FRAGILITY OF CALIFORNIA BRIDGES

DEVELOPMENT OF MODIFICATION FACTORS

A Dissertation

Presented to

The Academic Faculty

by

Farahnaz Soleimani

In Partial Fulfillment

of the Requirements for the Degree of

Doctor of Philosophy in the

School of Civil and Environmental Engineering

Georgia Institute of Technology

Georgia Institute of Technology
May 2017

FRAGILITY OF CALIFORNIA BRIDGES

DEVELOPMENT OF MODIFICATION FACTORS

Approved by:

Dr. Reginald DesRoches, Advisor
Karen and John Huff School Chair and Professor
School of Civil and Environmental Engineering
Georgia Institute of Technology

Dr. Jamie E. Padgett, Co-advisor
Associate Professor
School of Civil and Environmental Engineering
Rice University

Dr. Brani Vidakovic
Professor
H. Milton Stewart School of Industrial and System Engineering
Georgia Institute of Technology

Dr. Iris Tien
Assistant Professor
School of Civil and Environmental Engineering
Georgia Institute of Technology

Dr. Barry Goodno
Professor
School of Civil and Environmental Engineering
Georgia Institute of Technology

Date Approved: March 28, 2017

Dedication To

My Parents,

My Brother, Mohammadreza,

&

My Husband, Alireza

ACKNOWLEDGEMENTS

I am grateful for the people who have supported me during my academic career. First and foremost, I would like to express my sincere gratitude to my outstanding advisor, Dr. Reginald DesRoches. He has been supportive since the days I began working at Georgia Tech. He has offered the opportunity, guidance, knowledge, motivation, and camaraderie, which equipped me to pursue my academic interests. There is no way to convey my deep gratitude and respect for Dr. DesRoches. I could not have imagined having a better supervisor and extremely talented mentor. Much warmest gratitude is also extended to my wonderful co-advisor Dr. Jamie Padgett at Rice University. I have especially benefited from her truly professional support, sound advice, inspiration, enthusiasm, and continuous optimism.

I gratefully acknowledge the contributions and support I have received from the California Department of Transportation (Caltrans), and I would like to specially thank Cliff Roblee. This study has been supported, in part, by Caltrans through Project P266, Task 1780: Production development of generation-2 fragility models for California bridges. This study provides key insights regarding bridges with geometric irregularities, develops methodologies for generating fragility curves pertinent to the considered class of irregular bridges, and presents approaches to modify the process of developing probabilistic seismic demand models of irregular bridges. The curves shown in this thesis are illustrative and should not be used for deployment in ShakeCast, or other risk analysis software. However, the provided methodologies are intended to be used, in the future phases of this project, in order to generate final production set of fragilities for existing California bridges.

My sincere thanks go to the members of my doctoral committee: Dr. Barry Goodno, Dr. Brani Vidakovic, and Dr. Iris Tien. They generously invested time and support throughout the

development of this study and provided me valuable comments toward improving my work. A special note of acknowledgment is extended to Dr. Vidakovic who showed me the great power and potential of applying the statistical techniques to my problem. He was my guiding light to develop a broader perspective to my thesis. I owe him a special gratitude for providing his time, energy, outstanding teaching, great company, support, bright ideas, and intellectual contribution to assist me in many ways to present a productive work. I am grateful to my amazing friends whose support and friendship always helped me overcome the challenges in my life. However, I can not name each of them here. I am delighted to deeply appreciate each of them for being part of this journey.

Last but not least, I would like to express my deep and sincere gratitude to my family without whom I would never have enjoyed my accomplishments. My family has given up many things for me to pursue my passions. I wish to thank my parents for their unconditional support, continuous love, and encouragement throughout my life. I am grateful to my wonderful brother, Mohamadreza, who is a special person to me for always being there for me and for becoming a lifelong best friend. My beloved husband, Alireza, deserves special recognition. Without his patience and sacrifice, I could not pursue my passions. He has cherished with me every great moment, cheered me on, and celebrated each accomplishment, and supported me whenever I needed it. He has been my best friend and great companion, who loved, supported, encouraged, entertained, and helped me since the day we met.

TABLE OF CONTENTS

LIST OF TABLES

LIST OF FIGURES

SUMMARY

This research study concentrates on the effects of geometric irregularities on the seismic response and fragility analysis of bridges. The experiences of past earthquakes have affirmed that bridges with geometric irregularities or inconsistencies in configuration have a higher probability of damage than the regular, straight bridges. Although previous studies have explored the fragility analysis of different types of bridges, there is a lack of research that focuses on the effects of various types of geometric irregularities on the development of fragility curves. The current work aims to address this deficiency by focusing on the impacts of (i) skew angle, (ii) unbalanced stiffness of frames, and (iii) tall column bents on the seismic performance of concrete box-girder bridges in California.

This research first identifies the analytical modeling considerations associated with the design and construction of bridges in California. In the next step, bridge plans are extensively reviewed to determine the appropriate distribution of parameters needed to set up the various bridge components required for finite element modeling.

Following the analytical modeling of bridges, a sensitivity analysis is performed on different bridge attributes to classify all of the categories of bridges existing in California. This classification helps keep the number of simulations and computational efforts within a reasonable range. The impacts of each type of irregularity on the probabilistic seismic demand model and the vulnerability of bridges are investigated in the later phases of this project.

Finally, implementing statistical techniques, the results are compared to the responses of bridges with regular configurations. This results in the development of

modification factors that allow the fragility curves of regular bridges to be modified, taking irregularities into account. Eventually, the proposed modification factors for each type of irregularity are tested and finalized.

CHAPTER 1

INTRODUCTION

1.1 Problem Statement

Bridges, as a principal element of the highway transportation system, play a vital role in reducing traffic congestion in metropolises. Understanding the seismic behavior of highway bridges is imperative for maintaining a reliable and efficient transportation network. Earthquake vulnerability is one of the major factors threatening the functionality of highway bridges, particularly ones located in high-risk seismic zones. There is much existing literature on the seismic fragility analyses of many types of highway bridges in the United States (Mackie & Stojadinovic, 2005; Choi, et al., 2004; Nielson, 2005; Padgett & DesRoches, 2008; Ramanathan, 2012; Zhang & Huo, 2009; Jeong & Elnashai, 2007). Most studies on the seismic vulnerability of bridges can be applied to bridges that have regular geometry. However, it is well known that irregular bridges are particularly vulnerable to seismic damage (Buckle, 1994; Yashinsky, et al., 2010; Kawashima, et al., 2010).

Past earthquakes, such as the Northridge earthquake in California in 1994, the Kobe earthquake in Japan in 1995, and the earthquake off the coast of central Chile in 2010, revealed that bridges with irregularities such as skew, unbalanced stiffness frame, and tall column bents have a higher seismic damage risk than regular, straight bridges. Recent studies, which are outlined in the following section, show that the irregular bridge types exhibit distinctive seismic behavior when compared to regular, straight, bridges, and are potentially more susceptible to damage from a seismic event. The dominant

research focus on typical bridges and the clear evidence of higher damage risk in irregular bridges highlight the significance of a comprehensive study on the seismic behavior of irregular highway bridges.

1.2 Objective and Scope

This research seeks to add to the existing body of knowledge of the fragility analysis of typical bridges by addressing the issue of irregularities in bridge configurations. The intention is to provide a thorough understanding of the impacts of three types of irregularities on the seismic performance of bridges. The research will address skew, tall column height, and unbalanced stiffness frames, specifically focusing on bridges located in high seismic zones like California. A primary objective is to develop an approach that modifies the process of generating fragility curves by accounting for the aforementioned irregularities. In order to achieve these goals, modification (or adjustment) factors are established. The proposed adjustment factors contribute to the development of reliable fragility curves that are applicable to the class of irregular bridges.

The scope of this research is explained below:

- Identify the general modeling procedure and the appropriate distribution of parameters required for the finite element modeling. This step involves a comprehensive plan review of irregular bridge attributes, as well as a review of the various components of regular bridges.
- Classify all categories of the existing bridges in California into a feasible number of simulations, with respect to limited computational resources, through the following steps:

    - First, perform statistical analysis to classify regular bridges.
    - Second, use statistical distributions to determine the most common configurations of bridges for each type of irregularity.
    - Third, determine a set of bridge configurations for each class of irregular bridges, based on the insights acquired from the previous steps.
- Perform nonlinear time history analysis (NLTHA) on the selected set of bridges, using a suitable set of ground motions that corresponds to high seismic zones.
- Using the results of the NLTHA, obtain the seismic demands that correspond to the regular and irregular bridges.
- Evaluate the results of the analyses of regular and irregular bridges to find the impact of each irregularity on the seismic performance of the bridges.
- Establish a set of adjustment factors to modify the process for generating fragility curves that will account for the irregularities.
- Test the proposed modification factors for each type of irregularity.

1.3 Dissertation Outline

The content of this dissertation is organized into the following chapters:

- **Chapter 2** provides an overview of the damage experienced by irregular bridges in past earthquakes and demonstrates the need to address the existing research gap by evaluating the seismic performance of irregular bridges.
- **Chapter 3** explains the detailed aspects of the analytical modeling considerations and the distribution of parameters associated with various bridge components.

- **Chapter 4** delineates the classifications of bridge configurations for regular and irregular bridge types.
- **Chapter 5** describes the influential parameters for estimating the responses of irregular bridges.
- **Chapter 6** presents modified approaches for developing probabilistic seismic demand models of irregular bridges.
- **Chapter 7** describes the fragility analysis approach that is used in this study. It also discusses and illustrates the methodology used to develop adjustment factors for generating fragility curves of irregular bridges. **Chapter 7** provides the application of the proposed approaches to the California bridge system.
- **Chapter 8** summarizes the conclusions for the performance of irregular bridges and the generated fragility curves. Future research needs are also identified in this chapter.

CHAPTER 2

LITERATURE SEARCH

Bridges are critical links in a transportation network, and their seismic vulnerability can lead to large economic losses. Bridge vulnerability can be assessed by developing fragility curves that indicate the probability of reaching or exceeding a specific level of damage. The experiences of previous earthquakes, such as the Northridge earthquake in California in 1994, the Kobe earthquake in Japan in 1995, and the earthquake off the coast of central Chile in 2010, reveal that bridges with irregularities in their configurations have a higher chance of collapsing or sustaining severe damage than bridges constructed with typical configurations (Buckle, 1994; Yashinsky, et al., 2010; Kawashima, et al., 2010). Figure 2.1 shows pictures of damaged concrete bridges based on post-earthquake field observations (Sahs, et al., 2008). Bridges with typical geometric configurations are defined as straight bridges with zero skew angle and zero curvature, bridges with normal column heights, and bridges with balanced stiffness between frames.

2.1 Existing Research on Skewed Bridges

Among geometric irregularities, skew requires particular attention. Previous earthquakes have shown serious damage caused by the displacement or the unseating of the bridge decks in bridges with large skew angles (Kaviani, et al., 2012). Skewed bridges are commonly constructed in response to complex geometric constraints that necessitate using skew-angled abutments. As a result, the eccentric passive resistance of the abutment backfill initiates and promotes the in-plane rotation of the superstructure's

deck, which ultimately causes the unseating of the superstructure, leading the skewed bridge to collapse.

Figure 2.1: Field observations of the 1994 Northridge earthquake: (a) deck failure; (b) and (c) deck collapse; (d) deck and abutment displacements; (e) abutment connection failure; (f) abutment failure, and field observations of the 1989 Loma Prieta earthquake: (g) and (h) collapsed deck; (i) joint failure; (j) total failure; (k) column flexural failure; (l) column shear failure ((Sahs, et al., 2008))

Several research efforts have investigated the effects of skew angle on the seismic response of bridges (Abdel-Mohti & Peckan, 2008; Meng & Lui, 2000; Meng, et al., 2004; Maleki, 2005). Although these studies indicated that this class of bridges experiences larger column forces and deck displacement, they are limited to specific case studies on failed bridges and they considered a single bridge model. Catacoli (2014) proposed a nonlinear model to study the displacement demand of columns for skewed bridges with seat-type abutments. Maragakis and Jennings (1987) concluded that the response of skewed bridges is prominently governed by the skew angle, as well as the impact between the bridge deck and the abutment.

Several other researchers focusing on the seismic performance of skewed bridges highlighted extensive damage to the columns that was induced by the increased torsion in the column bents (Ghobarah & Tso, 1973; Tirasit & Kawashima, 2005). This torsional demand has been triggered primarily by bridge deck rotation. Ghobarah and Tso (1973) noted that highly skewed bridges collapsed mainly because of the coupled flexural-torsional motions of the deck.

2.1.1 Significant Parameters

Probabilistic seismic demand models (PSDMs) are essential tools used to describe the seismic demand of various components of a bridge in terms of the ground motion intensity measures. Researchers (Nielson & DesRoches, 2006; Padgett & DesRoches, 2008; Zhong, et al., 2008; Ramanathan, 2012) commonly utilize PSDMs to perform fragility analysis to characterize the conditional reliability of bridges. Several studies (Nielson & DesRoches, 2006; Dukes, et al., 2012; Padgett & DesRoches, 2007) have conducted sensitivity studies to identify the parameters that significantly affect the bridge

response to seismic demands. However, these studies typically focused on regular bridges and selected numerical parameters. The present study attempts to determine the influences of categorical and numerical parameters on the seismic response of irregular bridges.

Several research efforts have investigated the effects of skew angle, along with a few other parameters, on the seismic response of bridges (Abdel-Mohti & Peckan, 2008; Meng & Lui, 2000; Meng, et al., 2004; Maleki, 2005). For example, Abdel-Mohti & Peckan (2008) explored the seismic performance of a selected three-span concrete box-girder bridge with three different skew angles of 30°, 45°, and 60°. They compared bridges with two different cases of boundary conditions (with and without shear keys) and directions of applied ground motions. Four selected ground motions were applied for pushover and time history analysis using SAP2000. The results showed that skew angle and boundary conditions have significant effects on the bridge response. Meng & Lui (2000) analyzed a 60 degrees skewed box-girder bridge, the Foothill Boulevard Undercrossing, in SAP2000. The effects of deck flexibility, column base fixity, and the skew angle were investigated, and it was concluded that all three factors could drastically change the bridge response to a seismic event.

Kaviani, et al. (2012) performed a seismic assessment of selected skewed bridges in California. Three short California bridges with various structural parameters were selected. Sensitivity of the deck rotation and column-drift ratio were assessed according to five skew angles of 0°, 15°, 30°, 45°, and 60°, two span ratios 1.0 and 1.2, two column-height ratios 1.0 and 1.5, and three types of ground motions as soil-site, rock-site, and pulse-like with six angles of incidence, 0°, 30°, 60°, 90°, 120°, and 150°. It was

demonstrated that the monitored skewed bridge demands, including deck rotation and column-drift ratio, were higher than those of non-skewed bridges; these demands exhibited sensitivity to the characteristics of ground motions as well as to skew angles. Past studies investigated the influence of selected parameters, while the current study evaluates the entire modeling parameters to develop a comprehensive perspective on the impact of a broader range of parameters on the seismic response of irregular bridges.

Zakeri, et al. (2013) investigated the effect of skew angles, single and two-column bents, integral and seat-abutment types, and seismic design levels on the fragility curves of concrete box-girder bridges. Older bridges and bridges with integral abutment types showed less sensitivity to the skew angle; however, more recently designed bridges, bridges with seat-type abutments, and bridges with both single-column and two-column bents exhibited vulnerability to the variation of the skew angle. Although a basic understanding of the seismic behavior of skewed bridges has been developed, particularly in recent decades, a closer and more comprehensive investigation of the skew effect and modeling parameters on the seismic vulnerability needs to be conducted.

2.1.2 Fragility Analysis

Fragility analysis, which leads to the development of fragility curves, is a prominent approach used in damage assessment for various components of a bridge exposed to a seismic hazard. For each bridge, these curves determine the conditional probability of damage as a function of ground motion intensity. In this regard, researchers typically propose empirical (Shinozuka, et al., 2000) and analytical (Nielson, 2005) fragility curves for regular, straight bridges. Empirical approaches can only be used when sufficient earthquake records are available. Thus, the analytical approach is commonly

applied when sufficient records are not available. Analytical fragility curves were initially created by Yu, et al. (1991) and further extended by other researchers (Hwang, et al., 2000; Zhong, et al., 2008; Gardoni, et al., 2003). In the past two decades, the development of analytical fragility curves was an essential step towards the risk assessment of the existing highway transportation network (Choi, et al., 2004; Nielson, 2005; Mackie & Stojadinovic, 2005; Jeong & Elnashai, 2007; Padgett & DesRoches, 2008; Zhang & Huo, 2009; Ramanathan, 2012). Although previous studies have explored the fragility analysis of different types of bridges, there is currently limited research on the effects of various types of geometric irregularities on the development of fragility curves. The current work aims to address this deficiency by focusing on the impact of geometric irregularities on the seismic performance of concrete box-girder bridges. The specific irregularities to be addressed by this research are skew angle, unbalanced stiffness frame (i.e., short columns mixed with longer columns), and tall column bents.

There have been a few studies in this regard. Kaviani, et al. (2012) performed a seismic assessment of selected skewed bridges located in California. Three short bridges with various structural parameters were selected. It was demonstrated that the skewed bridge demands, including deck rotation and column-drift ratio, were higher than those for the non-skewed bridges. Among other studies in this area, Sullivan (2010) and Yang, et al. (2015) developed fragility curves for bridges with skew angles between 0 to 45 degrees that are located in moderate seismic zones. Sullivan (2010) conducted fragility analysis and developed the associated fragility curves for skewed and multi-span simply supported steel girder bridges. The proposed fragility curves indicate that bridge fragility is not noticeably influenced by low- to medium-skew angles (i.e., skew angles less than

30˚), but it is significantly affected by higher skew angles. Yang, et al. (2015) evaluated bridges with various designs and retrofitting strategies. They found that, overall, bridges with larger skew angles are more vulnerable to seismic excitations.

Although successful research on skew exists, a more thorough investigation should be conducted to discover an efficient framework for developing fragility curves that are applicable to existing skewed bridges in high-risk seismic zones. This research study aims to address this concern. Moreover, previous studies implemented conventional methodology for fragility analysis, and this research provides an updated methodology that facilitates prediction of fragility analysis for irregular bridges.

Box-girder bridges, commonly found in California, were selected to account for the effects of irregularities on estimating the bridge's seismic response. The approaches proposed in this study can be extended to various types of bridges in future research, which is the objective of ongoing research by the authors.

2.2 Existing Research on Tall and Unbalanced Stiffness Frame Bridges

2.2.1 Studies on Unbalanced and Tall Bridges

Other irregularities in bridge configurations include tall column bents and unbalanced stiffness frames. Bridges with these irregularities are typically constructed in specific regions with complex topography for the foundation layout, such as mountainous areas, deep valleys, or overcrossings. Consequently, based on the topography attributes, some of these bridges have columns higher than the typical range, while others have columns of variable height. At present, there is very limited research on this topic; hence,

there is a need to further assess the seismic performance of these irregular bridge configurations.

Utilizing post-earthquake observations, Zheng & Wenhua (2006) explored the four primary damage states of bridges with high or non-uniform columns in mountainous areas. Based on their study, the first damage state was associated with changes in the position of the abutment, abutment settlement, and damage to the superstructure deck. The second damage state was mainly related to the cracking and breaking of piers, in addition to the buckling of the steel reinforcement. The third damage state was caused by the inclination and deterioration of supports; the final damage state resulted in bridge collapse because of the failure of piers and supports, followed by the falling of the superstructure.

In the case of unbalanced frame bridges, the large relative displacement between adjacent piers with inconsistent column heights is the major factor affecting the superstructure's failure (Qian, et al., 2006). The combination of tall and short piers within a bridge exposed to earthquake excitation results in uneven force distribution between the piers (Qian, et al., 2006; Li, et al., 2001). Zheng & Wenhua (2006) also clarified the importance of following a separate seismic design procedure for tall-pier bridges. They recommended using stronger column bents to resist large bending moments, shear forces, and torques. All of these factors indicate the complex seismic response of bridges with unconventional column attributes.

Jara, et al. (2015) examined the effect of three different topologies of unequal column heights on the seismic demand of the bridge columns. The selected medium-length bridges included two cases of five-span bridges and one case of a six-span bridge.

Twelve ground motions and two soil types, soft and hard, were selected for analysis. Both unequal configurations and soil types showed significant impact on the pier damage index, particularly for columns located adjacent to the tallest column. Abbasi, et al. (2015) analyzed seismic fragility performance of older designs of box-girder viaduct bridges with an expansion joint and four levels of variations between the column heights. The studied bridge was a four-span bridge with three columns per bent. The results demonstrated that fragility of the considered bridges increases with increasing variation between the column heights. Moreover, among various components of the bridge, deformation of the bridge deck and the in-span hinge presented the highest sensitivity to the height variation. The seismic responses and performance of tall and unbalanced bridges have not been deeply studied; thus, there is a need to further assess the seismic performance of these irregular bridge configurations.

2.2.2 Seismic Performance Assessment of Bridge Columns

According to the plan review of existing box-girder bridges in California, the typical configuration of bridge columns consists of circular and rectangular cross-section shapes with constant cross-section dimensions along the column height, also known as prismatic columns. However, other column configurations exist that can drastically alter the seismic performance of columns and bridges. These configurations include oblong and flared columns. Although many of the bridges in the United States are supported by non-prismatic columns or non-typical cross-section shapes, most existing studies on fragility analysis (Mackie & Stojadinovic, 2005; Nielson, 2005; Padgett & DesRoches, 2008; Ramanathan, 2012; Yang, et al., 2015) focus on bridges supported by prismatic columns with circular or rectangular cross-sections. In order to determine the effects of

various column shapes, the current study attempts to evaluate the seismic performance of bridges with oblong and flared columns.

Using oblong column shapes in box-girder bridges can considerably reduce the amount of transverse reinforcement that is required, as the oblong cross-sections include interlocking spirals. These spirals confine the concrete core more effectively than single spiral confinements and rectangular hoops. Additionally, when a cross-section includes overlapping confinements, fabrication is easier for interlocking spirals than for overlapping rectangular hoops. Tanaka and Park (1993) tested four column specimens to study the behavior of columns with interlocking spirals: one with a rectangular shape that contained rectangular hoops, and three with oblong cross-sections that contained interlocking spirals. The tests applied constant axial loads, equal to ten percent of the axial capacity of the column, and cyclic horizontal loads to the tops of the columns. The experiments showed that the oblong-shaped columns outperformed the rectangular ones in the aspects of stable hysteresis loops, well-measured energy dissipation, and limited strength reduction up to a ductility demand of around 10.

Wu, et al. (2013) investigated the effect of transverse confinements on the performance of oblong and rectangular bridge columns in which either tie or spiral reinforcements were used. Four columns were tested, using combined axial and flexural loadings during the tests. The commonly used column cross-sections are circular and rectangular ones, while the spiral reinforcement scheme is typically advised for circular cross-sections. In order to take advantage of the benefits of spiral reinforcement, Wu, et al. proposed an innovative transverse reinforcement arrangement for rectangular-shaped columns, which included two central interlocking spiral reinforcements similar to the

oblong cross-section. Four small spirals at the corners of the rectangular cross-section were also added to the section. All of the tested columns displayed satisfying ductile behavior. Although the two oblong columns exhibited similar behavior, Wu, et al. (2013) illustrated the improved performance of rectangular columns with spiral reinforcement compared to the tied columns.

Ou, et al. (2014) focused solely on the shear behavior of oblong columns, with several different transverse reinforcement schemes, including the conventionally-tied two-spiral interlocking, and seven-spiral interlocking reinforcements. They proposed the seven-spiral configuration since the large size of the two-spiral oblong columns often poses challenges for fabrication and transportation. The tested columns with their proposed seven-spiral configuration effectively addressed the size issue and showed better performance compared to the conventionally-tied columns, while remaining interlocked during the entire experiment.

In addition to typical columns, which have a prismatic configuration, flare-shaped columns with one-way and two-way flares (Figure 2.2) also exist. Besides the architectural inclination, one-way flared columns are commonly used in bridges constructed after 1970 (approximately 42% of California box-girder bridges) to provide more support to the cap beam under eccentric live load. Flared columns are constructed by either integrating them to the superstructure (these are called connected flares), or by connecting them to the superstructure with a gap in between (these are called isolated flares, and are typically seen in bridges designed after 1990). Sanchez, et al. (1997) conducted experimental studies on flared columns and concluded that the seismic

performance of isolated flares is similar to prismatic columns. This study is limited to connected, one-way flared columns.

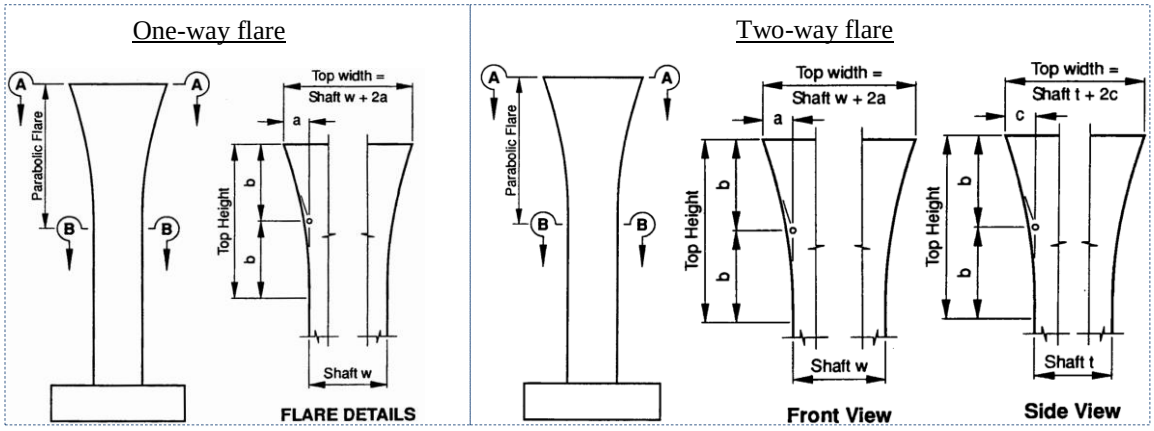

Figure 2.2: One-way and two-way flared columns (source: Caltrans Seismic Design Code (Caltrans, 2006))

Nada, et al. (2003) conducted an experimental and numerical study on four flared specimens in which two specimens were designed to display flexural dominate behavior, while the remaining shorter columns were designed to exhibit shear dominate demand. Each of the two column types contained different transverse designs. One was designed to have consistent confinement along the column height, and the other was designed to contain higher confinements at the top third of the column height. The columns were subjected to eleven ground motions simulated by a shake table. The study showed satisfactory ductile behavior for all tested specimens. Nada, et al. (2003) strongly recommended including a gap between the short columns and the superstructures since their analysis showed premature failure caused by brittle shear damage. With isolated columns, extensive shear cracks were observed. Since the gap was closed at a low ductility ratio, the load carrying capacity was increased as a consequence, which caused higher load transferring to the columns.

Wehbe, et al. (1997) examined four half-scaled flared bridge columns. The specimen designs were according to the 46th and 60th percentages of minimum confinements required by AASHTO. The columns were subjected to quasi-static cyclic lateral loadings. Two different longitudinal reinforcement arrangements were used in the tests. In one arrangement, reinforcements were placed along the flares, while in the other, reinforcements were located mainly in the core area. Test results showed higher vulnerability for the flared columns with longitudinal reinforcements distributed along the flares and not concentrated in the core area. This study also attempts to compare the seismic performance of bridge columns with various shapes.

2.3 Closure

Seismic performance assessment of highway bridges is an essential step toward maintaining a solid transportation network. Several research studies evaluated bridges and their columns as the most vulnerable elements of a bridge, via experimental and numerical studies. However, most of the research has focused on typical bridges and column types. This chapter provided an overview of the existing research on typical bridges, as well as the limited existing research on irregular bridges.

CHAPTER 3

ANALYTICAL MODELING APPROACH

The following section demonstrates the strategies and details of numerical modeling for global bridge models and their various components. The models are generated based on numerical and experimental analysis, observed performance of bridges during previous earthquakes, communications with collaborators from the California Department of Transportation (Caltrans), and a detailed review of real bridge plans collected from California archive. In the following, global layout of a bridge model is initially explained; then, the modeling procedure for the bridge components is described for the class of typical box-girder bridges (i.e., straight bridges with zero skew angles and normal and uniform column heights) and irregular box-girder bridges (i.e., skewed, tall, and unbalanced bridges). The differences between the numerical modeling of the irregular bridges and the regular bridges are explained for each of the components.

3.1 General Layout

In this study, the finite element platform, OpenSees (Mazzoni, et al., 2006), is used to generate three-dimensional (3-D) numerical models of the considered bridge categories and their corresponding configurations. Figure 3.1 demonstrates schematic diagrams of the analytical model for the regular and irregular bridge types that are considered in this study. Skewed bridges (Figure 3.1 (b)) include skewed-angle abutments, and, contrary to straight bridges (Figure 3.1 (a)), contain transverse deck elements are not perpendicular to the longitudinal deck elements. More explanations of the differences between skewed and straight bridges are provided in the component

modeling section. Tall bridges (Figure 3.1 (c)) are defined as those where the average column heights are higher than 1.5 times of the average column height of the regular bridges (i.e., $H_{tall} > 1.5 \times H_{normal}$, (Caltrans, 2013-2016)). Based on the seismic design criteria (Caltrans, 2006), a bridge is defined as having an unbalanced stiffness frame when different bents within the frame have a stiffness ratio of less than 75% (Figure 3.1 (d)). This criterion is converted to short and tall column height ratios later.

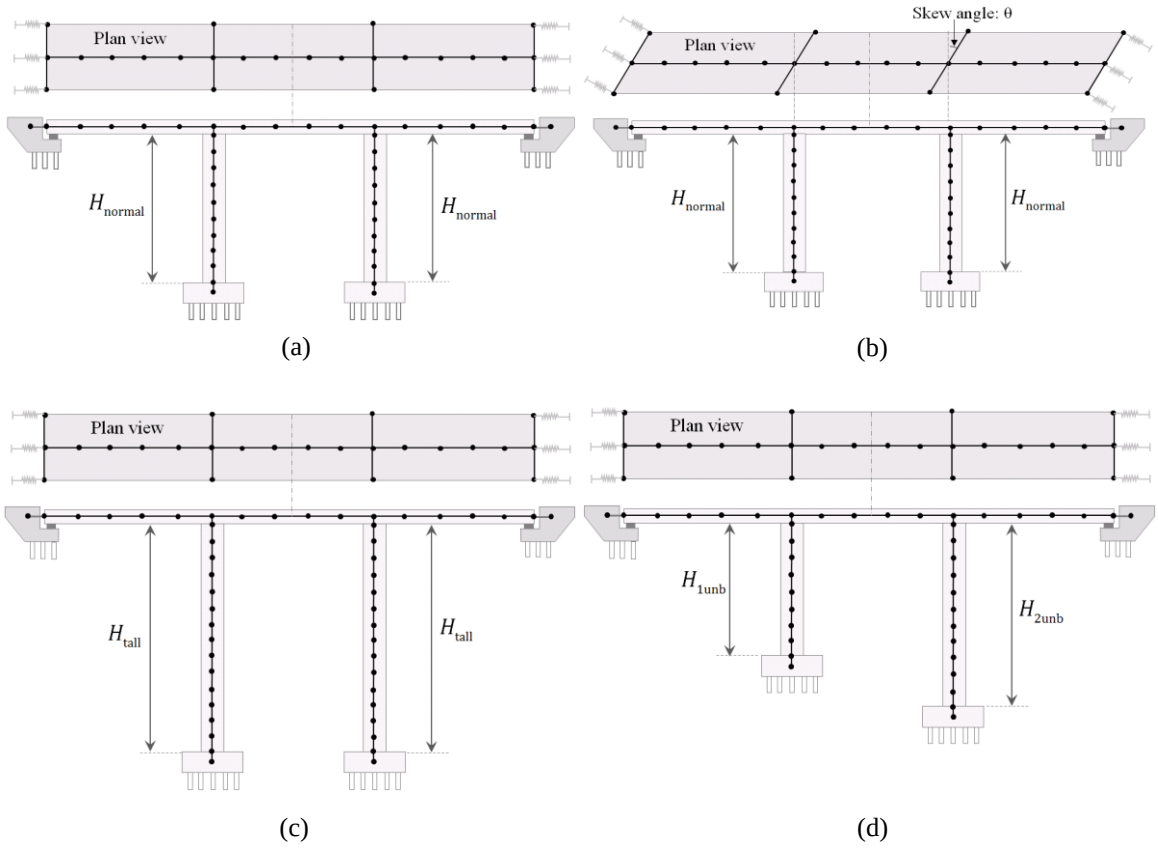

Figure 3.1: Schematic diagram of regular and irregular bridge layout

For each bridge type, various components of a box-girder bridge are modeled with their specific characteristics and are then integrated to generate the global analytical model of the bridge, as illustrated in Figure 3.2. The components can be primarily

classified as superstructure and substructure. A detailed description of the numerical modeling strategies for different components of a bridge is provided in the following section.

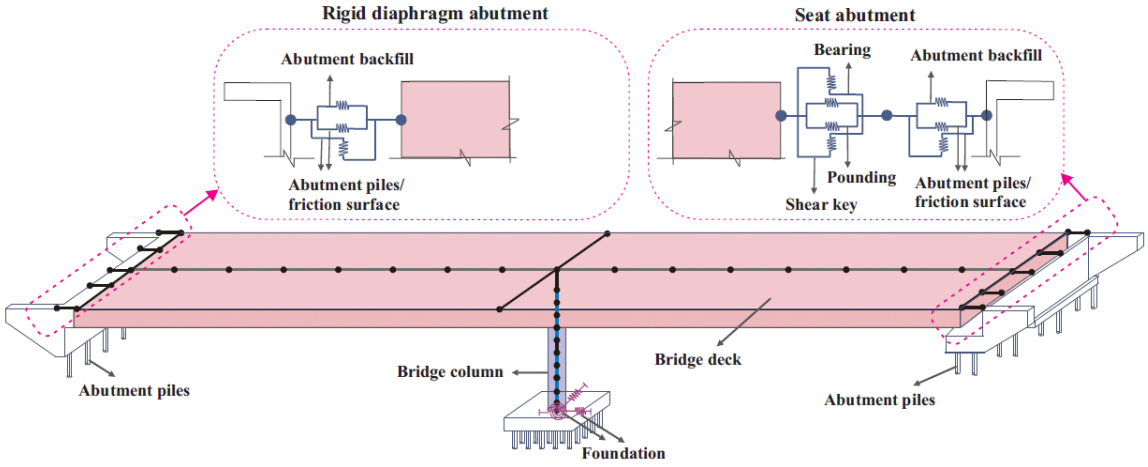

Figure 3.2: Illustration of various bridge components

3.2 Superstructure

The bridge deck consists of longitudinal and transverse elements known as girder elements (Figure 3.3). When a bridge is subjected to an earthquake, the superstructure typically remains elastic; hence the longitudinal deck elements and the transverse girder elements are modeled as elastic beam column elements in OpenSees with lumped masses applied on the element nodes. The properties of the elements are calculated based on the properties of a composite section.

The incorporation of skew into the analytical models of regular, straight bridges necessitates various modifications. Several bridge components are affected by changing the orientation of the bridge. For modeling skewed bridges, the transverse deck elements

are rotated to consider the corresponding skew angle of the bridge. Figure 3.3 illustrates the layout of the bridge deck for skewed bridges.

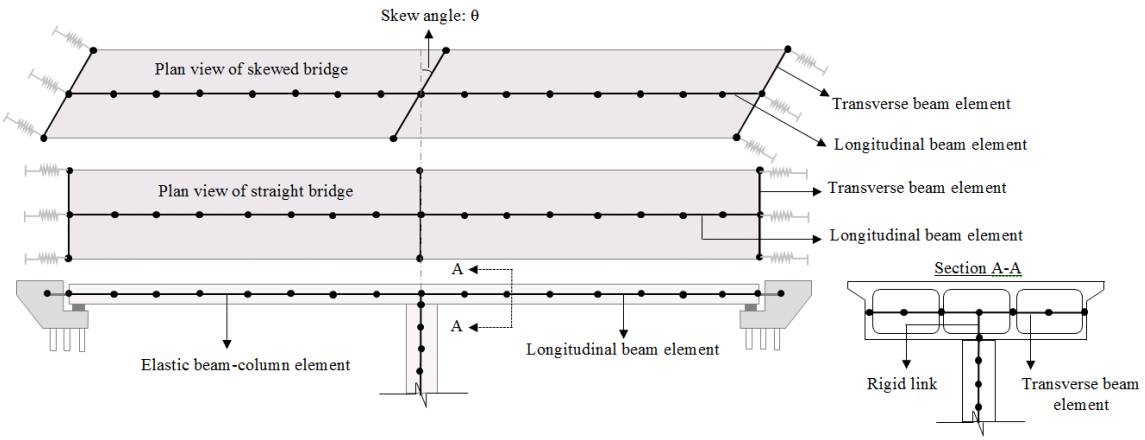

Figure 3.3: Illustration of box-girder bridge deck, the orientation of transverse deck elements in straight bridges versus skewed bridges, and the cross-sectional view of the bridge deck

3.3 Substructure

The bridge substructure consists of bent and column, abutment, foundation, pounding, bearing, and shear key. Modeling strategies for each of these components are presented below.

3.3.1 Column

Transverse deck elements are connected to columns using rigid links to ensure the moment and force transfer between the deck and column (Figure 3.3). The number of columns per bent in each bridge depends on various factors, including the deck width and the design code era. Consistent with previous studies (Nielson, 2005; Dukes, et al., 2012; Ramanathan, 2012), California bridges are designated as pre-1971 design era, 1971-1990 design era, or post-1990 design era, according to improvements that were added to the

seismic design codes. A review of the plans of real box-girder bridges in California showed that: the majority of bridges designed before 1971 have one or two columns per bent (Figure 3.4); bridges designed between 1971-1990 have one to four columns per bent; and bridges designed after 1990 have one to five columns per bent.

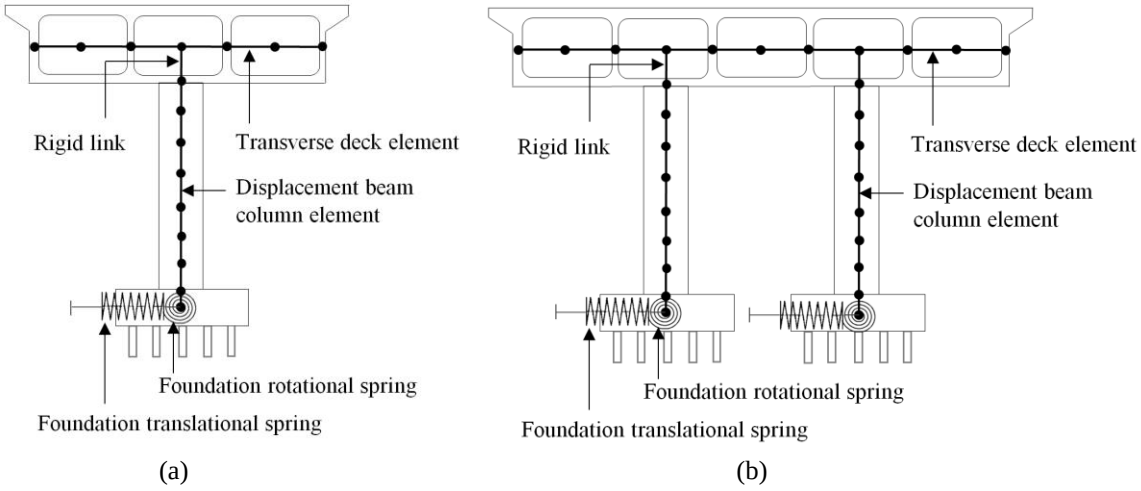

Figure 3.4: Illustration of number of column bents in pre-1971 bridges; (a) single column bent (SCB), (b) multi-column bents (MCB)

Single column bents are usually fixed at the column's base, and multi-column bents of bridges in the 1971-1990 and post-1990 design eras are pinned at the base, while 50% of pre-1971 bridges with multi-column bents have fixed-base columns. Choosing the number of column bents in each design era is related to the deck width. In this study, single column bent (SCB) and multi-column bent (MCB) are modeled using the displacement-based nonlinear beam column elements with fiber-defined cross-sections. The fiber section option in OpenSees provides the option to assign distinctive material properties to different locations on a cross-section. The fiber sections consisting of concrete and steel reinforcement are defined (Figure 3.5) using "concrete-07" and "steel-02" materials, respectively. As shown in Figure 3.5, different properties are considered

for the confined (core) concrete and the unconfined (cover) concrete parts employing the concrete models developed by Mander, et al. (1988). The model developed by Menegotto and Pinto (1973), later modified by Filippu, et al. (1983), is assigned to the numerical model to add isotropic strain hardening property (Figure 3.5) to the reinforcing steel.

The column's cross-section shape is another factor that varies with the design era. This study concentrates on the most common standardized column shapes in California box-girder bridges. According to the existing bridge configurations, column shapes are categorized into three main categories with layouts shown in Figure 3.5: Types I and II fall under the category of prismatic columns (Figure 3.5 (a)); while Type III is representative of flared columns that use stepped discretization (Figure 3.5 (b)) to create their numerical models. Type I columns are circular or square-shaped cross-sections in which two adjacent sides have equal lengths, while Type II columns are oblong or rectangularly-shaped, with unequal adjacent sides in the cross-sections. The three common cross-sections are shown in Figure 3.5 and all other existing cross-section shapes are idealized by one of these three common shapes. Appendix A provides the existing column cross-sections and the idealization details. As mentioned previously, in addition to a variety of cross-section shapes, flared columns are also present in California bridges. To test the importance of modeling flared columns for the purposes of this study, an initial case study evaluation was performed in this section to identify the effects of flares on the fragility curves.

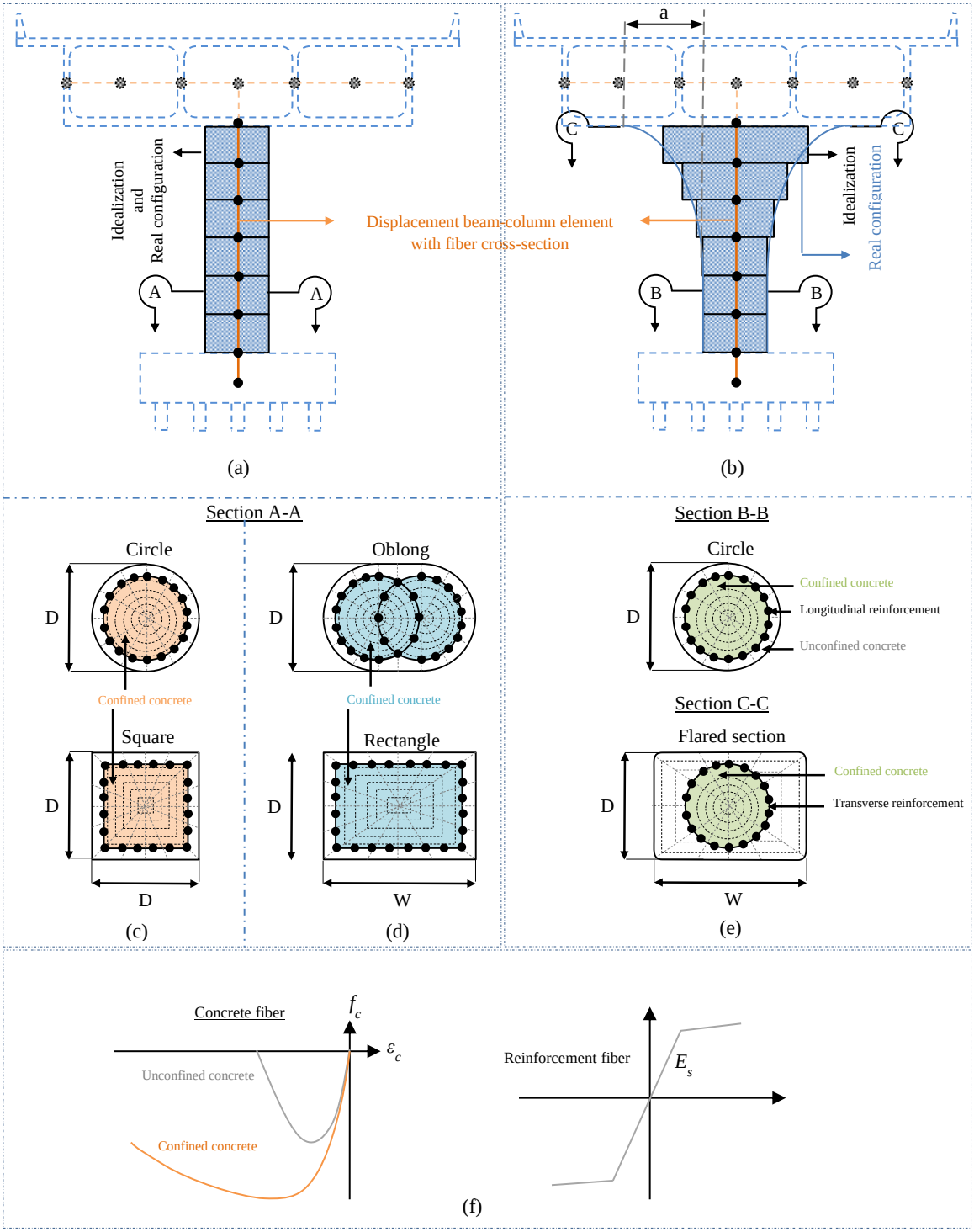

Figure 3.5: Column configurations in box-girder bridges: (a) Prismatic columns, (b) Flared columns, (c) Type I cross-section shapes, (d) Type II cross-section shapes, (e) Type III cross-section shapes, (f) OpenSees material objects assigned to the fiber cross-section

One initial step in an analytical study is to test the efficacy of modeling assumptions. In order to do that, this section focuses on a set of validation tests of the numerical modeling of bridge columns with the aforementioned column shapes. Four column tests were selected from previous experiments, and three-dimensional finite element models of the specimens were generated in OpenSees to determine how well the numerical models were able to capture experimental results. Based on a comparison of the numerical results and experiments data, insights are provided on each of the specimens. A detailed description of the four column tests is provided below.

To validate the numerical model of the Type I columns, a full-scale reinforced concrete (RC) bridge column test was chosen. This test was performed on the NEES Large High-Performance Outdoor Shake Table located at UCSD's Englekirk Structural Engineering Center. The RC cantilever column was designed according to Caltrans seismic design specifications and was supported on a fixed foundation. Figure 3.6 shows the test specimen and the setup for the experiment. The numerical modeling was conducted with the help of the finite element package called OpenSees. The numerical modeling parameters, shown in Table 3.1, are according to the provided values in the UCSD report (Schoettler, et al., 2012). The details of the column design and reinforcement are provided in Figure 3.6. The specimen was subjected to six ground motions (Figure 3.6) simulated by a shake table at UCSD. Similarly, the column's numerical model was subjected to the same set of motions. Nonlinear time history analysis was performed in OpenSees, and dynamic responses of the numerical model were captured. The responses include the column top displacement, the shear force at the base, and the bending moment at the column base. In this section, comparisons of the

numerical predictions with those measured during the experiments are provided. The response comparison of the full-time history analysis (Figure 3.7) confirms that the analytical and experimental results are in agreement.

To validate the numerical models of column Types II and III, full-scale RC bridge column tests by Tanaka and Park (1993), and Sanchez, et al. (1997) were chosen, respectively. The oblong cantilever column tested by Tanaka and Park (1993) was designed according to the column provisions in the New Zealand concrete design code. Sanchez, et al. (1997) constructed flared and prismatic columns according to Caltrans design code. Figure 3.8 and Figure 3.9 show the detailing of the column designs. In both studies, the columns were subjected to constant axial loads and cyclic horizontal loadings (Figure 3.8 and Figure 3.9). In the oblong cantilever column test, the cyclic horizontal load imposed on the specimen included one elastic cycle corresponding to a displacement ductility factor $\mu = \pm 0.75$, and two cycles for each of the factors $\mu = \pm 2, \pm 4, \pm 6, \pm 8$. In the Sanchez test, the displacement ductility factors used for applying the cyclic lateral loads were $\mu = \pm 1, \pm 1.5, \pm 2, \pm 3, \pm 4, \pm 5, \pm 6$ and $\mu = \pm 0.56, \pm 0.86, \pm 1.15, \pm 1.72, \pm 2.30, \pm 2.88, \pm 3.45$ for the prismatic and flared column, respectively. These experiments were simulated in OpenSees using similar cyclic loadings and performing cyclic pushover analysis. Then, the numerical results were compared with the experimental data. As shown in Figure 3.10, the numerical simulations are fairly able to predict the real columns' performance.

The validation process indicates that the numerical modeling technique used in this study can provide a realistic behavior model for bridge columns with various shapes. In the following section, a typical bridge column is modeled with the commonly used

structural characteristics and its seismic performance is evaluated by varying the column shape.

Table 3.1: Parameters used in the OpenSees model

Parameters	**Values**
Diameter of the column	1.22m (4 ft)
Column height	7.31m (24 ft)
Longitudinal reinforcements	18 #11
Transverse reinforcements (hoops)	Double #5 @152mm (6 in)
Clear cover	51 mm (2 in)
Concrete strength	41.9 MPa (6.1 ksi)
Modulus of elasticity	22877 MPa (3317 ksi)
Concrete compressive strain at maximum compressive stress	0.0026
Yield strength of longitudinal steel	518.5 Pa (75.2 ksi)
Yield strain of longitudinal steel	0.0026
Ultimate strength of longitudinal steel	706.7 MPa (102.4 ksi)
Modulus of elasticity of longitudinal steel	196057 MPa (28426 ksi)
ε_{sh} of longitudinal steel	0.011
E_{sh} of longitudinal steel	5515.5 MPa (800ksi)
ε_u of longitudinal steel	0.122
Yield strength of hoops	337.9 MPa (54.8 ksi)

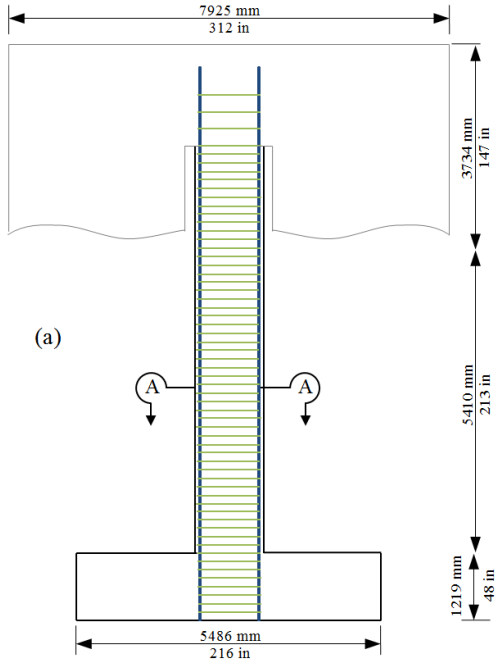

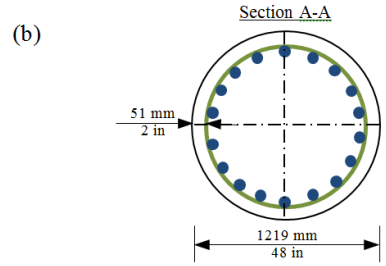

(c)

Selected ground motions

No.	Earthquake	Date	Moment magnitude	Station
EQ1	Loma Prieta	10/18/1989	6.9	Agnew State Hospital
EQ2	Loma Prieta	10/18/1989	6.9	Corralitos
EQ3	Loma Prieta	10/18/1989	6.9	LGPC
EQ4	Loma Prieta	10/18/1989	6.9	Corralitos
EQ5	Kobe	1/16/1995	6.9	Takatori
EQ6	Loma Prieta	10/18/1989	6.9	LGPC

Figure 3.6: (a) Details of the UCSD column design, (b) Reinforcement detailing of the UCSD column, (c) selected ground motions

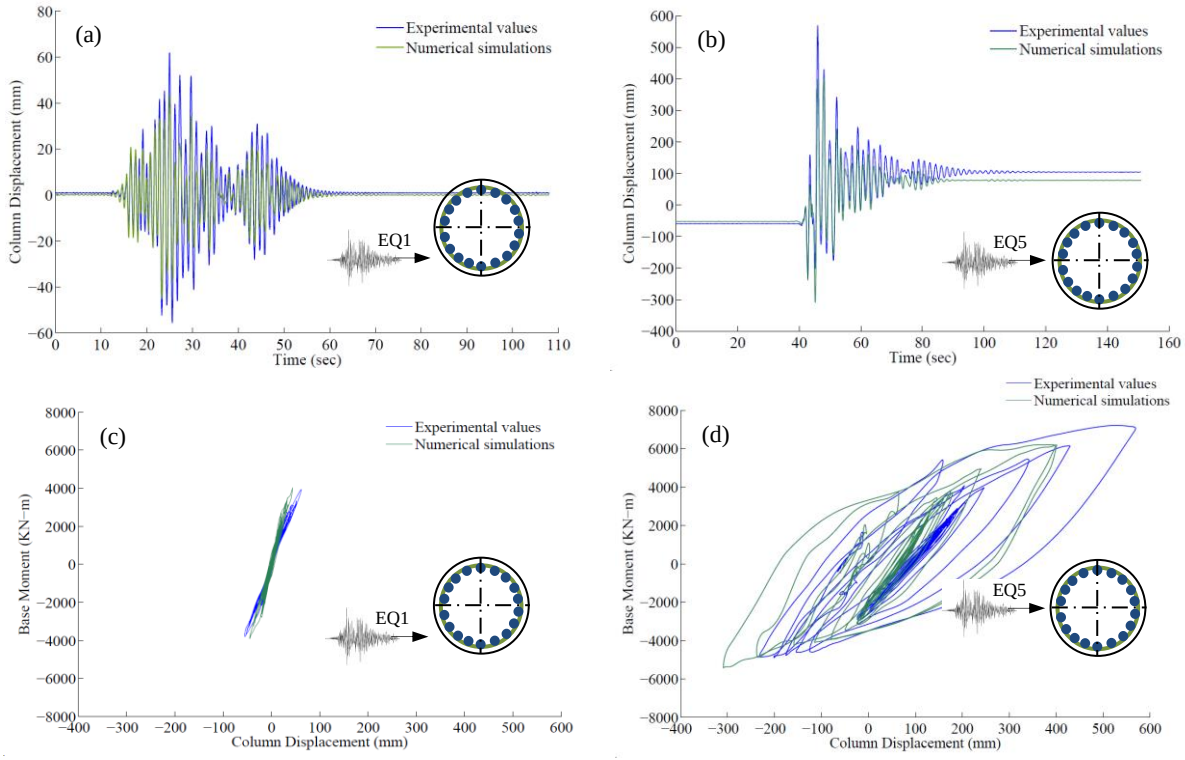

Figure 3.7: Comparison of the results for: (a) column top displacement (EQ1), (b) column top displacement (EQ5), (c) bending moment at column base (EQ1), and (d) bending moment at column base (EQ5)

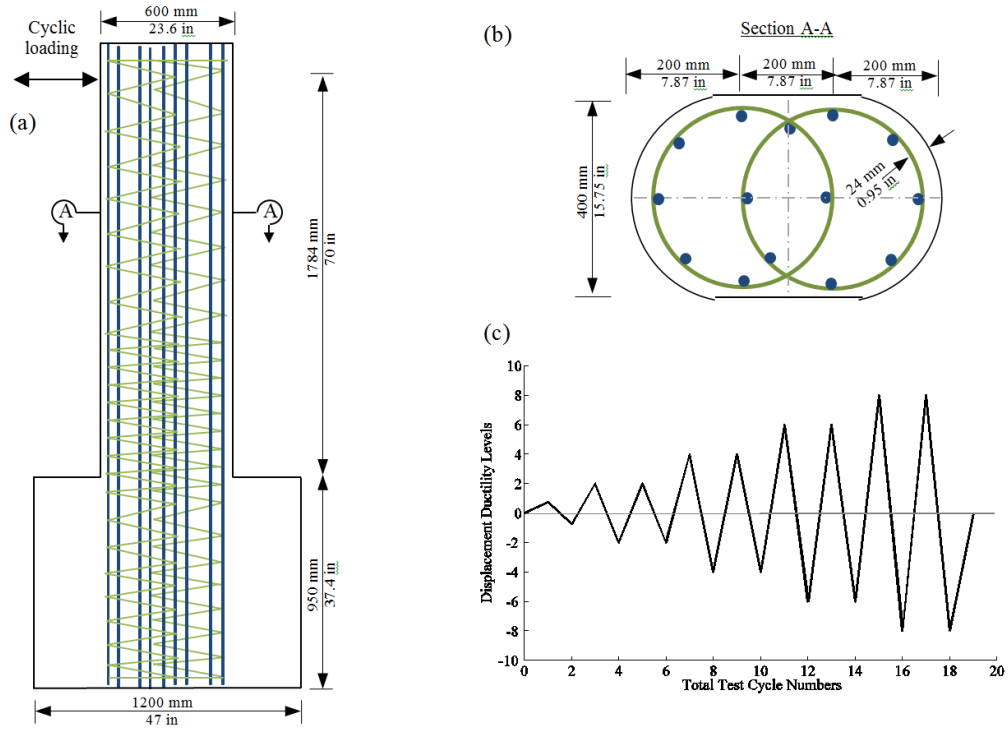

Figure 3.8: (a) Details of the column design, (b) Reinforcement detailing, (c) Displacement ductility levels

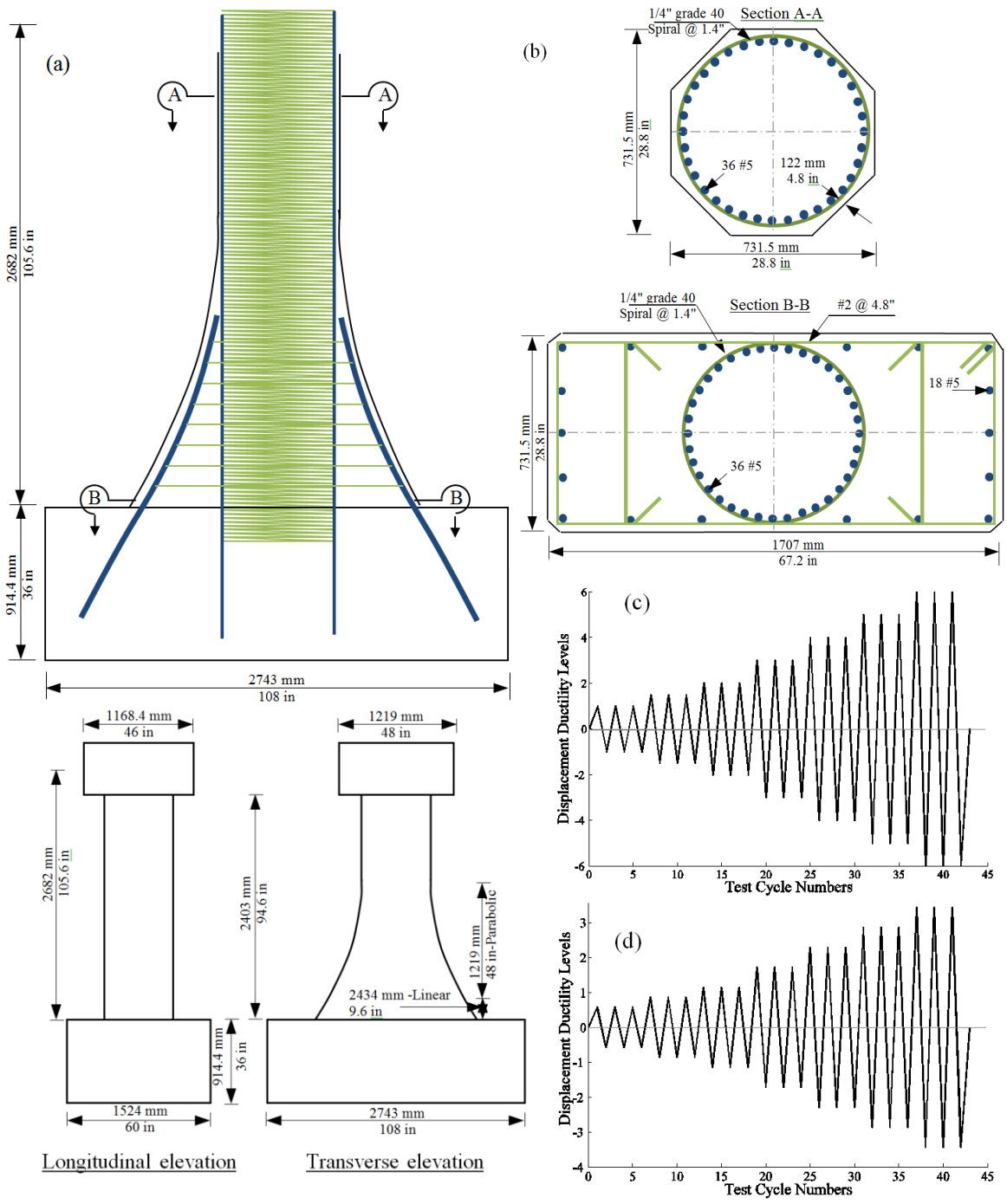

Figure 3.9: (a) Details of the column design, (b) Reinforcement detailing, (c) Displacement ductility levels for prismatic column, (d) Displacement ductility levels for flared column

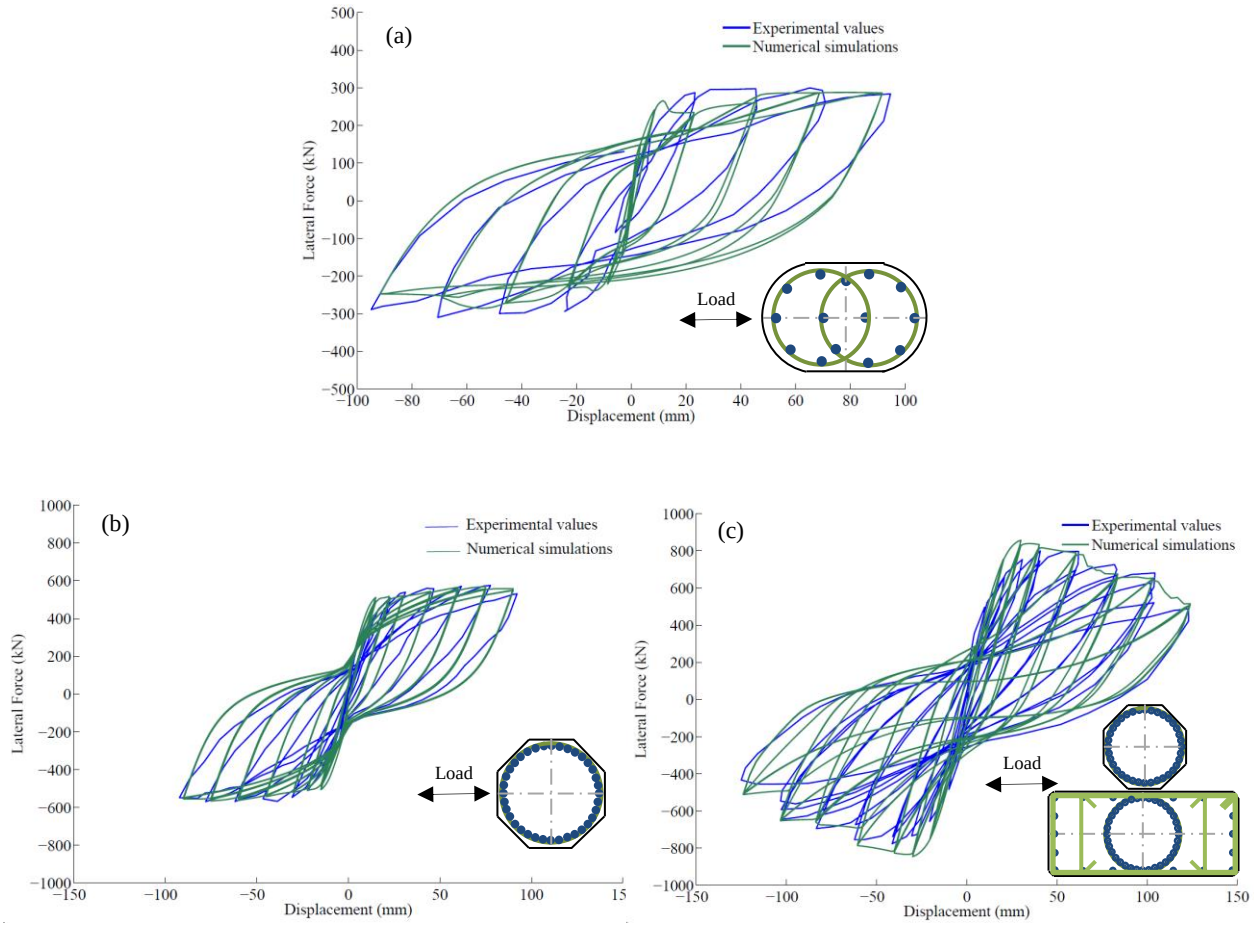

Figure 3.10: Lateral force versus lateral displacement hysteresis loops for (a) oblong column, (b) prismatic column, and (c) flared column

Analytical Comparison of the Columns' Performance

As mentioned above, a number of researchers studied the seismic performance of bridge columns with various shapes. However, the effect of column shape (cross-section and flares) on the fragility assessment of a bridge system is not well-known yet. The current study attempts to address this research gap by evaluating the seismic performance of a typical bridge column as an individual element and as a component of a bridge system. This numerical study is divided into two stages, in which the structural

characteristics of existing box-girder bridges in California are used to generate finite element models.

First, three-dimensional numerical models of a typical bridge column were created in OpenSees; the models include columns with various common shapes including circular, rectangular, and oblong cross-sections, as well as prismatic and flared columns. The numerical models were validated with previous experiments performed on the column shapes that are considered in this study. Then, seismic assessment of typical bridge columns was conducted through a set of monotonic and cyclic pushover analysis.

Second, a three-dimensional numerical model of a typical box-girder bridge was developed using a variety of column shapes. Using a selected set of ground motions, nonlinear time history analysis was performed on the models to derive structural responses. Next, the seismic performance of the bridge models was evaluated by comparing their probabilistic seismic demands, particularly the column displacement ductility. Since developing probabilistic seismic demand models is an essential step toward generating fragility curves, the comparison of the seismic demands provides initial insight into the influence of column shape on the fragility assessment of bridge components. In order to enhance the insight, the evaluation process was continued to produce fragility curves for the various bridge components and the bridge system. Assessment of the generated curves indicates the impact of column shapes on the bridge fragility assessment.

This section provides an investigation of the columns' behavior under both monotonic pushover and cyclic lateral loading. A general method of pushover analysis about two axes of longitudinal and transverse was applied. The columns were assumed to

be cantilever ones subjected to constant axial loads equal to their ten percentage axial capacity ($f_c^{'} A_g$).

The input parameters for the tested columns are presented in Table 3.2. A detailed plan review of existing bridges in California was conducted to extract the probability distributions of the required modeling parameters. These distributions are used in the bridge fragility analysis presented in the next section, while the mean values of the modeling parameters (Table 3.2) are selected for the analysis of the columns in the current section. Four main cases, circular prismatic (CP), rectangular prismatic (RP), oblong prismatic (OP), and flared columns (Fl), are considered in this study. The dimensions used in this section are the most common ones, based on review of the California bridge inventory. The bridge design details manual lists three standard column sizes as 4, 5.5, and 7 feet for an equivalent circular column. Reviewing the existing bridge plans revealed that the majority of circular single columns have a 5.5 feet diameter and the majority of circular multi-column bents have a 4 feet diameter. Similarly, the other cross-section dimensions are selected based on the existing bridge population. The column cross-section areas are approximately similar in the four considered cases. In order to have a fair comparison of only the effect of column shapes, it is essential to keep all structural characteristics such as reinforcement ratios and column height the same. In order to account for the differences in bridge design codes, separate analyses were performed for the specifications of bridges designed before and after 1970.

Table 3.2: Geometric parameters used in modeling cantilever columns for pushover analysis

Parameters	Column Name			
	CP	RP	OP	Fl
Cross-section	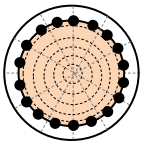	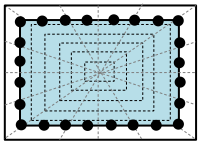	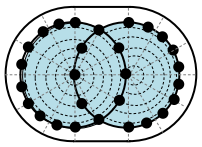	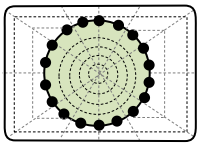
Type	I	II	II	III
Cross-section Dimensions (in)				
Single column	66	36 × 96	48 × 72	66 & a = 2' 9"
Multi-columns	48	36 × 48	36 × 48	48 & a = 2'
Cross-section Dimensions (mm)				
Single column	1676.4	914.4 × 2438.4	1219.2 × 1828.8	1676.4 & a = 838.2
Multi-columns	1219.2	914.4 × 1219.2	914.4 × 1219.2	1219.2 & a = 609.6
Column Height				
Pre-1970 (ft)	21.5	21.5	21.5	21.5
Pre-1970 (m)	6.55	6.55	6.55	6.55
Post-1970 (ft)	24.0	24.0	24.0	24.0
Post-1970 (m)	7.32	7.32	7.32	7.32
Longitudinal reinforcement (%)				
Pre-1970	1.9	1.9	1.9	1.9
Post-1970	2.35	2.35	2.35	2.35
Transverse reinforcement				
Pre-1970	#4 @ 12"	#4 @ 12"	#4 @ 12"	#4 @ 12"
Post-1970	#4 @ 3"	#4 @ 3"	#4 @ 3"	#4 @ 3"

First, monotonic pushover analysis was conducted on the columns in both longitudinal and transverse directions of the columns. As shown in Figure 3.11, two different patterns can be observed based on the direction of applied load, the arrangement of the longitudinal reinforcements, and the geometry of the confined concrete. In the longitudinal direction (Figure 3.11), the rectangular cross-section shows the highest strength because the steel reinforcement is arranged at the farthest distance from the center, which increases the moment of inertia and, subsequently, the stiffness and strength. Two additional cross-section shapes with similar modeling properties and cross-sectional area were analyzed to verify the comparisons. One (SP in Figure 3.11) is a square cross-section shape, and the other (36 × 48 rectangle, ERP in Figure 3.11) is a rectangular one with dimensions between the square (SP) and original rectangular (RP) section. The strength and stiffness increase as the shape changes from the circle (CP) to

the square (SP) and then to the two rectangles (RP and ERP); since the cross-section is elongated in the longitudinal direction that changes the reinforcement arrangements and the geometry of the confined concrete. This phenomenon is reversed in the transverse direction. The oblong columns have a response that is similar to the circular columns in the longitudinal direction and the rectangular columns in the transverse direction, due to the nearly similar arrangement of the rebar. The columns with flares display higher resistance than circular columns in both directions. That is the result of keeping the details of the non-flared sections of the flared column (from footing to half of the column height, Figure 3.5.b) identical to those of the prismatic columns, while the flared sections include an additional layer of reinforcement, similar to the layout shown in Figure 3.9, and the cross-section dimension increases along the column height. Clearly, circular columns have identical responses in both directions because of the symmetry of the shape and reinforcement. Additionally, increasing reinforcement ratios, while decreasing the confinement spacing, enhances the load-carrying capacity of the column during deformations.

Second, a cyclic pushover analysis was performed on the columns to examine the hysteretic loop. The displacement cycles are defined based on the yield displacement of the longitudinal reinforcements. The yield displacement was calculated using the deformation components including flexural deformation, bar slip, and shear deformation. Their contributions in the yield displacement experienced by a column specimen can be represented as $\Delta_y = \Delta_{flexural} + \Delta_{slip} + \Delta_{shear}$, and each of these deformations can be calculated based on empirical equations (Flores, 2004). The highest contribution corresponds to the flexural deformation that emerges when a moment load is generated in

the column, and a lateral displacement occurs at the end of the column. For a column that is considered to be fixed at both ends against rotation, a linear variation in curvature over the column height is assumed, and the flexural displacement contribution in the yield displacement can be calculated as $\Delta_{flexural} = \frac{L^2 \Phi_y}{6}$, where L and Φ_y are the column height and the curvature at the yield initiation point of the longitudinal reinforcements. The contribution of the shear and slip deformation are less than the flexural deformation; however, they will be counted in this study. The contribution of these deformations can be calculated using $\Delta_{shear} = \frac{2M_y}{GA_V}$ and $\Delta_{slip} = \frac{Ld_B F_{YL} \Phi_y}{8u}$, where M_y and A_V are the moment at first yield of the longitudinal reinforcement and the shear area of the column section, d_B and F_{YL} are the diameter and the yield stress of the longitudinal reinforcements, and $u = 6\sqrt{f_c'}$ is the bond stress between the longitudinal reinforcement and the footing. The calculation of the total yield displacement requires estimations for Φ_y and M_y using the moment-curvature relationships. This relationship is determined based on an OpenSees standard section analysis that relies on the assumption that plane sections remain plane. Based on the calculated yield displacements, the cyclic levels are set to be $\Delta = \pm 0.257, \pm 0.514, \pm 0.771, \pm 1.03, \pm 1.54, \pm 2.06, \pm 2.57, \pm 3.6, \pm 4.6, \pm 5.65, \pm 6.68, \pm 7.71$ (in). As shown in Figure 3.12, the cyclic behavior pattern across different cross-section shapes is similar to the observations from the monotonic pushover analysis (Figure 3.11.b). However, the strength degradation can be analyzed in the cyclic testing. This degradation happens at earlier levels in the flared columns, while it only occurs at the latest cycles for the other column shapes. The circular column shows a smooth degradation that increases during the last few cycles, and the rectangular and oblong ones

display a drastic decrease in the strength in the last cycle. In the following section, the influence of various column shapes on the seismic performance of the bridges is evaluated.

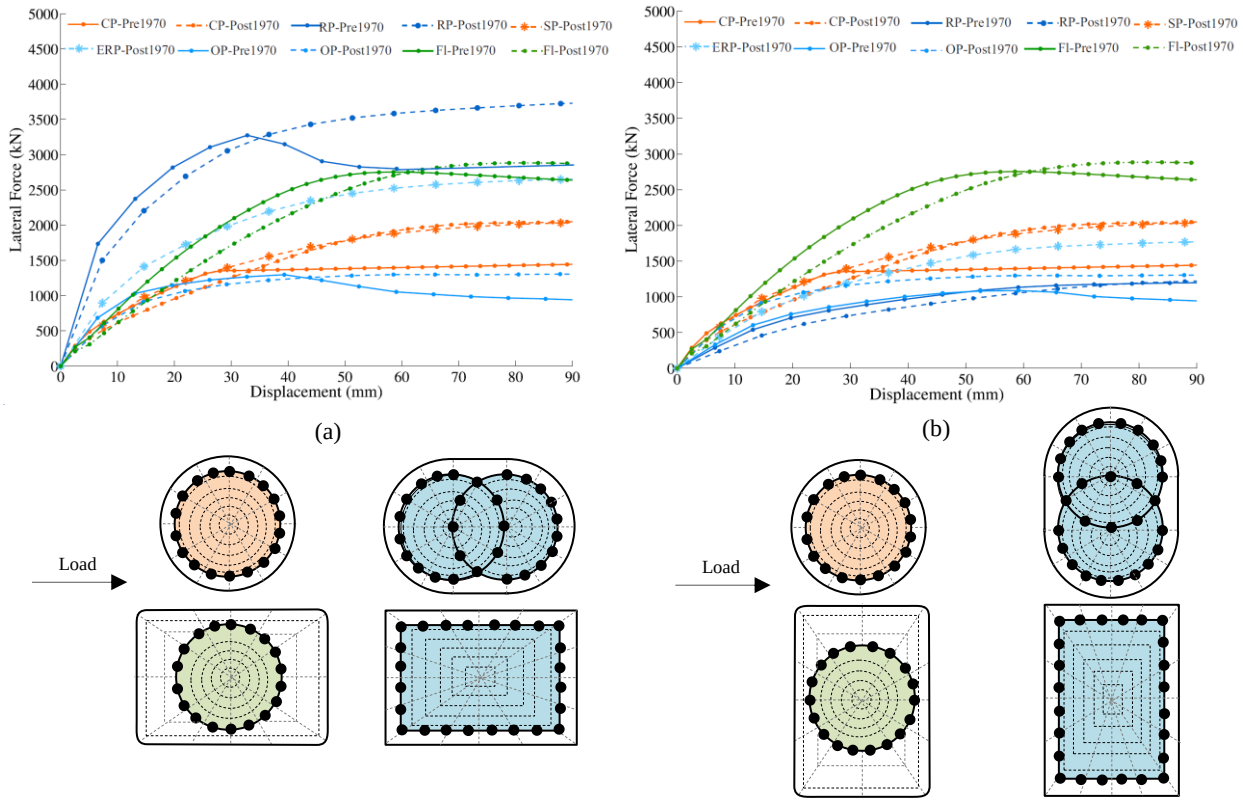

Figure 3.11: Comparison of monotonic pushover analysis of the columns in (a) longitudinal and (b) transverse directions

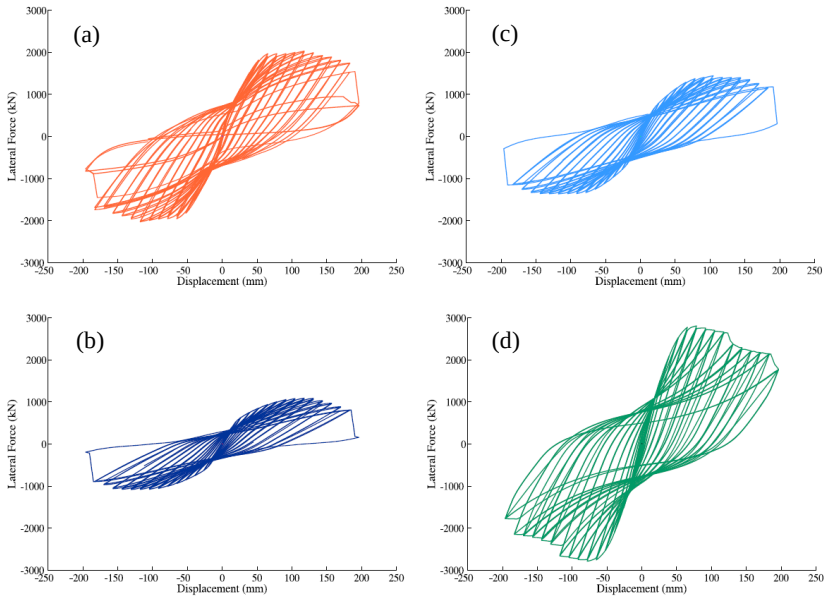

Figure 3.12: Comparison of cyclic pushover analysis for (a) CP, (b) RP, (c) OP, and (d) Fl, in the transverse direction

Seismic Analysis

A hypothetical box-girder bridge with the structural properties of California bridges was modeled in three-dimensions in OpenSees. The bridge layout and the backbone curves used in the components modeling are presented in Figure 3.13. A detailed plan review of the existing bridges in California was conducted to extract the probability distributions of the required modeling parameters (Table 3.4). Similar to the analysis provided in the previous section, the four cases of column shapes (CP, RP, OP, and Fl) were considered in the bridge study. Additionally, two separate sets of analysis were performed in order to account for the variations in reinforcement ratios and column heights in design codes written before and after 1970. As shown in Figure 3.13, each analysis needed to be conducted twice for the two types of rigid and seat abutments. Table 3.3 provides a description of bridge class varieties that are considered in this study.

Table 3.3: Description of nomenclature for bridge classes considered in this study

Nomenclature	Classification		
	Abutment	Design era	Number of columns per bent
DBSC	Rigid diaphragm (D)	Pre-1970 (B)	Single (SC)
SBSC	Seat Abutment (S)	Pre-1970 (B)	Single (SC)
DBMC	Rigid diaphragm (D)	Pre-1970 (B)	Multiple (≥ 2) (MC)
SBMC	Seat Abutment (S)	Pre-1970 (B)	Multiple (≥ 2) (MC)
DASC	Rigid diaphragm (D)	Post-1970 (A)	Single (SC)
SASC	Seat Abutment (S)	Post-1970 (A)	Single (SC)
DAMC	Rigid diaphragm (D)	Post-1970 (A)	Multiple (≥ 2) (MC)
SAMC	Seat Abutment (S)	Post-1970 (A)	Multiple (≥ 2) (MC)

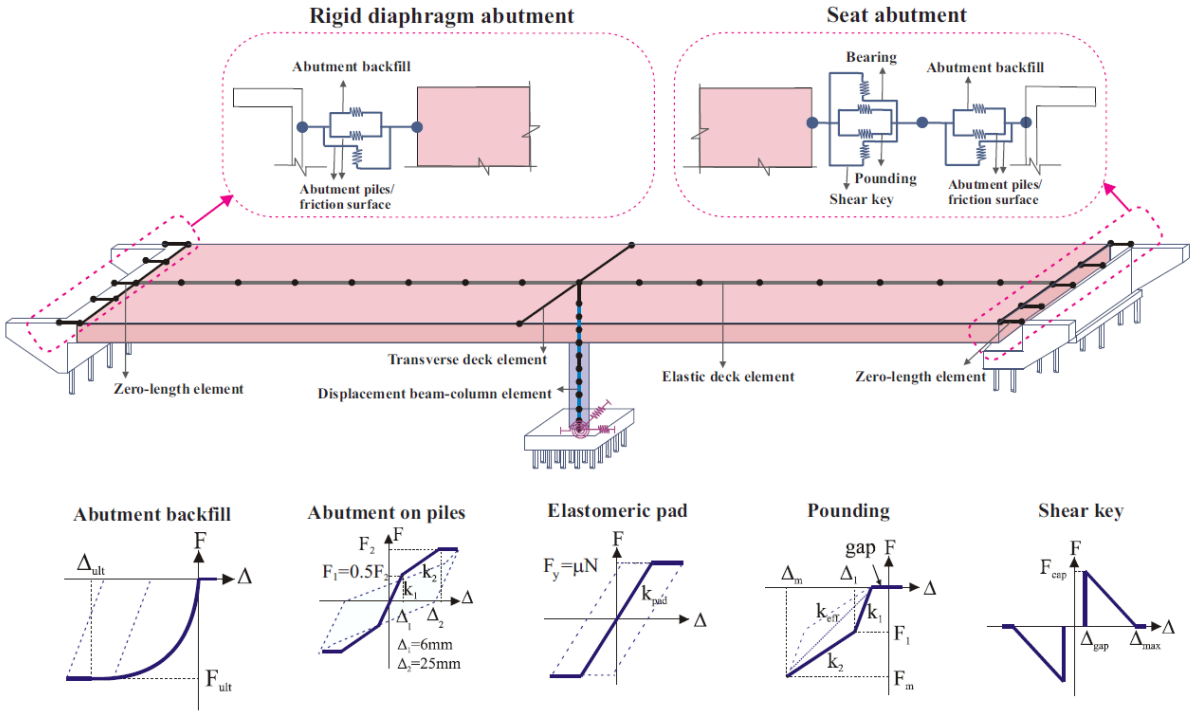

Figure 3.13: Numerical modeling of various bridge components

Nonlinear time history analysis (NLTHA) was performed on the bridge model using Baker's suite of 160 ground motions (Baker, et al., 2011). These excitations have longitudinal and orthogonal components, and are randomly oriented to the longitudinal and transverse directions of the bridge models. The results of this analysis provided the peak seismic response for each of the bridge components. The peak responses were used

to produce probabilistic seismic demand model (PSDM). A probabilistic seismic demand model (PSDM) is a regression model expressing the relationship between seismic demand (D) and ground motion intensity measure (IM) (Cornell, et al., 2002). Based on this regression model, the median value of the seismic demand (S_D) can be estimated for a specific intensity measure as

$$S_D = a.IM^b \quad , \tag{1}$$

where a and b are the regression coefficients that are obtained by performing a regression analysis on $D - IM$ pairs. Dispersion ($\beta_{D|IM}$) is calculated based on

$$\beta_{D|IM} = \sqrt{\frac{\sum_{i=1}^{N}(ln(D_i) - ln(S_D))^2}{N-2}} \quad , \ (N = \text{total number of data points}). \tag{2}$$

In order to generate fragility curves for the bridge system, the PSDM should be developed for each of the bridge components (e.g., columns, abutments, foundations). The bridge column vulnerability has a major contribution to the overall bridge system fragility. As a result, column displacement ductility, defined as the ratio of the ultimate displacement to the yield displacement, is assessed in the following. Figure 3.14 and Figure 3.15 depict the two-parameter lognormal probability distribution of the column ductility based on the ground motion intensity measure. For this study, Sa-1.0s (i.e., the spectral acceleration at 1.0 second) was chosen since it is the optimal intensity measure for box-girder bridges (Ramanathan, 2012).

Among the developed PSDMs, those of the oblong cross-sections have noticeably different slopes. More specifically, in all bridge types (Figure 3.14 and Figure 3.15), the slopes of the oblong column models are the lowest between the considered column

shapes. In contrast, the flared-shaped columns have the highest slopes of the PSDMs in almost all cases. No specific pattern is observed between circular and rectangular column shapes. These findings are not restricted to a particular abutment type, number of columns per bent, or the era when the bridge was designed.

Table 3.4: Uncertainty distribution considered in the bridge models

Parameter	Distribution Type	μ	σ
Concrete compressive strength (MPa)	Normal	29.03	3.59
Reinforcing steel yield strength (MPa)	Lognormal	465.0	37.30
Span length (mm)			
Two-span	Lognormal	31775	8738
Deck width (mm)			
Single column bent	Lognormal	9780	1980
Multi-column bent	Lognormal	11970	2418
Abutment backwall height (mm)			
Diaphragm abutments	Lognormal	3234	488
Seat-type abutments	Lognormal	2186	441
Abutments on piles - Lateral capacity/deck width (N/mm)			
Diaphragm abutment	Lognormal	1120	404
Seat-type abutment	Lognormal	1498	540
Elastomeric bearing pad			
Stiffness per deck width (N/mm/m)	Lognormal	908	327
Coefficient of friction for bearing pad	Normal	0.30	0.10
Gap (mm)			
Longitudinal (btw. deck & abutment wall)	Lognormal	23.5	12.5
Transverse (btw. deck and shear key)	Lognormal	12.8	2.58
Mass factor	Uniform	1.25	0.007
Damping	Normal	0.045	0.0125
Acceleration for shear key capacity (*g*)	Lognormal	1.00	0.20
Piles translational stiffness (N/mm)			
1% long. rebar	Normal	297716	140101
3% long. rebar	Normal	245178	105076
Piles rotational stiffness (N-m/rad)			
1% long. rebar	Normal	4.5×10^9	1.1×10^9
3% long. rebar	Normal	6.8×10^9	1.1×10^9

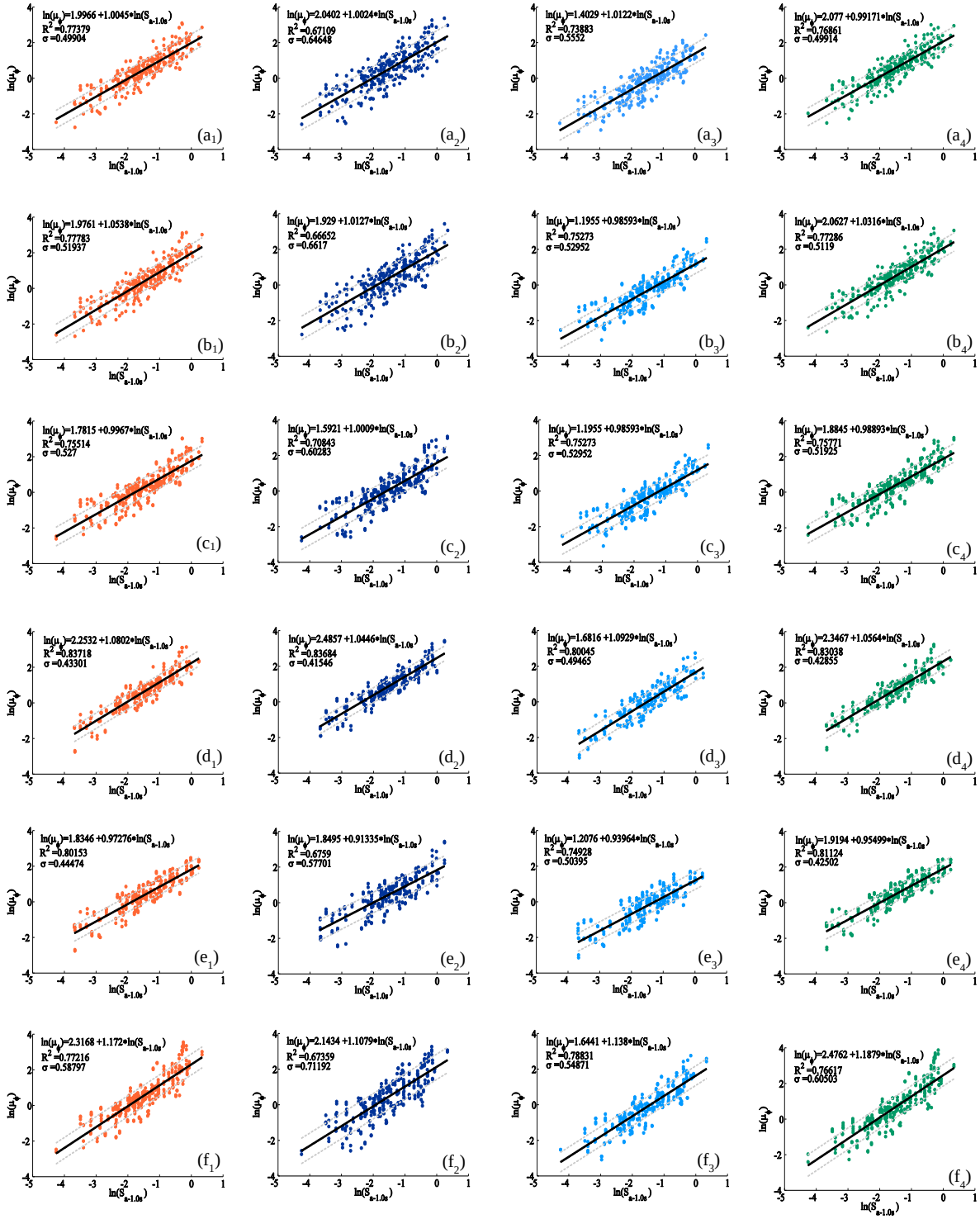

Figure 3.14: Probabilistic seismic demand models for column displacement ductility of bridges: (a) DBSC, (b) SBSC, (c) DBMC, (d) SBMC, (e) DASC, (f) SASC, ● 1-circular, ● 1-rectangular, ● 1-oblong, ● 1-flared shape

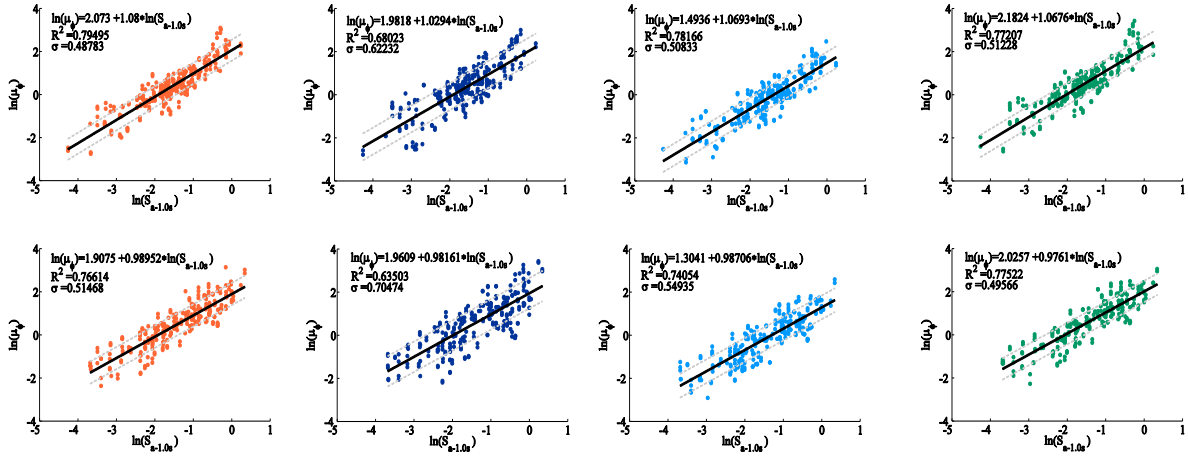

Figure 3.15: Probabilistic seismic demand models for column displacement ductility of bridges: (g) DAMC, (h) SAMC, ● 1-circular, ● 1-rectangular, ● 1-oblong, ● 1-flared shape

The developed PSDMs were used to establish the fragility curves. This research study also aims to investigate the effect of column shapes on the fragility analysis of a bridge, and follows the work of Nielson (2005) and Ramanathan (2012) to evaluate the fragility of bridge components at four different damage states: slight, moderate, extensive, and complete. At a chosen intensity measure, the probability that the seismic demand (D) of a component exceeds its capacity (C) can be assessed by fragility curves. A lognormal distribution of demand and capacity is assumed, and the probability of reaching or exceeding a specific damage state for a particular component is then estimated with the use of the probability equation

$$P[D > C|IM] = \Phi\left[\frac{ln(S_D/S_C)}{\sqrt{\beta_{D|IM}^2+\beta_C^2}}\right] , \qquad (12)$$

where, S_C is the median estimate of the capacity, β_C is the dispersion of the capacity, and $\Phi(\bullet)$ is the standard normal cumulative distribution function.

The limit states used for the displacement ductility are presented in Chapter 7. The other capacity values used in this study were similar to those used by Ramanathan

(2012). Figure 3.16 and Figure 3.17 demonstrate the fragility curves of bridge columns when different types of column shapes are used in the models. Each plot depicts the column vulnerability at slight, moderate, extensive, and collapse damage state. The plots that are placed in the same row correspond to an identical bridge type with the four considered column shapes, CP, RP, OP, and Fl. Hence, each column in the figures shows the fragility curves for various bridge types (e.g., different abutment types) but similar column shapes.

As is shown in Figure 3.16 and Figure 3.17, the column seismic vulnerability of seat-type abutment bridges is generally higher than that of integral-type bridges. Comparing the fragilities of each row reveals that the oblong column shapes are less fragile than any other column shape at four damage states. The results show that when oblong columns are used, the seismic vulnerability of the column decreases in bridges with either seat- or rigid-type abutments. In other words, oblong bridge columns are the least vulnerable ones due to the more effectively confined area of the cross-section. Although flared columns represent a higher strength compared to prismatic ones in the pushover analysis, they are more prone to damage in the time history analysis. In particular, the fragility curves of bridge columns indicate a higher probability of damage for bridges with flared columns than for bridges with straight columns. This is the result of the inconsistent cross-section along the column height, and, more specifically, the elongation of the cover concrete area.

Another finding is that at low and medium damage levels for bridges with multiple columns per bent, there is not a noticeable difference observed between the performances of columns with various shapes. However, these performances become

more distinctive at the higher levels. This is because the column shape plays a more significant role in providing the column's stiffness at larger displacement capacities and, accordingly, at larger deformations. More specifically, the column shape affects the reinforcing details, which define the column ductility demands and the seismic resistance.

The failure probabilities of bridge columns are presented in Table 3.5. Since circular column shapes are used in the majority of bridges (approximately 53% of California's box-girder bridges), the likelihood for damage for other column shapes is compared to the circular ones. The likelihood can be compared at any level of ground motion intensity; however, as an example, $0.5g$ is selected in the following. This comparison is provided as the absolute relative error ε in Table 3.5 and Figure 3.18. Comparing cases 1 to 4, at a spectral acceleration of $0.5g$, probabilities of moderate damage to the bridge column with circular, rectangular, oblong, and flared shapes are 81.8%, 73.3%, 57.8%, and 84.9%, respectively. For the same bridge type and at the same level of ground motion intensity, there is a 65.6%, 57.9%, 41.5%, and 69.3% possibility of observing extensive damage in bridge columns with circular, rectangular, oblong, and flared shapes, respectively. At the slight, moderate, extensive, and collapse damage levels, the maximum variations (relative errors), which are 25.02%, 30.78%, 38.42%, and 62.38% occur with oblong columns.

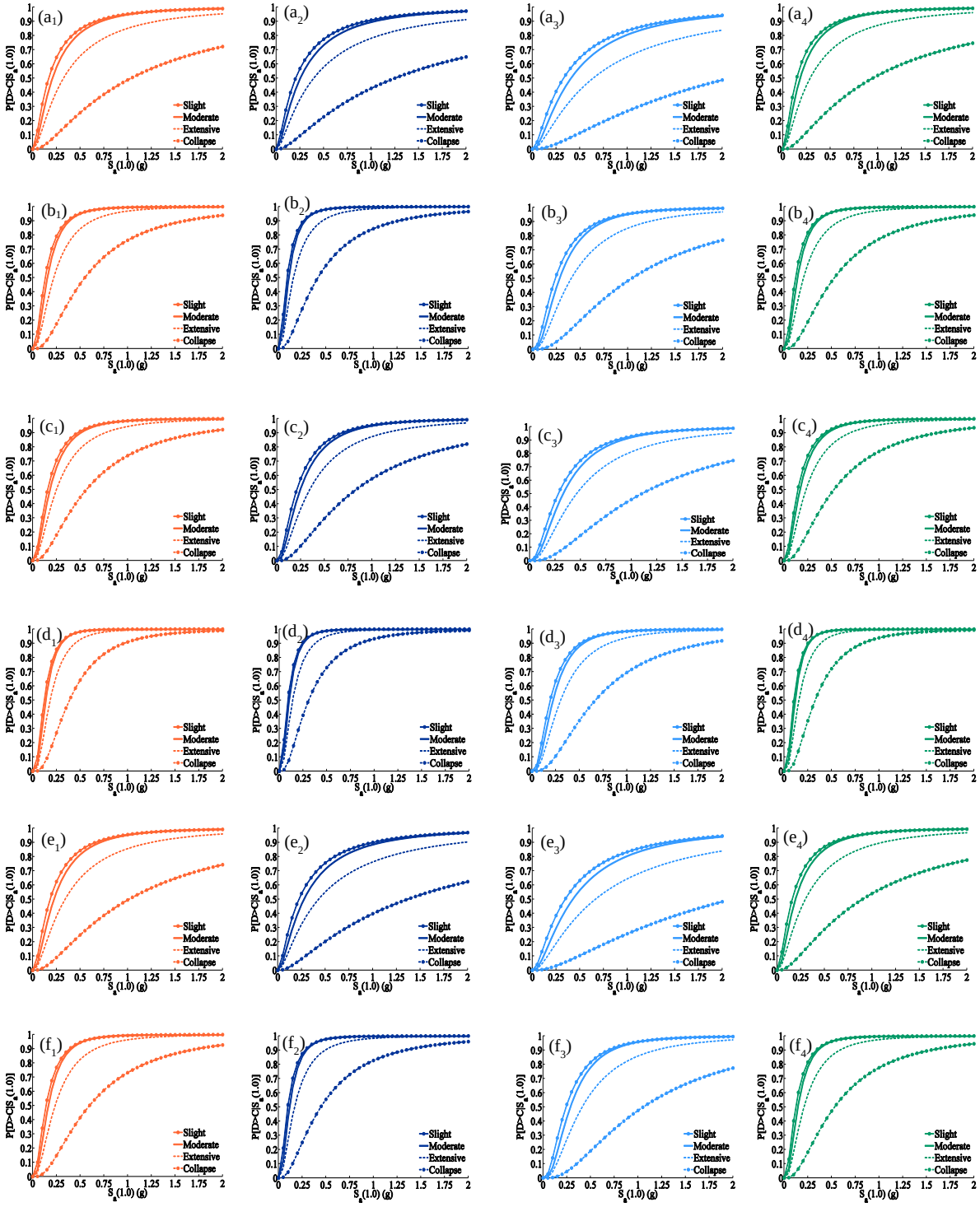

Figure 3.16: Fragility curves of the columns for bridges: (a) DBSC, (b) SBSC, (c) DBMC, (d) SBMC, (e) DASC, (f) SASC, ● 1-circular, ● 1-rectangular, ● 1-oblong, ● 1-flared shape

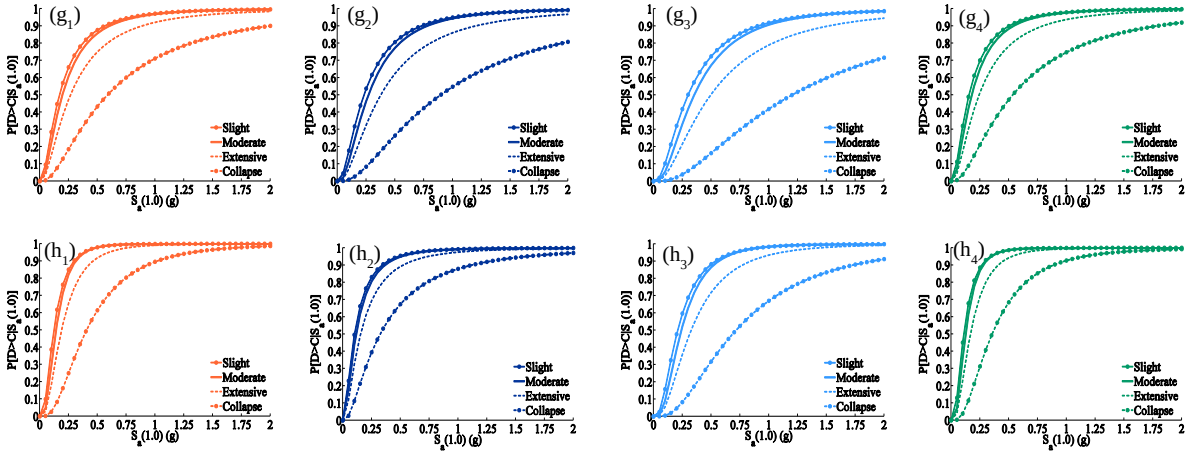

Figure 3.17: Fragility curves of the columns for bridges: (g) DAMC, (h) SAMC, ● 1-circular, ● 1-rectangular, ● 1-oblong, ● 1-flared shape

Figure A. 1 in Appendix A demonstrates the bridge system and components fragility curves. Apparently, in all cases, the most vulnerable components significantly affect the seismic fragility of the bridge system. In this study, it is observed that for the considered bridge types and column shapes, columns dominate the fragility of the whole bridge, and hence similar trends are observed in analyzing the system fragility curves as those of the column curves. However, the bridge system is more fragile than any of its components. The median and dispersion of the fragility functions for the four damage states are presented in table A.2. The first column of the table shows the bridge classes that are consistent with the ones assigned to the bridges in Table 3.5 and Table 3.3.

According to the generated fragility curves for bridges with integral abutment type, bridge system fragilities can be sorted based on their column shapes as oblong, rectangular, circular, and flared, with oblong columns showing the lowest fragility. Similarly, the ranking for bridges with seat-type abutments lists as oblong, circular, rectangular, and flared columns. However, in both types of abutments, the difference

between the system fragilities of bridges with oblong columns is more noticeable than the other considered shapes. This difference is enhanced at higher levels of damage. A closer look at the bridge component and system fragility curves shows that the abutment seat has a lower fragility probability for bridges with oblong columns than for any of the other considered column shapes. A similar behavior is observed for the displacement of the elastomeric bearing.

Table 3.5: Damage probabilities of the bridge columns at 0.5 g

Case	Type	Damage State							
		Slight		Moderate		Extensive		Collapse	
		P	ε (%)	P	ε (%)	P	ε (%)	P	ε (%)
DBSC	CP	0.845	-	0.818	-	0.656	-	0.257	-
DBSC	RP	0.774	8.46	0.733	10.46	0.579	11.82	0.227	11.49
DBSC	OP	0.644	23.89	0.578	29.32	0.415	36.69	0.114	55.59
DBSC	Fl	0.871	3.00	0.849	3.81	0.693	5.66	0.286	11.16
SBSC	CP	0.953	-	0.950	-	0.844	-	0.456	-
SBSC	RP	0.980	2.88	0.981	3.29	0.915	8.48	0.585	28.42
SBSC	OP	0.810	15.00	0.774	18.52	0.598	29.17	0.204	55.11
SBSC	Fl	0.960	0.77	0.960	1.01	0.860	1.96	0.473	3.78
DBMC	CP	0.910	-	0.897	-	0.788	-	0.445	-
DBMC	RP	0.827	9.12	0.797	11.18	0.655	16.80	0.297	33.26
DBMC	OP	0.748	17.85	0.703	21.72	0.538	31.71	0.189	57.58
DBMC	Fl	0.927	1.83	0.918	2.26	0.816	3.61	0.479	7.67
SBMC	CP	0.981	-	0.982	-	0.927	-	0.641	-
SBMC	RP	0.988	0.66	0.989	0.65	0.951	2.62	0.730	13.84
SBMC	OP	0.895	8.80	0.879	10.51	0.743	19.79	0.356	44.44
SBMC	Fl	0.989	0.74	0.990	0.76	0.952	2.68	0.722	12.58
DASC	CP	0.843	-	0.814	-	0.648	-	0.249	-
DASC	RP	0.755	10.38	0.710	12.77	0.551	14.92	0.203	18.49
DASC	OP	0.632	25.02	0.564	30.78	0.399	38.42	0.103	58.44
DASC	Fl	0.870	3.24	0.850	4.36	0.693	6.92	0.288	15.89
SASC	CP	0.945	-	0.942	-	0.825	-	0.415	-
SASC	RP	0.977	3.37	0.978	3.81	0.904	9.60	0.553	33.28
SASC	OP	0.814	13.88	0.778	17.43	0.593	28.13	0.190	54.18
SASC	Fl	0.961	1.74	0.961	1.97	0.860	4.34	0.470	13.33
DAMC	CP	0.876	-	0.857	-	0.749	-	0.433	-
DAMC	RP	0.806	7.97	0.773	9.83	0.624	16.77	0.264	38.98
DAMC	OP	0.724	17.36	0.672	21.61	0.504	32.77	0.163	62.38
DAMC	Fl	0.899	2.63	0.883	3.07	0.783	4.49	0.472	9.17
SAMC	CP	0.979	-	0.980	-	0.918	-	0.614	-
SAMC	RP	0.954	2.56	0.949	3.13	0.892	2.90	0.673	9.62
SAMC	OP	0.883	9.86	0.865	11.71	0.718	21.77	0.318	48.22
SAMC	Fl	0.986	0.72	0.987	0.79	0.942	2.60	0.684	11.36

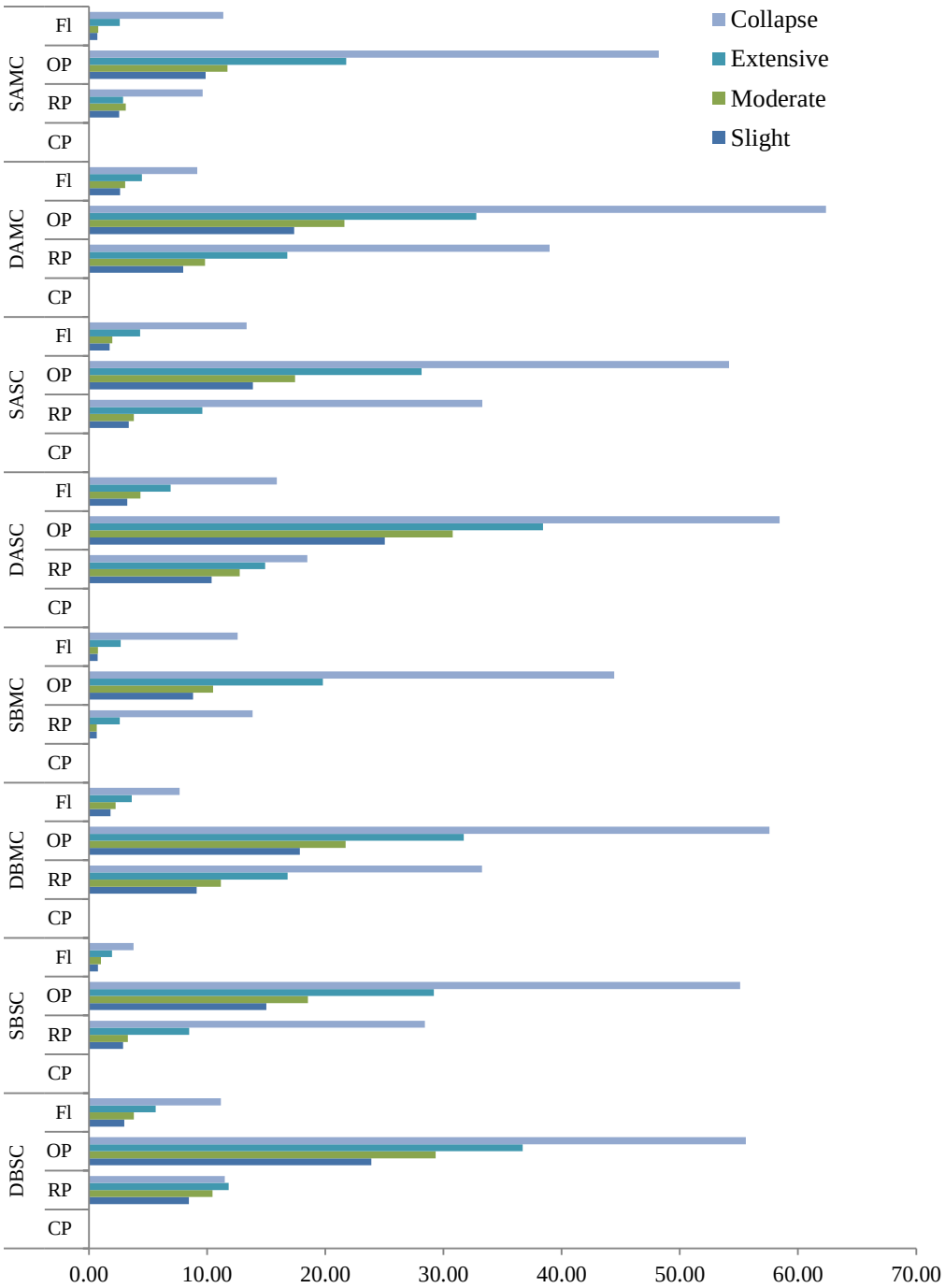

Figure 3.18: Relative errors for damage probabilities of the bridge columns at 0.5 g

Assessment of the generated curves indicates the impact of column shapes on the bridge fragilities. Among the considered column shapes, oblong and flared columns indicate the lowest and highest vulnerability, respectively. This is more noticeable at

higher levels of damage. Although bridges with seat abutments represent higher probability in the fragility analysis of the bridge column and system, similar trends are observed for the impact of column shapes on bridges with rigid and seat abutment types. Additionally, the findings are independent of the number of bridge columns per bent.

Generally, analytical modeling of columns, as the most susceptible component of a bridge under earthquake excitation, is challenging. Capturing and considering columns' responses is an essential part of the numerical analysis of a bridge. In this study, certain strategies were developed to consider failure modes of a column, and they were validated by the experimental results. The modes of column failure considered in this study, and the numerical approaches used to capture them, are explained in Appendix A.

For modeling skewed bridges, the columns are rotated in the direction of the skewed girders to consider the corresponding skew angle of the bridge (Figure 3.19).

Figure 3.19: Plan view of the bridge deck with the orientation of the columns in (a) straight bridges versus (b) skewed bridges

To date, there exists very limited research regarding bridges with unbalanced frames and tall column bents. Likewise, to the best of the author's knowledge, there are no data sets from experiments on these classes of bridges. Therefore, the only change that is considered in the present study for modeling bridges with unbalanced frames and tall column bents is the variation of the column heights. In this regard, four sources of bridge plans, listed as stream crossings, ramps, connectors, and viaducts were collected from BIRIS and were reviewed in detail to extract column height values. In order to have a

comprehensive database, approximately 600 plans were reviewed, and the results are analyzed as follows. The overall goal of this step is to set up a realistic sample of unbalanced or tall bridge profiles, which will be used to create synthetic unbalanced and tall bridge realizations to be utilized in analytical modeling of bridges. A brief summary of the implemented approach is presented in this section, and supplementary information can be found in Appendix B.

Global model for creating synthetic realizations

- **Common basis for column height normalization:** The average column heights (H_{ave}) of unbalanced or tall bridges are normalized by the average column heights (H_{base}) determined for the corresponding base models (i.e., representative regular bridge). Normalized-column-height (H_{ave} / H_{base}, Figure 3.20) values are then assigned to a variable called average bridge-height ratio. Those ratios meeting the column heights criteria to be considered as tall bridges (i.e., ratios higher than 1.5) are used for building the models for this class of bridges. Appropriate distributions of the average bridge-height ratios are identified (Figure 3.21) and implemented in the modeling of tall bridges.

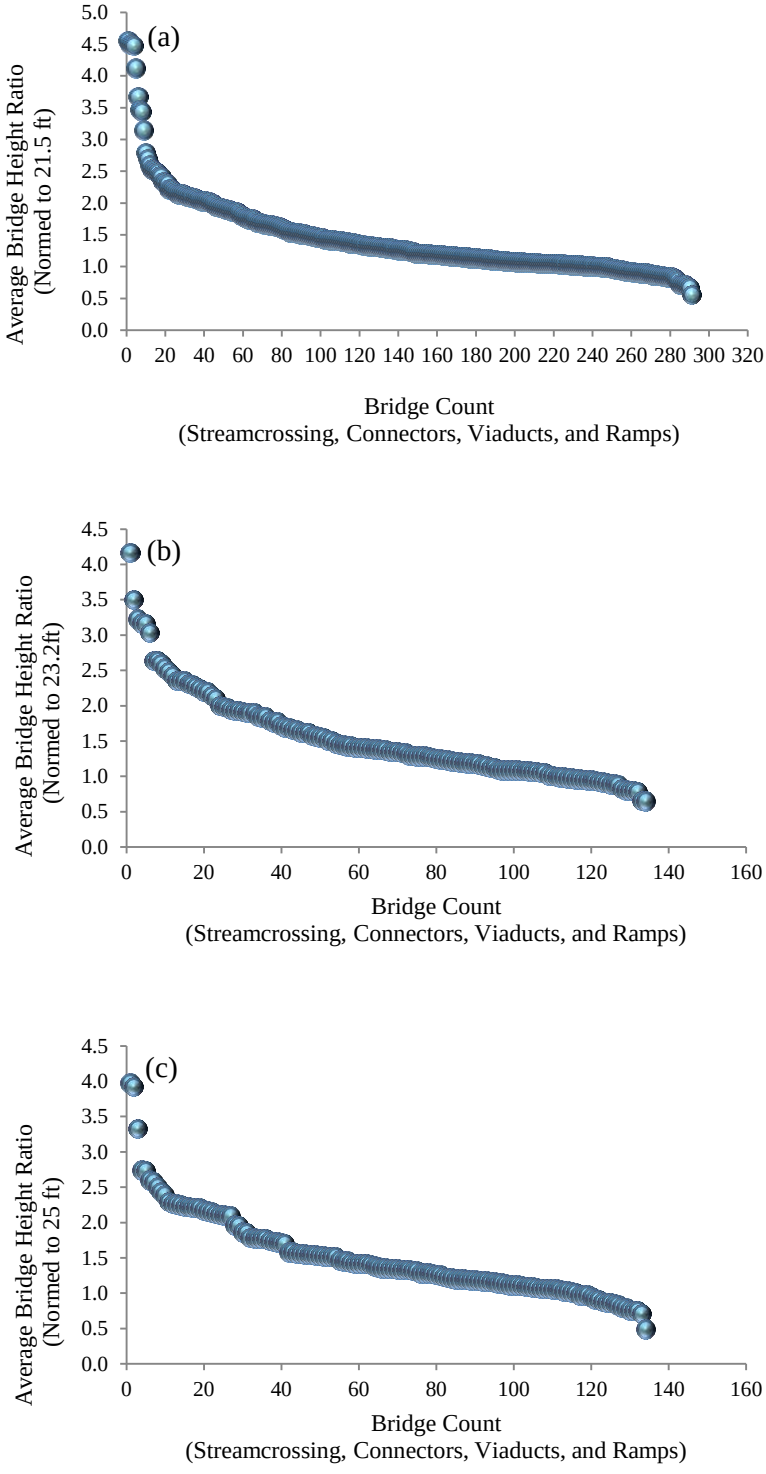

Figure 3.20: Average bridge column height ratios for bridges designed in (a) pre-1971, (b) 1971-1990, and (c) post-1990

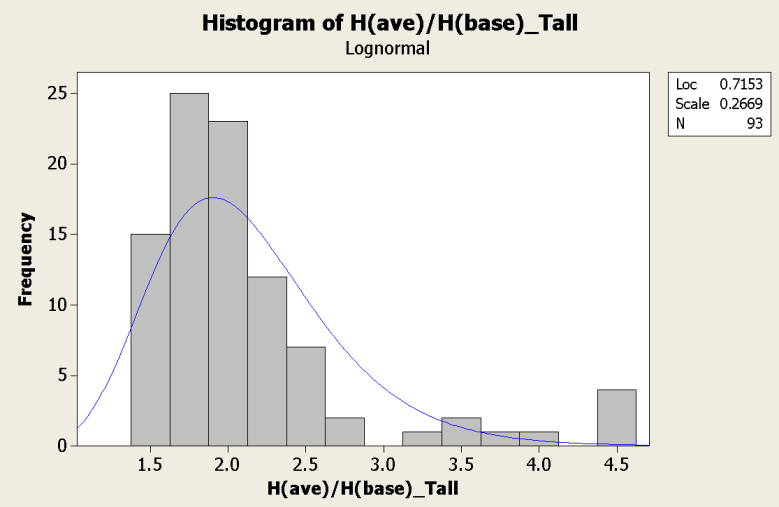

Figure 3.21: Distribution of average bridge column height ratios (for pre-1971 era)

❖ **Combined ratio model:** A single column-height-ratio is developed by normalizing the height of all of the columns in a bridge (H_i ; $i = 1,...,n$; n : number of columns in a bridge) to the bridge-average-height (H_{ave}). This yields ratios (H_i / H_{ave}) for each bridge that are centered on 1, but values extend both above and below the center (Figure 3.22). Based on the Caltrans Seismic Design Criteria (Caltrans, 2006), a bridge is defined as having a frame with unbalanced stiffness when different bents within the frame have a stiffness ratio of less than 75%. This criterion can be converted to column height ratios (H_i / H_{ave}) higher than 1.05 or lower than 0.95. Thus, the respective ratios are implemented in the modeling of bridges with unbalanced frames.

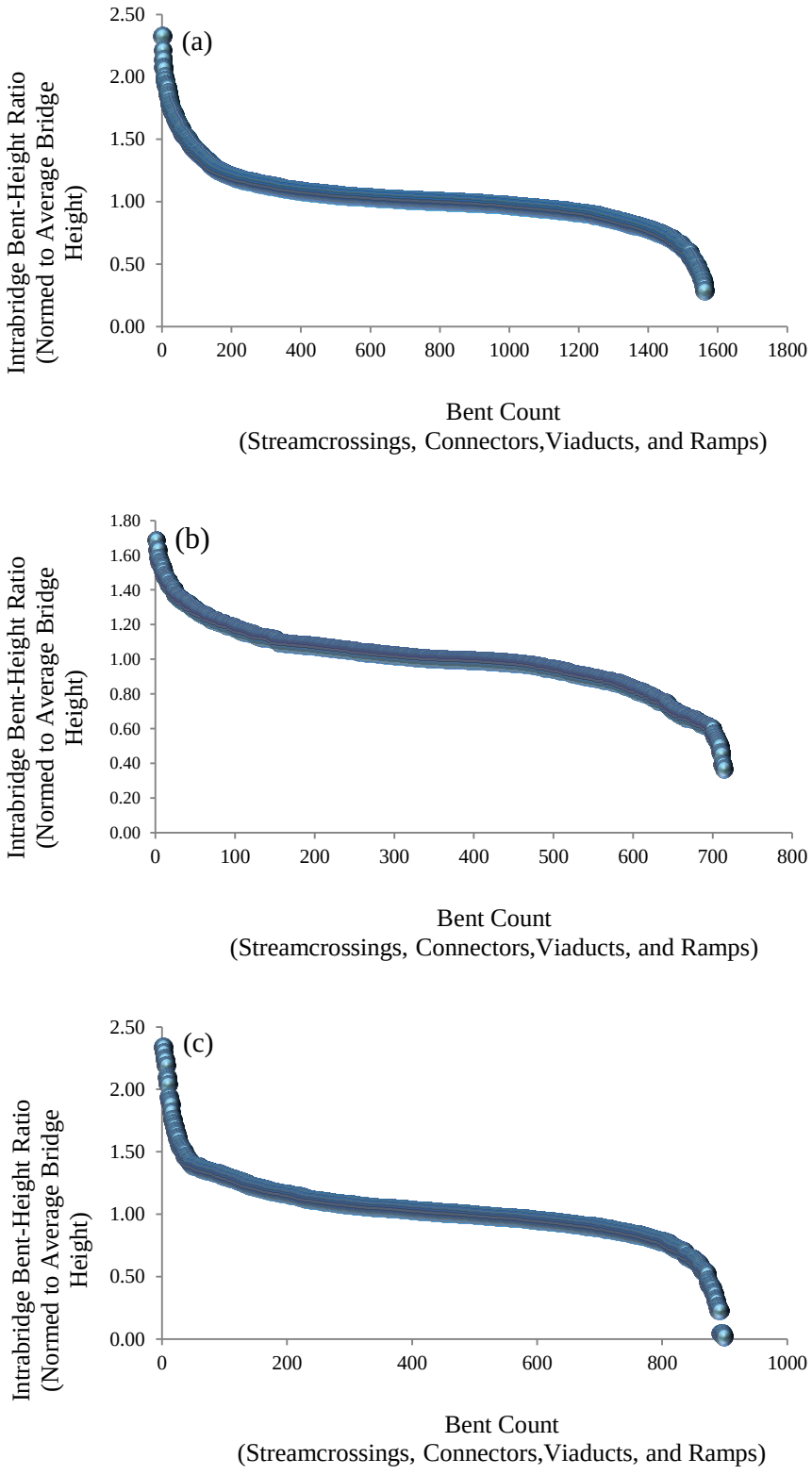

Figure 3.22: Intra-bridge bent-height ratio for bridges designed (a) pre-1971, (b) 1971-1990, and (c) post-1990

Assignment of the column height ratios:

The process of generating unbalanced bridges is illustrated in the following two examples.

Example 1: A slightly unbalanced three-span bridge (Figure 3.23)

- Column height ratio (0.91 < Ratio < 0.95) will be selected randomly to generate H_1.
- Column height ratio (1.05 < Ratio < 1.1) will be selected randomly to generate H_2.
- The stiffness ratios of the two columns are checked; bridges with ratios out of the slightly unbalanced range (55% < stiffness ratio < 75%) are removed. Random selection will be repeated until all generated column heights, H_1 and H_2, create a stiffness ratio between that falls in the 55-75% range.

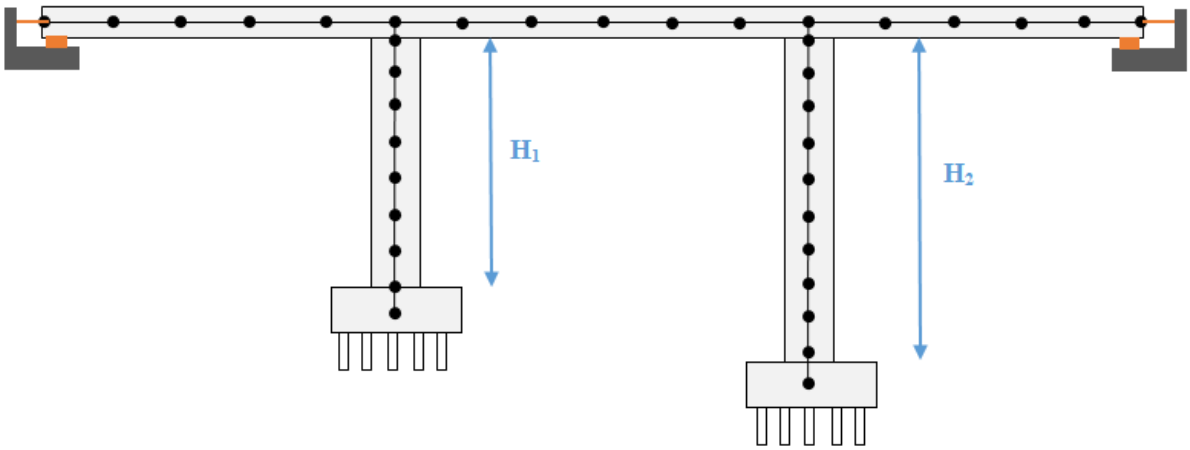

Figure 3.23: Layout of a slightly unbalanced three-span bridge

Example 2: A slightly unbalanced five-span bridge (Figure 3.24)

- Column height ratios (0.91 < Ratio < 0.95) and (1.05 < Ratio < 1.1) will be selected randomly to generate H_1, H_2, H_3, and H_4.
- The stiffness ratios of the adjacent columns will be checked to see if at least one of them satisfies the unbalanced criteria (e.g., 55% < stiffness ratio < 75%). If all of the values fall beyond the considered range (e.g., slightly unbalanced range, 55% < stiffness ratio < 75%), random selection will be repeated until the generated column heights create an unbalanced frame.

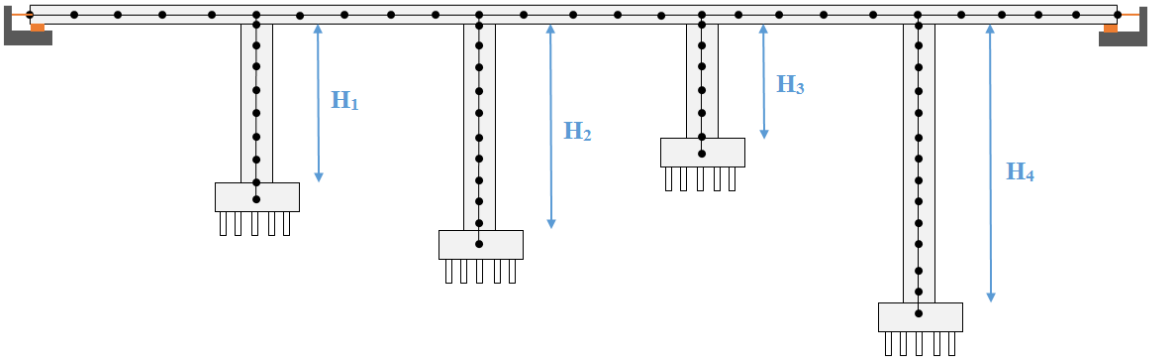

Figure 3.24: Layout of a slightly unbalanced five-span bridge

3.3.2 Abutment

Abutments are classified as either seat or rigid diaphragm types. A seat abutment allows the superstructure to move independently from the abutment, while a rigid diaphragm abutment is integrally connected to the superstructure. The statistical distribution of the abutment types is shown in Figure 3.25. It should be noted that the

rigid diaphragm abutment was commonly used in older bridges, and the seat abutment is typically used in more recently designed bridges.

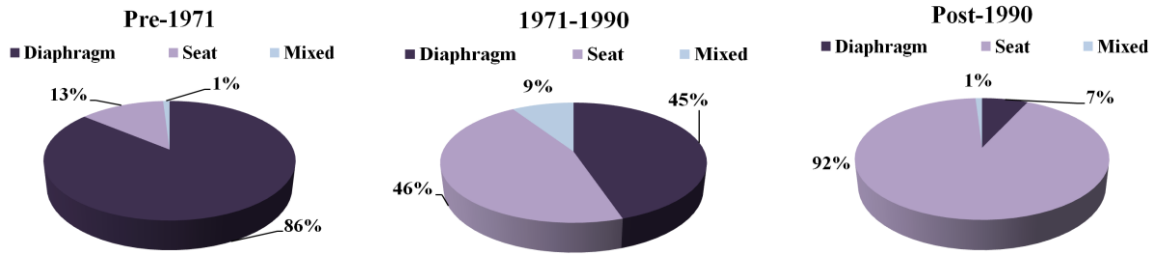

(a) (b) (c)

Figure 3.25: Statistical distribution of abutment types for bridges designed (a) pre-1971, (b) 1971-1990, and (c) post-1990

Diaphragm abutments are cast monolithic with the superstructure of the bridge. Since this type of abutment immediately engages the backfill soil during seismic action, it provides a great source of energy dissipation and reduces the likelihood of the unseating of the bridge deck. Since rigid diaphragm abutments are stiffer than the adjacent column bents, they absorb a larger portion of the imposed seismic force (Priestley, et al., 1996). The rigid diaphragm abutments are classified into the following four main configurations, as shown in Figure 3.26:

- Diaphragm abutments on piles
- Diaphragm abutments on spread footings
- Diaphragm abutments on ‘skirted’ piles
- Strutted diaphragms

The statistical distribution of the configurations is presented in Figure 3.27, which shows the majority of bridges in California have abutments resting on piles.

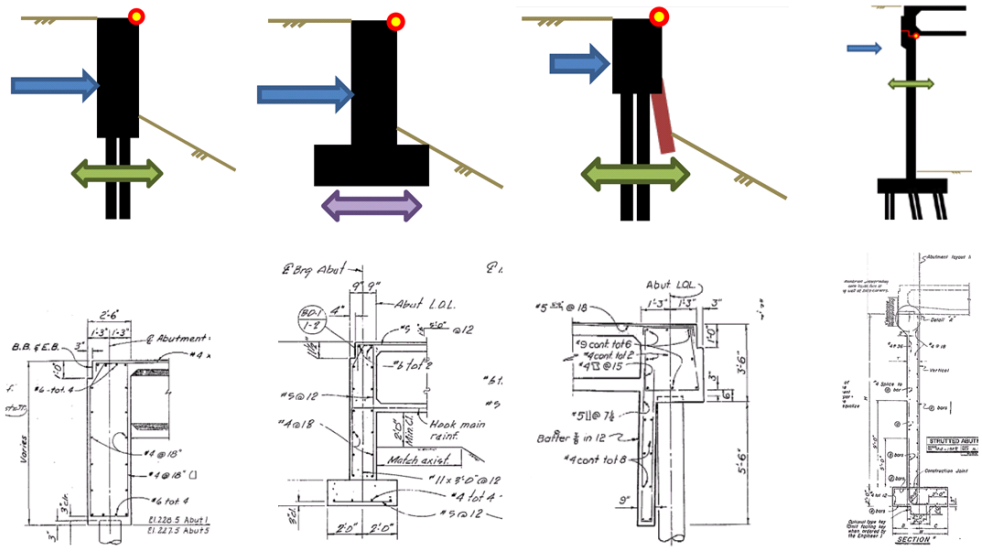

(a) (b) (c) (d)

Figure 3.26: Configurations of rigid diaphragm abutment; (a) resting on piles, b) resting on skirted piles, c) resting on spread footing, and d) strutted diaphragms (source: (Caltrans, 2013-2016))

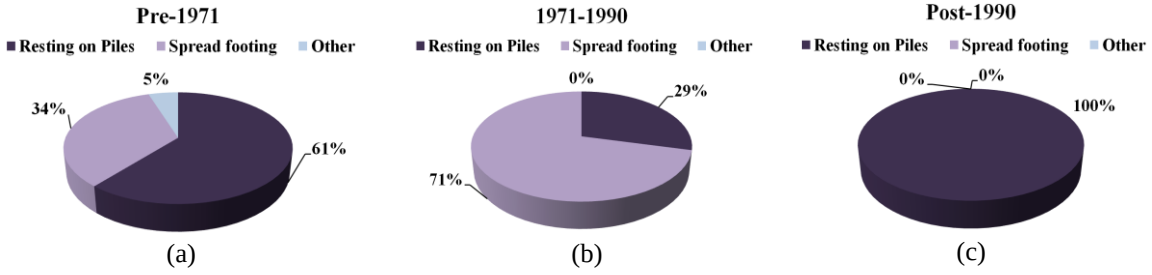

(a) (b) (c)

Figure 3.27: Statistical distribution of rigid diaphragm abutment for bridges designed (a) pre-1971, (b) 1971-1990, and (c) post-1990

Seat abutments provide a bearing support to the superstructure that is restrained by the abutment's backwall in the longitudinal direction and by the shear key in the transverse direction. In the case of seat abutments on piles, transverse resistance is also provided by the piles. The stiffness and resistance to seismic forces increase when the deck is in contact with the abutment's backwall in the longitudinal direction. However, as the superstructure moves away from the abutment, resistance depends primarily on the bearing pads and can cause unseating. The backwall of seat-type abutments is typically

designed to fail under passive response, and before damaging forces are transmitted to the lower portion of the abutment. The seat abutment is classified into the following three main configurations, as shown in Figure 3.28:

- Seat abutments on piles
- Seat abutments on spread footings
- Cantilever-type abutments (either on piles or on spread footings)

The statistical distribution of the configurations is presented in Figure 3.29.

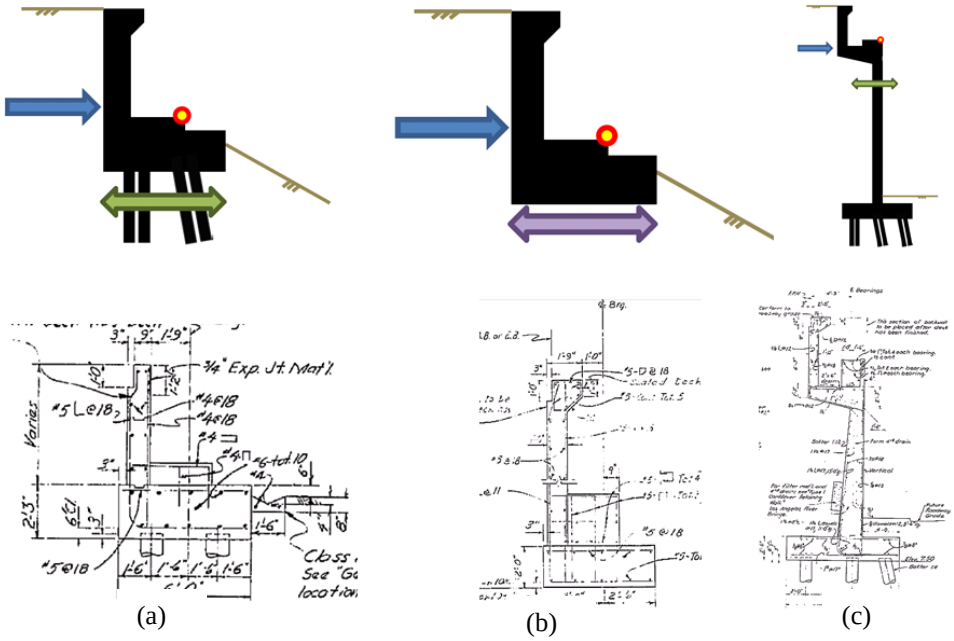

Figure 3.28: Configurations of seat abutment; (a) resting on piles, b) resting on spread footing, and c) cantilever-type (source: (Caltrans, 2013-2016))

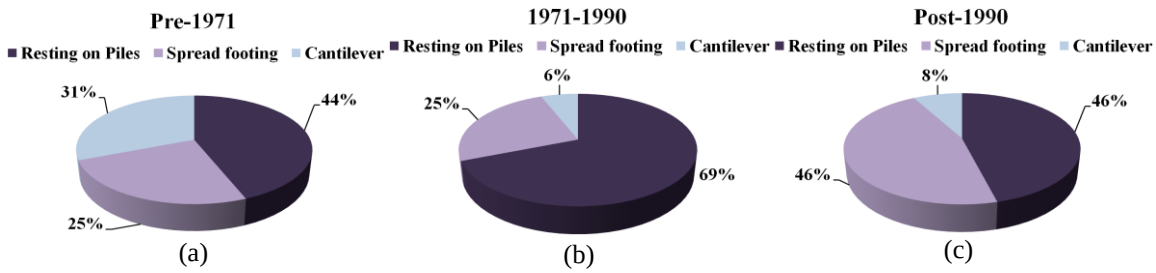

Figure 3.29: Statistical distribution of seat abutment type for bridges designed (a) pre-1971, (b) 1971-1990, and (c) post-1990

OpenSees' ZeroLength element is used to capture the response of the abutment backfill soil and the bi-directional forces, including abutment piles and frictional surface. The type of bi-directional force is selected according to the abutment configuration. The elements associated with the backfill soil and the bi-directional forces are connected in parallel. For cantilever-type abutments, the element representing the behavior of the wall stem flexure is connected in series with the bi-directional force elements. For modeling abutments including a haunch, impact and spring elements representing the shear capacity of the haunch are developed in series.

The abutment's resistance can be classified as either active or passive. An abutment's passive resistance develops when it moves toward the backfill soil, while active resistance appears when the abutment moves away from the backfill soil. Passive resistance is provided by the backfill soil and the piles; however, active resistance is provided by the piles (Caltrans, 2010).

The passive soil spring is modeled as a nonlinear elastic spring, as recommended by Shamsabadi and Yan (2008). The model is a function of the backwall height and the backfill soil type. The approximate equations used to calculate these forces, where H has dimensions of feet, are based on Shamsabadi and Yan's 2008 work:

$$F(y) = \frac{8y}{1+3y} H^{1.5} \qquad \text{for granular backfills}$$

$$F(y) = \frac{8y}{1+1.3y} H \qquad \text{for cohesive backfills}$$

H: the column height (ft)
F: the force (kip/ft)
y: deformation (in)

This model is based on a set of experiments conducted on bridge abutments with various abutment heights. Figure 3.30 shows the abutment force-deformation backbone curve, where F_{ult} is the maximum abutment force developed at the maximum displacement, y_{max}. The value of y_{ave} indicates the displacement corresponding to a force that is half of the maximum abutment force, and K is the average soil stiffness. Shamsabadi and Yan (2008) found that the maximum displacement of the backwall is *0.05H* and *0.1H* for granular (sandy soils) and cohesive (clayey soils) backfills, respectively. The response of the backfill soil is modeled using *HyperbolicGapMaterial*, in OpenSees, according to the recommendation of Shamsabadi and Yan (2008).

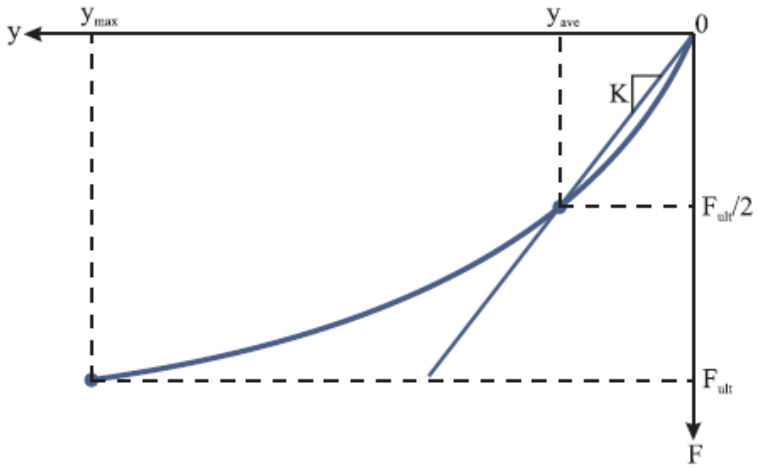

Figure 3.30: Force-deformation response of the abutment backfill soil

Frictional response applies to the abutments that are supported on spread footings or have a weak construction joint either above the footing or on the pile cap. Hence, the frictional surface can be the soil-concrete interface at the base of the footing or the concrete-concrete interface at the base of the stem wall. The force-versus-deformation curve corresponding to the frictional response is shown in Figure 3.31. The maximum response is calculated as the product of the coefficient of friction (μ) and the dead load reaction on the abutment (R). The frictional response is assumed to be involved in the active, passive, and transverse response of the abutments. A ZeroLength element with *ElasticPP* material is used to model the frictional response in OpenSees.

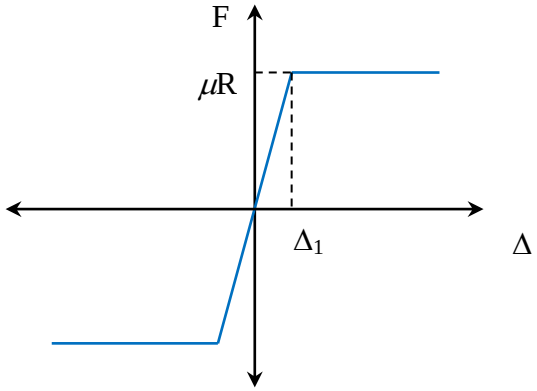

Figure 3.31: Force-deformation response of the abutment resting on spread footing

Piles provide longitudinal and transverse stiffness for the abutments resting on piles. The trilinear force-deformation response of the pile, along with the corresponding modeling parameters, is presented in Figure 3.32. The initial yield parameters (Δ_1, F_1) are determined based on the Caltrans 2014 draft of bridge design aids on 'Permissible Horizontal Loads for Standard Plan and Steel HP Piles' (Caltrans, 2013-2016). The plastic yielding parameters (Δ_2, F_2) are calculated based on the results of modeling various pile systems in LPILE (LPILE v6.0).

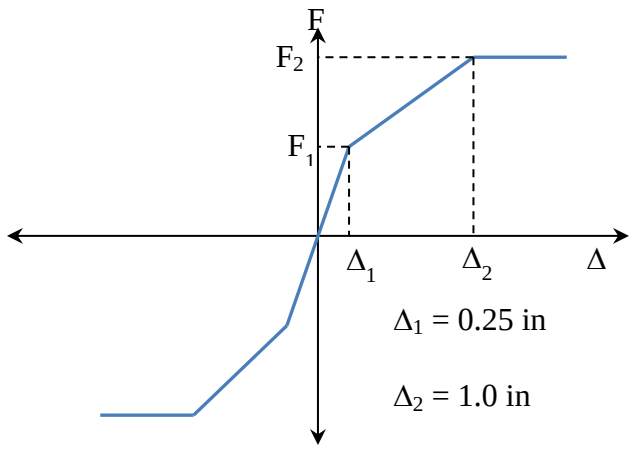

Figure 3.32: Force-deformation response of the abutment pile

For cantilever abutments, the flexural behavior of the abutment wall is assumed to be elastic perfectly plastic, as shown in Figure 3.33. The backbone curve is obtained through push-over analysis of the cantilever wall.

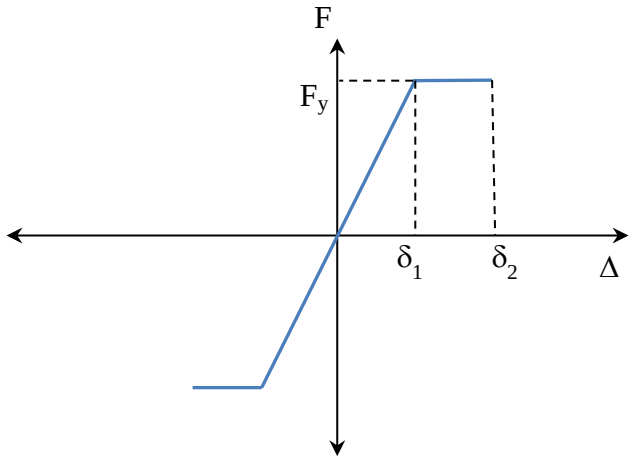

Figure 3.33: Force-deformation response of the cantilever abutment

For skewed bridges, the directions of the abutment elements are adjusted to make the passive pressure of the backfill act perpendicularly to the backwall. As noted in the Introduction, during a seismic event, the superstructure of a skewed bridge experiences significant rotation around the vertical axis of the bridge deck. Initially, the bridge deck pushes the abutment, and then the eccentricity of the backfill's reaction with respect to

the center of stiffness creates a rotational movement in the deck. Consequently, this rotation leads to the separation of the superstructure from the abutments at the acute corners. Figure 3.34 displays the rotation mechanism of skewed bridges. F_1 and F_2 represent the impact abutment forces at obtuse (F_1) and acute (F_2) corners.

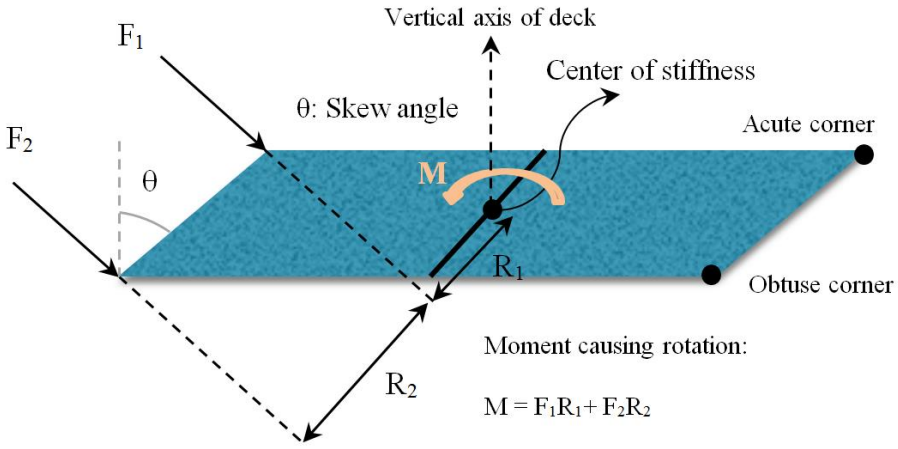

Figure 3.34: Rotation mechanism of skewed bridges

Researchers at Brigham Young University performed a set of large-scale experiments on bridge abutments with several skew angles. The comparison of the load-deformation backbone curves produced from these experiments with the results of numerical simulations (Shamsabadi & Rollins, 2014), indicated three major findings. First, the behavior of the skewed abutment is nonlinear with a nearly hyperbolic shape, similar to the straight abutment. Second, the skewed abutment forms an asymmetric passive soil wedge within the abutment backfill, primarily because of the deck rotation. Third, a significant reduction was noted in the passive force displacement capacity of the abutment backfill, and, interestingly, this reduction was a function of skew angle. As a result, herein, an exponential capacity reduction factor (R), introduced by Shamsabadi and Rollins (2014), is implemented to develop the force-deformation backbone curve

representing the skewed abutments as shown in Figure 3.35. This reduction factor is in the form of an exponential decay function defined as $R = e^{\frac{-\theta}{45^o}}$. Moreover, it is multiplied by the non-skewed abutment backbone curve (F_0) to find the backbone curve for the skewed abutment (F_θ), as $F_\theta = R \times F_0$.

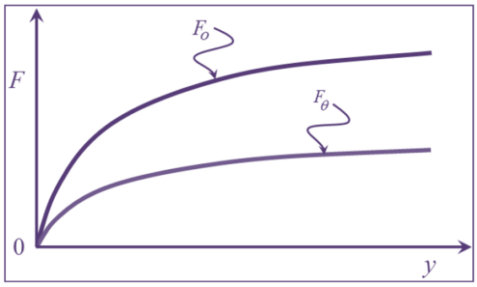

Figure 3.35: Backbone curve for skewed and non-skewed abutments

As mentioned previously, the skewed abutment develops an asymmetric passive soil wedge while the deck continues to rotate. Moreover, the backfill soil volume, mobilized per unit length of abutment wall, increases from the obtuse corner toward the acute corner. Reflecting these effects in the analytical model of the abutments requires assigning different properties to the nonlinear hyperbolic springs depending on their relative distance from the obtuse corner. This variation is considered linearly, following the recommendation of Kaviani, et al. (2012). The strength variation factor ($\beta = 0.3(\tan\theta / \tan 60^\circ)$) identified by Kaviani, et al. (2012) is computed as a function of skew angle.

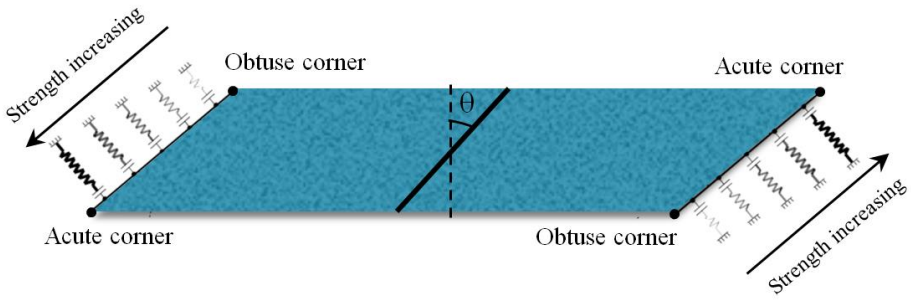

Figure 3.36: Configuration diagram of backfill soil springs

3.3.3 Foundation

Bridge foundations transfer structural loads to the underlying soil, and are classified into several types, including spread footings, integral pile shaft, and pile supported footings. Figure 3.37 shows a variety of foundation systems. The selection of appropriate foundation type depends primarily on the bridge's loading requirements and the site's soil conditions. Because the review of California bridge plans revealed the prevalence of pile-supported footings, spread footings, and integral pile shafts, these three types are considered in the present study. Corresponding portions of the numerical bridge model are assigned to each of the three foundation systems based on their respective statistical distribution (Figure 3.38). Using ZeroLength elements in OpenSees, translational and rotational springs are added to the base of the columns (Figure 3.39) to simulate the behaviors of bridge foundations.

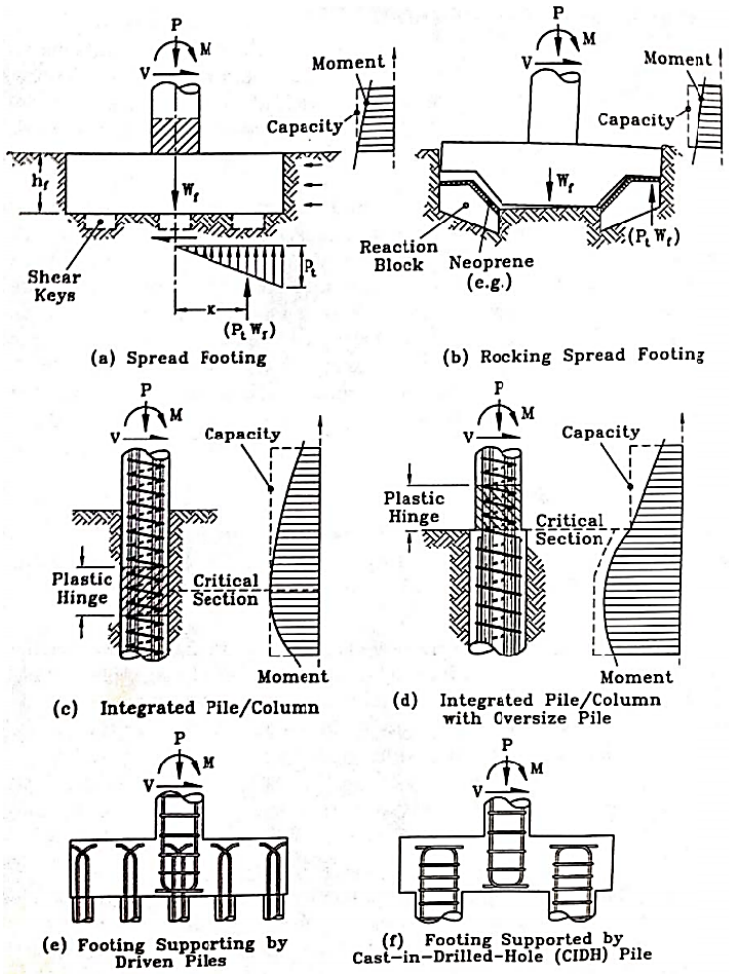

Figure 3.37: Bridge foundation systems (Source: **(Priestley, et al., 1996)**)

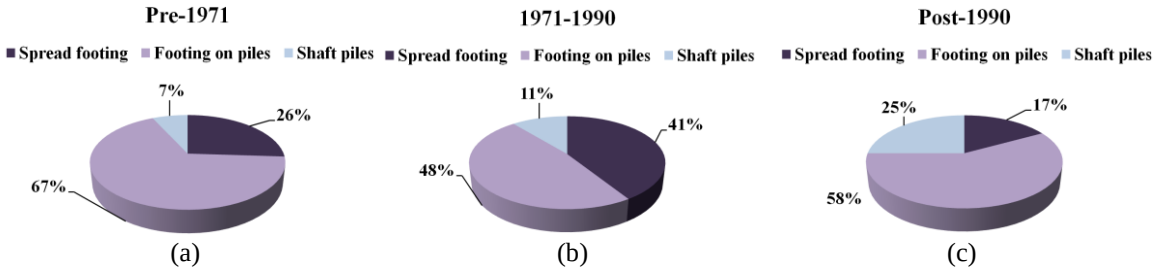

Figure 3.38: Statistical distribution of considered foundation systems for bridges designed (a) pre-1971, (b) 1971-1990, and (c) post-1990

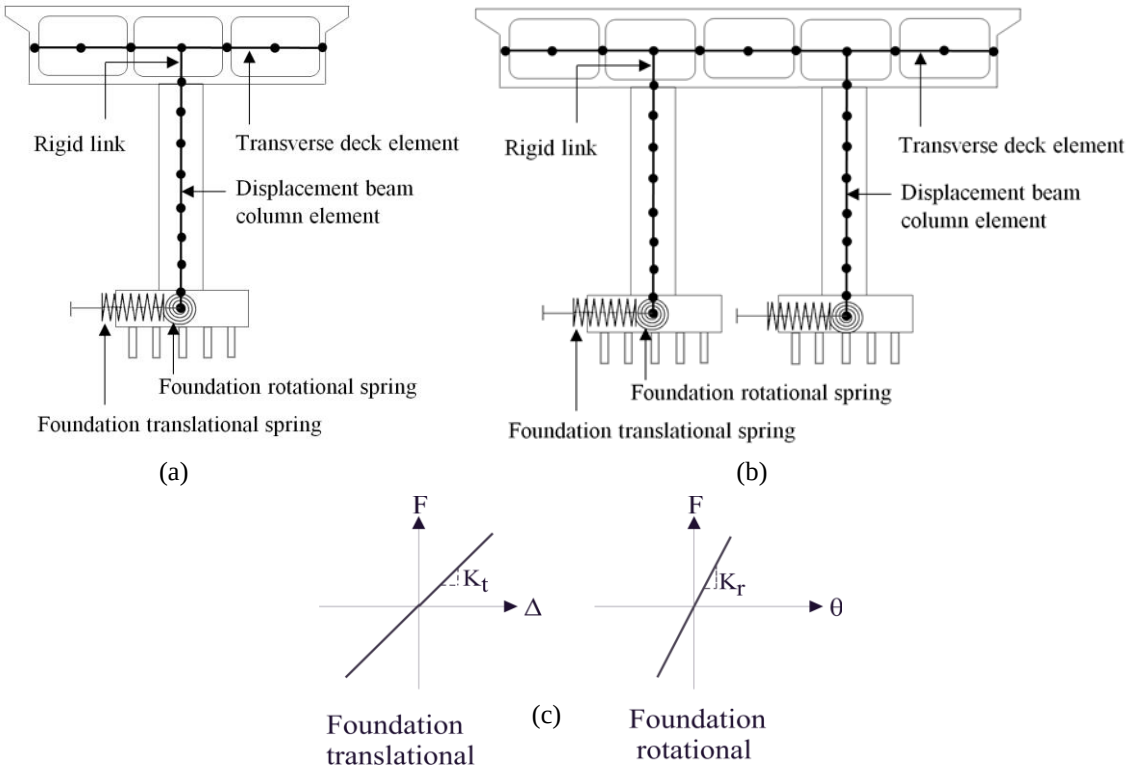

Figure 3.39: Bridge foundation elements added to the base of the columns; (a) single column bent; (b) multi-column bent; and (c) force-displacement of foundation elements

3.3.4 Pounding

Pounding or impact between the decks and/or the deck and abutment backwall is modeled using the contact element approach proposed by Muthukumar and DesRoches (2006) and is consistent with previous studies (Nielson, 2005; Ramanathan, 2012) (Figure 3.40). In skewed bridges, the interaction forces apply perpendicularly to the deck. Accordingly, the pounding elements are oriented along with the bridge deck.

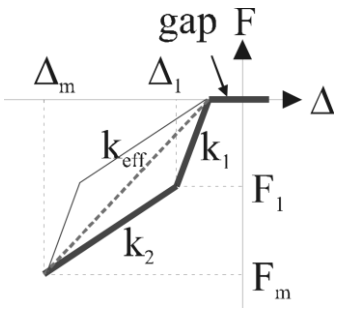

Figure 3.40: Analytical model for pounding between deck and abutment backwall (Source: (Muthukumar & DesRoches, 2006))

3.3.5 Bearing

Bridges with seat-type abutments rest on bearings. In the review of bridge plans in California, three types of bearings, listed as rocker, elastomeric, and friction bearing, were noted in bridges constructed prior to 1971, although only the elastomeric bearing type was found in bridges constructed after 1971. The statistical distribution of the bearings for various design eras is shown in Figure 3.41.

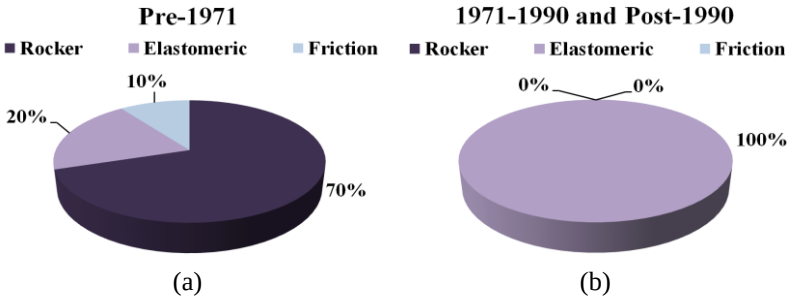

(a) (b)

Figure 3.41: Statistical distribution of bearings for bridges designed in (a) pre-1971, (b) 1971-1990 and post-1990

As shown in Figure 3.42, the elastomeric bearing is the most commonly used bearing noted in the plan review. This type of bearing usually transfers the horizontal forces by friction. The motions associated with the elastomeric and friction bearings are similar, and their behavior is characterized by sliding, which depends on the initial

stiffness. The responses of these types of bearings can be captured using elastic perfectly plastic material (Figure 3.42) (Steel01 material in OpenSees). ZeroLength element, in OpenSees, is implemented to model the bearing.

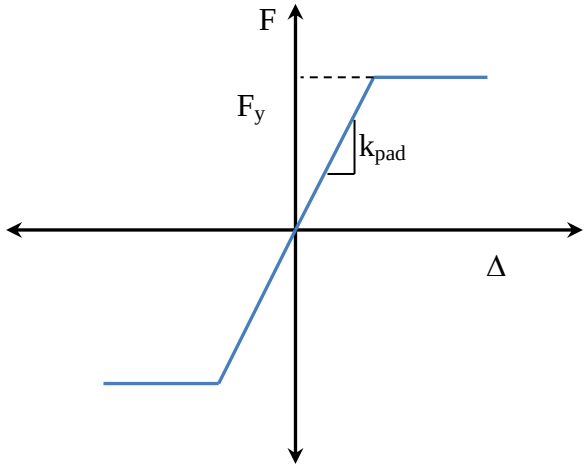

Figure 3.42: Force-deformation response of the elastomeric and friction bearings

The initial stiffness, $k_{pad} = GA/h$, is computed using the shear modulus (G) the cross-sectional area (A) and the bearing thickness (h) (Ramanathan, 2012). The yield force (F_y) in the force-deformation diagram, is calculated as the product of the normal force acting on the bearing (N) and the coefficient of friction (μ). The coefficient of friction that is a function of normal stress (σ_n) is derived from the experimental tests (Scharge, 1981) as $\mu = 0.05 + 0.4/\sigma_n$. An approach similar to what has been discussed here is used with different stiffness values to model the friction bearings, since their behavior pattern is similar to elastomeric bearings.

The rocker bearing is modeled according to the recommendations of an experimental study conducted by Mander, et al. (1996). The force-deformation behavior of bearings in the longitudinal direction is shown in Figure 3.43. The effect of debris

being plowed out is neglected in the current study. The transverse behavior of rocker bearings is modeled by the combination of a rectangular and a link element, as shown in Figure 3.44. The link element is used to capture slip and stiffness deterioration. In the skewed bridge models, the elements with respect to shear keys and bearings are not oriented, as is the same as the real bridge plans.

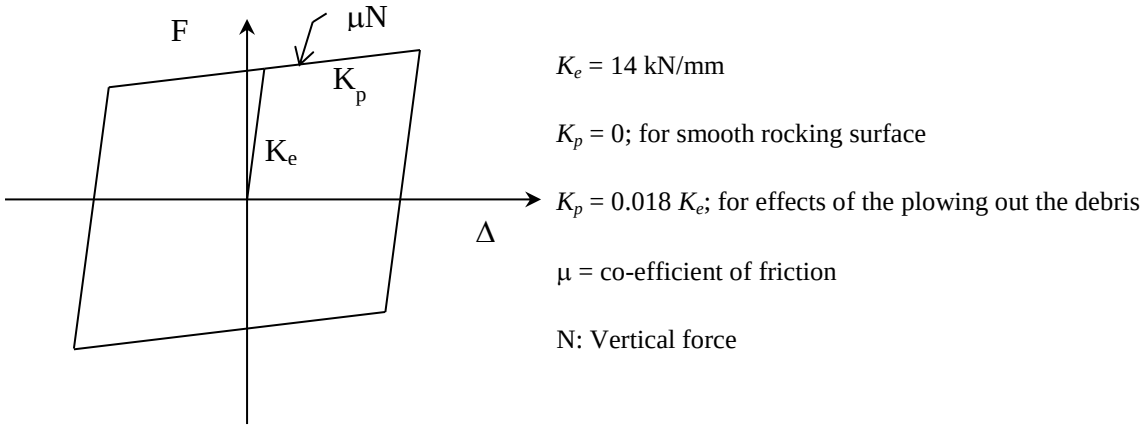

Figure 3.43: Force-deformation response of the rocker bearing in the longitudinal direction

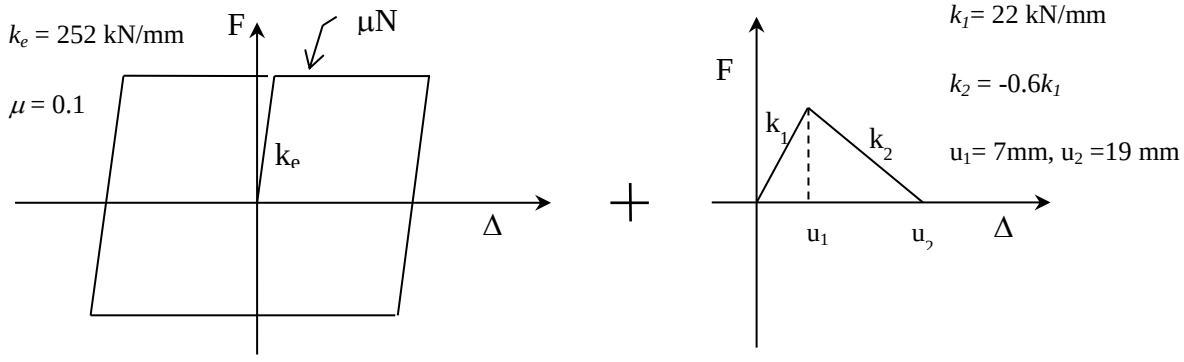

Figure 3.44: Force-deformation response of the rocker bearing in the transverse direction

3.3.6 Shear Key

Shear keys help constrain the relative transverse movement between the deck and the abutments and/or two adjacent deck segments. Potential failure of the shear keys can occur via one of the following four mechanisms: shear friction, flexure, shear, and bearing (Megally, et al., 2002). Shear key designs are categorized as isolated in newly emerging designs, or non-isolated in conventional designs (Caltrans, 2013-2016). However, only the non-isolated shear keys are considered in this study, as the isolated type is used only in recently designed bridges that are not found in the existing inventory.

The existing shear keys are designed for a dead-load reaction of 1 g, and the capacity of the shear key is estimated based on the dead-load reaction of the girder (Caltrans, 2013-2016). Megally, et al. (2002) presented the nonlinear force-deformation response of the abutment shear keys (Figure 3.45), which is adopted in the present study. Based on experimental results, the maximum displacement that the shear key undergoes before its capacity reduces to zero is about 3.5 inches, as shown in Figure 3.46. P_{cap} denotes the capacity of the shear key calculated as the product of the dead-load reaction and the acceleration. ZeroLength elements in OpenSees, characterized by this nonlinear force-deformation response, are used to capture the response of shear keys. In the skewed bridge models, the elements with respect to shear keys and bearings are not oriented, as is the same in real bridge plans.

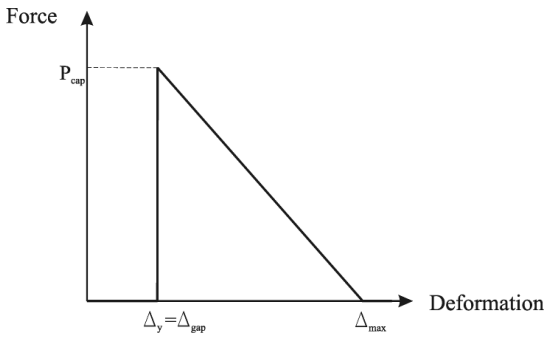

Figure 3.45: Force-deformation model for the shear key

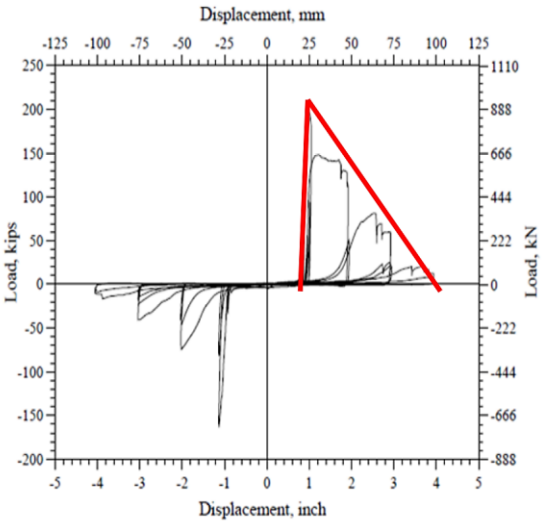

Figure 3.46: Load-displacement curves from the experimental testing of abutment shear keys (Source: **(Ramanathan, 2012)**)

3.4 Uncertainty in Modeling Parameters

Uncertainty in the structural modeling parameters is addressed in this study. Table 3.6 - Table 3.21 show the probability distribution of parameters associated with each of the modeling characteristics and their respective values, derived from a comprehensive review of the bridge plans of Caltrans bridge inventory (BIRIS). The values correspond to bridges designed prior to and after 1970. Additional details about the modeling parameters are provided by Mangalathu (2017).

Table 3.6: Probability distribution of modeling parameters for column material properties

Parameter	Design era	Units	Distribution				
			Type	Mean	Standard Deviation	Lower bound	Upper Bound
Concrete compressive strength	Pre-1970	ksi	Normal	3.90* (4.23)	0.48 (0.52)	2.94 (4.86)	5.19 (5.36)
	Post-1970	ksi	Normal	4.55	0.56	3.43	5.67
Steel yield strength	Pre-1970	ksi	Normal	57.3* (69.0)	4.5 (5.5)	49.0 (58.0)	67.0 (80.0)
	Post-1970	ksi	Normal	69.0	5.5	58.0	80.0

* 80% of the simulations are conducted with this value, and the remaining 20% are performed with the value in parenthesis.

Table 3.7: Probability distribution of modeling parameters for column height

Design era	Units	Distribution*					
		Type	Mean	Standard Deviation	Median	Lower bound	Upper Bound
Pre-1970	ft	Lognormal	3.06	0.13	21.5	16.5	28.0
1970-1990	ft	Lognormal	3.14	0.16	23.2	17.0	32.0
Post-1990	ft	Lognormal	3.22	0.18	25.0	17.5	36.0

* Mean and standard deviation of the associated normal distribution (in log space)

Table 3.8: Probability distribution of modeling parameters for column reinforcement details

Parameter	Design era	Units	Distribution				
			Type	Mean	Standard Deviation	Lower bound	Upper Bound
Longitudinal steel reinforcement ratio	All	-	Uniform	2.00	0.33	1.0	3.0
Transverse steel reinforcement ratio	Pre-1970	-	#4 @ 12 in. irrespective of the cross-section				
	Post-1970	-	Uniform	0.85	0.07	0.4	1.3

Table 3.9: Distribution of column cross-section shapes and dimensions

Design era	Type of bent	Column cross-section	Diameter	Length	Width	Mix (%)
Pre-1970	Single	Circular	48	-	-	10
			60	-	-	20
			72	-	-	20
		Rectangular	-	72	36	10
			-	96	36	15
			-	120	36	10
			-	96	48	15
	Multi	Circular	36	-	-	15
			48	-	-	20
			60	-	-	5
		Rectangular	-	42	30	20
			-	48	36	25
			-	60	42	10
			-	96	36	5
1970-1990	Single	Circular	60	-	-	10
			66	-	-	25
			72	-	-	15
			84	-	-	10
		Oblong	-	72	48	10
			-	96	48	15
			-	99	66	15
	Multi	Circular	48	-	-	35
			60	-	-	10
			66	-	-	20
			72	-	-	10
		Oblong	-	60	36	10
			-	72	48	15
Post-1990	Single	Circular	60	-	-	5
			66	-	-	15
			84	-	-	20
			108	-	-	10
		Oblong	-	72	48	5
			-	96	48	10
			-	99	66	25
			-	108	72	10
	Multi	Circular	48	-	-	30
			60	-	-	10
			66	-	-	25
			84	-	-	5
		Oblong	-	72	48	15
			-	99	66	10
			-	126	84	5

Table 3.10: Probability distribution of modeling parameters for abutment

Parameter	Design era	Type of abutment		Units	Distribution**				
					Type*	Mean	Standard Deviation	Lower bound	Upper bound
Abutment backwall height	Pre-1970	Diaphragm	On piles	ft	LN	2.35	0.15	8.0	14.0
			On spread	ft	LN	2.20	0.35	4.5	18.0
			Cantilever	ft	U	25.0	8.33	20.0	30.0
		Seat	On piles	ft	LN	1.95	0.20	5.0	10.5
			On spread	ft	LN	1.95	0.20	5.0	10.5
			Cantilever	ft	U	25.0	8.33	20.0	30.0
	1970-1990	Diaphragm	On piles	ft	LN	2.39	0.20	6.5	13.0
			On spread	ft	LN	2.37	0.09	9.5	12.5
			Cantilever	ft	-	-	-	-	-
		Seat	On piles	ft	LN	2.45	0.18	9.5	20.0
			On spread	ft	LN	2.50	0.09	10.5	14.5
			Cantilever	ft	-	-	-	-	-
	Post-1990	Diaphragm	On piles	ft	LN	2.45	0.18	9.5	20.0
			On spread	ft	-	-	-	-	-
			Cantilever	ft	-	-	-	-	-
		Seat	On piles	ft	LN	2.63	0.22	10.5	23.5
			On spread	ft	LN	2.58	0.14	11.0	19.0
			Cantilever	ft	-	-	-	-	-
Abutment pile stiffness (lateral capacity /deck width)	All	Diaphragm	On piles	kip/ft	LN	1.79	0.35	2.5	12.0
	All	Seat	On piles	kip/ft	LN	2.08	0.35	4.0	16.0
Coefficient of friction	All	Diaphragm /Seat	On spread	_	N	0.40	0.075	0.25	0.55
Yield displacement	All	Diaphragm /Seat	On spread	in	U	0.75	0.02	0.50	1.0
Abutment backfill soil (clay vs sand)	All	Diaphragm /Seat	All types		B	Equally split among all simulations			

* LN = lognormal, U = uniform, and B = Bernoulli distribution

** Mean and standard deviation of the associated normal distribution (in log space), in the case of a lognormal distribution

Table 3.11: Probability distribution of modeling parameters for bridge span length

Design era	Span range	No. of spans	Mix (%)	Superstructure: Reinforced (RC) Pre-stressed (PC)	Units	Span length distribution				
						Type	Mean	Standard Deviation	Lower bound	Upper Bound
Pre-1970	S11	1	50	RC	ft	Normal	80	25	35	130
			50	PC	ft	Normal	110	35	40	180
	S22	2	75	RC	ft	Normal	95	20	55	140
			25	PC	ft	Normal	135	35	75	230
	S34	3	55	RC	ft	Normal	90	25	50	160
		4	45	RC	ft	Normal	90	25	50	160
	S56	5	80	RC	ft	Normal	90	20	60	125
		6	20	RC	ft	Normal	90	20	60	125
1970-1990	S11	1	10	RC	ft	Normal	80	25	35	130
			35	PC	ft	Normal	130	35	50	220
Post-1900			15	RC	ft	Normal	105	40	35	200
			40	PC	ft	Normal	130	35	50	220
1970-1990	S22	2	5	RC	ft	Normal	95	20	55	140
			35	PC	ft	Normal	135	35	75	230
Post-1900	S22		10	RC	ft	Normal	135	35	85	200
			50	PC	ft	Normal	135	35	75	230
1970-1990	S34	3	10	RC	ft	Normal	90	25	50	160
			20	PC	ft	Normal	155	45	75	250
		4	5	RC	ft	Normal	90	25	50	160
			10	PC	ft	Normal	155	45	75	250
Post-1900	S34	3	5	RC	ft	Normal	110	35	55	190
			30	PC	ft	Normal	155	45	75	250
		4	5	RC	ft	Normal	110	35	55	190
			15	PC	ft	Normal	155	45	75	250
1970-1990	S56	5	10	RC	ft	Normal	90	20	60	125
			10	PC	ft	Normal	155	35	95	240
		6	5	RC	ft	Normal	90	20	60	125
			5	PC	ft	Normal	155	35	95	240
Post-1900	S56	5	15	RC	ft	Normal	125	35	75	165
			30	PC	ft	Normal	155	35	95	240
		6	5	RC	ft	Normal	125	35	75	165
			20	PC	ft	Normal	155	35	95	240

Table 3.12: Probability distribution of modeling parameters for span ratio (approach span/main span)

Design era	Span range	No. of spans	Mix (%)	Superstructure: Reinforced (RC) Pre-stressed (PC)	Span ratio distribution				
					Type	Mean	Standard Deviation	Lower bound	Upper Bound
Pre-1970	S11	1	50	RC	-	-	-	-	-
			50	PC	-	-	-	-	-
	S22	2	75	RC	-	-	-	-	-
			25	PC	-	-	-	-	-
	S34	3	55	RC	Normal	0.60	0.20	0.35	1.00
		4	45	RC	Normal	0.60	0.20	0.35	1.00
	S56	5	80	RC	Normal	0.60	0.20	0.35	1.00
		6	20	RC	Normal	0.60	0.20	0.35	1.00
1970-1990	S11	1	10	RC	-	-	-	-	-
			35	PC	-	-	-	-	-
Post-1900			15	RC	-	-	-	-	-
			40	PC	-	-	-	-	-
1970-1990	S22	2	5	RC	-	-	-	-	-
			35	PC	-	-	-	-	-
Post-1900	S22		10	RC	-	-	-	-	-
			50	PC	-	-	-	-	-
1970-1990	S34	3	10	RC	Normal	0.60	0.20	0.35	1.00
			20	PC	Normal	0.75	0.20	0.40	1.00
		4	5	RC	Normal	0.60	0.20	0.35	1.00
			10	PC	Normal	0.75	0.20	0.40	1.00
Post-1900	S34	3	5	RC	Normal	0.60	0.20	0.35	1.00
			30	PC	Normal	0.75	0.20	0.40	1.00
		4	5	RC	Normal	0.60	0.20	0.35	1.00
			15	PC	Normal	0.75	0.20	0.40	1.00
1970-1990	S56	5	10	RC	Normal	0.60	0.20	0.35	1.00
			10	PC	Normal	0.75	0.20	0.40	1.00
		6	5	RC	Normal	0.60	0.20	0.35	1.00
			5	PC	Normal	0.75	0.20	0.40	1.00
Post-1900	S56	5	15	RC	Normal	0.60	0.20	0.35	1.00
			30	PC	Normal	0.75	0.20	0.40	1.00
		6	5	RC	Normal	0.60	0.20	0.35	1.00
			20	PC	Normal	0.75	0.20	0.40	1.00

Table 3.13: Probability distribution of modeling parameters for deck width

Design era	No. of columns per bent	Mix (%)	Distribution					
			Unit	Type	Mean	Standard Deviation	Lower bound	Upper Bound
Pre-1970	1	25	ft	Normal	26.5	1.5	22	30
		50	ft	Normal	34	1.2	30	38
		25	ft	Normal	40	1.5	38	46
	2	15	ft	Normal	34	2.0	30	38
		25	ft	Normal	41	5	38	48
		15	ft	Normal	58	26	48	74
	3	10	ft	Normal	48	18	38	56
		15	ft	Normal	66	9	56	74
		5	ft	Normal	80	9	74	92
	4	5	ft	Normal	60	34	38	72
		10	ft	Normal	88	34	72	106
Post-1970	1	15	ft	Normal	28	1.2	22	30
		20	ft	Normal	34	4	30	38
		55	ft	Normal	42	2	38	46
		10	ft	Normal	50	14	46	60
	2	20	ft	Normal	43	7	36	50
		15	ft	Normal	57	8	50	66
		10	ft	Normal	73	22	66	88
	3	10	ft	Normal	59	18	50	68
		15	ft	Normal	79	20	68	88
		10	ft	Normal	98	20	88	108
	4	5	ft	Normal	75	32	58	90
		15	ft	Normal	107	38	90	128

Table 3.14: Modeling parameters for deck cross-section of a box-girder bridge

Deck cross-section properties	Unit	Pre-1970	1970-1990	Post-1990
Bottom flange thickness	in	6.0	6.5	7.0
Wall thickness	in	12.0	12.0	12.0

Table 3.15: Probability distribution of modeling parameters for cell types

Design era	No. of columns per bent	Cell distribution					
		Type	Mix (%)	Type	Mix (%)	Type	Mix (%)
Pre-1970	1	3 cell	100	-	-	-	-
		3 cell	70	5 cell	30	-	-
		3 cell	40	5 cell	60	-	-
	2	3 cell	50	5 cell	50	-	-
		3 cell	25	5 cell	75		
		5 cell	25	7 cell	50	9 cell	25
	3	5 cell	65	7 cell	35	-	-
		7 cell	50	9 cell	50	-	-
		9 cell	70	11 cell	30	-	-
	4	5 cell	25	7 cell	35	9 cell	40
		9 cell	25	11 cell	75	-	-
Post-1970	1	3 cell	100	-	-	-	-
		3 cell	85	5 cell	15		
		3 cell	75	5 cell	25	-	-
		3 cell	30	5 cell	50	7 cell	20
	2	3 cell	40	5 cell	60		
		5 cell	80	7 cell	20		
		5 cell	25	7 cell	50	9 cell	25
	3	5 cell	50	7 cell	50		
		7 cell	50	9 cell	50		
		7 cell	20	9 cell	40	11 cell	40
	4	5 cell	25	7 cell	40	9 cell	35
		9 cell	40	11 cell	35	13 cell	25

Table 3.16: Probability distribution of modeling parameters for bearing

Design era	Bearing types	Parameter	Units	Distribution**				
				Type*	Mean	Standard Deviation	Lower bound	Upper bound
Pre-190	Rocker	Coefficient of friction (longitudinal direction)	-	N	0.04	0.01	0.02	0.06
		Coefficient of friction (transverse direction)	-	N	0.10	0.02	0.06	0.14
	Elastomeric	Stiffness per feet of deck width	kip/in/ft	LN	0.40	0.35	0.70	3.0
		Coefficient of friction	-	N	0.30	0.10	0.10	0.50
	Friction	Coefficient of friction	-	U	0.50	0.03	0.20	0.80
		Yield displacement	in	U	0.07	0.0003	0.04	0.10
1970-1990	Elastomeric	Stiffness per feet of deck width	kip/in/ft	LN	0.77	0.52	0.7	6.0
		Coefficient of friction	-	N	0.30	0.10	0.10	0.50
Post-1990	Elastomeric	Stiffness per feet of deck width	kip/in/ft	LN	0.00	0.45	0.4	2.5
		Coefficient of friction	-	N	0.30	0.10	0.10	0.50

* N = normal, LN = lognormal, U = uniform, and B = Bernoulli distribution.

** Mean and standard deviation of the associated normal distribution (in log space), in the case of a lognormal distribution

Table 3.17: Probability distribution of modeling parameters for foundation rotational stiffness ($\times 10^6$ kip-in/rad)

Design era	Type of bent	Type of footing	Foundation fixity	Mix (%)	Transverse to bridge direction distribution*				
					Type	Mean	Standard Deviation	Lower bound	Upper Bound
Pre-1970	single	pile	fixed	100	Lognormal	25.0	2.5	10	62.5
		spread	fixed		Lognormal	25.0	2.5	10	62.5
	multiple	pile	pinned	37.5	Lognormal	2.5	2.5	1.0	6.3
			fixed	12.5	Lognormal	4.0	2.5	1.6	10.0
		spread	pinned	37.5	Lognormal	2.5	2.5	1.0	6.3
			fixed	12.5	Lognormal	4.0	2.5	1.6	10.0
1970-1990	single	pile	fixed	50	Lognormal	80.0	2.5	32.0	200.0
		spread	fixed	50	Lognormal	50.0	2.5	20.0	125.0
	multiple	pile	pinned	25	Lognormal	12.0	2.5	4.8	30.0
			fixed	25	Lognormal	18.0	2.5	7.2	15.0
		spread	pinned	25	Lognormal	12.0	2.5	4.8	30.0
			fixed	25	Lognormal	18.0	2.5	7.2	15.0
Post-1990	single	pile	fixed	90	Lognormal	190.0	2.5	76.0	475.0
		spread	fixed	10	Lognormal	50.0	2.5	20.0	125.0
	multiple	pile	pinned	50	Lognormal	20.0	2.5	8.0	50.0
			fixed	0	Lognormal	30.0	2.5	12.0	75.0
		spread	pinned	50	Lognormal	20.0	2.5	8.0	50.0
			fixed	0	Lognormal	30.0	2.5	12.0	75.0

* Mean and standard deviation of the associated normal distribution (in log space)

Table 3.18: Probability distribution of modeling parameters for foundation rotational stiffness

Design era	Type of bent	Type of footing	Foundation fixity	Trans/Long stiffness ratio distribution*				
				Type	Mean	Standard Deviation	Lower bound	Upper Bound
Pre-1970	single	pile	fixed	Lognormal	1.5	1.5	1.0	2.25
		spread	fixed	Lognormal	1.5	1.5	1.0	2.25
	multiple	pile	pinned	Lognormal	1.0	1.5	0.67	1.50
			fixed	Lognormal	1.0	1.5	0.67	1.50
		spread	pinned	Lognormal	1.0	1.5	0.67	1.50
			fixed	Lognormal	1.0	1.5	0.67	1.50
1970-1990	single	pile	fixed	Lognormal	1.5	1.5	1.0	2.25
		spread	fixed	Lognormal	1.3	1.3	1.0	1.70
	multiple	pile	pinned	Lognormal	1.0	1.5	0.67	1.5
			fixed	Lognormal	1.0	1.5	0.67	1.5
		spread	pinned	Lognormal	1.0	1.5	0.67	1.5
			fixed	Lognormal	1.0	1.5	0.67	1.5
Post-1990	single	pile	fixed	Lognormal	1.15	1.15	1.00	1.32
		spread	fixed	Lognormal	1.15	1.15	1.00	1.32
	multiple	pile	pinned	Lognormal	1.20	1.25	0.96	1.50
			fixed	Lognormal	1.20	1.25	0.96	1.50
		spread	pinned	Lognormal	1.20	1.25	0.96	1.50
			fixed	Lognormal	1.20	1.25	0.96	1.50

* Mean and standard deviation of the associated normal distribution (in log space)

Table 3.19: Probability distribution of modeling parameters for foundation translational stiffness (kip/in)

Design era	Type of bent	Type of footing	Foundation fixity	Mix (%)	Transverse to bridge direction distribution*				
					Type	Mean	Standard Deviation	Lower bound	Upper Bound
Pre-1970	single	pile	fixed	100	Lognormal	1250.0	2.5	500.0	3125.0
		spread	fixed		Lognormal	1250.0	2.5	500.0	3125.0
	multiple	pile	pinned	37.5	Lognormal	625.0	2.5	250.0	1562.5
			fixed	12.5	Lognormal	625.0	2.5	250.0	1562.5
		spread	pinned	37.5	Lognormal	625.0	2.5	250.0	1562.5
			fixed	12.5	Lognormal	625.0	2.5	250.0	1562.5
1970-1990	single	pile	fixed	50	Lognormal	2000.0	2.5	800.0	5000.0
		spread	fixed	40	Lognormal	2000.0	2.5	800.0	5000.0
	multiple	pile	pinned	25	Lognormal	1000.0	2.5	400.0	2500.0
			fixed	12.5	Lognormal	1000.0	2.5	400.0	2500.0
		spread	pinned	25	Lognormal	1000.0	2.5	400.0	2500.0
			fixed	12.5	Lognormal	1000.0	2.5	400.0	2500.0
Post-1990	single	pile	fixed	65	Lognormal	2500.0	2.5	1000.0	6250.0
		spread	fixed	10	Lognormal	2500.0	2.5	1000.0	6250.0
	multiple	pile	pinned	35	Lognormal	1000.0	2.5	400.0	2500.0
			fixed	0	Lognormal	1000.0	2.5	400.0	2500.0
		spread	pinned	35	Lognormal	1000.0	2.5	400.0	2500.0
			fixed	0	Lognormal	1000.0	2.5	400.0	2500.0

* Mean and standard deviation of the associated normal distribution (in log space)

Table 3.20: Probability distribution of modeling parameters for foundation translational stiffness

Design era	Type of bent	Type of footing	Foundation fixity	Trans/Long stiffness ratio distribution*				
				Type	Mean	Standard Deviation	Lower bound	Upper Bound
Pre-1970	single	pile	fixed	Lognormal	1.0	1.0	1.0	1.0
		spread	fixed	Lognormal	1.0	1.0	1.0	1.0
	multiple	pile	pinned	Lognormal	1.0	1.0	1.0	1.0
			fixed	Lognormal	1.0	1.0	1.0	1.0
		spread	pinned	Lognormal	1.0	1.0	1.0	1.0
			fixed	Lognormal	1.0	1.0	1.0	1.0
1970-1990	single	pile	fixed	Lognormal	1.0	1.0	1.0	1.0
		spread	fixed	Lognormal	1.0	1.0	1.0	1.0
	multiple	pile	pinned	Lognormal	1.0	1.0	1.0	1.0
			fixed	Lognormal	1.0	1.0	1.0	1.0
		spread	pinned	Lognormal	1.0	1.0	1.0	1.0
			fixed	Lognormal	1.0	1.0	1.0	1.0
Post-1990	single	pile	fixed	Lognormal	1.0	1.0	1.0	1.0
		spread	fixed	Lognormal	1.0	1.0	1.0	1.0
	multiple	pile	pinned	Lognormal	1.0	1.0	1.0	1.0
			fixed	Lognormal	1.0	1.0	1.0	1.0
		spread	pinned	Lognormal	1.0	1.0	1.0	1.0
			fixed	Lognormal	1.0	1.0	1.0	1.0

* Mean and standard deviation of the associated normal distribution (in log space)

Table 3.21: Additional uncertain parameters

Parameter	Units	Distribution*				
		Type	Mean	Standard Deviation	Lower bound	Upper bound
Damping	-	Normal	0.045	0.0125	0.02	0.07
Mass factor		Uniform	1.05	0.0033	0.95	1.15
Shear key acceleration	g	Lognormal	0.0	0.20	0.8	1.20
Gap						
deck and superstructure	in	Lognormal	-0.20	0.50	0.30	2.20
superstructure and shear key	in	Uniform	0.75	0.19	0.00	1.50

* Mean and standard deviation of the associated normal distribution (in log space), in the case of a lognormal distribution

3.5 Closure

The strategies used to generate numerical modeling of various components of a bridge were presented in this section. Bridge columns are known to be the most vulnerable components of a bridge, and operate as the core substructure elements of the bridge support system. Post-earthquake evidence reveals that large deformations of and extensive damage to bridge columns are linked to the force and deformation capacity of the columns. Since research on the seismic vulnerability of bridges with various column shapes is limited, the major part of this section aimed to address this deficiency by evaluating the seismic performance of a variety of common column shapes. The effect of common bridge column shapes on the seismic performance of bridges was analytically assessed in this section using pushover analysis of individual columns and fragility analysis of a hypothetical bridge. The structural characteristics of the existing box-girder bridges located in California were utilized to generate finite element models. Three-dimensional numerical models of a typical bridge column with common circular, rectangular, and oblong cross-sections, as well as prismatic and flared columns, were created in OpenSees. The numerical models were validated by previous experiments, and account for the uncertainties in modeling the bridge components. Assessment of the generated curves indicates the impact of column shapes on the bridge fragilities.

CHAPTER 4

CLASSIFICATION OF BRIDGE CONFIGURATIONS

4.1 General Grouping of the Class of Regular Bridges

As each class of bridge has a variety of configurations (e.g., number of spans, abutment type, and interior support type), it is not manageable to perform simulations for all possible combinations of bridge attributes, while respecting time and resource constraints. Considering all possible combinations would require thousands of production runs. Therefore, an initial sensitivity study was incorporated with the expertise of civil engineers in order to maintain a reasonable computational load. A brief summary of the findings of the sensitivity study, and its methodology, is explained in this section.

In order to gain insight about the most significant bridge attributes to be considered in the generation of fragility curves, seismic bridge responses are compared using statistical techniques (Figure 4.1). For this purpose, a method known as Analysis of Variance (ANOVA) is applied. ANOVA is a statistical method commonly used to analyze the variations between the means associated with different groups of a database. This method assumes the independent observations, the normal distribution of residuals, and the constant variance in the groups. ANOVA evaluates significant differences between the means of two or more independent groups of observations (Vidakovic, 2011). Figure 4.1 shows a simple example of a sample bridge and its 11 possible configurations. In order to investigate the significant differences between the means, ANOVA tests the equality of mean values corresponding to various groups of observations using the following statistical hypothesis test (Figure 4.1):

H_0: $\mu_1 = \mu_2 = ... = \mu_k$, k = total number of groups

H_1: $\mu_i \neq \mu_j$, i and $j = 1, 2, \cdots, k$.

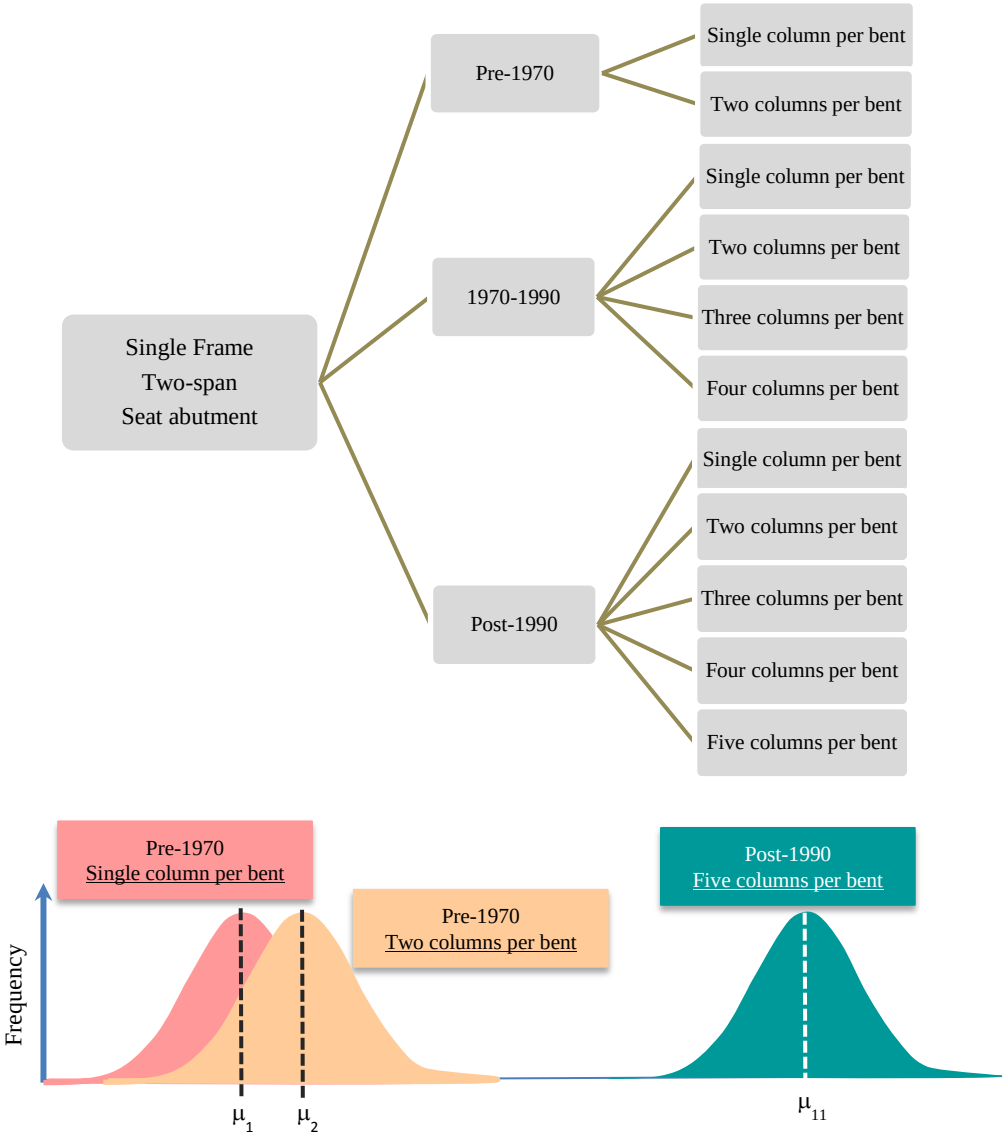

Figure 4.1: Illustration of the variety of bridge configurations and responses

The *F*–statistics are used to perform the hypothesis test. The value of *F* (with k-1 and n – k degrees of freedom) is computed as:

$$F = \frac{SST_r / (\mathrm{k}-1)}{SSE / (n-k)}$$

where, in this equation, SST_r is the treatment sum of squares and can be obtained by $SST = SST_r + SSE$ using the total sum of squares ($SST = \sum_{i=1}^{k}\sum_{j=1}^{n_i}(y_{ij} - \bar{y})^2$) and the sum of squares due to error ($SSE = \sum_{i=1}^{k}\sum_{j=1}^{n_i}(y_{ij} - \bar{y}_i)^2$). Using these computed F values, the probability that the variation between groups occurred by chance can be derived as $p - \text{value} = 1 - Fcdf\left(F, k-1, N-k\right)$. The p–value is the evidence against the null hypothesis, or the probability that the variation between groups occurred by chance. Typically, a cutoff value of 0.05 is selected in ANOVA, and if the p–value is less than the cutoff value, the null hypothesis (H_0: $\mu_1 = \mu_2 = ... = \mu_k$) is rejected. In another words, if the p–value is larger than the cutoff value of 0.05, there is a 95% confidence value that bridge responses will be similar. In this way, bridges with similar seismic responses can be classified into a single group, and one numerical simulation per each group can be performed that will represent the seismic responses of the group. This classification significantly reduces the computational costs for developing fragility curves in the later tasks of this project.

Although ANOVA mainly contributes to the classification of bridges, it only provides the p–values. Therefore, an additional statistical technique must be applied to classify bridges by comparing the obtained p–values. The Fisher Method is another complementary statistical tool to compare different groups of observations. In this method, initially, the group with the highest sensitivity is identified, and then a statistical hypothesis test (ANOVA) is performed to check the equality of the mean value of other groups to the identified highly sensitive group. These two groups can be classified under

one category if the difference between their means is negligible. However, if a significant difference is observed, the process continues to check the group with the second highest sensitivity. This procedure is repeated to classify all groups of observations with similar values. An example of the Fisher Method output is shown in Table 4.1 and Figure 4.2. Figure 4.3 summarizes the process of identifying bridge classes.

Table 4.1: An example of Fisher output for the curvature ductility of bridge column

Bridge configuration	**Mean* value of the bridge response**	**Classification of bridges**	
Pre-1970, Two columns per bent	7.77	A	
Post-1990, Five columns per bent	6.36	A	
1970-1990, Four columns per bent	6.30	A	
Post-1990, Four columns per bent	6.23	A	
Post-1990, Three columns per bent	5.99	A	
1970-1990, Three columns per bent	5.93	A	
Post-1990, Two columns per bent	5.87	A	
1970-1990, Two columns per bent	5.86	A	
Pre-1970, Single column per bent	3.49		B
1970-1990, Single columns per bent	3.48		B
Post-1990, Single columns per bent	2.86		B

* mean values are shown in logarithmic scale

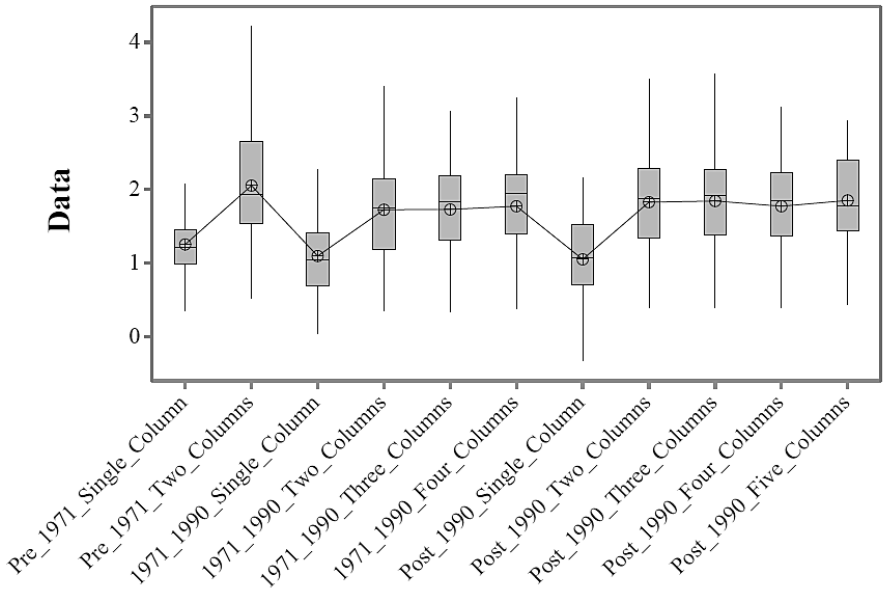

Figure 4.2: Box-plot of the bridge responses presented in Table 4.1

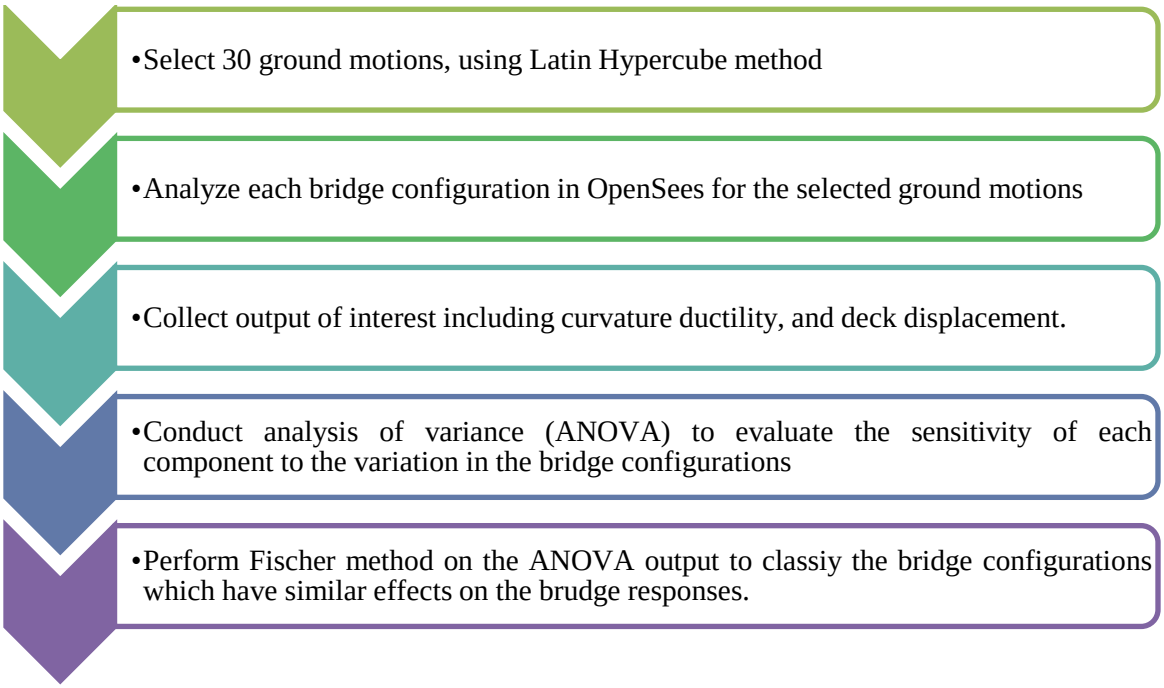

Figure 4.3: Process of classifying bridges with different configurations

The classification procedure was carried out for the box-girder bridge type with various permutations of the number of spans, abutment types, interior supports, number of columns per bent, design eras, and number of frames. Those bridges with significant differences between their responses (column curvature ductility and abutment passive, active, and transverse responses) needed to be analyzed individually in the production runs. A sample of results is shown in Figure 4.4. The main findings of this sensitivity study can be organized as the following:

- Number of spans: Single span and two-span bridges need to be analyzed individually. However, bridges with three and four spans can be analyzed in a similar group, S34, because of their observed close behavior. Similarly, bridges with five and six spans, seven and eight spans, and with nine or more spans can be analyzed in three groups of S56, S78, S99, respectively.

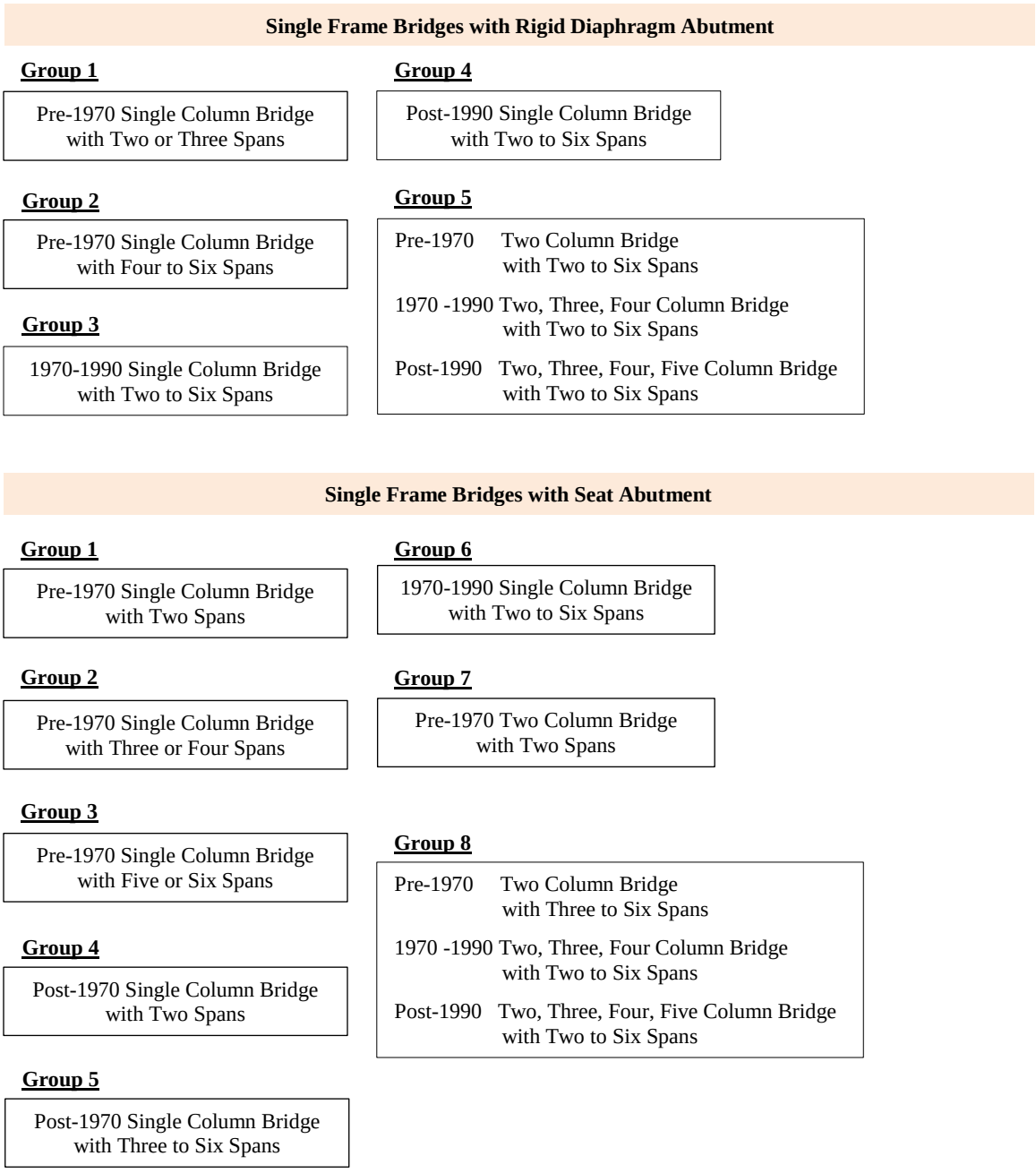

Figure 4.4: Process of classifying bridges with different configurations

- Abutment types: significant differences were noted between the responses of bridges with rigid abutments and bridges with seat-type abutments.
- Interior supports: A similar trend was observed between the responses of bridges with multiple columns per bent; however, the response of bridges supported on a

single column bent showed distinctive results when compared to bridges with multi-column bents. Therefore, single column bent bridges are considered individually, and multi-column bent bridges are classified in a similar group in the production runs.

- Design eras: Based on sensitivity results, bridges designed before 1970 should be considered separately from bridges designed in more recent eras. Bridges from the 1970-1990 and post-1990 design eras can be studied in a similar group.
- Number of frames: The sensitivity study also considered various simplified framing configurations. Responses for the two-frame systems were clearly unique, but distinction between the responses of bridge with a higher number (> 2) of frames was not observed.

The intent of this initial study was to gain insights regarding the most significant bridge attribute to be considered in the future tasks of the project. Eventually, 129 bridge configurations were specified for the concrete box-girder bridge type. The fragility analysis of these 129 groups of bridges is not in the scope of the present study and is implemented in a separate phase of the project (Caltrans project number CT1780), which is proceeding in parallel with the phase presented here.

4.2 Classification of the Class of Irregular Bridges

Obviously, it is not feasible to consider all 129 specified regular bridge classes herein, since each must be evaluated for the effect of a range of various irregularities, which certainly increases the number of simulations. To address this concern, the list of 129 bridge classes was filtered by the common bridge configurations in each type of

irregularity (i.e., skew, tall column bents, unbalanced frame). The distributions of irregular bridges are presented in Figure 4.5 and Figure 4.6. The figures show skew appears more commonly in single-span and single-frame bridges. Similarly, an unbalanced stiffness frame or columns taller than normal appear most frequently in single-frame bridges, followed by two-frame bridges.

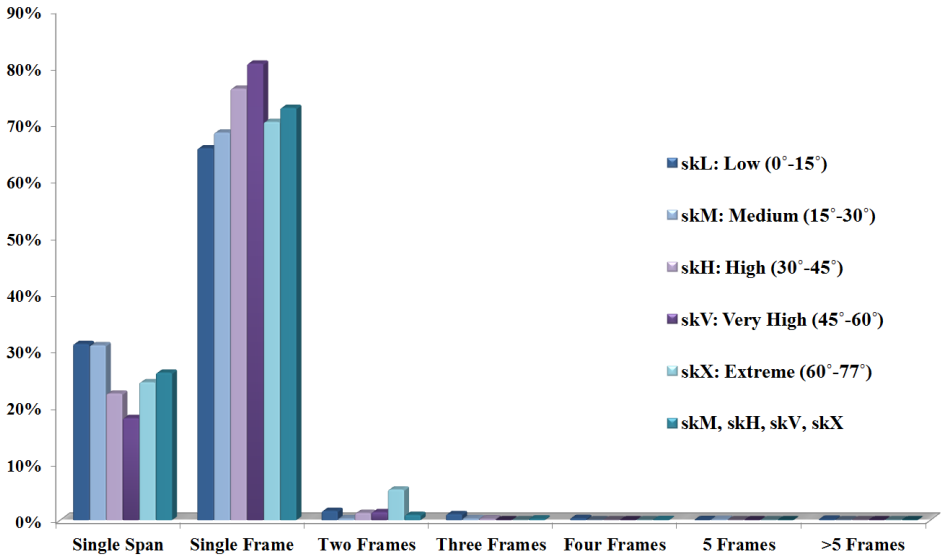

Figure 4.5: Distribution of skewed bridges in each range of skew angle

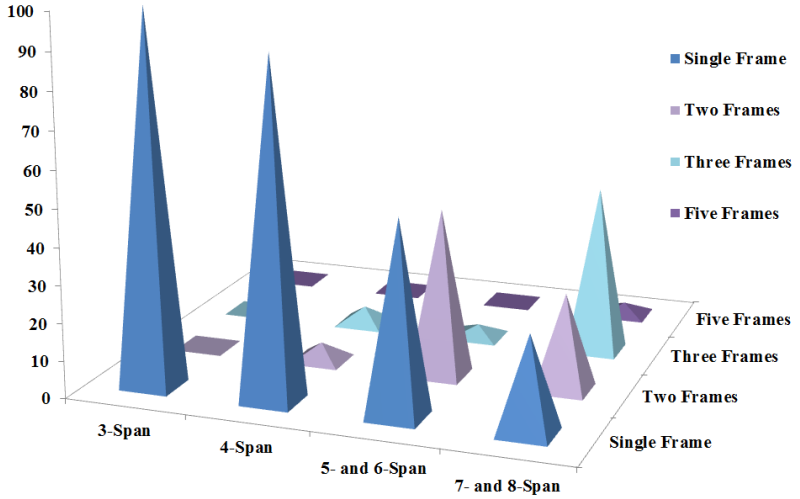

Figure 4.6: Distribution of bridges with unbalanced frames or tall column bents

By evaluating the distribution of irregular bridges and the classification provided in the last section, bridge configurations for the study of the effect of irregularities were selected. The proposed configurations for the study of the class of skewed, unbalanced, and tall bridges are shown in Figure 4.7, Figure 4.8 , and Figure 4.9, respectively.

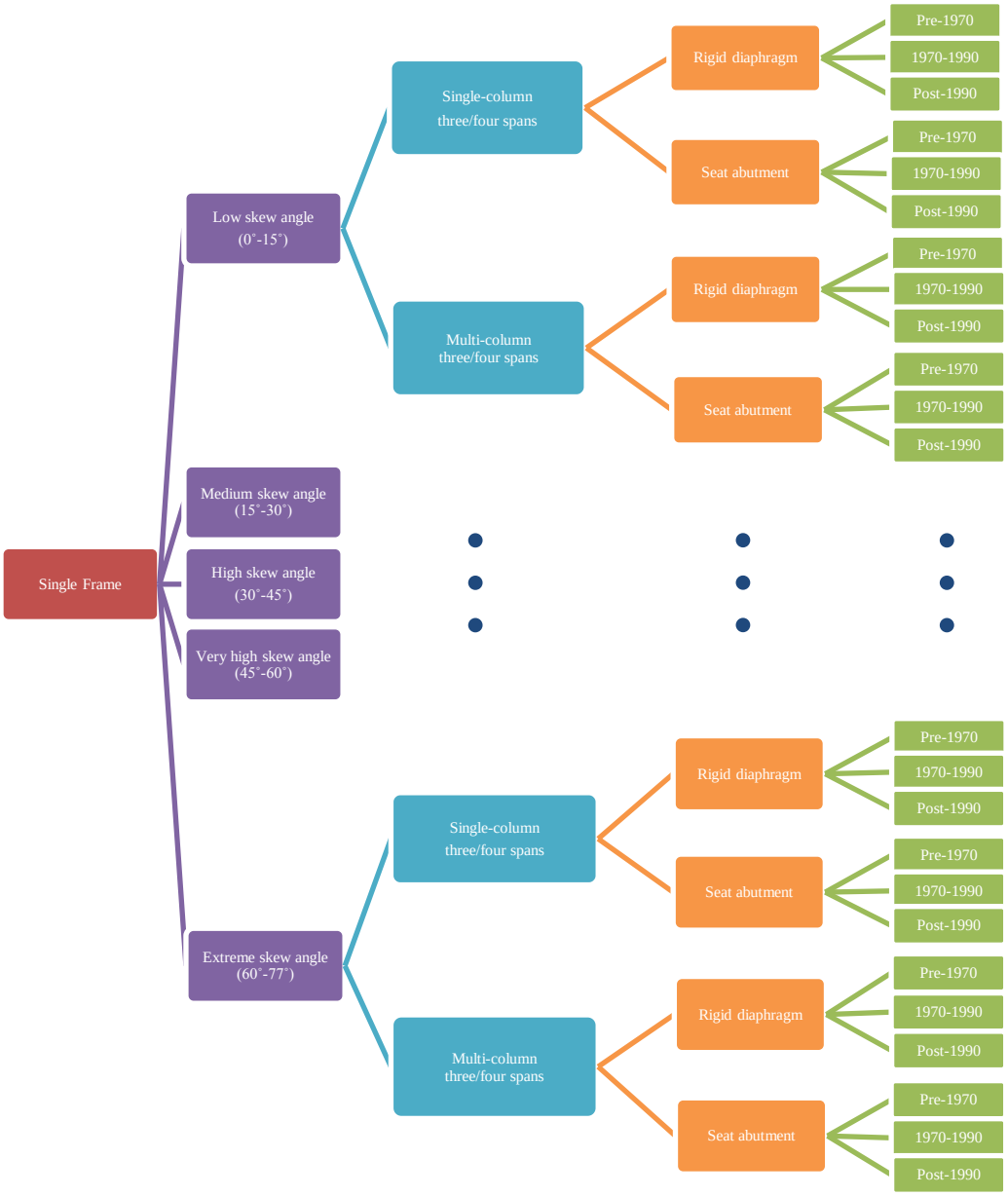

Figure 4.7: Bridges for the consideration of skew

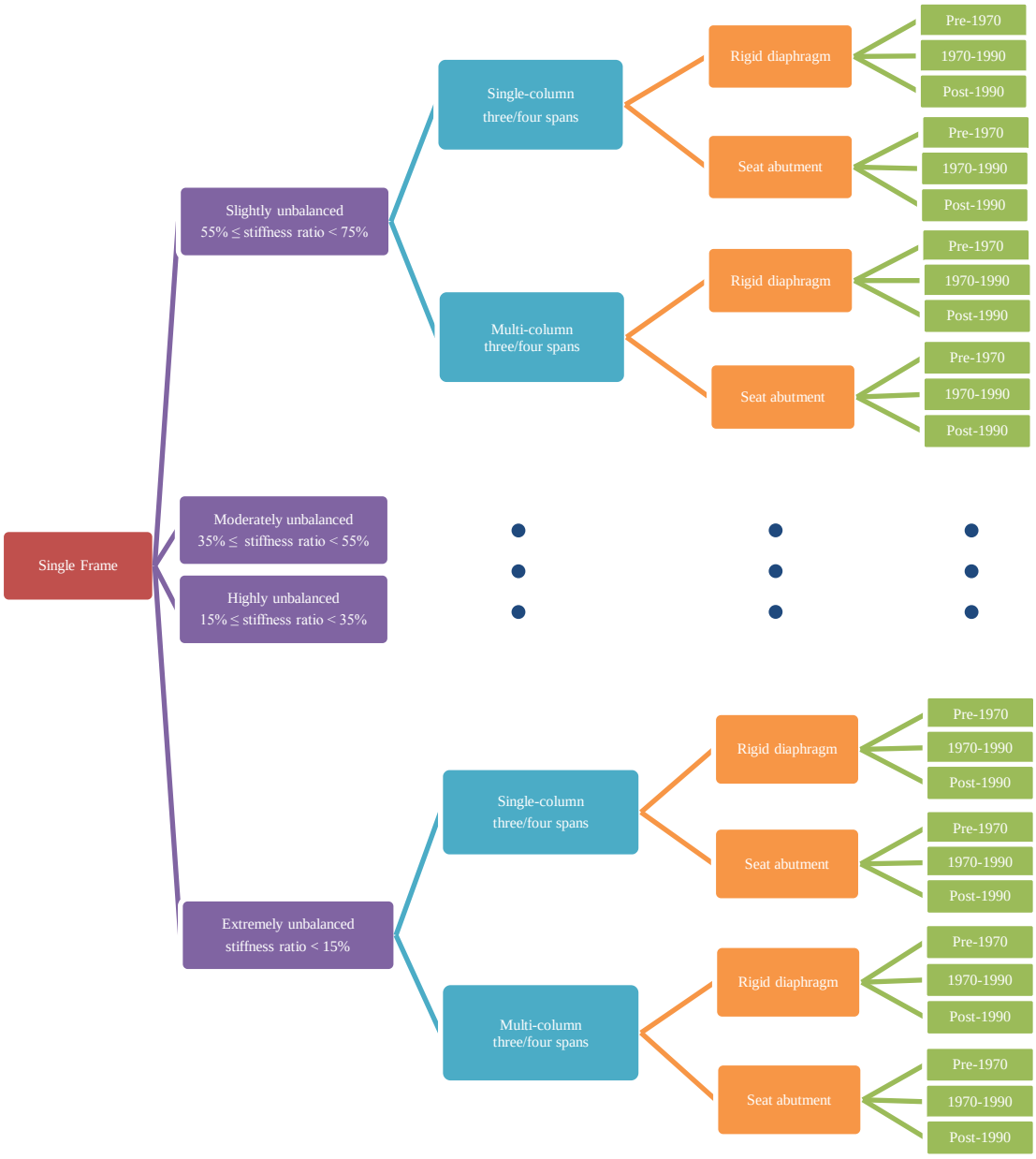

Figure 4.8: Bridges for consideration of unbalanced frames

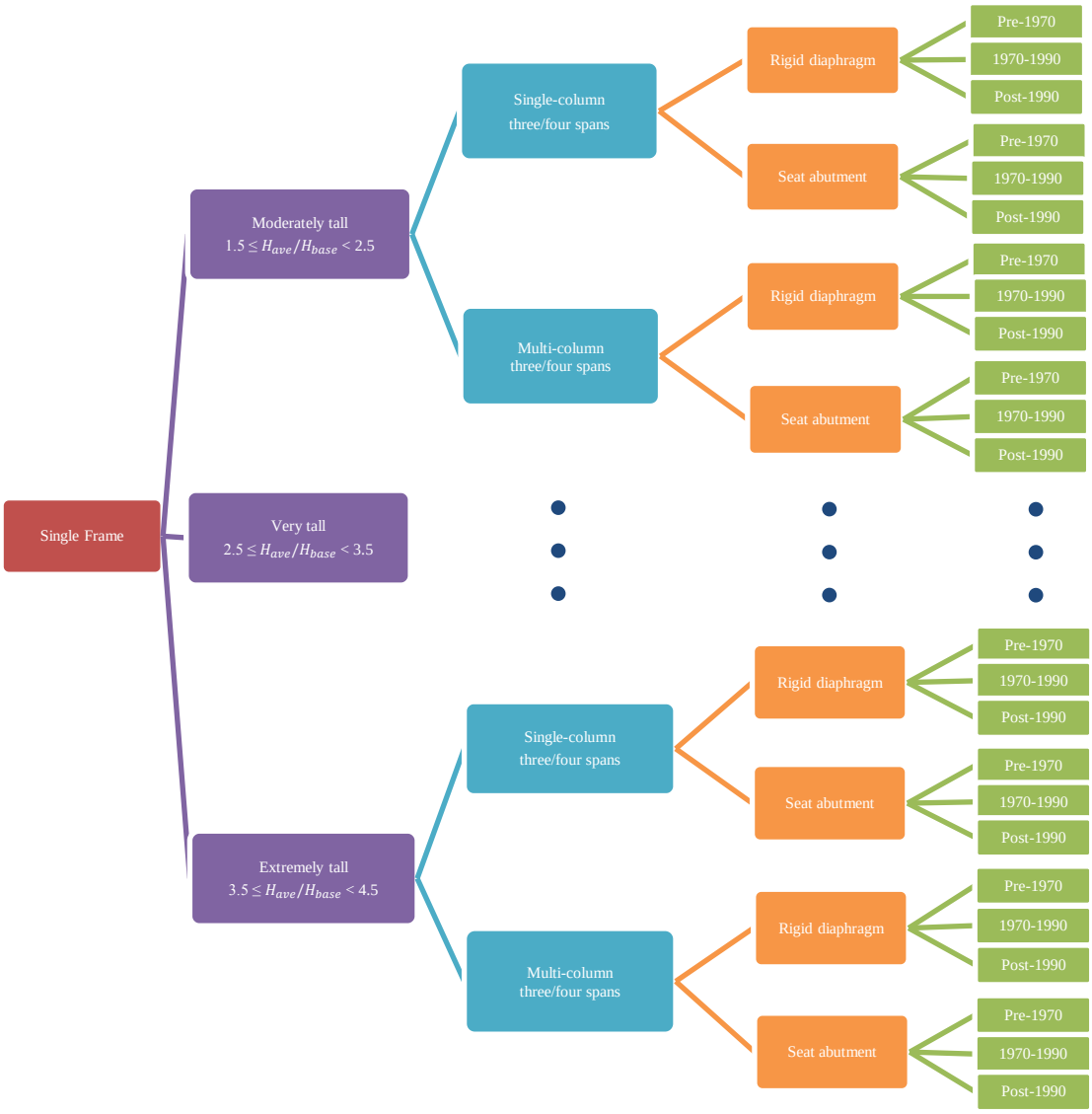

Figure 4.9: Bridges for consideration of tall column bents

A summary of the classification for irregular bridges follows:

- Twelve bridge configurations were identified for developing adjustment factors of skewed bridges. In this study, skew angles are divided into five main ranges: low (0˚-15˚), medium (15˚-30˚), high (30˚-45˚), very high (45˚-60˚), and extreme (60˚-77˚, the maximum value in the database for the existing bridges in California). A total of 60 (12×5=60) permutations is identified for studying skew.

- The selected skewed configurations systematically explore the effect of skew on single-frame seat-type structures for two design eras and two main support types.
- In this study, the column height ratio of tall bridges is divided into three different ranges: moderately tall ($1.5 \leq H_{ave} / H_{base} < 2.5$), very tall ($2.5 \leq H_{ave} / H_{base} < 3.5$), and extremely tall ($3.5 \leq H_{ave} / H_{base} < 4.5$).
- For bridges with unbalanced stiffness frames, four ranges of column height ratios are considered: slightly unbalanced (55% ≤ stiffness ratio < 75%), moderately unbalanced (35% ≤ stiffness ratio < 55%), highly unbalanced (15% ≤ stiffness ratio < 35%), and extremely unbalanced (stiffness ratio < 15%).
- Twelve bridge configurations were specified for evaluating bridges with unbalanced frames and tall column bents. Thirty-six (12×3=36) simulations are required for tall bridges, and 48 (12×4=48) simulations are required for unbalanced frame bridges.

The primary objective of this study is to develop an efficient framework to consider the effects of geometric irregularities in generating seismic demand models and fragility curves. For this purpose, the present work mainly focus on the most common configurations detected for irregular bridges. Based on the provided summary of the classification, in total, 144 permutations are required for the study of irregular bridges. It is apparent that the geometric irregularity is not a common feature in multi-frame bridges; hence this study concentrates on the single-frame bridges as the most common type in the irregular concrete box-girder bridge category.

4.3 Closure

As each class of bridge has a variety of configurations, it is not feasible to perform simulations for all possible combinations of bridge attributes while respecting time and resource constraints. Considering all possible combinations would result in thousands of production runs. Therefore, an initial sensitivity study was performed to keep computational loads reasonable. Explanations of the sensitivity study methodology and findings were provided in this chapter. Eventually, 129 bridge configurations were specified for the box-girder bridge type.

Clearly, it is not feasible to consider all 129 specified regular bridges herein, since each of these bridges needs to be evaluated for the effect of a range of various irregularities, which certainly increases the number of simulations. To address this concern, the list of 129 bridges was filtered based on an identification of the most common bridge configurations for each type of irregularity (i.e., skew, tall column bents, unbalanced frame). Finally, the list of common irregular bridge configurations for consideration in this study was provided.

CHAPTER 5

IDENTIFICATION OF INFLUENTIAL PARAMETERS

Developing probabilistic seismic demand models is a key element in seismic risk assessment of structures such as bridges. Identifying the influential parameters related to the seismic response of a structure is a crucial step toward evaluating its seismic vulnerability. Most previous related sensitivity studies have focused on regular bridges with typical configurations, although observed damage from past earthquakes affirms that, when compared to regular bridges, those with irregularities or geometric inconsistencies in the configuration are more susceptible to noticeable damage. In this chapter, using state-of-the-art statistical methodology, the influence of various parameters on the resulting probabilistic seismic demand is investigated. This study concentrates on concrete box-girder bridges with three geometric irregularity types: (i) skew angle, (ii) a frame with unbalanced stiffness, and (iii) tall column heights; a comprehensive sensitivity of a broad range of probabilistic modeling parameters on the seismic response is assessed. The statistical analysis reveals that the common parameters of ground motion intensity, longitudinal reinforcement ratio, column diameter, number of columns per bent, column height, span length, and concrete compressive strength significantly influence the seismic response of the three studied irregular bridges (Soleimani, et al., 2017). The individual influential parameters affecting each class of irregularity are highlighted and discussed.

The primary objective of this chapter is to improve the understanding of the seismic performance of irregular bridges by using statistical sensitivity studies. This is contrary to the aforementioned studies, which commonly focused on developing regional

assessment algorithms for typical bridges irrespective of the uncertainties existing in irregular configurations. One of the leading steps toward developing a more reliable and realistic seismic fragility framework for irregular bridges is the completion of systematic sensitivity analysis to identify the influential uncertain parameters that are related to key responses. Moreover, this study aims to determine characteristics corresponding to the general configuration of irregular bridges that have the most significant effect on the bridge response. Regression analysis incorporated with hypothesis testing is a popular approach that helps identify the impact of parameters involved in the response. Although the selected parameters in previous studies were commonly selective and quantitative variables, this study evaluates the effect of a more comprehensive list of modeling parameters and includes both quantitative and qualitative ones using statistical tools such as Categorical Regression Analysis, Lasso regression, and partial F-statistics. This study addresses a wide range of irregularities that are found in the existing California bridge inventory. The considered ranges include skew angles varying from zero to 77˚, tall column-height ratios (i.e., the ratio of the average column height of a tall bridge to the average column height of a normal bridge) ranging from 1.5 to 4.5, and an unbalanced frame with stiffness ratios (i.e., the stiffness ratio between different bents within a bridge frame) changing from 75% to lower than 15%. The details of the irregularity ranges are provided in Section 5.1.

This chapter also reviews the general procedure for generating three-dimensional bridge models in OpenSees. An accessible inventory of existing irregular bridges located in California was the basis for establishing bridge component characteristics. This study considers a complete list of uncertain characteristics as input parameters for statistical

analysis. Critical seismic responses serve as outputs of the statistical model and are captured by performing nonlinear time history analysis.

The remainder of the chapter is arranged as follows. In Subsections 5.1.1 and 5.1.2, implemented statistical approaches that deal with both numerical and categorical variables are described. Following that, Subsection 5.1.3 presents the implementation process and Subsections 5.2-5.4 compare the results in three main aspects. First, the effects of parameters are discussed separately for various ranges within each irregularity type. Second, comparisons are made between irregularity types and their associated significant parameters. Third, weights of significant parameters are examined to measure their effectiveness in predicting bridge responses. The chapter concludes by detecting common influential parameters, although the relative significance of the various predictors changes over different bridge responses and irregularity ranges.

5.1 Statistical Analysis Framework

In order to detect the influential parameters on the seismic responses of irregular bridges, this study deals with a problem that involves both numerical and categorical variables. In the following, Categorical Regression Analysis, applicable to the models with only categorical variables, is explained through an illustrative example. Then, a detailed explanation is provided for the Lasso regression that treats categorical variables similarly to the process used in the categorical regression analysis. Later, Lasso regression is implemented to identify the parameter weights in predicting bridge responses.

5.1.1 Categorical Regression Analysis

The majority of regression models focus on variables that are measured with a numerical scale. However, in this study, some of the parameters considered are qualitative (ordinal and categorical) (Table 5.2). Contrary to numerical variables, the effect of categorical variables cannot be estimated using standard regression models. Thus, a categorical regression method is applied herein to incorporate the qualitative variables into the regression model.

The categorical regression method introduces a set of indicator or dummy variables to account for the different levels of a variable, and, even more importantly, to obtain variables in the regression model that have simple interpretations. For example, to introduce the effect of two separate levels of a variable such as abutment type into a binary regression model, an indicator variable is defined as:

$$x = \begin{cases} 0 & \text{if the variable is in category \#1} \\ 1 & \text{if the variable is in category \#2} \end{cases} \quad (1)$$

In some applications, such as design era, the variable is not binary but is multi-categorical. When categorical variables with more than two levels are included in a regression model, additional steps are required to ensure consistency and interpretability of the results. These steps consist of recoding categorical variables into a number of separate variables. Hence, in a general case, a variable with k possible levels of category is modeled by $k - 1$ indicator variables. For example, if a categorical variable X has five levels, then it will be transformed into four separate variables $(x_1, \dots, x_4)$ that will be used in the multiple regression model and contain the same information as the initial single categorical variable. The indicator variables are assigned either zero or unit values, representing each level of the category. Thus, the binary coding takes the following form:

$$x_i = \begin{cases} 1 \text{ if the variable is in category i} \\ 0 \text{ otherwise} \end{cases}, \quad (2)$$

where $i = 1, \ldots, k-1$, and the k^{th} category is selected as the reference. In this approach, indicator variables can be included in the hypothesis testing, similar to any other variable. Their mean differences can be estimated with a linear model by representing groups with a set of $k-1$ variables, where k is the total number of groups. An alternate coding approach is using -1 and 1 instead of 0 and 1. The only difference between these two coding strategies is raised in the interpretation.

According to this standard, when the response y depends solely on one categorical variable, X, the predictor is modeled by multiple dummy variables as

$$E(y) = \beta_0 + \beta_1 x_1 + \cdots + \beta_{k-1} x_{k-1}. \quad (3)$$

Interpretation of this categorical model follows directly from determining the response for different categories of X. If the model is in the k^{th} category, $E(y) = \beta_0$, which means the intercept in the categorical regression model represents the expected response for the reference category (i.e., the k^{th} level). If the model is in the i^{th} category, then $E(y) = \beta_0 + \beta_i$, which means each slope β_i in the model indicates the increase or decrease of the expected response in comparison to the reference category k. Hence, the results can be interpreted as the change in the expected transition from one category to another.

The categorical regression analysis yields a model that is mathematically identical to analysis of variance (ANOVA), with similar interpretations and statistical inferences. Consequently, the categorical regression weights are equal to the ANOVA mean differences. Both of these techniques retain the information on how the k groups differ from one another, which determine the influence of the parameters considered.

5.1.2 Lasso Regression

Conventional regression techniques typically follow the standard least squares framework by considering all possible covariates in the model, in spite of the fact that the resulting estimates are not often satisfactory. The first concern is associated with the prediction accuracy, as the estimates generated by the least squares method can have large variances. The second challenge relates to the interpretation of the developed regression model, which is intricate when a model has a large number of predictors.

In order to address these problems, approaches known as the variable subset selection techniques (Miller, 2002; John, et al., 1994) are applied. These techniques, such as Best-Subset Selection (Hocking & Leslie, 1967), Forward-Stagewise Regression (Hastie, et al., 2007), and Forward-Stepwise and Backward-Stepwise Selection (Derksen & Keselman, 1992), improve the prediction accuracy. Generally, the subset selection reduces the variance of the estimates and prunes some of the predictors with less impact on the overall regression model. Although these techniques produce improved models, they utilize a discrete process in which a variable is either retained or discarded. As a result, these techniques may perform poorly at reducing the prediction error of the full regression model.

Shrinkage methods (Tibshirani, 1996) use a continuous process rather than the discrete scheme, which noticeably reduces the variance and the prediction error. These methods minimize the residual sum of squares subject to a constraint on the magnitude or the cardinality of the coefficients, which is their main distinction from the previously mentioned approaches. Such restriction controls the model complexity, which subsequently controls the variance of the predicted values and improves the overall

prediction accuracy. Ridge Regression and Lasso Regression are among the most well-known shrinkage techniques, although Lasso surpasses Ridge in several aspects that are explained further. A more comprehensive study and comparison of these methods is presented by James, et al. (2013).

Lasso (Least Absolute Shrinkage and Selection Operator) is a robust statistical regression technique. It is mainly applicable to the problems that arise from having a large number of covariates from which the influential set must be determined. Consider y_i as the i^{th} response that depends upon the variables x_{ij} , $i = 1, \dots, n$ and $j = 1, \dots, p$, where n and p denote the number of collected data for the response and the number of regressors, respectively. Lasso estimates the coefficients of the regression model through the convex constrained minimization

$$\hat{\beta}^{Lasso} = \underset{\beta}{\operatorname{argmin}} \sum_{i=1}^{n} \left(Y_i - \beta_0 - \sum_{j=1}^{p} x_{ij}\beta_j \right)^2 , \text{ Subject To: } \sum_{j=1}^{p} |\beta_j| \leq \text{t (constant)}, \quad (4)$$

which minimizes the residual sum of squares, subject to an ℓ_1-norm constraint on the coefficients. Such constraint is shown to promote sparsity among β coefficients.

This problem has an equivalent matrix form

$$\hat{\beta}^{Lasso} = \underset{\beta}{\operatorname{argmin}} \{ \underbrace{\|\mathbf{Y} - \mathbf{X}\boldsymbol{\beta}\|_2^2}_{\text{Loss term}} + \underbrace{\lambda \|\boldsymbol{\beta}\|_1}_{\text{Penalty function}} \} , \quad (5)$$

where X , Y , and β are the matrix form of regressors x_{ij}, vector of responses y_i, and vector of regression coefficients, respectively. The tuning parameter λ is directly related to the constant t and controls the generated models, such that when λ is sufficiently large, t is equivalently small.

The advantage of using Lasso over Ridge Regression is related to the penalty function, which is the source of difference between their performances. In this regard,

Lasso applies an ℓ_1-norm penalty on the coefficient vector β (i.e., $\|\beta\|_1 = \sum_{j=1}^{p}|\beta_j|$), while Ridge imposes an ℓ_2-norm constraint on β (i.e., $\|\beta\|_2 = \sum_{j=1}^{p}\beta_j^2$). Thanks to the geometric structure of the ℓ_1-ball, the coefficient estimates of the parameters x_{ij} with the least impact on the response y_i are forced to be exactly zero.

Figure 5.1 shows the geometrical illustration of Equation 5 and the interpretation of the Lasso and Ridge Regression constraints for a model with two parameters. Technically speaking, the first point of contact between a sub-level set of the loss and the penalty ball characterizes the optimal solution. This initial contact point can be located at a corner of the diamond-shaped Lasso region and thus one of the two coefficients vanishes to zero. As the number of parameters directly affects the number of corners in the Lasso penalty ball, an increase in the problem dimension increases the possibility of more vanishing coefficients. This phenomenon is unlikely to occur in the case of Ridge Regression, simply because of the rounded boundary of the penalty ball.

A critical step in solving a problem using Lasso Regression is finding the optimum value for the tuning parameter λ. In the extreme limit, $\lambda = 0$ reduces the problem to the least square problem, while increasing λ increases the sparsity of the resulting coefficients, until a null model is obtained. In this study, the typical ten-fold cross-validation is performed to determine the optimum value of λ for which the error calculated by the cross-validation method is smallest (Tibshirani, 1996; James, et al., 2013; Vidakovic, 2011).

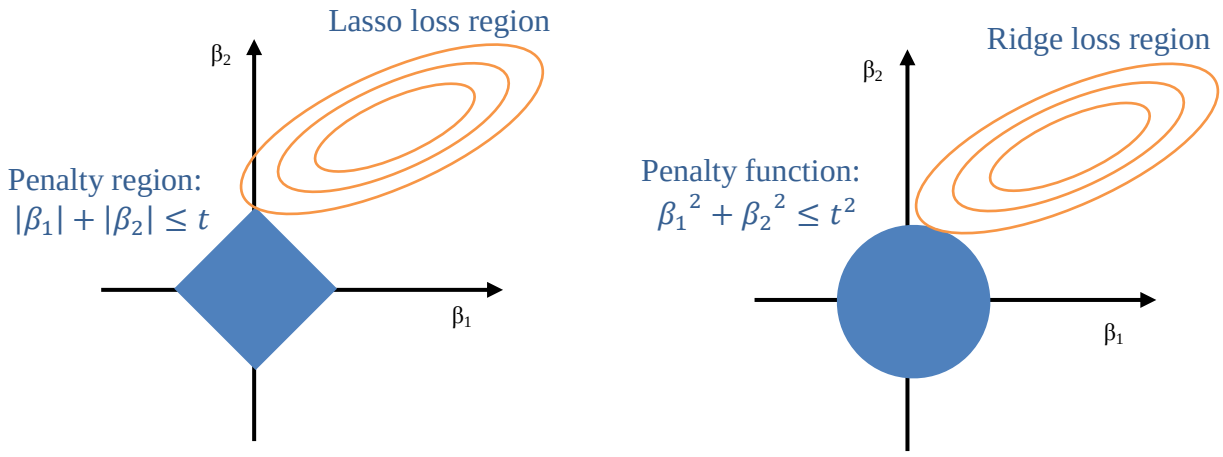

Figure 5.1: Illustration of equation 6 and the difference between the constraints of Lasso and Ridge

5.1.3 Implementation of Statistical Methods

Numerical Modeling of Bridges

For the purpose of this study, the single-frame box-girder concrete bridge type was selected, and OpenSees was used to develop three-dimensional numerical models. To incorporate the uncertainty into the numerical modeling of bridges, probabilistic geometric and material parameters (Ramanathan, 2012) were selected for the numerical simulations. Figure 5.2 illustrates the general layout of the numerical modeling of bridges. The incorporation of skew into the analytical modeling of straight bridges necessitates various modifications, including recently-developed modeling strategies based on the experimental and numerical studies of skewed bridges (Shamsabadi & Rollins, 2014; Kaviani, et al., 2012) discussed in Chapter 3. In this study, skew angles are divided into 5 ranges: low (0˚-15˚), medium (15˚-30˚), high (30˚-45˚), very high (45˚-60˚), and extreme (60˚-77˚), which is noted as the maximum value in the database for the existing bridges in California. In the simulation process, skew angles are distributed uniformly in each range and assigned randomly to the bridge samples.

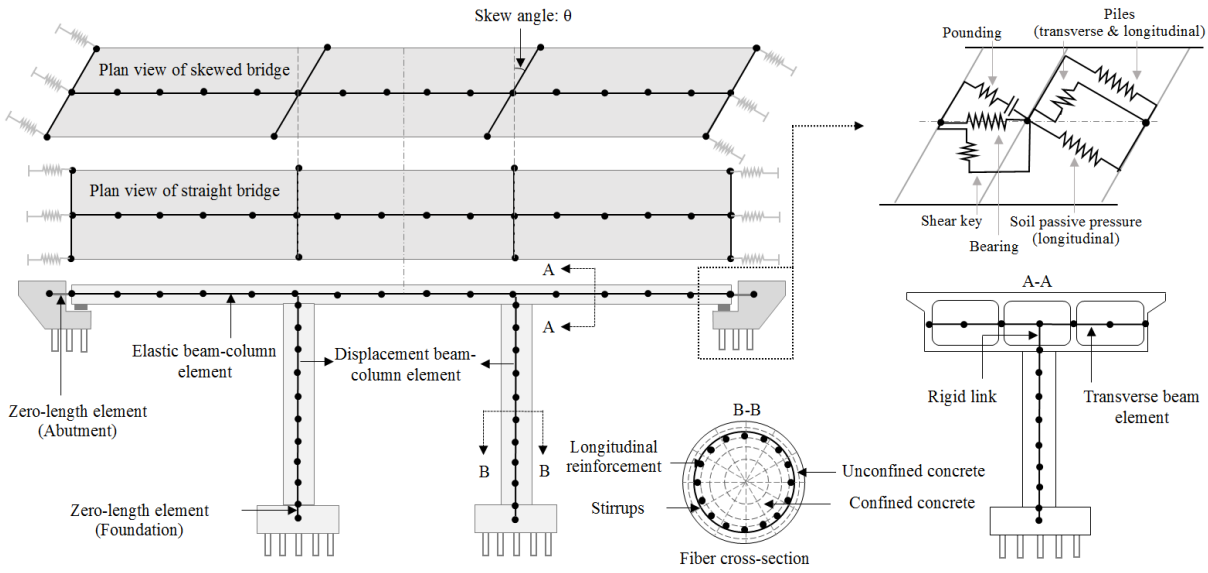

Figure 5.2: Typical layout of a single-frame, three-span, box-girder bridge

To date, limited research exists regarding bridges with tall column bents and a frame with unbalanced stiffness. Likewise, to the best of the authors' knowledge, there are no data sets from experiments on these classes of bridges. Therefore, the only change that is considered in the present study for modeling bridges with unbalanced frames and tall column bents is the variation of the column heights. In this regard, four groups of California box-girder bridge plans (stream crossings, ramps, connectors, and viaducts) were reviewed in detail to extract column height values in order to have a comprehensive database. The overall goal of this step was to set up a realistic sample of unbalanced or tall bridge profiles to use for creating synthetic unbalanced and tall bridge realizations in the analytical modeling of bridges. The average column heights (H_{ave}) of unbalanced or tall bridges were normalized by the average column heights (H_{base}) of the base models (i.e., regular bridges with normal column heights and balanced stiffness frames). Those ratios of H_{ave}/H_{base} which meet the column heights criteria to be considered as tall bridges (i.e., ratios higher than 1.5) are used to build the models for this class of bridges.

As an example, the ratios for bridges designed in the Pre-1971 era are shown in Figure 5.3a. The column height ratio of tall bridges is divided into three different ranges, as shown in Figure 5.3b, including: moderately tall ($1.5 \leq H_{ave}/H_{base} < 2.5$), very tall ($2.5 \leq H_{ave}/H_{base} < 3.5$), and extremely tall ($3.5 \leq H_{ave}/H_{base} < 4.5$).

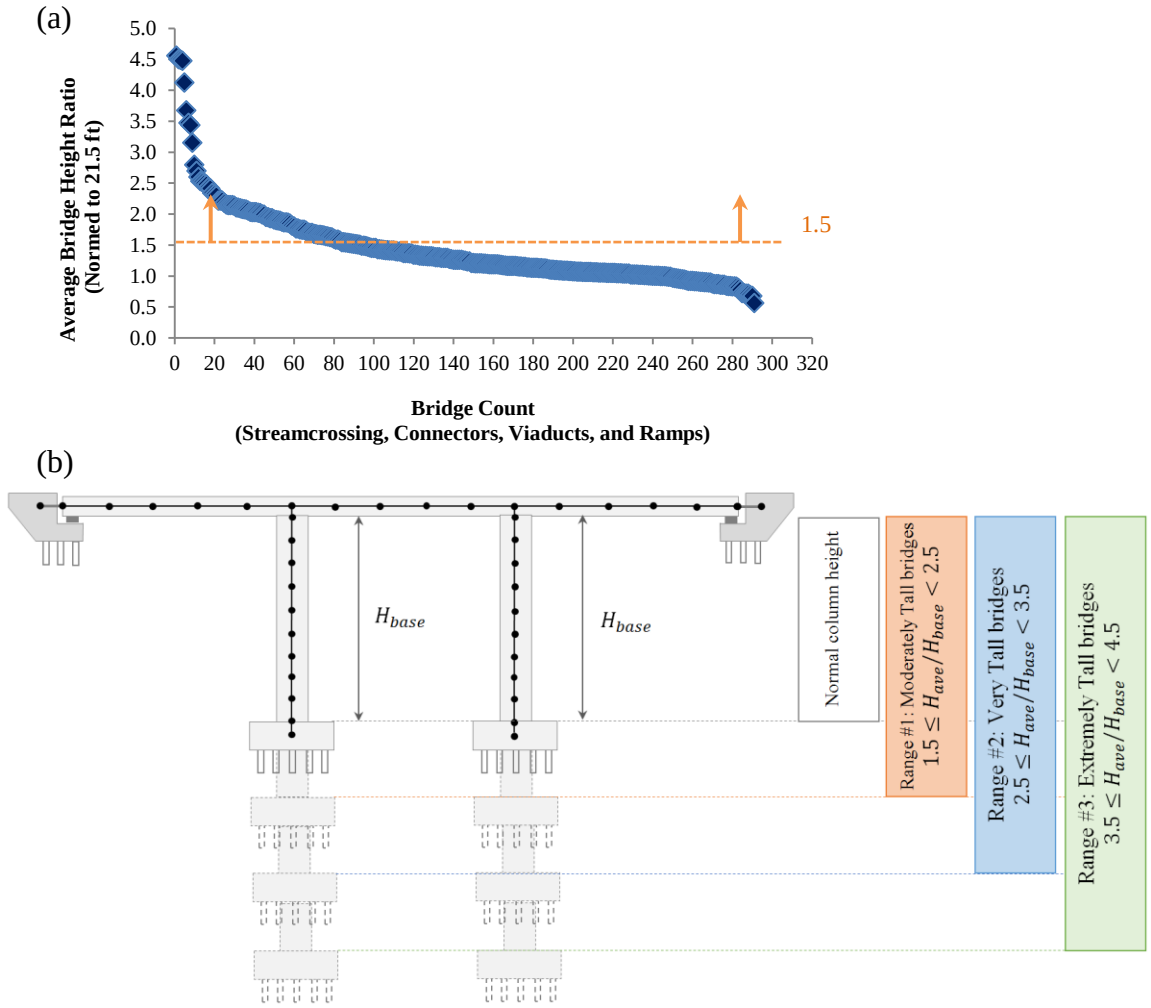

Figure 5.3: (a) Average bridge column height ratios for bridges designed in Pre-1971; (b) Considered configurations for tall bridges

A single column-height-ratio is developed by normalizing the height of all the columns in a bridge ($H_i\,; i = 1, \ldots, n$ and $n =$ number of columns in a bridge) to the bridge-average-height (H_{ave}). This yields ratios (H_i/H_{ave}) for each bridge that are centered on 1, but values extend both above and below the center (Figure 5.4a). Based on

the Caltrans Seismic Design Criteria (Caltrans, 2006), a bridge is defined as having a frame with unbalanced stiffness when different bents within the frame have a stiffness ratio of less than 75%. Since stiffness is a function of modulus of elasticity, moment of inertia, and column height, the criteria assigned to the stiffness ratio of an unbalanced frame can be converted to a criterion for the column heights, by assuming similar modulus of elasticity and moment of inertia for different bents in a frame. This criterion is converted to column height ratios by normalizing the short (H_1) and tall (H_2) column heights of a bridge by the average column height, as shown in Figure 5.4b. The ratios of H_1/H_{ave} and H_2/H_{ave} are calculated as 0.95 and 1.05, respectively. Thus, the respective ratios (i.e., higher than 1.05 and lower than 0.95, Figure 5.4a) are implemented in the modeling of bridges with unbalanced frames. For bridges with unbalanced stiffness, four ranges of column height ratios are considered, as shown in Figure 5.4b: slightly unbalanced (55% $\leq$ stiffness ratio < 75%), moderately unbalanced (35% $\leq$ stiffness ratio < 55%), highly unbalanced (15% $\leq$ stiffness ratio < 35%), and extremely unbalanced (stiffness ratio < 15%). The corresponding column height ratios for the short column H_1/H_{ave} and for the tall column H_2/H_{ave} are provided in Figure 5.4b.

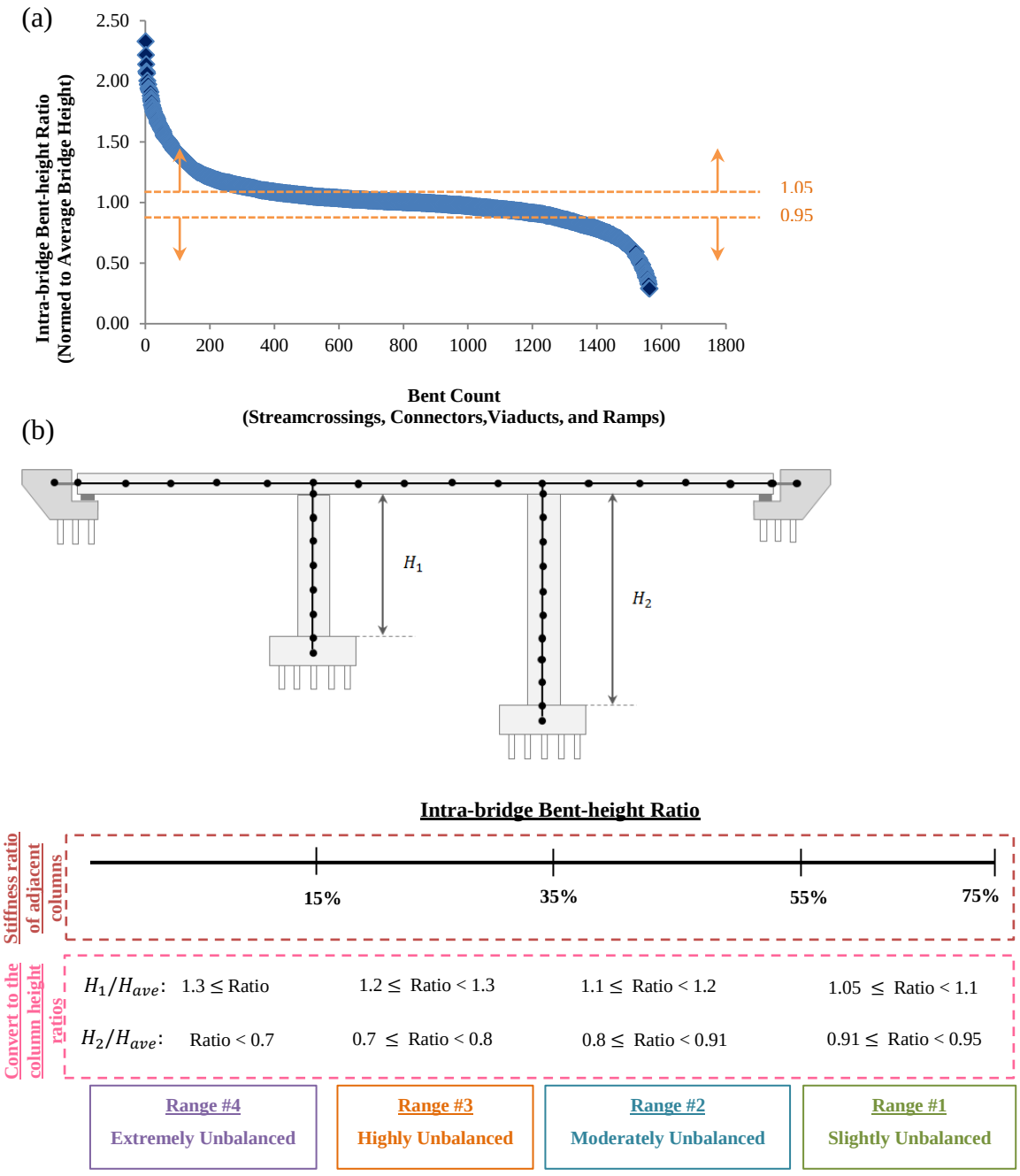

Figure 5.4: (a) Intra-bridge bent-height ratios for bridges designed in Pre-1971; (b) Considered configurations for bridges with unbalanced stiffness frame

Statistical Parameters

Table 5.1 summarizes the various levels of irregularities discussed above. The three-dimensional bridge models were created in OpenSees for each level of irregularity,

two types of abutments (i.e., rigid diaphragm and seat-abutment types), and the specifications of various design eras. The bridge deck elements were typically modeled using elastic beam column elements, as the bridge deck remains elastic during earthquake. The bridge columns were modeled using displacement beam column elements with fiber cross-sections (Soleimani, et al., 2016). The column elements are connected to the deck elements and bridge footing by rigid links and foundation springs, respectively. More details about numerical modeling of box-girder bridges, including details of modeling of pounding and bearing elements, can be found in the previous studies (Nielson & DesRoches, 2006; Ramanathan, 2012) and Chapter 3 of this study.

The statistical parameters in this study can be classified into two main groups of categorical and numerical parameters. In this study, $S_{a\text{-}1.0s}$ (i.e., the spectral acceleration at 1.0 second) was assigned to the first potential predictor X_1 and chosen as the measure of the ground motion intensity, since it has been found to be the optimal intensity measure for classes of box-girder bridges (Ramanathan, 2012). The associated parameters of the two groups are listed in Table 5.2. To incorporate the uncertainty into the numerical modeling of bridges, probabilistic geometric and material parameters were selected for the numerical simulations (Table 5.3). The column height values and the distribution parameters are listed in Table 5.4. All column height values follow the lognormal distribution.

Table 5.1: Summary of the considered ranges for irregularity parameters

Irregular Parameters	Levels
Skew	Low, Medium, High, Very high, Extreme
Tall	Moderately Tall, Very tall, Extremely tall
Unbalanced	Slight, Moderate, High, Extreme

Table 5.2: Description of the potential predictors for the statistical analysis

	Parameter	Categories	Assigned Variable
Categorical Input Parameters	Abutment type	Rigid diaphragm, seat	X_2
	Design era	Pre-1971, 1971-1990, Post-1990	X_3
	Number of columns per bent	Single, Two, Three, Four, Five	X_4
	Soil type	Clay, Sand	X_5
	Superstructure box type	Reinforced concrete, Pre-stressed concrete	X_6
	Number of box cells	Three, Five, Seven, Nine, Eleven, Fifteen	X_7
	Direction of applied excitation	Longitudinal, Transverse	X_8

	Parameter	Unit	Assigned Variable	Parameter	Unit	Assigned Variable
Numerical Input Parameters	Span length	(ft)	X_9	Restrainer yield deformation	(in)	X_{27}
	Column height	(ft)	X_{10}	Number of restrainers	N/A	X_{28}
	Deck width	(ft)	X_{11}	Concrete compressive strength	(ksi)	X_{29}
	Girder spacing	(in)	X_{12}	Reinforcing steel yield strength	(ksi)	X_{30}
	Top flange thickness	(in)	X_{13}	Shear key capacity	(kip)	X_{31}
	Bottom flange thickness	(in)	X_{14}	Multiplicative factor for coefficient of friction of bearing pads	N/A	X_{32}
	Wall thickness	(in)	X_{15}	Shear modulus of elastomeric bearing pads	(ksi)	X_{33}
	Depth of superstructure	(in)	X_{16}	Transverse gap between deck and shear keys	(in)	X_{34}
	Column diameter	(in)	X_{17}	Longitudinal gap between deck and abutment	(in)	X_{35}
	Longitudinal reinforcement ratio	N/A	X_{18}	Pile stiffness	(kip/in)	X_{36}
	Confinement spacing	(in)	X_{19}	Mass factor	N/A	X_{37}
	Abutment backwall height	(ft)	X_{20}	Damping	%	X_{38}
	Pile spacing	(ft)	X_{21}	Ground motion time step	(sec)	X_{39}
	Foundation translational stiffness	(kip/in)	X_{22}	Skew angle	(degree)	X_{40}
	Foundation rotational stiffness	(kip-in/rad)	X_{23}	Tall ratio	N/A	X_{41}
	Restrainer length	(ft)	X_{24}	H1_ratio	N/A	X_{42}
	Initial slack in restrainer cable	(in)	X_{25}	H2_ratio	N/A	X_{43}
	Restrainer stiffness	(kip/in)	X_{26}			

Table 5.3: Distribution of modeling parameters (source: review of bridge plans and Ramanathan **(2012)**)

Parameter	Unit	Distribution	Distribution parameters	
			Factor 1*	Factor 2**
Span length	(ft)	Empirical	114.8	40.5
Deck width	(ft)	Empirical	67.2	42.2
Girder spacing	(in)	Empirical	114	39.4
Top flange thickness	(in)	Empirical		
Reinforced concrete			8.4	1.1
Pre-stressed concrete			8.2	1.0
Bottom flange thickness	(in)	Uniform	4.5	6.5
Wall thickness	(in)	Uniform	10	12
Depth of superstructure	(in)	Uniform		
Reinforced concrete		Uniform	0.055* Span length	0.06* Span length
Pre-stressed concrete		Uniform	0.04* Span length	0.045* Span length
Column diameter	(in)	Randomly assign 25% of simulation to each 48, 60, 66, 72		
Longitudinal reinforcement ratio	N/A	Uniform		
Pre-1970 design era			1.4	2.4
1970-1990 design era			1.0	3.7
Post-1990 design era			1.0	3.5
Confinement spacing	(in)	Uniform		
Pre-1970 design era			Spacing: 12 in	
1970-1990 design era			0.3	0.9
Post-1990 design era			0.4	1.7
Abutment backwall height	(ft)	Uniform	3.5	8.5
Pile spacing	(ft)	Uniform	5.5	7
Foundation translational stiffness	(kip/in)	Normal		
Single column - 6 ft dia column 1% long. steel			1700	800
Single column - 6 ft dia column 3% long. steel			1400	600
Multi-columns - 3 ft dia column 1.5% long. steel			800	600
Foundation rotational stiffness	(kip-in/rad)	Normal		
Single column - 6 ft dia column 1% long. steel			$4.1x10^7$	$1.2x10^7$
Single column - 6 ft dia column 3% long. steel			$6.5x10^7$	$1.0x10^7$
Multi-columns - 3 ft dia column 1.5% long. steel			0	0
Restrainer length	(ft)	Uniform	8	20
Initial slack in restrainer cable	(in)	Uniform	0.25	1.0
Restrainer stiffness	(kip/in)	Uniform	32.5	13.0
Restrainer yield deformation	(in)	Uniform	1.5	3.5
Number of restrainers	N/A	Uniform	8	50
Concrete compressive strength	(ksi)	Normal	5.0	0.63
Reinforcing steel yield strength	(ksi)	Lognormal	4.21	0.08
Shear key capacity	(kip)			
Multiplicative factor for coefficient of friction of bearing pads	N/A	Lognormal	0	0.1
Shear modulus of elastomeric bearing pads	(ksi)	Uniform	80	250
Transverse gap between deck and shear keys	(in)	Uniform	0	1.5
Longitudinal gap between deck and abutment	(in)	Uniform	0	6.0
Pile stiffness	(kip/in)	Lognormal	80	0.3
Mass factor	N/A	Uniform	1.1	1.4
Damping	%	Normal	0.045	0.0125

*, ** Factors 1 and 2 represents the mean and standard deviation for normal, lognormal, and empirical distributions; lower bound and upper bound for uniform distribution

Table 5.4: Uncertainty distribution parameters for the column height according to the bridge inventory

Parameter	Design era	Min	Max	Mean	Standard deviation
Normal column heights	Pre-1971	16.40 (ft)	28.20 (ft)	3.068	0.136
(H_{base})	1971-1990	16.50 (ft)	32.80 (ft)	3.147	0.171
	Post-1990	16.80 (ft)	37.10 (ft)	3.218	0.198
Ratio for tall column heights	Pre-1971	0.56	4.56	0.715	0.267
(H_{ave}/H_{base})	1971-1990	0.65	4.17	0.729	0.237
	Post-1990	0.49	3.97	0.697	0.232
Ratio for unbalanced frames	Pre-1971	0.29	2.33	-0.005	0.237
(H_i/H_{ave})	1971-1990	0.37	1.69	-0.023	0.208
	Post-1990	0.23	2.34	0.0005	0.270

Seismic Analysis

In order to perform seismic analysis, 160 sets of ground motions selected by Baker (2011) for probabilistic seismic response assessment of bridges in California were adopted in this study to cover a range of ground motion intensity levels and characteristics. For each of the required finite element models discussed earlier, 160 numerical bridge models were generated by sampling across the distribution of the modeling parameters using Latin Hypercube Sampling. Then, the generated bridge models and the ground motions were paired randomly. Nonlinear time history analysis (NLTHA) was performed on the bridge models, with 11,520 simulations in total; the simulations considered twelve irregularity levels with reference to the levels listed in Table 5.1, two abutment types, and three different design eras (Table 5.2). The analysis results provided the seismic response of each bridge component, and the peak responses were commonly used to develop the PSDMs. The seismic responses monitored in NLTHA are listed in Table 5.5, and the impact of variables is evaluated on each of these responses individually.

The statistical techniques explained in the previous sections assume a linear relationship between the response and predictors. However, Cornell, et al. (2002) proved that the relationship between the bridge seismic response (S_D) and the ground motion intensity (IM) is expressed as a power function $S_D = a(IM)^b$. In logarithmic scale, this regression is converted to a simple linear model $\ln(S_D) = \ln(a) + b\ln(IM)$ where $\ln(a)$ and b are the regression coefficients. Therefore, in this study, in order to implement the statistical techniques, the logarithmic format needed to be considered for the relationship between the bridge responses (e.g., column curvature ductility φ) and the potential predictors (e.g., column height). To extract the effect of various parameters in this study (Table 5.2), seismic demands ($\ln(Y_i)$) shown in Table 5.5 are regressed against the ground motion intensity ($X_1 = \ln(IM)$) as well as the remaining predictors ($X_2, \dots, X_{43}$) that are considered in the transformed logarithmic form. In the following sections, the results of the sensitivity studies are presented to determine the effect of each parameter on the bridge responses.

Table 5.5: Seismic demand of various components of a bridge

Component	Engineering Demand Parameter	Units	Assigned Variable
Columns	Curvature	$(\text{in})^{-1}$	Y_1
Deck	Displacement	(in)	Y_2
Foundation rotation	Rotation	(radian)	Y_3
Foundation translation	Displacement	(in)	Y_4
Active abutment displacement	Displacement	(in)	Y_5
Passive abutment displacement	Displacement	(in)	Y_6
Transverse abutment displacement	Displacement	(in)	Y_7
Elastomeric bearing pads	Displacement	(in)	Y_8
Shear key	Displacement	(in)	Y_9

Implementing Lasso regression, a sensitivity study was completed to assess the effect of varying the entire list of modeling covariates (Table 5.2) on the responses of key bridge components, including columns, abutments, and bearings (Table 5.5).

In order to assess the influence of potential predictors, a sensitivity analysis was performed on each irregularity range individually. For example, for the case of unbalanced bridges, analysis was conducted for each of the four different ranges of column heights: slightly, moderately, highly, and extremely unbalanced. The results for each range are discussed in Section 5.2. These results provide insights as to which categorical and numerical bridge parameters are most important for predicting the seismic response of irregular bridges, and whether the set of predictors changes as the *level of irregularity* (e.g., angle of skew) changes. Additionally, to provide an overall perspective of irregular bridge performance, another analysis was performed by considering all different ranges of irregularities in a single group. In this case, the results of the family of tall, unbalanced, and skewed bridges can be compared to identify which predictors are more important for different *types of bridge irregularity*. Corresponding findings are discussed in Section 5.3, while the order of importance for the detected influential parameters for different types of bridge irregularity is discussed in Section 5.4.

5.2 Analysis of the Results for Various Levels of Irregularity

A detailed investigation of the results for each irregularity range is discussed in this section. The findings presented in this section benefit structural engineers working in the design or retrofit fields by enhancing their understanding of irregular bridge performances, particularly for each range of irregularity. Selected results are shown in the

tables (Table 5.6, Table 5.7, and Table 5.8), while a comprehensive list of findings is provided in the content of the following subsections. The evaluated responses and the potential predictors are listed in rows and columns, respectively. The shaded cells indicate that the parameter located in that column is identified as an important predictor for estimating the response in the corresponding row. In all cases, the ground motion intensity measure is identified as a certain predictor, as was anticipated according to previous studies (Cornell, et al., 2002; Ramanathan, 2012).

Tall bridges

As explained earlier, three different ranges of tall bridges are investigated in this study. The impact of parameters on the responses is varies among ranges of moderately tall, very tall, and extremely tall bridges. An example of results for the extremely tall level is shown in Table 5.6.

Eliminated parameters from all responses in all three ranges of the tall bridge family are the superstructure box type and the wall thickness. In addition, the restrainer length and the restrainer yield deformation are among the eliminated list of parameters for the very tall bridges. The least important parameters, defined here as those which contribute to only one of the bridge responses, are:

- girder spacing and restrainer stiffness, for moderately tall bridges;
- superstructure type, top flange thickness, and reinforcing steel yield strength, for very tall bridges;
- superstructure type, bottom flange thickness, restrainer stiffness, and the initial slack in restrainer, for extremely tall bridges.

The results indicate that most important parameters for predicting the bridge response for three tall ranges are the mass factor, the normal column height, and the tall ratio. The last two define the bridge column dimension. The following parameters are also identified among the influential parameters for most cases: the abutment backwall height for all responses of moderately tall and very tall bridges; the soil type for extremely tall bridges; and the pile spacing for moderately tall bridges.

Table 5.6: Identified influential parameters for extremely tall bridges

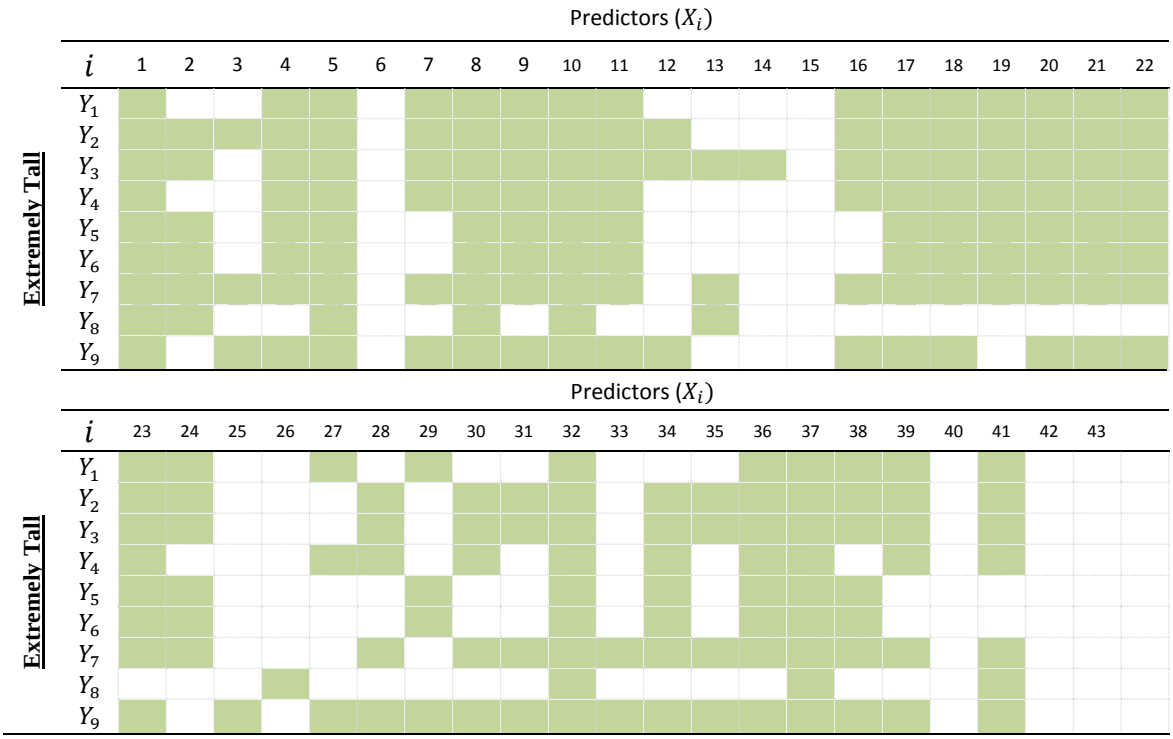

Several parameters are found to be influential in predicting all responses except bearing displacement. The list includes:

- number of columns per bent, span length, deck width, column diameter, and foundation translational and rotational stiffness, for all three ranges;
- abutment backwall height, for extremely tall bridges;

- ground motion time step, for moderately tall and very tall bridges;
- pile stiffness and pile spacing, for very tall and extremely tall bridges.

Aside from the overall bridge response, a number of parameters are highlighted in tables because of their influence on specific responses. As an example, the number of cells affects deck displacement and foundation translation and rotation in all three categories of tall bridges. The direction of applied ground motion is a certain predictor for all responses of extremely tall bridges; however, in the case of very tall and moderately tall bridges, it affects only some of the responses, including column curvature, deck displacement, foundation translational and rotational responses, and transverse abutment response. This shows the sensitivity of bridge responses varies with changes in the irregularity range. In another case, even though damping ratio affects moderately tall bridge responses, it shows less impact as the tall ratio increases. Likewise, the influence of parameters depends on the regarded bridge responses. For instance, the superstructure depth is recognized as a predictor for column curvature ductility, deck displacement, foundation translation and rotation, and transverse abutment response, while it is not listed as an identified predictor of shear key and bearing displacement. Another example is the shear key capacity, which mostly controls the shear key response, transverse abutment displacement, and foundation translation in all irregularity ranges; however, this variable rarely affects the other responses. Shear key, deck, and foundation translational and rotational displacements rely on the transverse gap between the bridge deck and the shear key.

As previously stated, Lasso uses the most significant potential predictors in the final regression model and eliminates the ones with negligible effects. In some problems,

potential correlation appears between the variables, and Lasso retains the ones with remarkable effects to reduce complexity. Design era demonstrates this concept, as it is recognized as an important predictor in only a few scenarios: deck displacement of very tall and extremely tall bridges; shear key displacement of all three ranges; and the transverse abutment displacement of extremely tall bridges. This finding should be interpreted cautiously, as it does not simply denote the minimal effect of the design era on the bridge response; rather, the results indicate that some other predictors correlated to the design era are previously included in the model. For this problem, longitudinal reinforcement ratio and confinement spacing (which are both functions of design era) are specified as critical parameters, particularly for estimating the column curvature, deck displacement, and foundation responses. Similarly, abutment type is determined to be a predictor for all responses of extremely tall bridges, while it is a predictor in a small set of responses for very tall and moderately tall bridges, because other parameters like the longitudinal gap between deck and abutment are previously accounted for in the model and are sufficient to predict the response.

Overall, when considering the class of tall bridges, a number of geometric specifications such as the column height and tall ratio are identified as the most influential predictors. Among the material properties, concrete compressive strength shows the highest effectiveness on the bridge response. The influence of some parameters shows similar trends for various irregularity ranges, and they could eventually be classified as the most or least influential predictors, although the effect of some other parameters depends on particular responses or unique irregularity range.

Unbalanced bridges

As mentioned earlier, four different ranges of unbalanced bridges are evaluated in this study. An example of the results for the extremely unbalanced level is shown in Table 5.7. The important observed trends are explained herein and more details are provided in the tables.

In the class of unbalanced bridges, the most significant parameters identified for almost all bridge responses are listed as the longitudinal reinforcement ratio, direction of applied ground motion, pile stiffness, and geometric attributes including span length, column height (along with the short and tall ratios), deck width, and column diameter. These geometric features are found to be less effective on shear key and bearing displacement. The bearing response in the highly and extremely unbalanced range does not show sensitivity to the pile stiffness. In addition, foundation translational stiffness is highlighted in most of the responses of the unbalanced class, excluding foundation rotation of moderately and extremely unbalanced bridges and shear key displacement of ranges 2 to 4.

The bridge responses show more sensitivity to a number of parameters as the unbalanced irregularity range moves from the slight to the extreme. The abutment backwall height, soil type, pile spacing and stiffness, and concrete compressive strength are examples of these parameters. Moreover, the column height, particularly the shorter column height, impacts more responses as the irregularity range increases. Additional examples are the transverse gap between deck and shear key, and the longitudinal gap between deck and abutment with no effect on the column curvature, deck displacement, and foundation rotation in the slightly unbalanced range. Unlike that scenario, as the

irregularity range increases to the extreme, the bridge response displays less sensitivity to some of the parameters, including superstructure type and girder spacing.

Table 5.7: Identified influential parameters for extremely unbalanced bridges

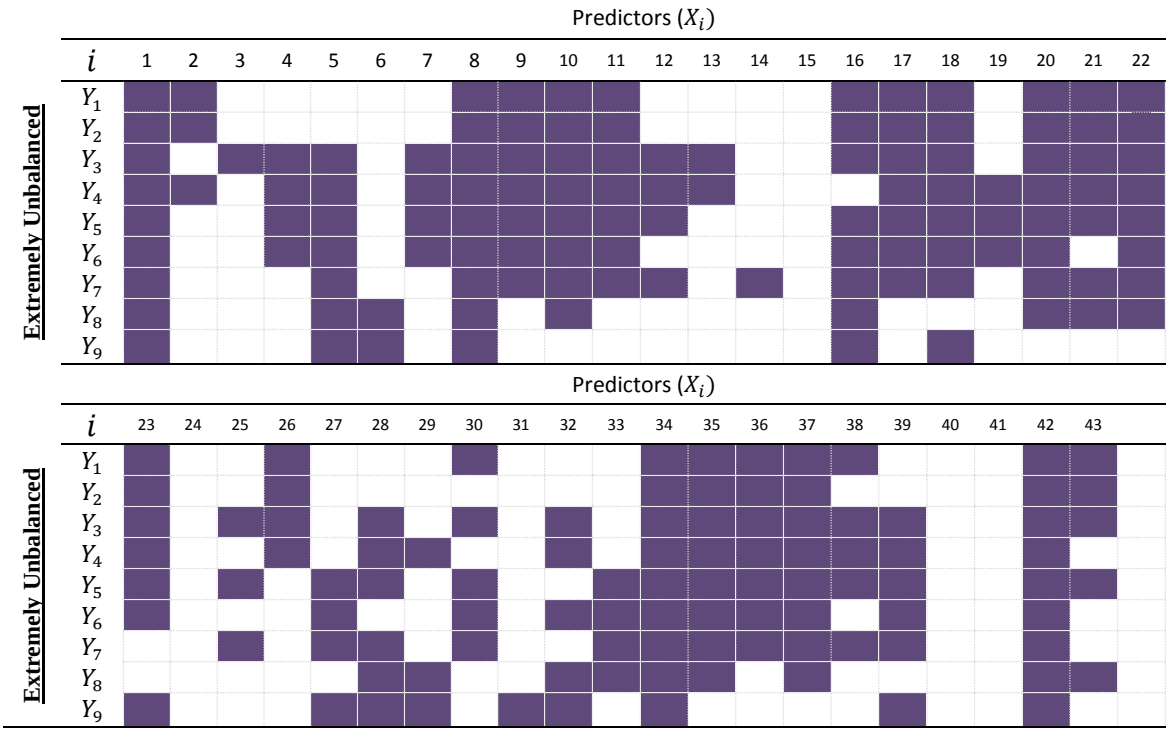

Parameters with the least impact on the responses include wall and flange thickness. The superstructure depth affects the abutment responses in all ranges of unbalanced irregularity; additionally, it influences deck, foundation, and shear key responses of slightly, moderately, and highly unbalanced bridges. Abutment backwall height is an important predictor to capture the abutment and bearing responses in all cases. In addition, the backwall height is highlighted as a predictor of deck displacement for moderately and extremely unbalanced bridges, of foundation translational displacement for slightly and extremely unbalanced bridges, and of the column curvature ductility for extremely unbalanced bridges. Shear key capacity only influences shear key

displacement in the range of moderately, highly, and extremely unbalanced bridges, while it affects the abutment response of slightly unbalanced bridges.

Skewed bridges

As noted in Section 2, five ranges of skew angles are considered in this study. An example of the results for the extremely skewed level is shown in Table 5.8. When considering skewed bridges, this study determined that wall thickness, superstructure depth, and bottom flange thickness are the least important predictors for most of the responses. On the other hand, span length, longitudinal reinforcement ratio, and pile stiffness are among the most important predictors for all bridge responses in the entire range of skewed bridges. Column height is highlighted in most of the responses and skew angles. According to the analysis results, multiple parameters influence most of the bridge responses; however they indicate less importance in estimating the shear key and bearing responses in some ranges of skew angles. These variables include soil type, confinement spacing, mass factor, deck width, foundation translational and rotational stiffness, and top flange thickness. Another group of parameters are those with effects on all responses except the shear key. Examples of these are abutment backwall height and pile spacing for all skewed bridges, and column diameter, which has less impact on shear key for bridges with low to very high skew angles.

Other significant bridge attributes for the class of skewed bridges are the longitudinal gap between deck and abutment, the transverse gap between deck and shear key, and the skew angle. The longitudinal gap affects most of the skewed bridge responses; some exceptions are shear key displacement of bridges with low to medium skew angles, and foundation rotation and transverse abutment displacement in a few

skew range. The transverse gap influences all responses of bridges with low and extreme skew angles, though it is mostly critical for the abutment, shear key, and bearing response of moderate, high, and very high classes.

The analysis indicates skew angle is most effective in predicting the majority of bridge responses listed as column curvature, deck displacement, foundation rotation, abutment active and passive displacements, and bearing and shear key responses. It is, however, not significant in predicting the shear key displacement for low to medium skew levels. Compared to the aforementioned responses, the skew angle is found to be less effective at controlling the foundation translation and transverse abutment displacement of moderately, highly, and very highly skewed bridges.

Table 5.8: Identified influential parameters for extremely skewed bridges

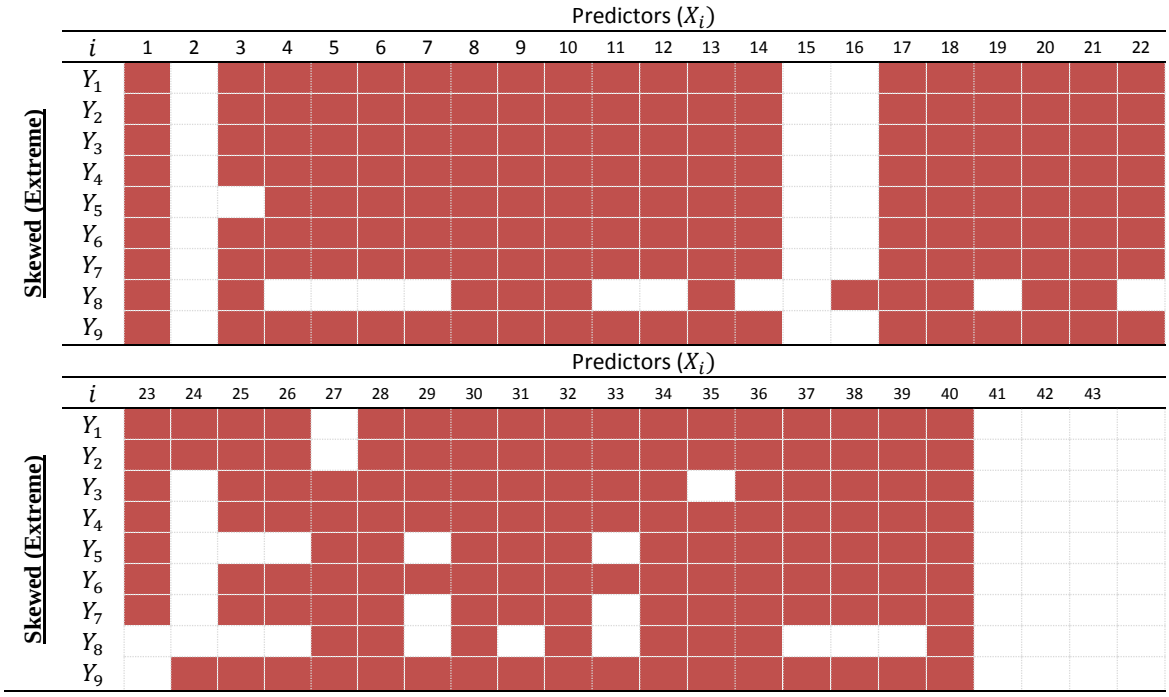

The impact of parameters varies within different skew angles, which is similar to both tall and unbalanced bridges. For instance, the superstructure type and number of box

cells present impact reduction as the skew angle increases from low to very high, despite the fact that they are important predictors for extremely skewed bridges. Overall, the sensitivity of almost all bridge responses is enhanced for the extremely skewed bridges when compared to the other ranges.

5.3 Analysis of the Results for Different Types of Bridge Irregularity

The previous section explained the effects of input parameters on the seismic response for each irregularity range of interest. While the comparisons do provide a comprehensive assessment of each individual range, they make the task of finding a general conclusion intricate. This section provides the analysis for the whole family of tall (Figure 5.5 in this section), unbalanced (Figure D.1 in Appendix D), and skewed bridges (Figure D.2 in Appendix D) by considering all ranges in a single group instead of focusing the analysis on individual ranges. This makes the results of the three different irregularity types comparable.

The results confirm the significant influence of ground motion intensity in all cases. The longitudinal gap between deck and abutment, a function of abutment type, is an influential predictor in the total list. However, the variable corresponding to the abutment type has more importance for tall classes since it contributes to every one of the responses. Deck width appears less important in the unbalanced class, while it appears significant in most of the responses in the tall and skewed categories. Although superstructure type has no impact on any of the responses of tall bridges, it does have an effect in most cases of the other two irregularity types. Wall thickness has no impact on any of the responses. However, several parameters are detected as influential predictors

for the majority of scenarios regardless of the irregularity type. Such variables are the column's height and diameter, the number of columns per bent, the span length, the abutment backwall height, the pile's stiffness and spacing, the foundation translational stiffness, the soil type, the transverse gap between deck and shear key, the mass factor, the damping ratio, and the ground motion characteristics.

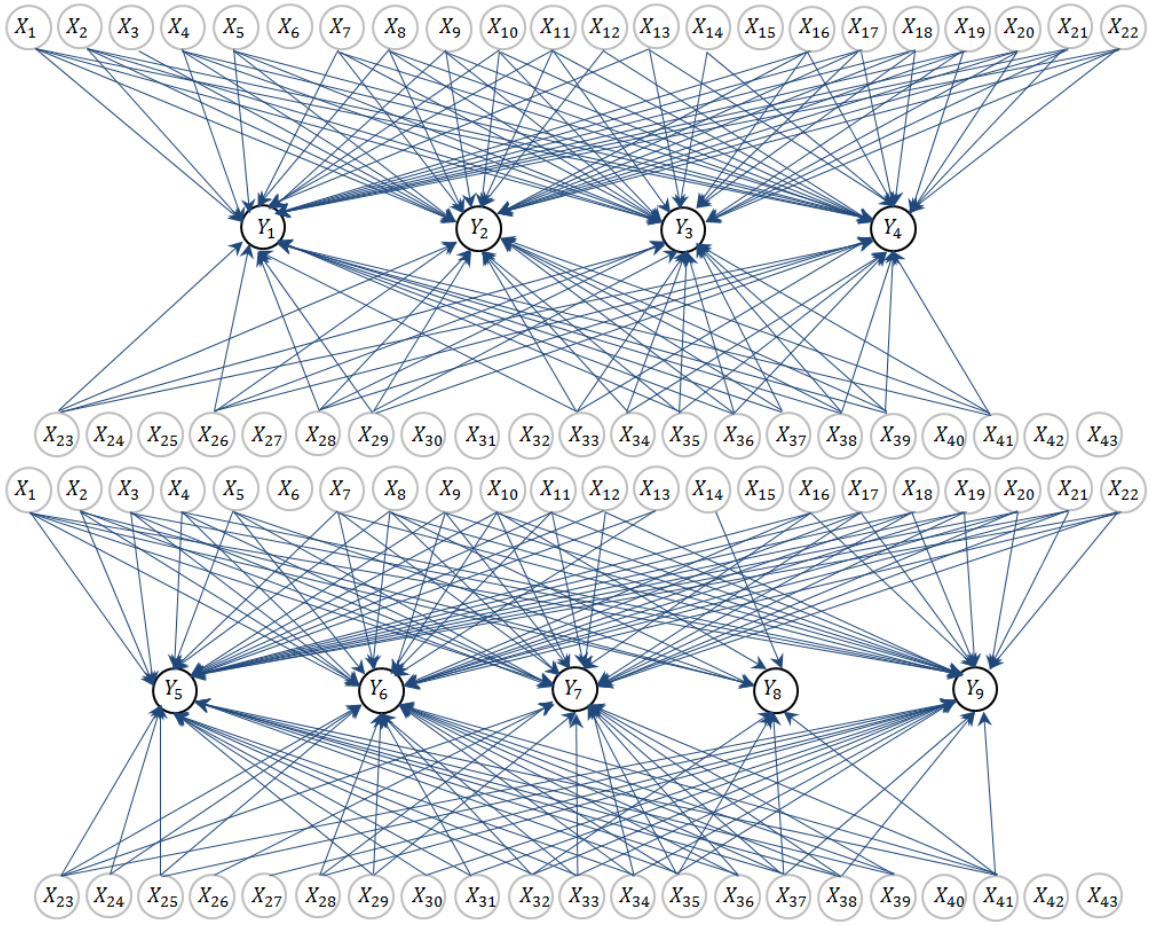

Figure 5.5: System network diagram for the class of tall bridges (Appendix E)

Evidently, more predictors are involved in the final response model of skewed bridges, compared to those of unbalanced and tall bridges, indicating higher sensitivity of skewed bridges to the modeling parameters. Additionally, a number of parameters are detected to be more effective for skewed bridges than the other two irregularity types.

Design era is an example of this, even though the reinforcement detailing that is a function of design era is imperative in most scenarios, irrespective of the irregularity class. Additional parameters include girder spacing, foundation rotational stiffness, material properties, and shear key capacity. The aforementioned observation relates to the distinctive seismic behavior of skewed bridges and their tendency to experience larger deck displacements and unseating between the deck and the abutment.

5.4 Comparative Analysis of Influential Parameters

Although the applied regression analysis selected the influential predictors from among the entire list of possible covariates, it remains challenging to rank the final predictors. A reliable and well-known technique to compare the importance of predictors is the partial F-test statistic (Vidakovic, 2011). In this study, the partial F-test is applied to test the hypothesis that q coefficients are zero while the full model includes l coefficients. This method compares the residual sum of squares (RSS) for two separate regression models: the full model (which represents the final Lasso regression model), and the reduced model (which accounts for the full model eliminating the variable of interest X_i). This method provides

$$F = \frac{\frac{RSS_{reduced} - RSS_{full}}{q}}{\frac{RSS_{full}}{m - l}} \quad , \tag{8}$$

representing the ratio of two variances. The denominator equals the mean squared error of the full model divided by its degrees of freedom $m - l$. The numerator computes the difference in the RSS produced by the q variables, divided by the number of eliminated variables. Table 5.9 provides a comparative analysis of the influential parameters on the

bridge column responses. Higher F-values are equivalent to the lower probability of rejecting the hypothesis that q coefficients are zero. Consequently, the variables with higher F-values have a higher impact on the estimated response Y_i. In this study, the test was performed on individual variables ($q = 1$) to compare their relative importance.

The contribution of each parameter to the seismic response can be evaluated using Table 5.9. The ground motion intensity with the highest F-value is recognized as the most influential parameter in all three irregularity types. For the other parameters, the horizontal bars represent the single parameter contribution in estimating the response.

According to the results, the column height and tall ratio are most heavily involved in the predicted response of tall bridges since both control the column's overall strength. Third in the list of significant features is the longitudinal reinforcement ratio dominating the column's ductility and seismic performance, followed by span length because of its contribution to the force and dead load applied to the columns. Subsequent components are pile spacing, column diameter, concrete compressive strength, number of columns per bent, and mass factor, mainly associated with the column's seismic resistance. Moreover, one of the main observed damage states relates to the cracking and breaking of tall piers, in addition to the buckling of their steel reinforcements. Consequently, stronger column bents must be designed for tall bridges to resist large bending moments, shear forces, and torques.

Regarding bridges with unbalanced frame, the comparative analysis results assign the highest impact to the longitudinal reinforcement ratio, span length, short and tall column height ratios, concrete compressive strength, number of columns per bent, and foundation translational stiffness. Similar to the category of tall bridges, many of the

parameters primarily define the column's strength and ductility, which eventually impacts the general seismic performance of the bridge, as columns are known to be the most vulnerable bridge components. As stated in the Introduction, according to post-earthquake investigations, unequal force distribution within the columns of an unbalanced bridge causes the column's damage, which leads to the superstructure's failure. A number of noted significant parameters, including the span length and the column-height ratios, control the force distribution among various columns within a bridge frame. As a result, particular attention is required to increase the seismic resistance of shorter columns, especially the ones adjacent to the very tall columns, and enhance the overall performance of the bridge.

Skew increases the sensitivity of bridge responses to the uncertain parameters. The results show the longitudinal reinforcement ratios, column diameter, number of restrainers, mass factor, number of columns per bent, column height, pile spacing and stiffness, design era, shear key capacity, skew angle, confinement spacing, and deck width to be of greater importance than the remaining significant predictors. Post-earthquake investigations of skewed bridges showed serious damage caused by displacement or unseating of the bridge deck and larger demands including column forces. The results indicate that every one of the outlined parameters significantly contributes in both demands. The column specifications such as column diameter, height, and reinforcement detailing provide the general column's durability. Span length, deck width, pile properties, skew angle, and shear key capacity contribute more than the other demands such as the deck displacements, which indirectly have an effect on the column's demand.

Table 5.9: Comparative analysis of the identified influential parameters

Tall Bridge Class		Unbalanced Bridge Class		Skewed Bridge Class	
Partial F-test result	Regressors X_i	Partial F-test result	Regressors X_i	Partial F-test result	Regressors X_i
F	i	F	i	F	i
841.34	1	6347.1	1	2577.7	1
140.81	41	370.94	18	178.82	18
109.32	10	109.82	9	61.288	17
96.924	18	37.025	42	49.072	28
40.857	9	25.951	29	31.284	37
23.062	21	22.980	43	18.469	13
19.209	17	21.492	13	12.650	12
16.681	29	18.589	37	11.892	4
15.644	37	16.517	8	11.210	10
14.857	13	15.786	7	10.788	21
13.240	33	10.771	4	9.4173	3
12.455	4	6.1803	22	7.9154	36
12.317	28	2.9170	39	6.8257	31
12.254	39	2.6458	38	6.6300	40
9.8648	7	2.5959	6	6.0540	19
5.1979	2	2.1159	34	4.8201	11
5.0957	19	1.2465	19	3.6175	6
3.8813	8	1.0973	21	3.6167	16
2.3597	16	0.6394	35	3.6146	9
2.0457	38	0.3347	20	2.6915	23
1.3606	20	0.3155	5	2.0644	8
1.2597	36	0.2522	10	1.6892	33
1.1826	5	0.0342	17	1.3645	32
1.1703	23	0.0109	23	1.2809	20
0.8765	22	0.0093	2	1.1881	29
0.1750	35	0.0086	24	0.9322	7
0.0094	11	0.0085	27	0.8733	25
0.0086	26			0.8681	27
				0.8649	2
				0.8611	26
				0.8574	5
				0.5333	30
				0.4928	35
				0.3908	22
				0.1407	39
				0.0378	34
				0.0108	38

The significance of individual influential parameters contributing to each class of irregularity is compared above in Table 5.9. The statistical analysis reveals that the commonly detected parameters of ground motion intensity, longitudinal reinforcement ratio, column diameter, number of columns per bent, column height, span length, and concrete compressive strength significantly influence the response of all three studied

types of irregular bridges. Amongst these, longitudinal reinforcement ratio dominates the column response, as the horizontal bars in Table 5.9 show.

5.5 Closure

In order to improve our understanding of the seismic performance of irregular bridges, this study examines the influential parameters of irregular bridges by performing sensitivity analyses of skewed, tall columns, and unbalanced bridge frames. This study is intended to enhance the knowledge regarding the effects of a broad range of parameters associated with finite element bridge models on the seismic response of bridges with geometric irregularities in their configuration.

In contrast to previous sensitivity studies, this study conducts categorical regression analysis to uncover the influence of variables affecting seismic response. This is advantageous because a number of the parameters that describe the characteristics of irregular bridges can easily be categorized to simplify database development and inform vulnerability modeling. A robust and reliable statistical tool, Lasso regression, is implemented in this study; this allows for the involvement of both categorical and numerical covariates in the regression model. The presented results reveal that the influence of a given parameter varies with increasing irregularity ranges. For instance, bridges with skew angles beyond the medium level (and particularly beyond 60˚) display higher sensitivity to the modeling parameters. Similar trends are observed for tall and unbalanced categories.

This study implements statistical techniques that explicitly identify which parameters influence bridge responses related to the column, deck, foundation, abutment,

bearing, and shear key; the techniques also highlight which parameters are the most and least influential. Although the relative significance of the various predictors changes over different bridge responses and irregularity ranges, there are many common influential parameters; these include ground motion intensity, longitudinal reinforcement ratio, column diameter, number of columns per bent, column height, span length, and concrete compressive strength.

The influential parameters identified in this chapter should be included in the seismic demand modeling of irregular bridges. In order to accomplish this, bridge databases must be enhanced to provide realistic information for the influential parameters. Where the information is not accessible, suitable uncertainty in the assignment of these parameters needs to be considered in the modeling of bridge performance. It is found that irregularity parameters play essential roles in the seismic response estimations in almost all scenarios. Although the statistical approach is applied herein for identifying significant parameters affecting concrete box-bridges, similar methodology could be applied to other bridge types such as steel-girder, T-girder, and slab bridges. Since the current study was performed based on representative bridge models with existing bridge characteristics, the results are advantageous in informing regional seismic risk and fragility assessment of irregular bridges.

CHAPTER 6

MODIFIED PROBABILISTIC SEISMIC RESPONSE ANALYSIS

6.1 General Procedure for the Development of Probabilistic Seismic Demand Models

Performing seismic risk analysis on bridges involves several steps. The initial step includes the random pairing of an equal number of bridge samples with a suitable set of ground motions. The list of ground motions used in this project was assembled by Caltrans using the NGA-2 database and is provided in Appendix F. These excitations have longitudinal and orthogonal components, and are randomly oriented to the longitudinal and transverse directions of the bridge models. To consider the uncertainty associated with the modeling parameters, random bridge samples are generated utilizing the Latin Hypercube sampling technique (Ayyub & Lai, 1989) based on the cumulative distribution function that corresponds to each of the modeling parameters (Chapter 3).

The next steps involve performing nonlinear time history analysis (NLTHA) on each bridge sample to estimate the seismic demand of the bridge components. The results of this analysis provide the peak seismic response of the specified engineering demand parameters (EDPs) (Table 6.1). Monitoring the key demand parameters is an essential step in the risk assessment of bridges. The EDPs are described through probabilistic seismic demand models (PSDMs); these are regression models that express the relationship between the seismic demands (D) and the ground motion intensities (IM) (Cornell, et al., 2002). In the current study, spectral acceleration at 1.0 sec, $S_{a-1.0s}$, is selected as *IM*, since it has been found to be the optimal intensity measure for the

selected class of box-girder bridges (Ramanathan, 2012). Based on the lognormal assumption (Song & Ellingwood, 1999; Cornell, et al., 2002), the median value of the seismic demand (S_d) can be estimated as a function of ground motion intensity as

$$S_d = a.IM^b \tag{1}$$

where a and b are the regression coefficients that are obtained by performing a regression analysis on $D-IM$ pairs. Dispersion ($\beta_{d|IM}$) is calculated as

$$\beta_{d|IM} = \sqrt{\frac{\sum_{i=1}^{n}(\ln(D_i) - \ln(S_d))^2}{N-2}} \quad , N = \text{total number of data points.} \tag{2}$$

It is often easier to illustrate PSDM in a transformed space (Figure 6.1). Therefore, the linear representation of Equation 1 is given by taking the natural logarithm of both sides of the equation as

$$\ln(S_d) = \ln(a) + b.\ln(IM). \tag{3}$$

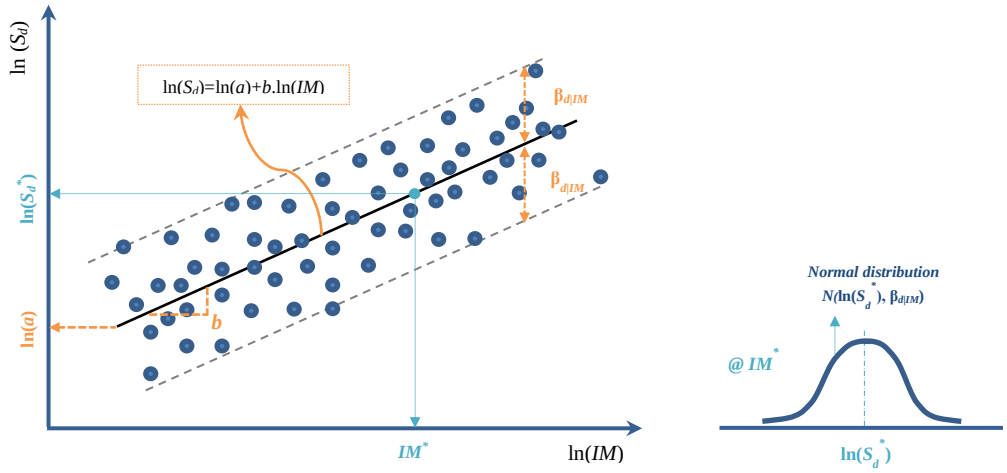

Figure 6.1: Illustration of a typical PSDM in the transformed space

Table 6.1: The common* list of engineering demand parameters

Component	Engineering demand parameter	Notation	Units
Columns	Curvature ductility	ϕ_c	1/inch
Abutment seat	Displacement	δ_{seat}	Inches
Unseating	Displacement	δ_{unseat}	Inches
Bearing	Displacement	δ_{brng}	Inches
Deck	Displacement	δ_{deck}	Inches
Foundation translation	Displacement	δ_{fnd}	Inches
Foundation rotation	Rotation	θ_f	Radians
Passive abutment response	Displacement	δ_p	Inches
Active abutment response	Displacement	δ_a	Inches
Transverse abutment response	Displacement	δ_t	Inches
Shear key	Displacement	δ_{key}	Inches

* Additional engineering demand parameters may be added for individual bridge classes

The primary objective of this research study is to develop an approach that will modify the process of generating fragility curves by accounting for the effect of aforementioned irregularities. In order to achieve this goal, the present study explores alternative methods for developing modified PSDMs. The methodologies are explained in the following section.

6.2 Development of Probabilistic Seismic Demand Models for Irregular Bridges

Using the procedure explained in the previous section, NLTHA is performed on both regular (base models) and irregular bridges (models with irregularities: i.e., skew angle, unbalanced stiffness frame, and tall column heights). The analysis results are further compared, and an approach is developed to establish modified PSDMs applicable to the class of irregular bridges. Figure 6.2 illustrates the general process.

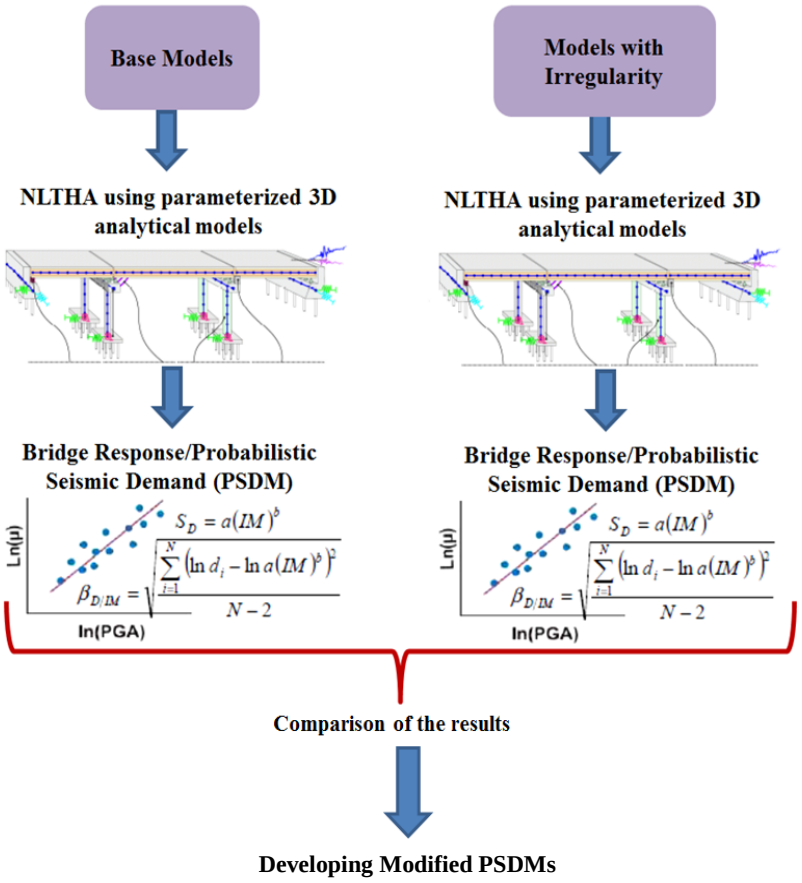

Figure 6.2: The general procedure for developing modified PSDMs

6.2.1 Modification of PSDMs Using Optimization Technique

Based on the comparison illustrated in Figure 6.2, a general form is derived for Equation 1 and for each kind of irregularity (i.e., skew, unbalanced frame, and tall). This general form can be written as

$$S_d(\theta, IM) = h(\theta).IM^{g(\theta)}, \quad (4)$$

where θ represents the bridge geometric irregularity (e.g., skew angle). The functions $h(\theta)$ and $g(\theta)$ are intended to be an efficient format that is simple to implement, and which concurrently provides a decent approximation of the demands. Finding the appropriate format for the functions, $h(\theta)$ and $g(\theta)$, depends on the variation of $S_d(\theta, IM)$ with respect to changes in the irregularity parameter (e.g., skew angle (θ)). If

this variation is monotonic and is slowly increasing/decreasing (similar to the example presented in the next section), $h(\theta)$ and $g(\theta)$ can be well approximated by linear functions as

$$\begin{cases} h(\theta) = a_0 + a_1.\theta \\ g(\theta) = b_0 + b_1.\theta \end{cases} \quad (5)$$

where $a_0, a_1, b_0, and\ b_1$ are constants. To select the best values for these constants, mathematical optimization techniques, programmed in Matlab, are implemented. As $S_d(\theta, IM)$ has a non-linear format (Equation 4), a non-linear least squares (NLLS) problem should be solved in the optimization process. The Levenberg–Marquardt method (Madsen, et al., 1999; Madsen, et al., 2004) is used to solve this problem in Matlab. It is desired to find the optimal parameters (i.e., constants $a_0, a_1, b_0, and\ b_1$) such that $S_d(\theta, IM)$ values, obtained from Equation 4, best fit the data obtained from the seismic demand results of the NLTHA for irregular bridges while minimizing the least squares of errors.

Consider a vector called **x** with entries $a_0, a_1, b_0, and\ b_1$, (i.e., $\mathbf{X}=[a_0 \quad a_1 \quad b_0 \quad b_1]^T$). The residuals are computed by Equation 6:

$$\mathbf{v}_j(\mathbf{x},\theta) = y_j - (a_0 + a_1\theta)(IM)_j^{(b_0+b_1\theta)} \quad , j = 1, 2, \cdots, nGM$$
$$\mathbf{f}(\mathbf{x}) = \begin{bmatrix} \mathbf{v}(\mathbf{x},\theta_1) \\ \mathbf{v}(\mathbf{x},\theta_2) \\ \vdots \\ \mathbf{v}(\mathbf{x},\theta_{nSk}) \end{bmatrix} \quad (6)$$

In these equations, *nSk* corresponds to the number of parameters respective to the considered irregularity type (i.e., skew angle, unbalanced stiffness frame, and tall column bents), and *nGM* represents the number of ground motions.

The objective is to minimize $\|\mathbf{f}(\mathbf{x})\|$ or equivalently, to find optimal $\mathbf{X}$ as $\boldsymbol{X}^*$:

$$\boldsymbol{X}^* = argmin_X\{F(\mathbf{X})\}\ , \tag{7}$$

where $\mathrm{F}(\mathbf{x})$ is the objective function in NLLS problem, and can be defined in the form of a sum of squares as

$$\begin{aligned}\mathrm{F}(\mathbf{x}) &= \frac{1}{2}\sum_{i=1}^{nSk}\sum_{j=1}^{nGM}(y_j - (x_1 + x_2\theta_i)(IM)_j^{(x_3+x_4\theta_i)})^2 \\ &= \frac{1}{2}\|\mathbf{f}(\mathbf{x})\|^2 = \frac{1}{2}\mathbf{f}(\mathbf{x})^{\mathrm{T}}\mathbf{f}(\mathbf{x})\end{aligned} \tag{8}$$

The function defined in Equation 8 is minimized where it gains zero gradients that are derived by:

$$\mathrm{F}'(\mathbf{x}) = \mathbf{J}(\mathbf{x})^{\mathrm{T}}\mathbf{f}(\mathbf{x})\ , \tag{9}$$

where $\mathbf{J} \in R^{(nGM\times nSk)\times nPar}$ ($nPar$ = size of vector $\mathbf{x}$)) represents the Jacobian matrix of $\mathrm{f}(\mathbf{x})$ and comprises the first partial derivatives of $\mathrm{f}(\mathbf{x})$ with respect to the corresponding parameters (Equation 10).

$$\mathbf{J}(\mathbf{x}) = \left[\frac{\partial\mathbf{f}(\mathbf{x})}{\partial x_1}, \frac{\partial\mathbf{f}(\mathbf{x})}{\partial x_2}, ..., \frac{\partial\mathbf{f}(\mathbf{x})}{\partial x_k}\right]\quad , k = 1, 2, \cdots, nPar \tag{10}$$

Based on Equation 6, $nPar$ is equal to 4; however, if another form is proposed instead of Equation 6, $nPar$ will vary accordingly. The components of the Jacobian matrix are computed based on Equation 10 and Equation 6, as the following:

$$\frac{\partial \mathbf{v}(\mathbf{x})}{\partial x_1} = -IM_j^{(b_0+b_1\theta_i)}$$
$$\frac{\partial \mathbf{v}(\mathbf{x})}{\partial x_2} = -\theta_i IM_j^{(b_0+b_1\theta_i)}$$
$$\frac{\partial \mathbf{v}(\mathbf{x})}{\partial x_3} = -(a_0+a_1\theta_i)\ln(IM_j)IM_j^{(b_0+b_1\theta_i)} \quad (11)$$
$$\frac{\partial \mathbf{v}(\mathbf{x})}{\partial x_4} = -\theta_i(a_0+a_1\theta_i)\ln(IM_j)IM_j^{(b_0+b_1\theta_i)}$$

Using the explained optimization technique, the optimal solution $\boldsymbol{X}^*$ is found, which leads to form Equation 4 as

$$S_d(\theta, IM) = (a_0^* + a_1^*.\theta).IM^{(b_0^*+b_1^*.\theta)} \quad (12)$$

This is the best fit to the seismic demand results of the NLTHA. This formula provides an estimation of the median values of the desired seismic demand as a function of the irregularity in the bridge configuration. The formula can be developed for any of the components of a bridge whose seismic response needs to be evaluated. Accordingly, the dispersion is calculated as

$$\beta_{d|IM} = \sqrt{\frac{\sum_{i=1}^{n}(\ln(D_i) - \ln(a_0^* + a_1^*.\theta) - (b_0^* + b_1^*.\theta).\ln(IM))^2}{N-2}} \quad . \quad (13)$$

Similarly, corresponding formulas, called modified PSDMs, are derived for bridges with each type of irregularity.

In this section, a case study example is presented to demonstrate the procedure explained above. For this purpose, a two-span single-frame box-girder bridge designed in the post-1990 era is selected and analyzed. Skew was selected as the type of irregularity. NLTHA was performed on the selected bridge with skew angles of 0˚, 15˚, 30˚, 45˚, and 60˚, using the Baker's suite of 160 ground motions (Baker, et al., 2011). Using the

optimization technique, the modified PSDM function, $S_d(\theta, IM) = (a_0^* + a_1^*.\theta).IM^{(b_0^*+b_1^*.\theta)}$ was derived for this specific bridge. For example,

$$S_d(\theta, IM) = (8.1509 + 0.1024.\theta).IM^{(1.4316+0.001.\theta)} \quad (14)$$

was obtained for the abutment response and skew angles $0^\circ \leq \theta \leq 60^\circ$. This formula provides an estimation of the median value of the seismic demand as a function of two factors, the bridge skew angle and the intensity measure. Another estimation of the median value can be obtained using the results of the NLTHA of the bridge (with skew angles equal to 0˚, 15˚, 30˚, 45˚, and 60˚) and implementing Equation 1, which is a function of a single factor, the ground motion intensity or IM .

The approximated values of the median responses are compared in Figure 6.3. Estimating values using the NLTHA results requires finite element modeling of a bridge for each of the desired skew angles (in the range of 0˚ to 60˚) and time history analyses for hundreds of ground motions, which necessitates extensive computational costs. By using the proposed approach, the modified PSDM function can be developed with analytical modeling and analysis of a much smaller set of skew angles (in this example, 5 skew angles were used), and a general trend can be identified throughout the whole range. Using this approach significantly reduces the computational costs. The proposed modified PSDM formula provides a decent approximation of the median value of the seismic demand for any desired skew angle within the range (e.g., 0˚ to 60˚) for which the formula was derived. The modified PSDM formula, for the case study example in this section, was derived from a wide range of skew angles. Certainly, the accuracy of estimation can be improved by narrowing the range (e.g., 15˚ to 30˚).

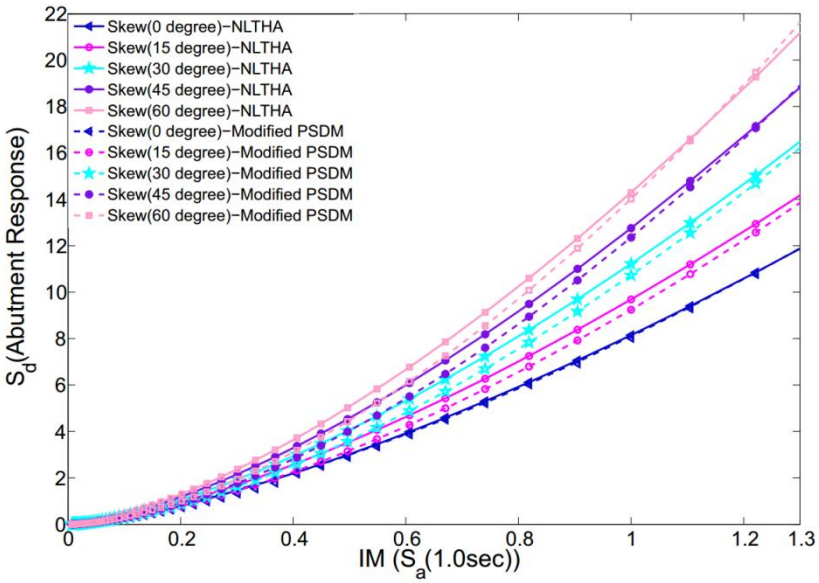

Figure 6.3: Comparison of the estimators for the median value of the demand

This research study also aims to investigate the effects of irregularities on bridge fragility. For illustration, Figure 6.4 shows a comparison of the fragility curves for several skew angles of the bridge in the case study example. It is notable that the probability of exceeding a damage state increases along with the skew angle. More details about fragility curves are provided in the next chapter.

In this section, a general form for PSDM was derived using mathematical optimization technique. The model coefficients (i.e., the parameters $a_0, a_1, b_0,$ and b_1) were optimized. Although this mathematical approach gives the best fit to the data, it does not provide a confidence interval for the derived coefficients. In order to estimate the confidence interval, the model is formulated in a Bayesian framework in the following section to make statistical inferences about the optimized parameters.

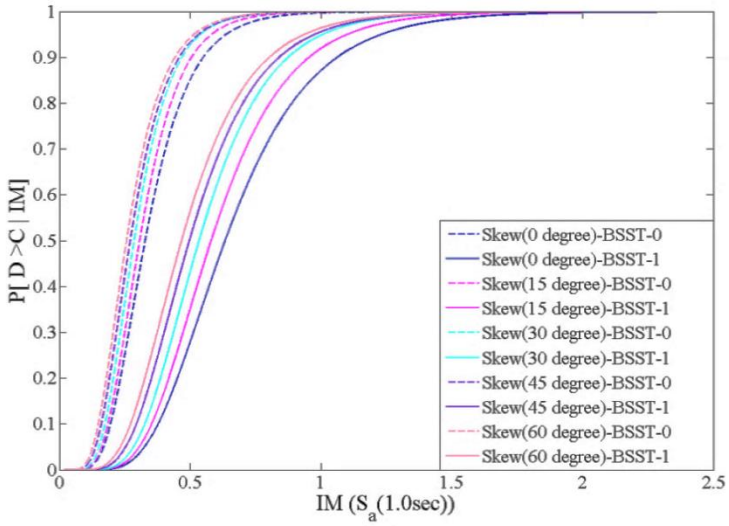

Figure 6.4: Comparison of the fragility curves for a range of skew angles (corresponds to the abutment response)

6.2.2 Development of the Credible Interval Using Bayesian Approach

The two dominant statistical inference approaches, known as frequentist (classical) statistics and Bayesian statistics, differ in their treatment of parameters. Let's consider parameter γ_i with an unknown quantity, and the goal of making an inference about γ_i. Frequentist statistics assumes the value of γ_i has a fixed but unknown quantity. Since the value of the parameter γ_i is unknown, the frequentist statistics approach performs many trials to estimate the parameter value using samples from a population. In this approach, the parameter uncertainty cannot be described with a probability distribution because the parameter value is assumed to be fixed and not random.

In contrast, Bayesian statistics considers the parameters that are not observable as random variables in the model. The main advantage of implementing this approach is that the parameter uncertainty is described by a probability distribution, and so the statistical inference can be automated via Bayesian updating. The Bayesian philosophy is conceptually simple. It starts with initial knowledge regarding the parameter of interest,

updates that knowledge using the observed data and the technique provided by Bayes' theorem, and arrives at an ultimate summary of the parameters.

A prior distribution is a statistical expression of our belief about a parameter before conducting simulations. This belief is commonly based on pre-defined assumptions such as theoretical considerations, expert opinions, and previous experiments when practically possible. In this case, the informative prior distribution is expressed in terms of a known probability density, $f(\gamma_i)$ (e.g., Gaussian, Beta, Binomial), to reflect our knowledge of the parameter. Providing prior information about a parameter before gathering enough data is not often possible, so the prior must be set so that the data may speak for itself and control the Bayesian updating. For non-informative prior, the distribution can be set to an equal probability of all parameter values within a certain range that is similar to a uniform distribution. The non-informative prior has a minimal effect on the posterior distribution.

Bayes' theorem shows how the prior distribution can be updated to the posterior distribution in the light of additional information. The Bayesian approach connects the parameters and the simulation data through the likelihood function, $f(x|\gamma_i)$. This conditional distribution incorporates the observed data in the prior distribution. The Bayesian approach is implemented to calculate and interpret the posterior or predictive probability distribution $f(\gamma_i|x)$, which is derived as a consequence of two antecedents: the prior distribution and the likelihood function (i.e., $\text{Posterior} \propto \text{Likelihood} \times \text{Prior}$). For a model M with parameter γ_i and the simulation data x, the Bayes' theorem is defined as

$$f(\gamma_i|x, M) = \frac{f(x|\gamma_i, M)f(\gamma_i|M)}{f(x, M)}, \tag{15}$$

where $f(x, M)$ denotes the marginal likelihood.

The posterior (or predictive) distribution is used to find the credible interval, which is an analogous term to the confidence interval. The Bayesian credible interval and the frequentist confidence interval differ in their approaches to treating parameters. In Bayesian statistics, parameters are considered as random variables and bounds of a credible interval are assumed to be fixed, but this is reversed in frequentist statistics. In order to identify a 95% credible interval, the 0.025 and 0.975 quantiles of the posterior distribution are determined. The highest posterior density (HPD) interval can also be extracted through the statistical inference. Although the intervals approximated via the HPD and the equal tails are identical for symmetric distributions, the intervals differ for asymmetric distributions. The Bayesian process is clarified in the following example.

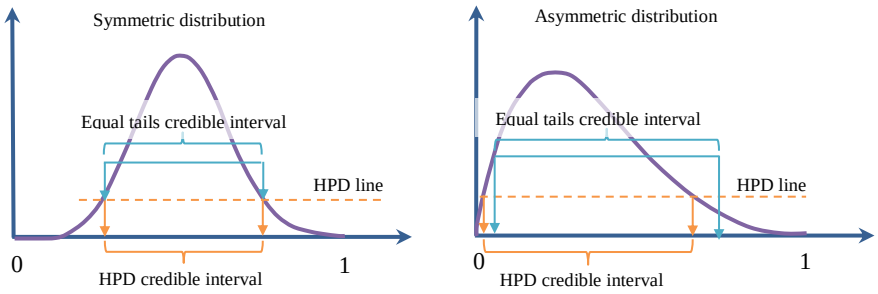

Figure 6.5: Differences between the equal tails interval and HPD interval

A simple example is flipping a coin with head and tail sides where γ_i denotes the probability of the coin landing head-side-up. Both non-informative (Case I) and informative (Case II) distributions are used to illustrate the impact of prior distribution. As Figure 6.6 displays, the non-informative prior presents a uniform distribution on the interval of [0,1]. However, experience shows that the concentration of the probability of the coin landing head-side-up is around 0.5. This turns into an informative prior distribution expressed as a *Beta* distribution in Figure 6.6.

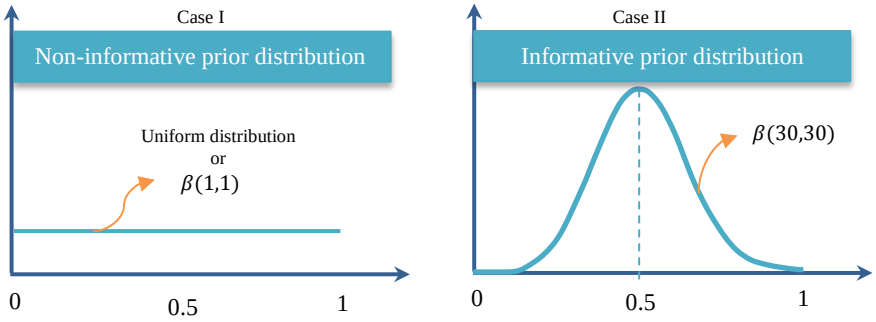

Figure 6.6: Illustrative example of the prior probability distributions for Bayesian statistics

The likelihood function can be derived by quantifying the results of a simple experiment. If 4 heads-up landings are observed when the coin is flipped 10 times, the likelihood function can be expressed as $Binomial(10,4,\theta)$ (Figure 6.7). Then, Bayesian statistics updates the prior distributions using the experimental results.

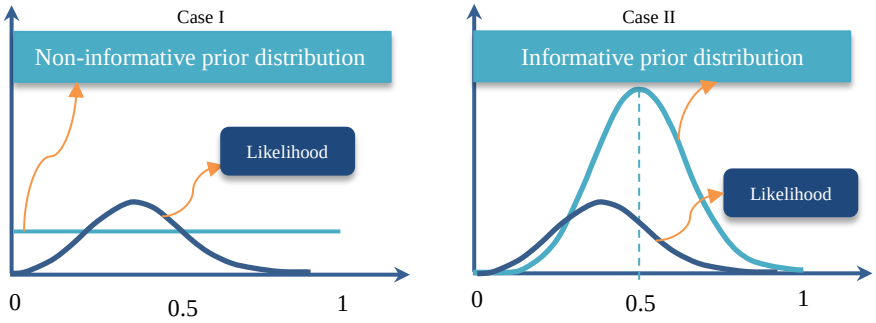

Figure 6.7: Illustrative example of the likelihood with the prior probability distributions for Bayesian statistics

In Case I, the posterior probability is equivalent to the likelihood function (Figure 6.8). This happens because of using a completely non-informative prior. In the Case II, the posterior probability computed using Bayesian statistics equals to a *Beta* distribution (posterior = $\beta(34,36)$). As shown in Figure 6.8, the posterior distribution is very close to the prior distribution because of using a strong, informative prior and small sample size when conducting the experiment. By increasing the sample size (e.g., by flipping the coin 50 times), the likelihood will have a greater influence on the posterior (Figure 6.9).

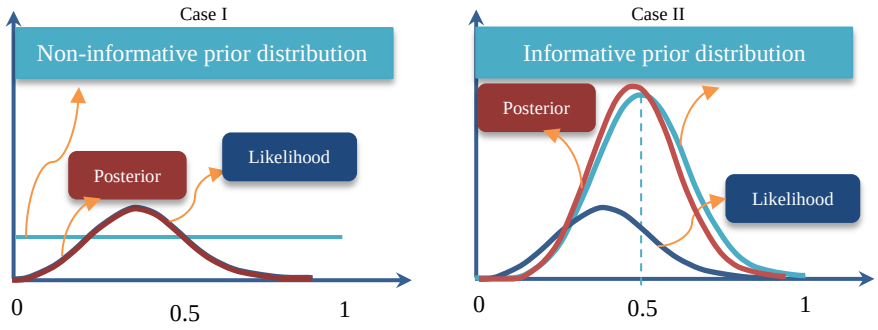

Figure 6.8: Illustrative example of the posterior distribution obtained from Bayesian statistics

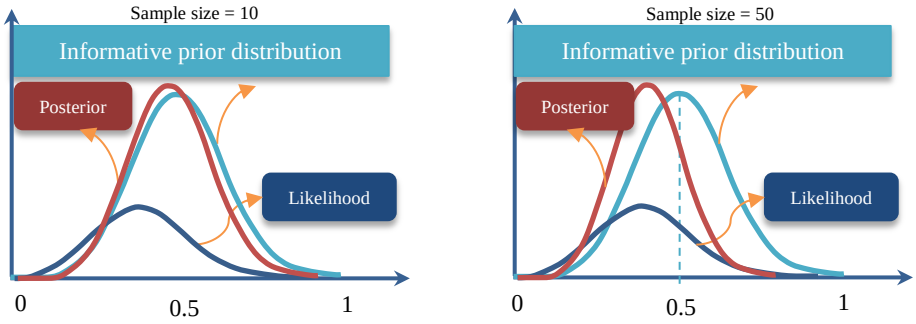

Figure 6.9: Illustrative example of the effect of sample size on posterior distribution obtained from Bayesian statistics

As stated earlier, the posterior distribution can be analyzed to extract statistical inference estimates such as mean, median, mode, and credible interval. For the coin example, with Case II, the posterior mean is calculated as 0.4857. Any desired percentage of a credible interval can be calculated according to the posterior distribution. For example, in order to identify a 95% credible interval (Figure 6.10.a), the 0.025 and 0.975 quantiles of the posterior distribution are determined for the coin example as $P(0.37 < \gamma_i < 0.60) = 0.95$. Similarly, the HPD credible interval is found by drawing a horizontal line through the posterior distribution density and moving the line over the density plot until the probability within the range matches the 95% probability (Figure 6.10.b). Additionally, the chance that the value of the parameter of interest will be in a particular

interval can be approximated. Figure 6.10.c shows that the probability of being between 0.4 and 0.5 is approximately 43%.

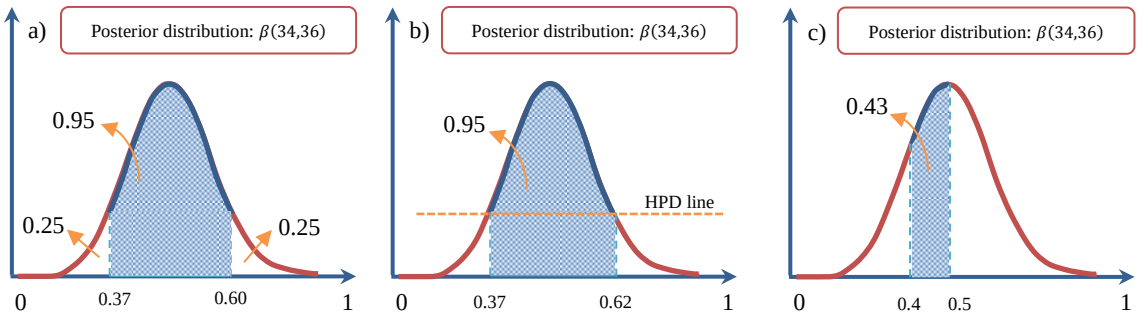

Figure 6.10: Statistical inference of the posterior distribution: (a) 95% of credible interval; (b) 95% HPD credible interval; (c) probability of the parameter to be in a particular interval

In the previous section of this chapter, the modified PSDM function (Equation 12) was developed using mathematical optimization methodology to estimate the median value of the seismic demand as a function of two factors, the bridge geometric irregularity (e.g., skew angle ($0^{\circ} \leq \theta \leq 60^{\circ}$)) and intensity measure. For the case study example, the optimum values for the PSDM coefficients (i.e., $a_0, a_1, b_0, and\ b_1$) of the abutment response were provided in Equation 14. In the current chapter, the model is formulated in the Bayesian framework to predict the distribution of the PSDM coefficients, and moreover, to assess the credible interval. The model is programmed in WinBUGS (Spiegelhalter, et al., 2003; Vidakovic, 2011), which is the statistical software used to conduct the Bayesian analysis. The number of simulations used to approximate the posterior distribution was 1,000,000. The obtained posterior probability distributions for individual coefficients are shown in Figure 6.11. The statistical inference quantities are described in Table **6.2**, and the corresponding statistical evaluation is listed in Table 6.3.

Table 6.2: Description of the statistical inference quantities corresponding to the posterior distributions (Spiegelhalter, et al., 2003)

Quantity	Description
Mean	An approximation for the μ of the posterior distribution of the unknown quantity
Median	An approximation for the median or 50th percentile of the posterior distribution
Std	An approximation for the standard deviation σ of the posterior distribution
MC error	The computational accuracy of the posterior mean
Val2.5pc	The 2.5th percentile of the posterior distribution
Val5.0pc	The 5.0th percentile of the posterior distribution
Val95.0pc	The 95.0th percentile of the posterior distribution
Val97.5pc	The 97.5th percentile of the posterior distribution

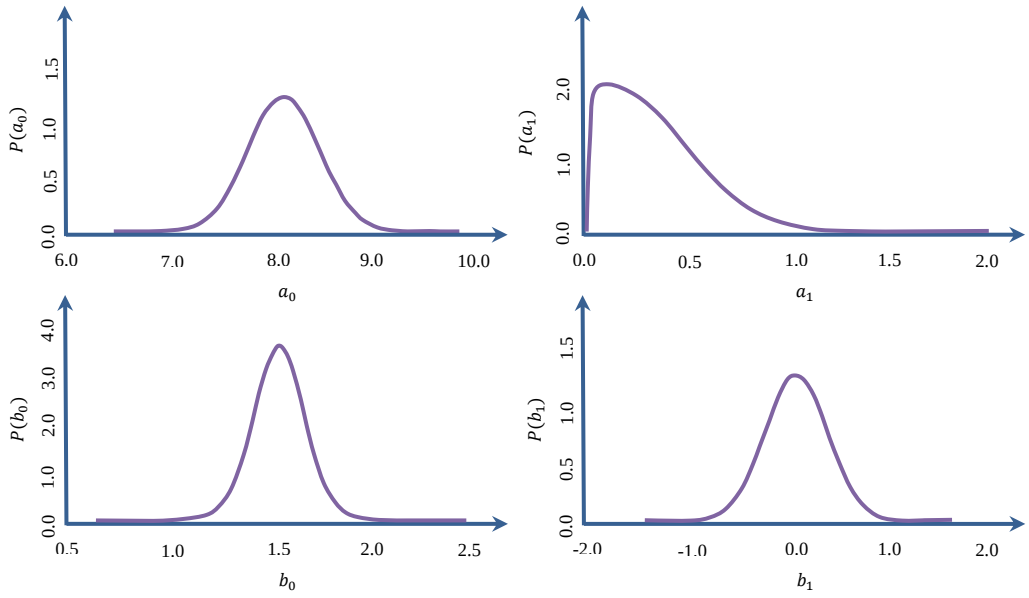

Figure 6.11: The estimated posterior distributions for the coefficients of PSDM

Table 6.3: The statistical inference of the posterior distributions

Parameter	Mean	median	Std	MC_error	val2.5pc	val5.0pc	val95.0pc	val97.5pc
a_0	8.103	8.103	0.3131	7.93E-04	7.489	7.588	8.618	8.717
a_1	0.2921	0.2549	0.2094	2.03E-04	0.01283	0.02551	0.6894	0.7823
b_0	1.491	1.492	0.1131	2.88E-04	1.265	1.305	1.675	1.714
b_1	-1.15E-03	-3.40E-03	0.3164	3.23E-04	-0.6207	-0.5201	0.5201	0.6196

6.2.3 Comparison of the Probabilistic Seismic Demand Models

This study focuses on predicting bridge fragilities for the class of concrete box-girder bridges located in California. As a part of the assessment, PSDMs are initially developed to be further used in the generation of fragility curves. Although the computations outlined in Equation 1 (i.e., the conventional form of PSDM) have been widely used (Mackie & Stojadinovic, 2005; Cornell, et al., 2002; Nielson, 2005; Ramanathan, 2012), it is not the only possible form to express PSDMs. Also, as stated earlier in the Introduction, most previous studies have focused on regular bridges, and past earthquakes have shown that irregular bridges have seismic performances that are distinct from regular bridges. Three different approaches are proposed in this study to develop PSDMs of bridges with the aforementioned geometric irregularities. First, in Chapter 5, significant parameters affecting the seismic responses of irregular bridges were identified using finite element bridge models and statistical tools. As a result, multivariate PSDMs were constructed using the identified influential parameters (e.g., Appendix E). Second, a modified form of PSDMs was established in Chapter 6, Subsection 6.2.1, by implementing mathematical optimization techniques. Third, in Chapter 6, Subsection 6.2.2, Bayesian updating was applied on PSDMs to make statistical inferences on the model.

Conclusions about the prediction accuracy of the three different PSDMs can be made based on a point-to-point comparison (i.e., comparing the testing data points that are the peak seismic responses, scattered points in Figure 6.12, and the predictive response using each of the three PSDMs) or based on the summation of all point-to-point comparisons in the entire NLTHA (i.e., $\sum_{i=1}^{n}\left(ds_i - dp_i\right)^2$). To make an overall conclusion, the

values are compared using the following measure of the coefficient of determination (Golub & Van Loan, 1996):

$$R - Squared \text{ or } R^2 = 1 - \frac{SSE}{SST}$$

$$= 1 - \frac{\sum_i^n (ds_i - dp_i)^2}{\sum_i^n \left(ds_i - Mean(ds)\right)^2} \ , \qquad (16)$$

in which *dp* and *ds* are, respectively, the predictive and simulation seismic responses (or demand) and n is the number of data points. The statistical value $R - Squared$ represents the goodness of fit of the models, or how well the models predict the data.

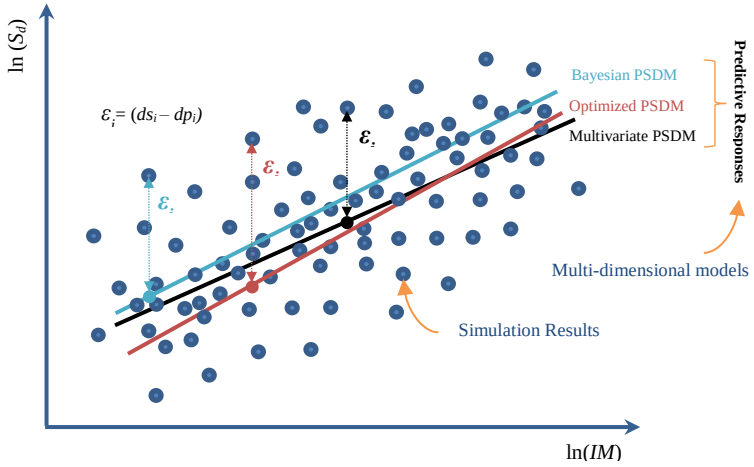

Figure 6.12: Illustration of error calculation for a typical PSDM in the transformed space

In order to compare these models, $R - Squared$ is computed for each of the generated PSDMs using the training data set (i.e., the simulation data set used to develop the models). Another set of data (i.e., the testing data) is prepared by performing a separate NLTHA on the finite element models. The derived probabilistic seismic demand models for skewed, tall, and unbalanced bridges are provided in Appendix G and the goodness of fit comparison is given in Table 6.4 and Figure 6.13.

Table 6.4: Comparison of the goodness of fit of the models

Model	*R-Squared(Training data)*			*R-Squared(Testing data)*		
	Skewed bridge	Tall bridge	Unbalanced bridge	Skewed bridge	Tall bridge	Unbalanced bridge
Conventional PSDM	0.746	0.779	0.714	0.711	0.823	0.657
Optimized PSDM	0.790	0.816	0.769	0.696	0.839	0.701
Bayesian Model	0.763	0.772	0.766	0.649	0.767	0.701
Multivariate PSDM	0.736	0.716	0.743	0.686	0.634	0.700

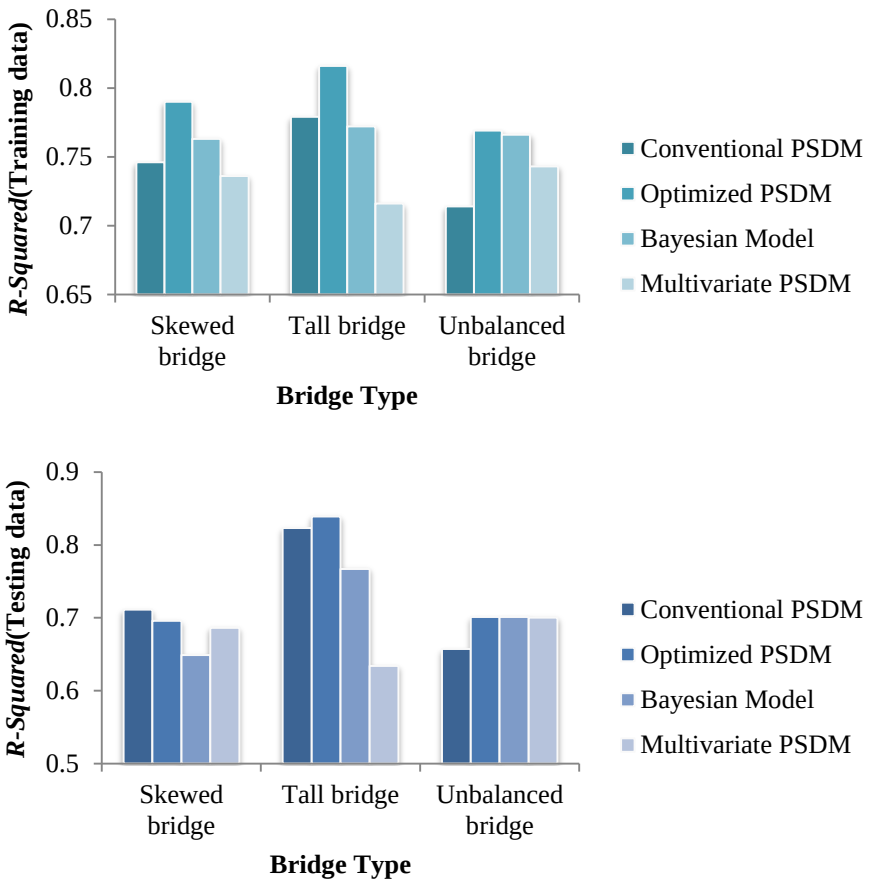

Figure 6.13: Comparison of the goodness of fit of the models

According to the predictive capabilities (Table 6.4 and Figure 6.13) of the models, overall, the predictive responses using any of the PSDM forms agree with the bridge simulation data points with reasonable precision, even though some models provide improved accuracy. Among all models, the Optimized PSDM is the most reliable model

with the highest $R-Squared$ values in almost all cases. This model is highly effective at predicting the seismic responses. The conventional approach uses the simulation results for developing seismic demand models in which intensive NLTHA must be conducted, which make the procedure of developing PSDMs impractical. Multivariate models are proposed as an alternative approach when the bridge characteristics are known and can serve as the predictor variables in the multi-dimensional models. However, increasing the number of input parameters in a model does not necessarily improve the accuracy, and it can even spoil the model's simplicity. Although the Multivariate PSDM has a lower accuracy compared to the Optimized PSDM and Bayesian PSDM, in some cases (e.g., unbalanced bridges), it performs better than the Conventional PSDM. In general, the Multivariate PSDM provides a good ($R^2_{training} > 0.7$ and $R^2_{testing} > 0.6$) approximation of the seismic demand and can produce PSDMs at low computational costs. In some cases (e.g., unbalanced bridges), the Bayesian PSDM shows higher R^2 values and, in some other cases (e.g., tall bridges), it shows lower R^2 values than the Conventional PSDM.

It is concluded that optimization techniques that are coupled with Bayesian statistics can be used to efficiently predict the seismic demand of bridges with geometric irregularities. In another words, the model can be developed by implementing the optimization approach and the credible intervals can be approximated using the Bayesian approach, since the Optimized PSDM provides the best fit to the data and Bayesian updating can compensate for optimization's drawbacks by computing the credible intervals.

6.3 Closure

To efficiently explore the seismic responses of existing irregular bridges in California, modified forms of probabilistic seismic demand models (PSDMs) were investigated and established in this chapter using three methodologies. The proposed models consider the effects of geometric irregularities and also provide a practical solution when there is a high computational demand. The multivariate model is derived based on the influential parameters identified in Chapter 5. A general form of modified PSDM was derived in the present chapter using mathematical optimization techniques. Although this approach provides the best fit for the seismic demands, it does not provide a confidence interval for the derived coefficients. In order to estimate the confidence intervals, the model is formulated in a Bayesian framework. Bayesian statistics provides a robust statistical tool for inferring the probability distribution of the parameters of interest; it was used to calculate and interpret the posterior distribution. Finally, the prediction accuracy of the proposed models was evaluated in this chapter through the goodness of fit comparison.

CHAPTER 7

DEVELOPMENT OF ADJUSTMENT FACTORS FOR FRAGILITY CURVES

7.1 General Procedure of Fragility Analysis

The seismic vulnerability evaluation of bridges facilitates post-earthquake emergency responses and determines of suitable retrofit strategies. This assessment can be performed by implementing a probabilistic approach in the form of fragility curves for the bridge components and the bridge system. In order to get some indications of the functionality level of irregular bridges, this chapter evaluates the bridge fragility at four different damage states: slight, moderate, extensive, and complete. General descriptions of various levels of damage for bridge components (i.e., Component Damage Threshold (CDT)) and the bridge system (i.e., Bridge System State Threshold (BSST)) are given in Table 7.1 and Table 7.2, using an approach from previous research (Nielson, 2005; Ramanathan, 2012).

At a chosen intensity measure, the probability that the seismic demand (D) of a component exceeds its capacity (C) can be assessed through fragility curves. Assuming a lognormal distribution of demand and capacity (Song & Ellingwood, 1999; Cornell, et al., 2002) in conjunction with the first order reliability theory, the probability of reaching or exceeding a specific damage state for a particular component is estimated as

$$\mathrm{P}[D > C \mid \mathrm{IM}] = \Phi\left[\frac{\ln(S_d / S_c)}{\sqrt{\beta_{d/IM}^2 + \beta_c^2}}\right], \tag{1}$$

where S_d represents the median estimate of the demand, S_c is the median estimate of the capacity, $\beta_{d/IM}$ represents the dispersion of the demand, β_c is the dispersion of the capacity, and $\Phi(\bullet)$ corresponds to the standard normal cumulative distribution function.

Table 7.1: Qualitative damage levels for the bridge components

Damage Levels	CDT-0	CDT-1	CDT-2	CDT-3
Description of damage	Aesthetic damage	Repairable minor functional damage	Repairable major functional damage	Component replacement

Table 7.2: Description of different damage states for the bridge system

	Bridge system damage levels			
	BSST-0 Slight	BSST-1 Moderate	BSST-2 Extensive	BSST-4 Complete
Shake Cast Inspection Priority levels	Low	Medium	Medium-High	High
Likely Immediate Post-Event Traffic State	Open to normal public traffic – No Restrictions	Open to Limited public traffic – speed/weight/lane restrictions	Emergency vehicles only – speed/weight/lane restrictions	Closed (until shored/braced) – potential for collapse
Traffic Operation				
Closure/detour needed	Very unlikely	Unlikely	Likely	Very Likely
Traffic restrictions needed	Unlikely	Likely	Very Likely	Very Likely
Emergency Repair				
Shoring/bracing needed	Very Unlikely	Unlikely	Likely	Very Likely
Roadway leveling needed	Unlikely	Likely	Very Likely	Very Likely
Primary Components	CDT-0 to 1	CDT-1 to 2	CDT-2 to 3	Above CDT-3
Secondary Components	CDT-0	CDT-1	NA	NA

Figure 7.1 and Figure 7.2 illustrate the process for generating fragility curves. The general procedure of developing PSDMs by conducting three-dimensional nonlinear full time history analyses was explained in Chapter 6, Section 6.1. In calculating fragilities (Equation 1), the required demand parameters S_d and $\beta_{d/IM}$ for each bridge component are estimated from the PSDMs, and the corresponding capacity parameters are obtained from the limit states. The median and dispersion values associated with the capacity models,

also known as the limit states, are determined based on a lognormal distribution assumption.

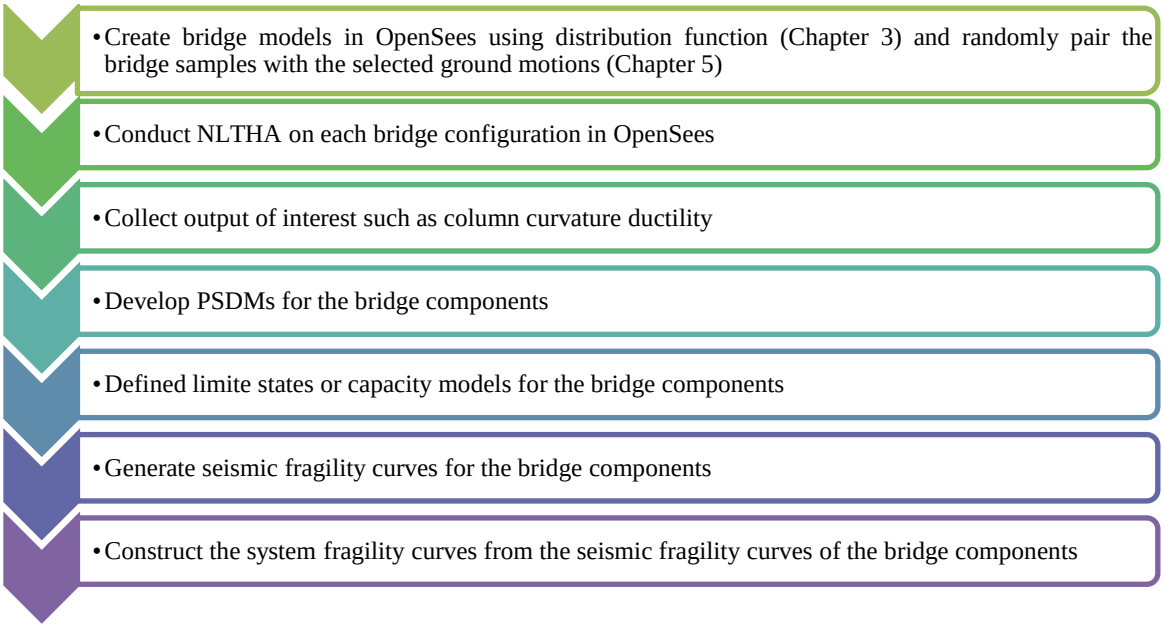

Figure 7.1: Process of generating fragility curves

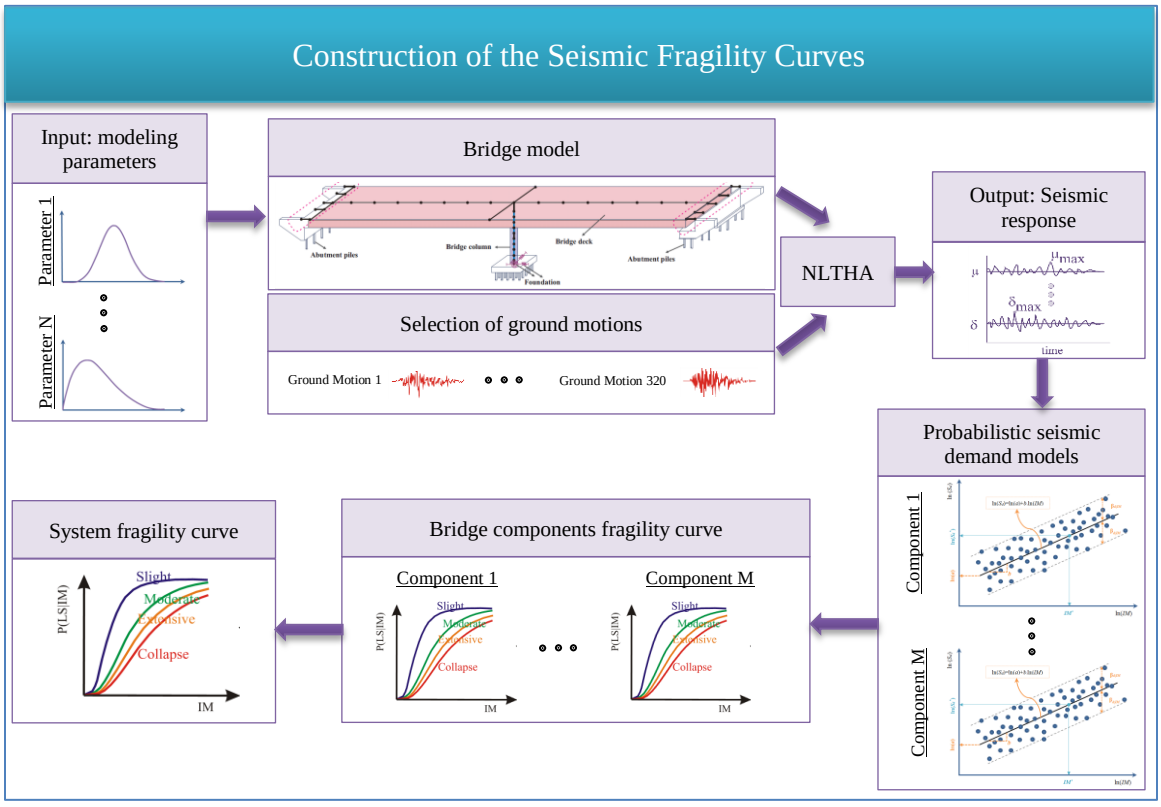

Figure 7.2: Illustration of the steps for generating fragility curves

The bridge components that are monitored in this study are divided into two categories. With primary components such as bridge column, failure of the components can significantly affect the stability of a bridge; consequently, failure of a primary component mandates the closure of the damaged bridge. Secondary components such as bearing have less effect on the general functionality of a bridge. The results of the last phase of this project (DesRoches, et al., 2012) showed that column limit states need further investigation to improve the accuracy of the fragility estimations. Therefore, in the current phase of this project, sampled bridge column tests have been reviewed, and the experimental results have been interpreted to develop the capacity models, as explained in Appendix H. The summary of the Column Capacity Limit States (CCLS) and their definitions are provided in Table 7.3 and Table 7.4. The limit states that are used to develop fragility curves for various bridge components in this study are listed in Table 7.5. Consequently, the component fragility curves are constructed by applying the capacity models along with the PSDMs in Equation 1.

Table 7.3: Qualitative damage levels for the bridge columns

Column capacity limit states (CCLS)	Component state	Component damage	Component repair
CCLS-0 (Slight)	None or aesthetic	EQ-related minor cracking	Seal and paint
CCLS-1 (Moderate)	Minor repairs needed	Minor spalling of cover concrete	Epoxy inject, minor removal/patch
CCLS-2 (Extensive)	Major repairs needed, but function intact	Exposed core, confinement yield	Major removal/patch. Add jacket.
CCLS-3 (Complete)	Irreparable damage, function compromised	Bar bucking, large drift, core crushing	Remove/Replace column (or bridge)

Table 7.4: Quantitative damage levels for the bridge columns (Appendix H)

Bridge design eras	Statistical parameter	Displacement ductility				Curvature ductility			
		CCLS-0	CCLS-1	CCLS-2	CCLS-3	CCLS-0	CCLS-1	CCLS-2	CCLS-3
Pre-1970	Mean	0.82	1.58	2.93	4.56	0.82	2.25	4.99	8.57
	Median	0.80	1.51	3.00	4.00	**0.80**	**2.30**	**5.20**	**8.80**
	lower bound	0.80	1.00	1.50	2.00	0.80	1.00	1.54	2.56
	upper bound	1.00	2.05	5.04	8.27	1.00	3.65	8.28	14.10
1970-1990	Mean	1.02	3.02	4.65	6.29	1.32	5.64	8.22	11.49
	Median	1.00	2.65	4.59	6.30	**1.00**	**5.00**	**8.00**	**11.00**
	Lower bound	0.69	1.00	2.88	3.45	0.69	1.60	4.15	7.32
	Upper bound	2.00	6.00	8.00	10.00	3.75	14.77	20.28	25.79
Post-1990	Mean	1.20	2.98	5.45	7.86	1.45	5.63	11.73	18.05
	Median	1.00	2.68	5.00	8.13	**1.00**	**5.00**	**11.00**	**17.50**
	lower bound	0.70	1.40	2.20	3.80	0.50	2.00	4.72	9.71
	upper bound	2.00	6.00	10.00	12.00	3.94	18.47	23.67	30.19

Table 7.5: Statistical parameters for the capacity models of the bridge components (Table 7.4 and DesRoches, et al., 2012)

	Bridge component	EDP	Units	Median value (S_c)				Dispersion (β_c)
				CDT-0	CDT-1	CDT-2	CDT-3	
Primary components	Columns							
	Pre-1970	Curvature ductility	NA	0.8	2.0	5.0	8.0	0.35
	1970-1990	Curvature ductility	NA	1.0	5.0	8.0	11.0	0.35
	Post-1990	Curvature ductility	NA	1.0	5.0	11.0	17.0	0.35
	Abutment seat							
	Pre-1970	Displacement	Inches	0.5	1.0	2.0	3.0	0.35
	1970-1990	Displacement	Inches	1.0	4.5	10.0	15.0	0.35
	Post-1990	Displacement	Inches	1.5	4.5	14.0	21.0	0.35
Secondary components	Joint Seal	Displacement	Inches	2.0	5.0	NA	NA	0.35
	Bearings	Displacement	Inches	1.0	4.0	NA	NA	0.35
	Shear keys	Displacement	Inches	1.0	5.0	NA	NA	0.35
	Deck	Displacement	Inches	4.0	12.0	NA	NA	0.35
	Bent foundation							
	Translation	Displacement	Inches	1.0	4.0	NA	NA	0.35
	Rotation	Rotation	Radian	1.5	6.0	NA	NA	0.35
	Abutment displacement							
	Passive	Displacement	Inches	3.0	10.0	NA	NA	0.35
	Active	Displacement	Inches	1.5	4.0	NA	NA	0.35
	Transverse	Displacement	Inches	1.0	4.0	NA	NA	0.35

As shown in Figure 7.1 and Figure 7.2, the next step is constructing system fragility curves using the generated curves for individual bridge components. In this regard, a joint probabilistic method is typically applied (Nielson, 2005; Ramanathan, 2012). For the joint probabilistic seismic demand model (JSPDM), Monte Carlo simulations using 1,000,000 trial runs are performed on the demand and capacity models. This results in an approximation for a fragility value that states the probability of demand exceeding the capacity at one specific level of ground motion intensity (*IM*). This process is repeated to estimate the fragility values at other ground motion levels and plot the computed fragility values in the form of a system fragility curve. The lower and upper bounds of the system fragility curves are found as

$$\max_{i=1:nc}\left(P[D>C|IM]_{i^{th}component}\right) \le P[D>C|IM]_{System}$$

$$\le 1-\prod_{i=1}^{nc}\left(1-P[D>C|IM]_{i^{th}component}\right) \quad (2)$$

As shown in Figure 7.3, the lower bound underestimates the system fragility, while the upper bound provides a conservative overestimation of the bridge fragility.

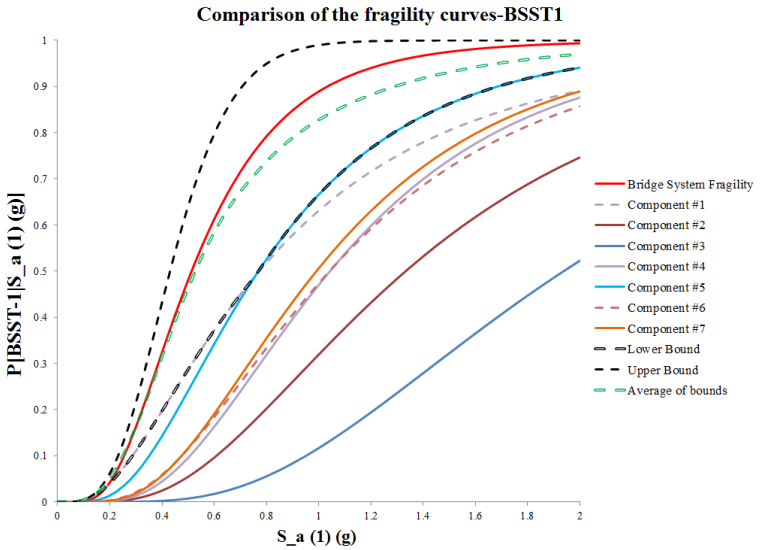

Figure 7.3: An example of a system fragility curve and the lower, upper bounds

The results of the fragility analysis for the bridge models (Chapter 4) selected for the scope of this study are presented in the following section. For simplicity, the nomenclature is assigned to the irregular bridges as given in Table 7.6, according to the irregularity ranges discussed in Section 5.1.3. In Table 7.6, BM stands for the base models, which are regular bridge models without any types of irregularity (i.e., bridge models with zero skew angle, straight decks, normal column heights, and balanced stiffness frames). In addition to the irregularity parameters, the selected box-girder bridges are different in several configurations. Therefore, an additional nomenclature list based on various design eras, abutment types, and number of columns per bent is provided in Appendix I, Table I. 1.

Table 7.6: The assigned nomenclature for irregular bridges

Nomenclature	Geometric Irregularity	Range of irregular parameter
BM	NA	NA
SKL	Skew angle	Low
SKM		Medium
SKH		High
SKVH		Very High
SKEx		Extreme
MTL	Tall column bents	Moderately tall
VTL		Very tall
ExTL		Extremely tall
SUnb	Unbalanced stiffness frames	Slightly unbalanced
MUnb		Moderately unbalanced
HUnb		Highly unbalanced
ExUnb		Extremely unbalanced

7.2 Development of Adjustment Factors

The components and system fragility curves for each specific bridge are generated using the methodology explained in the previous section. The fragility analysis results are presented in Subsections 7.2.1., 7.2.2., and 7.2.3. for tall, unbalanced, and skewed bridge

classes, respectively. The fragilities are further compared with those of regular bridges, and an approach is developed to establish appropriate adjustment factors for estimating the fragility of bridges with geometric irregularities. Adjustment factors are multiplicative factors that are determined based on the comparison of the fragility quantities in order to estimate the fragility values corresponding to a particular geometric irregularity. The computed adjustment factors are compared with HAZUS-MH modification factors in Subsection 7.2.4.

7.2.1 Tall Bridges

As mentioned in the previous chapters, this study explores the seismic performance of the family of tall bridges in three ranges of column heights. The median (λ) and dispersion (ζ) of the generated fragility curves are given in Table 7.7 and Figure 7.4. Then, the fragility values of tall bridges are compared to the fragility values of the base models, and the adjustment factors (ω_λ and ω_ζ) are established, as presented in Table 7.8.

Table 7.7: Fragility parameters for the tall bridge types (specifications: multi-span continuous concrete box-girder bridges with seat abutments, single column per bent, and circular column cross-sections)

Bridge design era	Bridge type	BSST-0		BSST-1		BSST-2		BSST-3	
		λ	ζ	λ	ζ	λ	ζ	λ	ζ
Pre-1970	BM	0.102	0.499	0.200	0.488	0.382	0.489	0.540	0.485
	MTL	0.078	0.509	0.140	0.525	0.247	0.531	0.342	0.519
	VTL	0.059	0.528	0.103	0.540	0.174	0.530	0.235	0.535
	ExTL	0.049	0.561	0.087	0.566	0.148	0.566	0.206	0.568
1970-1990	BM	0.100	0.660	0.515	0.651	0.957	0.802	1.343	0.809
	MTL	0.071	0.610	0.374	0.549	0.832	0.736	1.236	0.746
	VTL	0.046	0.658	0.256	0.627	0.637	0.789	0.965	0.858
	ExTL	0.037	0.686	0.207	0.673	0.580	0.824	0.870	0.882
Post-1990	BM	0.095	0.651	0.515	0.653	1.296	0.772	2.052	0.770
	MTL	0.069	0.605	0.373	0.562	0.990	0.675	1.543	0.651
	VTL	0.045	0.658	0.256	0.626	0.707	0.735	1.068	0.693
	ExTL	0.037	0.682	0.206	0.672	0.602	0.784	0.925	0.809

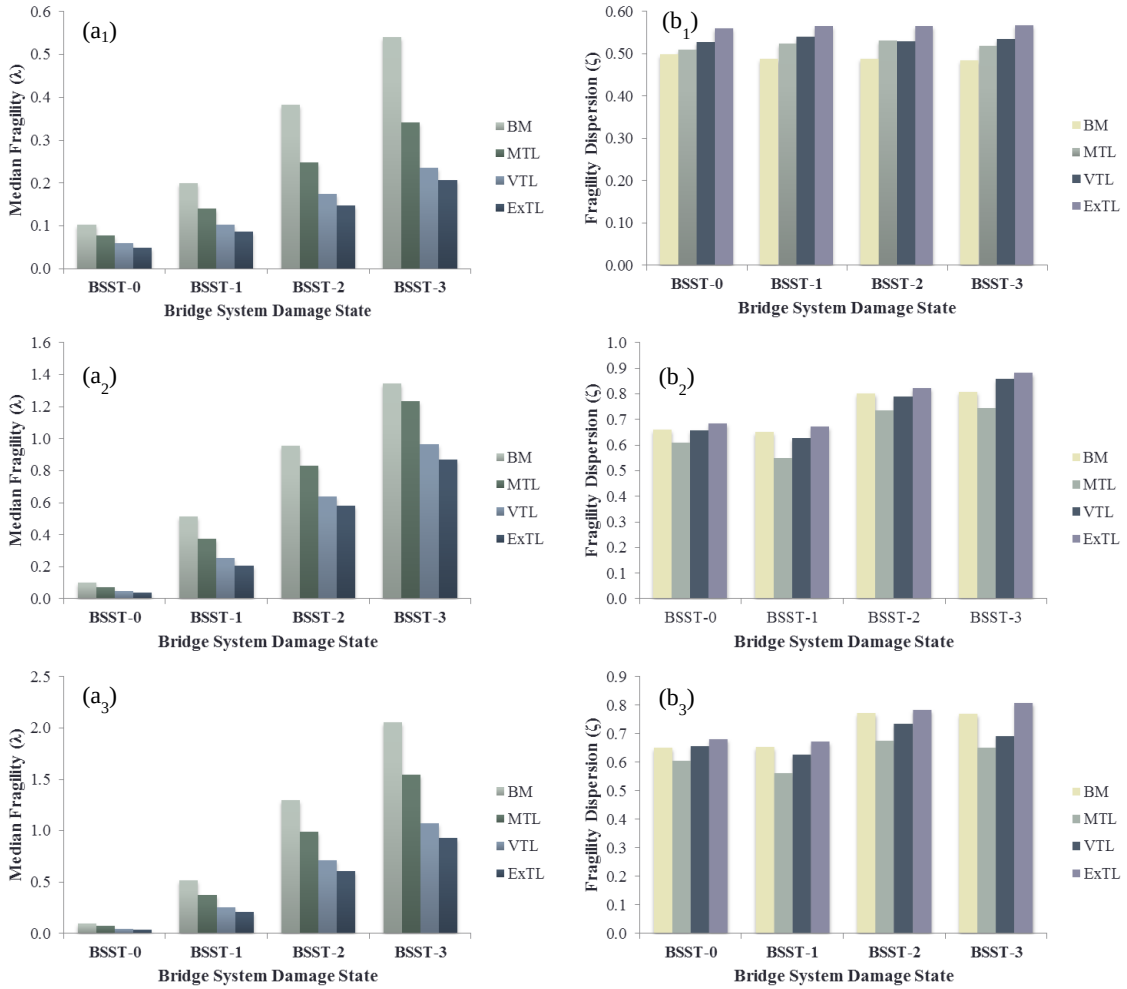

Figure 7.4: Comparison of the median and dispersion of the bridge system fragility curves for the tall bridge types: (1) pre-1970 design era; (2) 1970-1990 design era; (3) post-1990 design era

The results shown in Table 7.7 and Figure 7.4 illustrate that, for the three design eras, as the column height increases, the median fragility values decrease, which leads to higher seismic vulnerability. In the pre-1970 era, the variability between the medians of regular bridges and the tall class of bridges is higher at the higher levels of damage. However, this variation is constant for the 1970-1990 era. The difference between the medians is negligible at the slight damage state for the 1970-1990 and post-1990 eras. For bridges designed after 1990, the medians show higher variation at the complete damage level than at the other levels. On the other hand, the dispersion increases across

the levels of irregularity. Compared to the dispersion of the regular bridges, all tall classes have higher dispersions for the pre-1970 era, while there is a slight decrease in the MTL and VTL dispersion values. In general, for each design era, the dispersion values of different bridge classes are in a similar range.

Table 7.8: Fragility adjustment factors for the tall bridge types (specifications: multi-span continuous concrete box-girder bridges with seat abutments, single column per bent, and circular column cross-sections)

Bridge design era	Bridge type	BSST-0		BSST-1		BSST-2		BSST-3	
		ω_λ	ω_ζ	ω_λ	ω_ζ	ω_λ	ω_ζ	ω_λ	ω_ζ
Pre-1970	BM	1.000	1.000	1.000	1.000	1.000	1.000	1.000	1.000
	MTL	0.765	1.020	0.700	1.076	0.647	1.086	0.633	1.070
	VTL	0.578	1.058	0.515	1.107	0.455	1.084	0.435	1.103
	ExTL	0.480	1.124	0.435	1.160	0.387	1.157	0.381	1.171
1970-1990	BM	1.000	1.000	1.000	1.000	1.000	1.000	1.000	1.000
	MTL	0.710	0.924	0.726	0.843	0.869	0.918	0.920	0.922
	VTL	0.460	0.997	0.497	0.963	0.666	0.984	0.719	1.061
	ExTL	0.370	1.039	0.402	1.034	0.606	1.027	0.648	1.090
Post-1990	BM	1.000	1.000	1.000	1.000	1.000	1.000	1.000	1.000
	MTL	0.726	0.929	0.724	0.861	0.764	0.874	0.752	0.845
	VTL	0.474	1.011	0.497	0.959	0.546	0.952	0.520	0.900
	ExTL	0.389	1.048	0.400	1.029	0.465	1.016	0.451	1.051

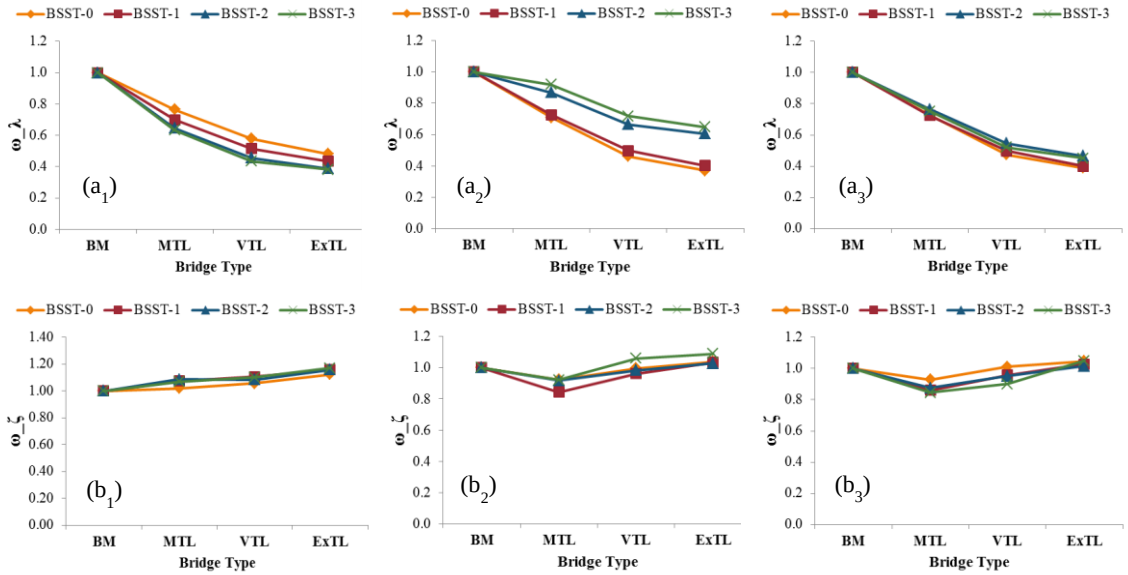

Figure 7.5: Comparison of the median and dispersion adjustment factors of the bridge system fragility curves for the tall bridge types: (1) pre-1970 design era; (2) 1970-1990 design era; (3) post-1990 design era

As shown in Table 7.8 and Figure 7.5, the adjustment factors corresponding to the median fragilities change from 0.37 to 1 in each of design eras. For the post-1990 era, it is observed that these factors are comparable within the four levels of damage. However, for the other design eras, these adjustment factors decrease as the damage state increases. In the pre-1970 bridge design era, the calculated factors related to the dispersion are slightly larger than unity for all tall classes. For bridges designed from 1970-1990, the complete damage state has the highest adjustment factor among all damage levels. For bridges designed after 1990, these factors reduce at higher damage levels.

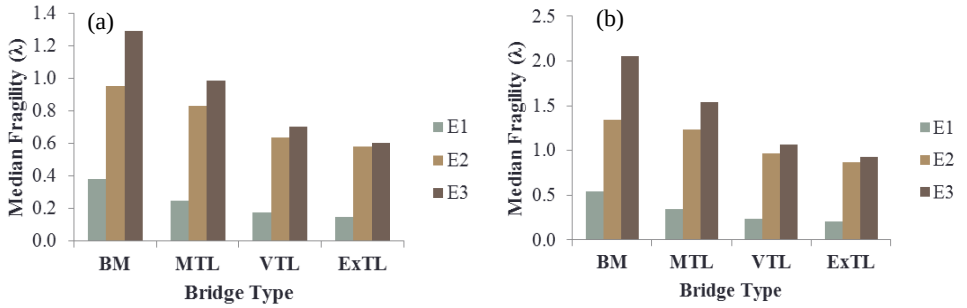

Figure 7.6: Comparison of the median system fragilities of tall bridges based on various design eras: (a) BBST-2; (b) BBST-3

It is seen from Figure 7.6 that, for all bridge configurations, bridges designed post-1990 and pre-1970 demonstrate the least and the most vulnerability, respectively. Also, bridges designed between 1970-1990 are less vulnerable than bridges designed before 1970. The observed enhanced seismic performance of bridges designed more recently is attributable to considerable improvements in the seismic bridge design codes following the 1971 San Fernando and the 1989 Loma Prieta earthquakes. The difference between the vulnerability of recently-designed bridges and older bridges is more noticeable at higher degrees of irregularity (e.g., extremely tall bridges). However, the

difference between the median fragilities of bridges designed from 1970-1990 and after 1990 is small, even for extremely tall and very tall bridges.

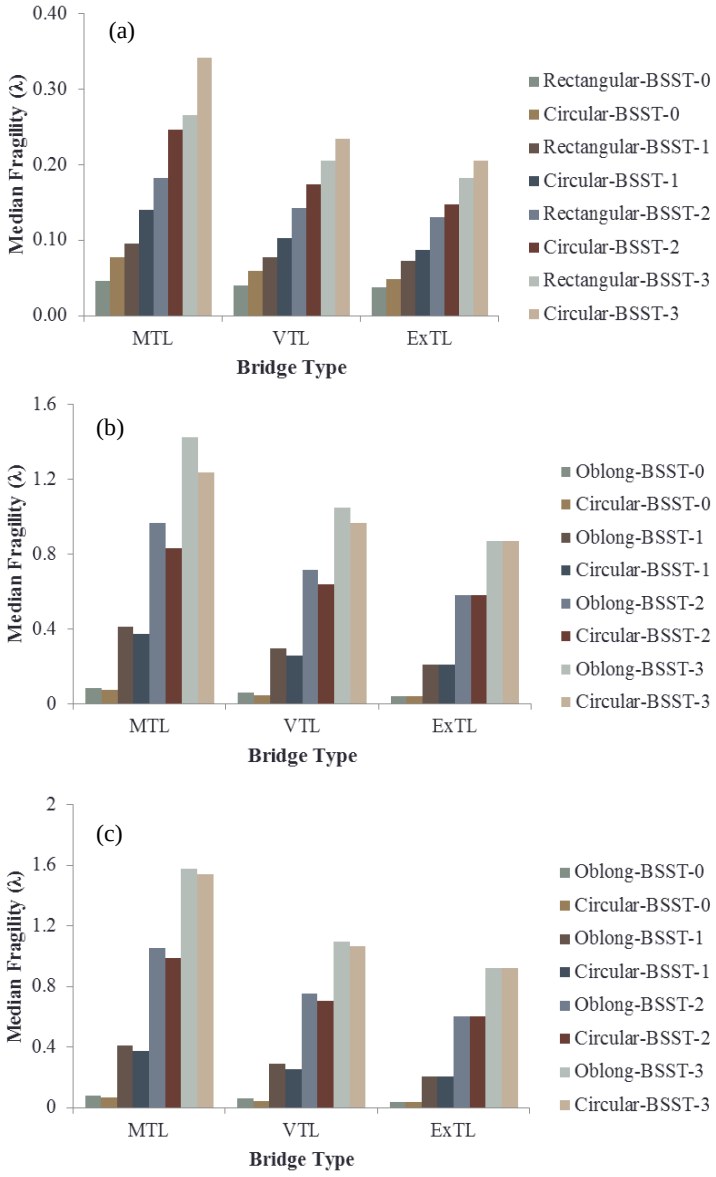

Figure 7.7: Comparison of the median system fragilities of tall bridges based on various column cross-section shapes: (a) pre-1970 design era; (b) 1970-1990 design era; (c) post-1990 design era

The median fragilities for bridges with various shapes of column cross-sections are compared in Figure 7.7. It is apparent that, for the older bridges, circular columns perform better than rectangular ones at all damage states. For the more recently-designed bridges, oblong columns perform better than the circular ones at slight and moderate

damage levels. For extremely tall bridges, there is a negligible difference between the medians of various columns shapes at all damage states.

The fragility parameters for very tall bridges with various configurations are presented in Table 7.9. A comparison of the results for the seat and rigid abutment types shows that, for bridges with single, two, and multiple columns per bent, the median difference is minor at the slight and moderate damage states, while major differences are observed at the extensive and complete damage states. This is more noticeable for bridges with two columns per bent. As an example, at BSST-3, the medians for TC-Rg-E3 and TC-St-E3 are 4.687 and 0.788 (i.e., 83.2% reduction), respectively while the medians for MC-Rg-E3 and MC-St-E3 are 2.387 and 0.831 (i.e., 65.2% reduction), respectively (Figure 7.8). It is seen from Figure 7.9 that the median changes among various numbers of columns per bent are negligible at BSST-0. It is also seen that at BSST-1, tall bridges with multi-column bents are more vulnerable than those with single column bents.

Table 7.9: Fragility parameters for the tall bridge types (specifications: multi-span continuous concrete box-girder bridges with circular column cross-sections and various abutment types and number of columns per bent)

Bridge type*	BSST-0		BSST-1		BSST-2		BSST-3	
	λ	ζ	λ	ζ	λ	ζ	λ	ζ
SC-Rg-E2	0.076	0.597	0.323	0.557	1.328	1.107	1.975	1.106
SC-St-E2	0.046	0.658	0.256	0.627	0.637	0.789	0.965	0.858
TC-Rg-E2	0.025	0.93	0.225	1.134	1.703	0.623	2.479	0.649
TC-St-E2	0.038	0.582	0.199	0.581	0.502	0.68	0.744	0.679
MC-Rg-E2	0.042	0.598	0.227	0.668	1.167	1.069	1.595	1.073
MC-St-E2	0.02	0.744	0.177	0.67	0.481	0.838	0.747	0.889
SC-Rg-E3	0.077	0.611	0.326	0.554	1.967	1.12	3.374	1.099
SC-St-E3	0.045	0.658	0.256	0.626	0.707	0.735	1.068	0.693
TC-Rg-E3	0.025	0.917	0.227	1.126	2.509	0.751	4.687	0.854
TC-St-E3	0.038	0.584	0.194	0.571	0.529	0.639	0.788	0.635
MC-Rg-E3	0.042	0.597	0.227	0.67	1.585	1.073	2.387	1.043
MC-St-E3	0.019	0.753	0.178	0.674	0.538	0.782	0.831	0.797

* refer to Appendix-I, Table I.1 for the nomenclature

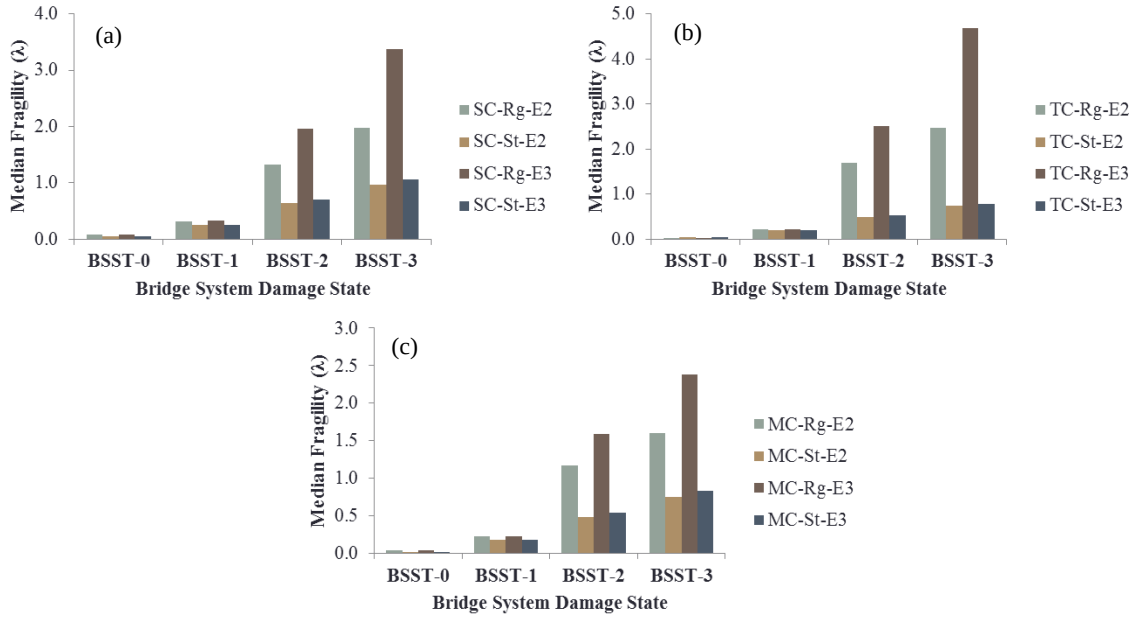

Figure 7.8: Comparison of the median system fragilities of tall bridges based on various abutment types; (a) single column per bent: (b) two columns per bent; (c) three columns per bent

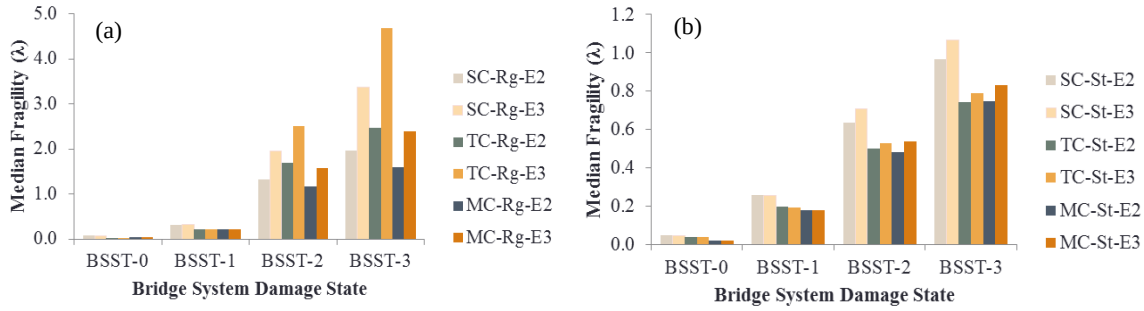

Figure 7.9: Comparison of the median system fragilities of tall bridges based on different number of columns per bent: (a) rigid diaphragm abutment; (b) seat type abutment

To assess the effectiveness of the tall bridges' columns on the resulting fragility curves, Figure 7.10 shows a sample of the fragility curves constructed for the four levels of damage corresponding to slight, moderate, extensive, and complete. It is apparent that the column height has a significant impact on the fragilities at the moderate, extensive, and complete damage states (i.e., BSST-1, BSST-2, and BSST-3). More variations are observed for the extensive and complete damage states, at which the increase in the vulnerability is more noticeable between the regular bridge model (BM) and the MTL, and also between the MTL and the VTL. However, the increase rate is lower between the VTL and the ExTL. Similarly, at BSST-0, the fragility curve of the ExTL is very close that of the VTL.

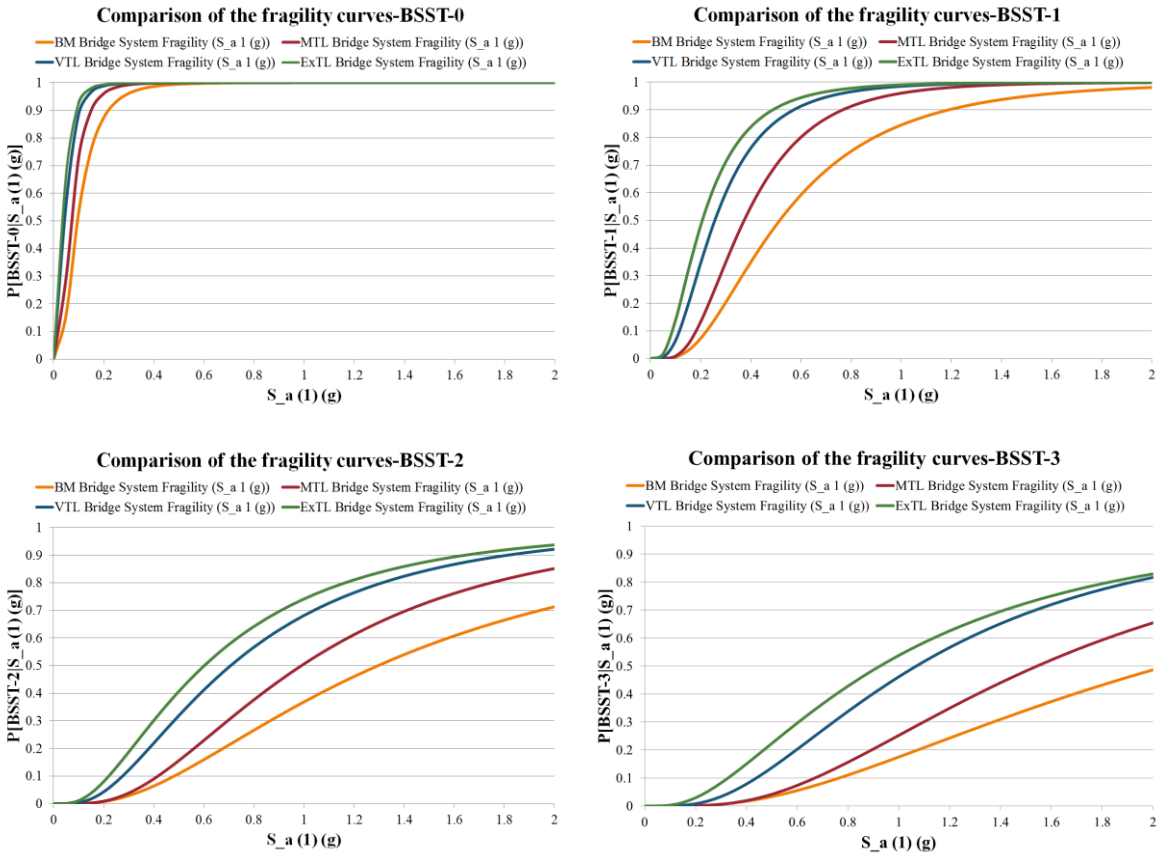

Figure 7.10: Comparison of the system fragility curves for the class of tall bridges (specifications: SC-St-E3 and circular column cross-sections)

7.2.2 Unbalanced Bridges

This study investigates the seismic performance of the family of unbalanced bridges in four ranges of bridge frame stiffness ratios, as shown in Table 7.6 and Chapter 5. The median (λ) and dispersion (ζ) of the generated fragility curves are given in Table 7.10, and a comparison is provided in Figure 7.11. Then the fragility values of the tall bridges are compared to the fragilities of the base models, and the adjustment factors (ω_λ and ω_ζ) are established, as presented in Table 7.11 and Figure 7.12.

Table 7.10: Fragility parameters for the unbalanced bridge types (specifications: multi-span continuous concrete box-girder bridges with seat abutments, single column per bent, and circular column cross-sections)

Bridge design era	Bridge type	BSST-0		BSST-1		BSST-2		BSST-3	
		λ	ζ	λ	ζ	λ	ζ	λ	ζ
Pre-1970	BM	0.110	0.486	0.217	0.490	0.414	0.499	0.595	0.510
	SUnb	0.105	0.509	0.216	0.525	0.415	0.521	0.603	0.531
	MUnb	0.106	0.519	0.209	0.533	0.407	0.529	0.589	0.533
	HUnb	0.107	0.519	0.211	0.509	0.404	0.511	0.584	0.524
	ExUnb	0.112	0.572	0.222	0.575	0.428	0.571	0.623	0.576
1970-1990	BM	0.129	0.536	0.620	0.525	1.145	0.575	1.540	0.587
	SUnb	0.128	0.548	0.602	0.519	1.089	0.574	1.457	0.580
	MUnb	0.124	0.543	0.581	0.523	1.036	0.574	1.377	0.580
	HUnb	0.116	0.543	0.533	0.527	0.932	0.596	1.236	0.595
	ExUnb	0.118	0.57	0.500	0.539	0.865	0.629	1.115	0.632
Post-1990	BM	0.131	0.543	0.625	0.516	1.491	0.563	2.238	0.587
	SUnb	0.129	0.542	0.603	0.523	1.386	0.571	2.080	0.580
	MUnb	0.123	0.548	0.577	0.519	1.330	0.564	1.975	0.570
	HUnb	0.116	0.54	0.531	0.524	1.196	0.581	1.755	0.583
	ExUnb	0.115	0.553	0.502	0.536	1.104	0.628	1.558	0.632

It is seen that the median values of various bridge classes are similar at the slight damage state, which indicates the minimal influence of the unbalanced stiffness frames at this level of damage. Regarding other damage states, for the class of irregular bridges designed after 1970, the median fragility decreases as the irregularity range increases, as shown in Figure 7.11. This observation is more noticeable at the higher levels of damage. A general trend for median values is not observed for bridges designed before 1970, but it

is seen that the dispersion increases by increasing the levels of irregularity. For more recently-designed bridges, the results show similar dispersions for all tall ranges at BSST-0 and BSST-1, while the data indicates an increase for extremely unbalanced bridges at BSST-2 and BSST-3.

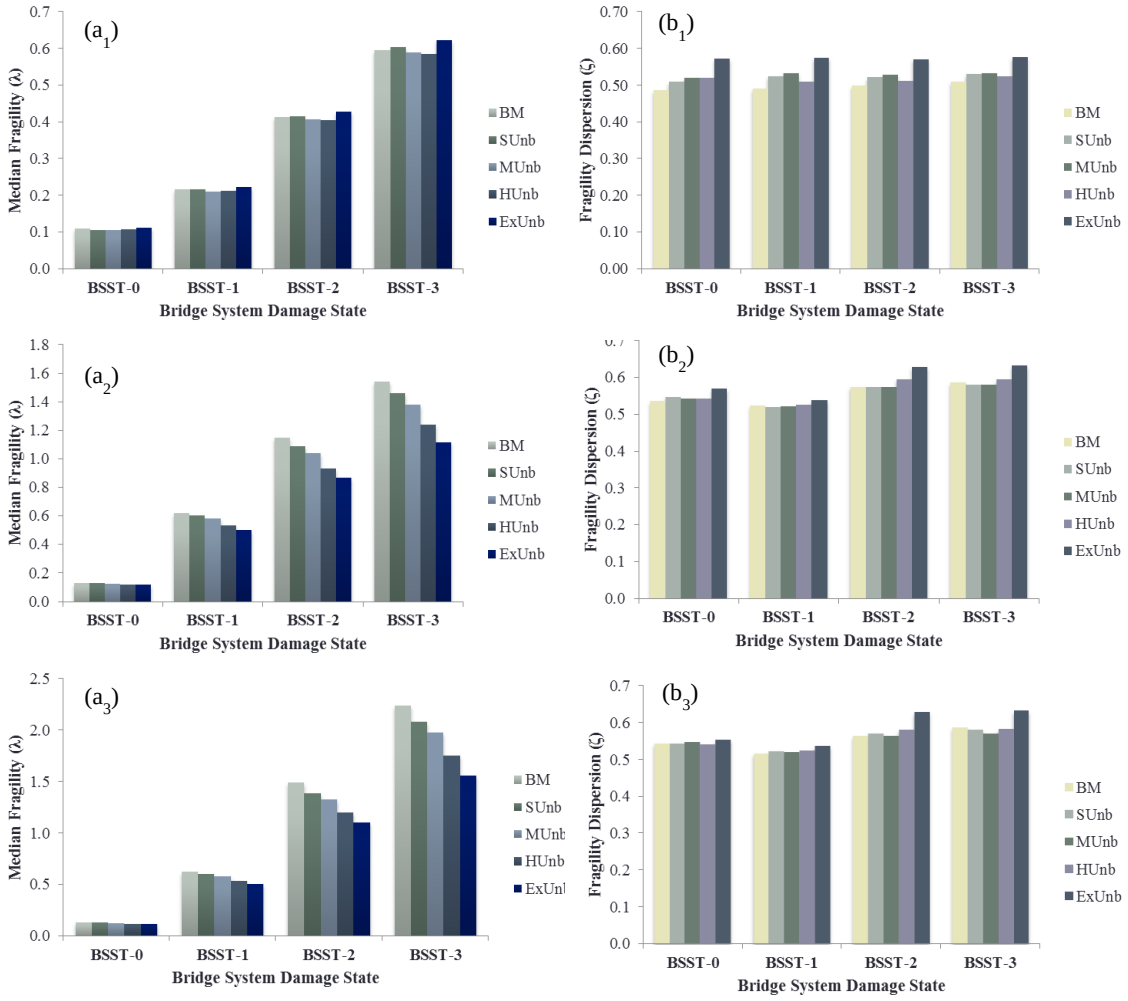

Figure 7.11: Comparison of the median and dispersion of the bridge system fragility curves for the unbalanced bridge types: (1) pre-1970 design era; (2) 1970-1990 design era; (3) post-1990 design era

As shown in Figure 7.12, the adjustment factors corresponding to the median fragility perturb around one for bridges designed before 1970. These factors reduce as both the levels of irregularity and damage increase. The adjustment factors of BSST-2 and BSST-3 are very close in almost all cases. Although the adjustment factors

corresponding to dispersion increase as the level of irregularity increases, the factors do not vary significantly across different damage states.

Table 7.11: Fragility adjustment factors for the unbalanced bridge types (specifications: multi-span continuous concrete box-girder bridges with seat abutments, single column per bent, and circular column cross-sections)

Bridge design era	Bridge type	BSST-0		BSST-1		BSST-2		BSST-3	
		ω_λ	ω_ζ	ω_λ	ω_ζ	ω_λ	ω_ζ	ω_λ	ω_ζ
Pre-1970	BM	1.000	1.000	1.000	1.000	1.000	1.000	1.000	1.000
	SUnb	0.955	1.047	0.995	1.071	1.002	1.044	1.013	1.041
	MUnb	0.964	1.068	0.963	1.088	0.983	1.060	0.990	1.045
	HUnb	0.973	1.068	0.972	1.039	0.976	1.024	0.982	1.027
	ExUnb	1.018	1.177	1.023	1.173	1.034	1.144	1.047	1.129
1970-1990	BM	1.000	1.000	1.000	1.000	1.000	1.000	1.000	1.000
	SUnb	0.992	1.022	0.971	0.989	0.951	0.998	0.946	0.988
	MUnb	0.961	1.013	0.937	0.996	0.905	0.998	0.894	0.988
	HUnb	0.899	1.013	0.860	1.004	0.814	1.037	0.803	1.014
	ExUnb	0.915	1.063	0.806	1.027	0.755	1.094	0.724	1.077
Post-1990	BM	1.000	1.000	1.000	1.000	1.000	1.000	1.000	1.000
	SUnb	0.985	0.998	0.965	1.014	0.930	1.014	0.929	0.988
	MUnb	0.939	1.009	0.923	1.006	0.892	1.002	0.882	0.971
	HUnb	0.885	0.994	0.850	1.016	0.802	1.032	0.784	0.993
	ExUnb	0.878	1.018	0.803	1.039	0.740	1.115	0.696	1.077

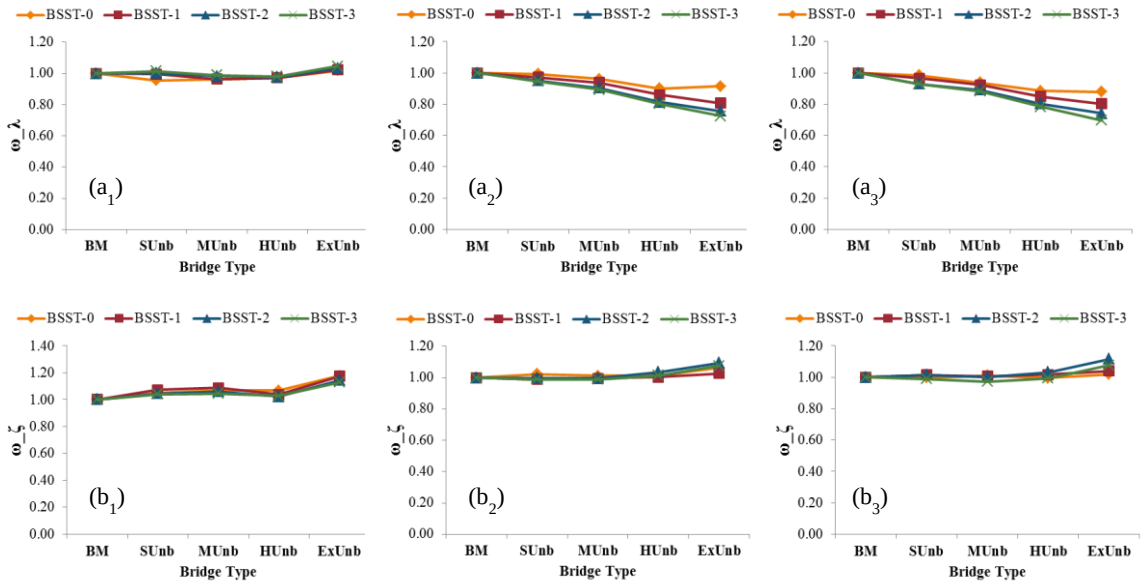

Figure 7.12: Comparison of the median and dispersion adjustment factors of the bridge system fragility curves for the unbalanced bridge types; (1) pre-1970 design era; (2) 1970-1990 design era; (3) post-1990 design era

Regarding various bridge design eras (Figure 7.13), more recently-designed bridges demonstrate improved performance when compared to older bridges, which is due to changes in bridge design requirements. This is generally true for all bridge classes, irrespective of irregularity types. The same trend was observed for tall bridges in the previous section.

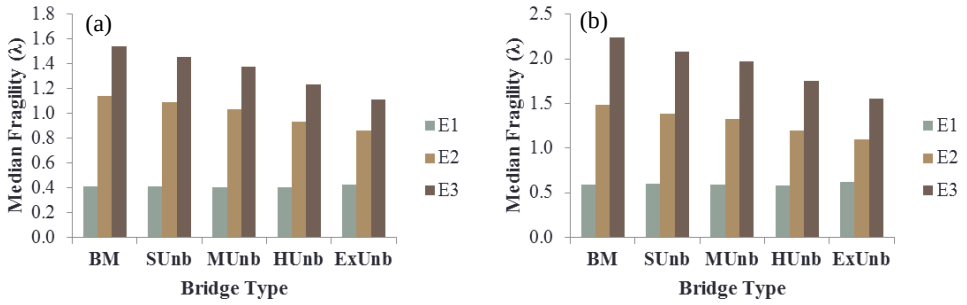

Figure 7.13: Comparison of the median system fragilities of unbalanced bridges based on various design eras: (a) BBST-2; (b) BBST-3

Figure 7.14 illustrates that circular columns perform better than rectangular columns in older bridges with unbalanced stiffness frames, irrespective of the damage levels and irregularity ranges. For bridges designed after 1970, bridges with oblong columns are less vulnerable than those with circular columns; this holds true for all damage levels except the slight damage state, in which the oblong and circular columns perform similarly. Also, the effect of unbalanced stiffness frames in Figure 7.14 is more noticeable for bridges designed after 1970.

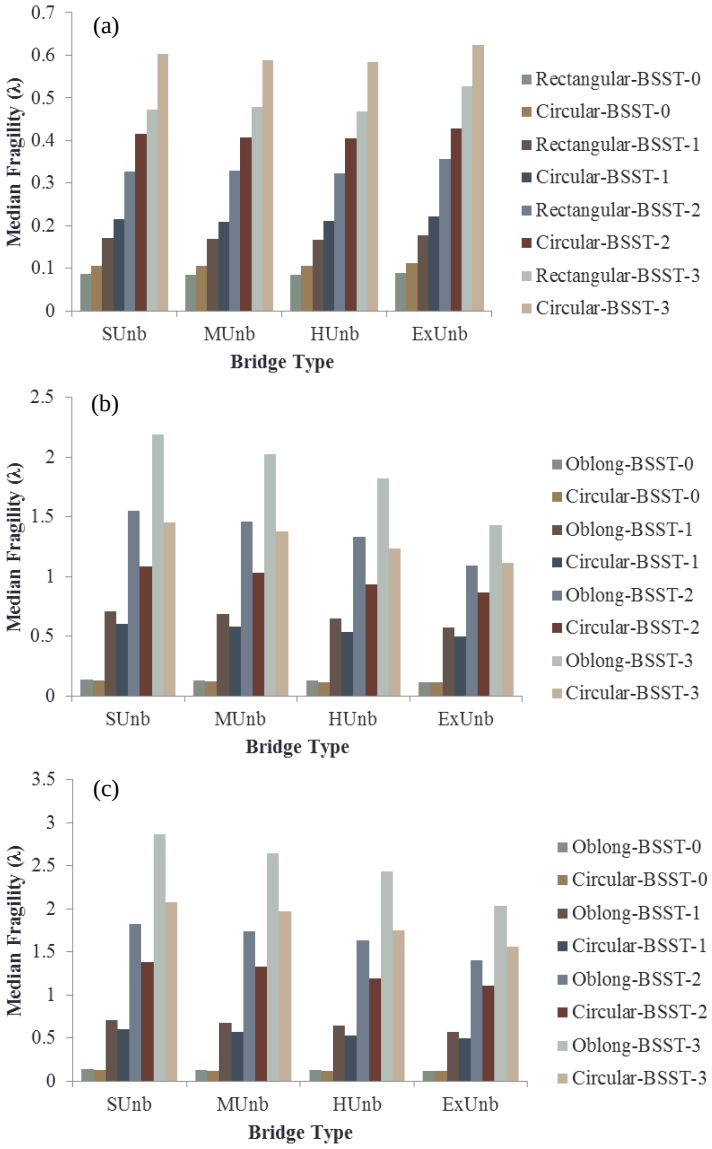

Figure 7.14: Comparison of the median system fragilities of unbalanced bridges based on various column cross-section shapes: (a) pre-1970 design era; (b) 1970-1990 design era; (c) post-1990 design era

The fragility parameters for the highly unbalanced bridge class with various configurations are presented in Table 7.12, and their values are compared in Figure 7.15 and Figure 7.16. As shown in Figure 7.15, bridges with seat abutments are more vulnerable than bridges with rigid diaphragm abutment, which is similar to the class of tall bridges. However, the difference between the median fragility is almost negligible at the slight damage state. In terms of the number of columns per bent, the differences between the vulnerability of bridges with seat or rigid abutments are more evident in single- and two-column bridges than in multi-column ones. Moreover, bridges with single and multiple columns per bent have the highest and lowest median fragilities, respectively, as shown in Figure 7.16.

Table 7.12: Fragility parameters for the unbalanced bridge types (specifications: multi-span continuous concrete box-girder bridges with circular column cross-sections and various abutment types and number of columns per bent)

Bridge type*	BSST-0		BSST-1		BSST-2		BSST-3	
	λ	ζ	λ	ζ	λ	ζ	λ	ζ
SC-Rg-E2	0.150	0.512	0.589	0.497	1.318	0.555	1.752	0.555
SC-St-E2	0.116	0.543	0.533	0.527	0.932	0.596	1.236	0.595
TC-Rg-E2	0.100	0.524	0.456	0.528	0.985	0.564	1.309	0.560
TC-St-E2	0.085	0.466	0.378	0.478	0.670	0.542	0.894	0.557
MC-Rg-E2	0.100	0.532	0.354	0.523	0.636	0.628	0.804	0.631
MC-St-E2	0.073	0.559	0.327	0.55	0.544	0.649	0.727	0.661
SC-Rg-E3	0.149	0.503	0.588	0.496	1.748	0.553	2.569	0.556
SC-St-E3	0.116	0.54	0.531	0.524	1.196	0.581	1.755	0.583
TC-Rg-E3	0.101	0.54	0.454	0.528	1.318	0.558	1.961	0.559
TC-St-E3	0.085	0.48	0.375	0.482	0.846	0.528	1.238	0.53
MC-Rg-E3	0.101	0.537	0.356	0.532	0.798	0.630	1.102	0.632
MC-St-E3	0.074	0.561	0.327	0.549	0.715	0.638	1.062	0.647

* refer to Appendix I, Table I.1 for the nomenclature

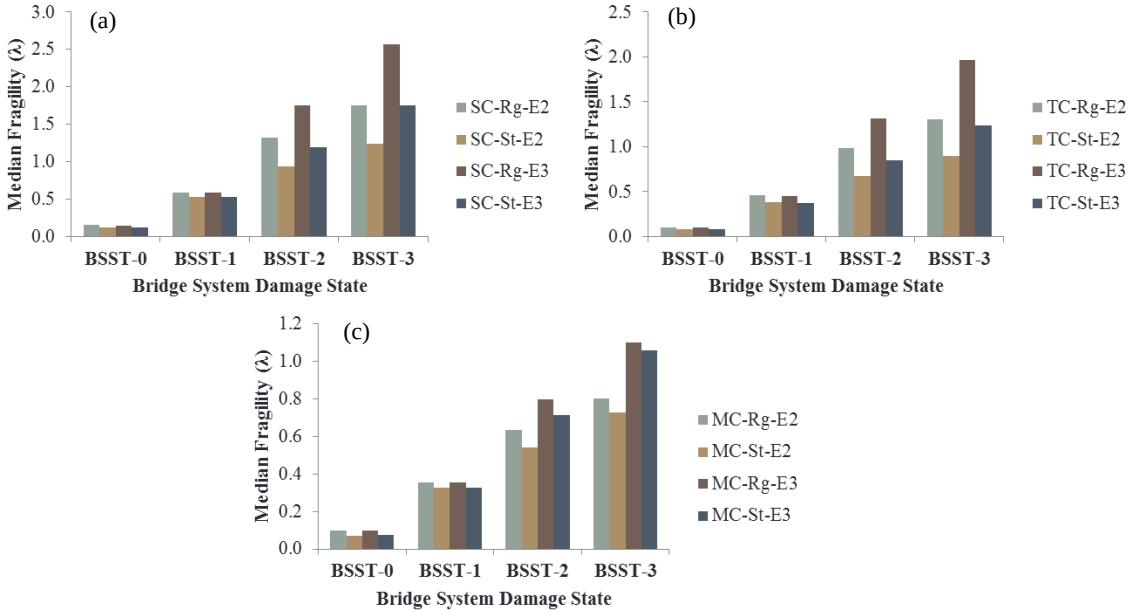

Figure 7.15: Comparison of the median system fragilities of unbalanced bridges based on various abutment types: (a) single column per bent; (b) two columns per bent; (c) three columns per bent

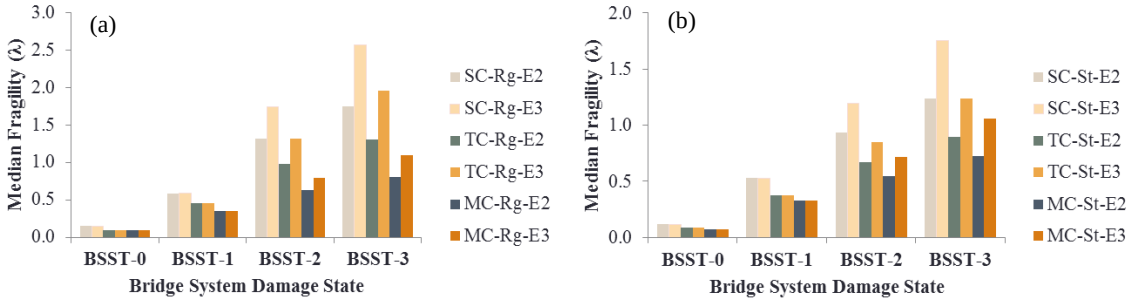

Figure 7.16: Comparison of the median system fragilities of unbalanced bridges based on different number of columns per bent: (a) rigid diaphragm abutment; (b) seat type abutment

To analyze the effects of unbalanced stiffness frames, the fragility curves for the four unbalanced bridge classes are compared to those of regular bridges, as shown in Figure 7.17. Through these comparisons, it appears that unequal column heights have little influence on fragilities at the slight damage state. More variations are seen at higher damage levels. The increase rate of the fragility curves is fairly constant across various ranges of irregularity. However, the SUnb and MUnb fragility curves vary slightly at the extensive and complete damage levels. Overall, it can be concluded that vulnerability increases at higher degrees of irregularity for bridges with unbalanced stiffness frames.

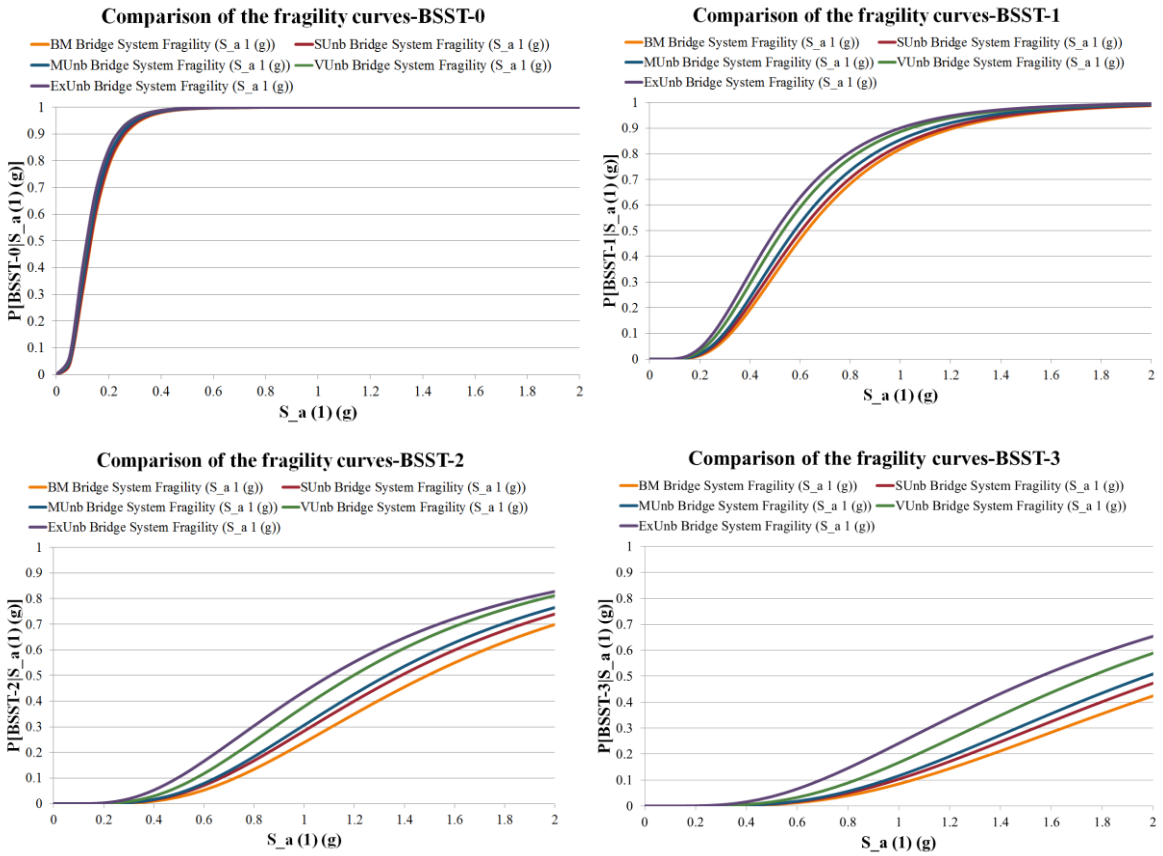

Figure 7.17: Comparison of the system fragility curves for the class of unbalanced bridges (specifications: SC-St-E3 and circular column cross-sections)

7.2.3 Skewed Bridges

As mentioned in previous chapters and Table 7.6, this study explores the seismic performance of the family of tall bridges at five ranges of skew angles. The median (λ) and dispersion (ζ) of the generated fragility curves are given in Table 7.7. Then the fragility values of tall bridges are compared to the fragilities of the base models, and adjustment factors (ω_λ and ω_ζ) are established, as presented in Table 7.14.

Table 7.13: Fragility parameters for the skewed bridge types (specifications: multi-span continuous concrete box-girder bridges with seat abutments, single column per bent, and circular column cross-sections)

Bridge design era	Bridge type	BSST-0		BSST-1		BSST-2		BSST-3	
		λ	ζ	λ	ζ	λ	ζ	λ	ζ
Pre-1970	BM	0.102	0.499	0.200	0.488	0.382	0.489	0.540	0.485
	SKL	0.099	0.506	0.197	0.497	0.376	0.499	0.533	0.498
	SKM	0.085	0.538	0.181	0.542	0.348	0.547	0.500	0.561
	SKH	0.084	0.514	0.180	0.523	0.343	0.530	0.491	0.545
	SKVH	0.083	0.489	0.178	0.504	0.337	0.512	0.482	0.528
	SKEx	0.065	0.381	0.139	0.393	0.263	0.399	0.376	0.411
1970-1990	BM	0.100	0.660	0.515	0.651	0.957	0.802	1.343	0.809
	SKL	0.097	0.641	0.507	0.632	0.944	0.769	1.293	0.776
	SKM	0.085	0.552	0.470	0.545	0.883	0.614	1.054	0.623
	SKH	0.085	0.551	0.465	0.541	0.850	0.603	1.012	0.609
	SKVH	0.086	0.550	0.460	0.536	0.818	0.591	0.969	0.595
	SKEx	0.067	0.429	0.358	0.418	0.637	0.461	0.755	0.464
Post-1990	BM	0.095	0.651	0.515	0.653	1.296	0.772	2.052	0.770
	SKL	0.093	0.635	0.506	0.635	1.271	0.743	2.021	0.741
	SKM	0.081	0.562	0.462	0.548	1.155	0.609	1.873	0.606
	SKH	0.081	0.549	0.455	0.543	1.110	0.598	1.797	0.600
	SKVH	0.081	0.535	0.448	0.538	1.066	0.586	1.721	0.594
	SKEx	0.063	0.417	0.349	0.419	0.830	0.752	1.341	0.762

The median fragility is fairly similar for SKL and BM, and then it reduces from SKL to SKM (Figure 7.18). Bridges in the categories of SKH and SKVH have slightly lower median fragilities than those in the SKM. Then the median values reduce significantly from SKVH to SKEx. This phenomenon is more evident at higher levels of damage. It is also seen from Figure 7.18 that the dispersion varies based on the variable

skew angle, and there is a noticeable change at SKM and higher skewed ranges. For older bridges, dispersion of SKL is close to the BM dispersion, and the dispersion increases from BM to SKM, but this trend is reversed after the SKM category for most cases. For bridges designed after 1970, the dispersion decreases as the skew angle increases, and the SKM, SKH, and SKVH have very similar dispersions.

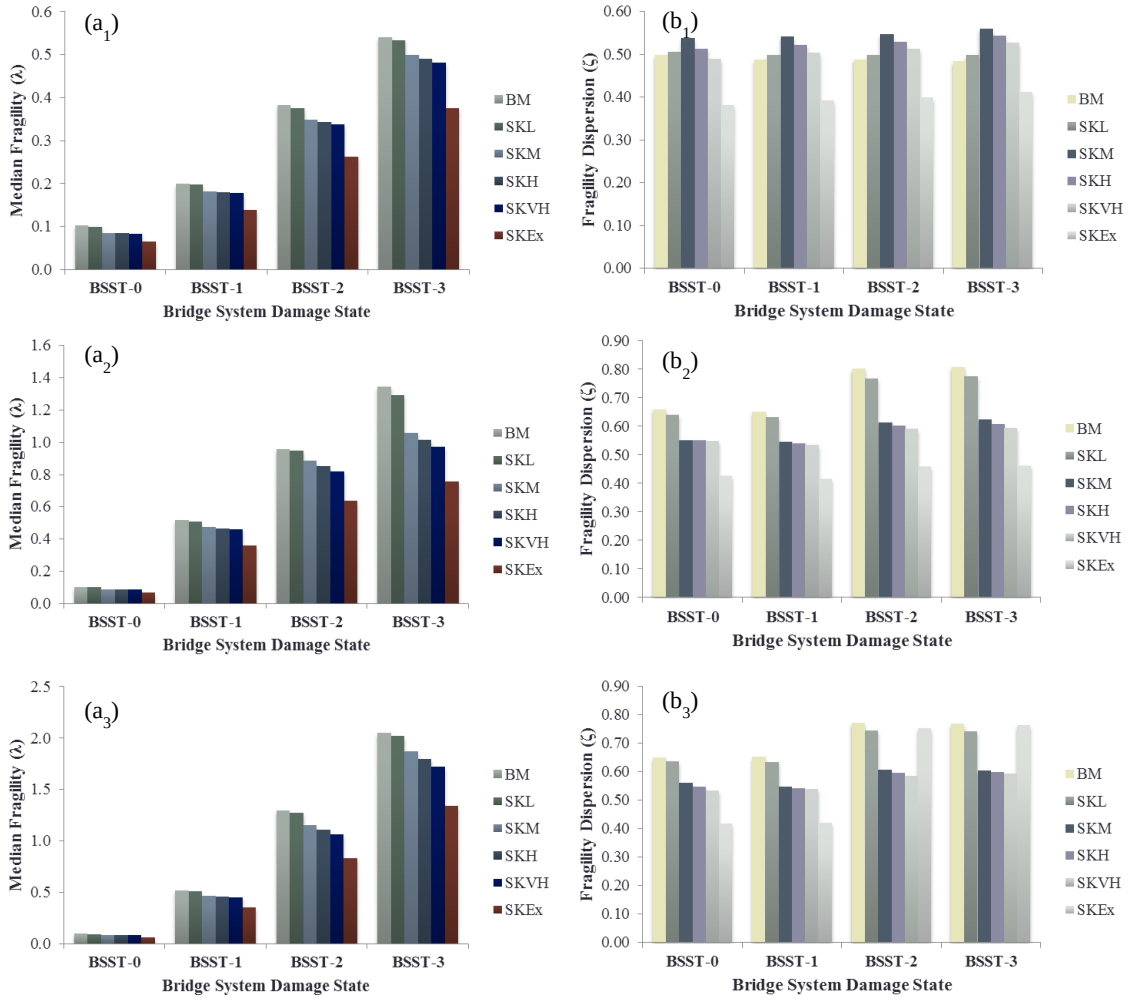

Figure 7.18: Comparison of the median and dispersion of the bridge system fragility curves for the skewed bridge types: (1) pre-1970 design era; (2) 1970-1990 design era; (3) post-1990 design era

The adjustment factors corresponding to the median fragility across the various skew ranges are fairly close (Table **7.14** and Figure 7.19). A significant decrease is observed at the complete damage state for bridges designed in the 1970-1990 era. The comparison of these adjustment factors indicates a notable decrease from SKVH to SKEx. It is seen that the adjustment factors corresponding to the dispersion are highest and lowest at BSST-3 and BSST-0, respectively, for older bridges. Also, the values related to BSST-1 are similar to the values for BSST-2. For more recent design eras, the factors are similar at lower damage levels (BSST-0 and BSST-1) and are higher than the factors at higher damage levels (BSST-2 and BSST-3).

Table 7.14: Fragility adjustment factors for the skewed bridge types (specifications: multi-span continuous concrete box-girder bridges with seat abutments, single column per bent, and circular column cross-sections)

Bridge design era	Bridge type	BSST-0		BSST-1		BSST-2		BSST-3	
		ω_λ	ω_ζ	ω_λ	ω_ζ	ω_λ	ω_ζ	ω_λ	ω_ζ
Pre-1970	BM	1.000	1.000	1.000	1.000	1.000	1.000	1.000	1.000
	SKL	0.971	1.014	0.984	1.019	0.984	1.021	0.987	1.027
	SKM	0.837	1.078	0.906	1.111	0.910	1.119	0.926	1.157
	SKH	0.826	1.029	0.898	1.072	0.897	1.083	0.909	1.123
	SKVH	0.815	0.980	0.890	1.033	0.883	1.047	0.892	1.089
	SKEx	0.635	0.764	0.694	0.805	0.688	0.816	0.695	0.848
1970-1990	BM	1.000	1.000	1.000	1.000	1.000	1.000	1.000	1.000
	SKL	0.973	0.971	0.985	0.972	0.986	0.959	0.962	0.960
	SKM	0.846	0.836	0.914	0.837	0.923	0.766	0.785	0.770
	SKH	0.852	0.835	0.903	0.830	0.889	0.751	0.753	0.753
	SKVH	0.859	0.833	0.893	0.823	0.854	0.737	0.722	0.735
	SKEx	0.669	0.649	0.696	0.642	0.666	0.574	0.562	0.573
Post-1990	BM	1.000	1.000	1.000	1.000	1.000	1.000	1.000	1.000
	SKL	0.974	0.976	0.982	0.972	0.981	0.963	0.985	0.963
	SKM	0.854	0.863	0.896	0.839	0.891	0.789	0.913	0.787
	SKH	0.854	0.843	0.883	0.832	0.857	0.774	0.876	0.779
	SKVH	0.854	0.822	0.871	0.824	0.822	0.759	0.838	0.771
	SKEx	0.665	0.640	0.678	0.642	0.641	0.974	0.653	0.990

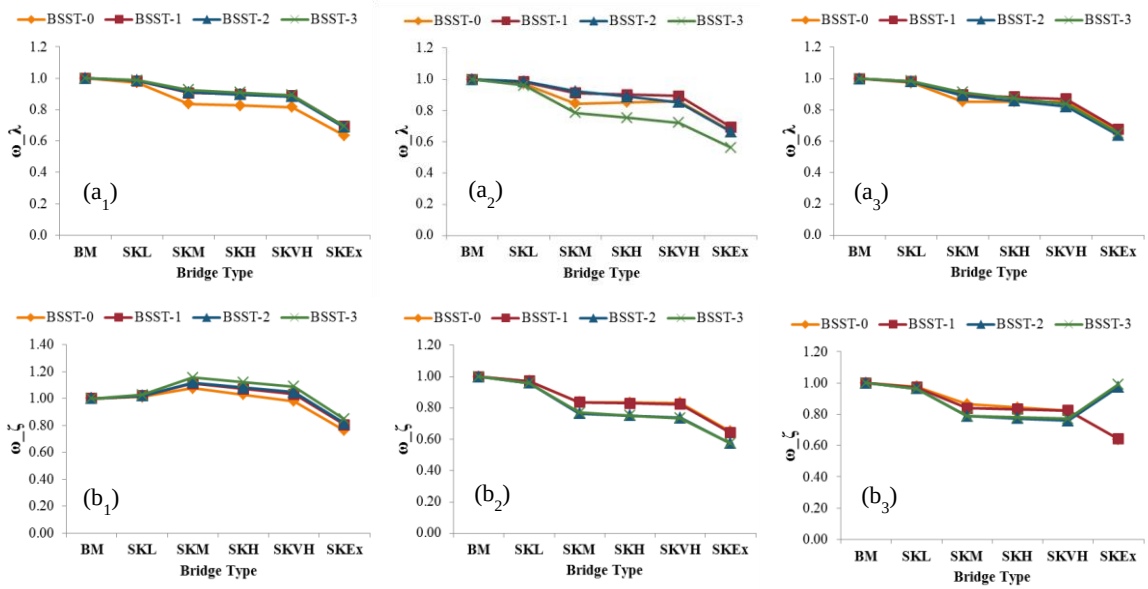

Figure 7.19: Comparison of the median and dispersion adjustment factors of the bridge system fragility curves for the skewed bridge types: (1) pre-1970 design era; (2) 1970-1990 design era; (3) post-1990 design era

Figure 7.20 compares the median fragilities across various design eras. The results are similar to those explained at the tall and unbalanced section. Figure 7.21 demonstrates changes in the median fragility based on various bridge column shapes. For older bridges, bridges with circular columns are less vulnerable than bridges with rectangular columns. For more recently-designed bridges, bridges with oblong columns show better performance than bridges with circular columns; this is more apparent at the complete damage state.

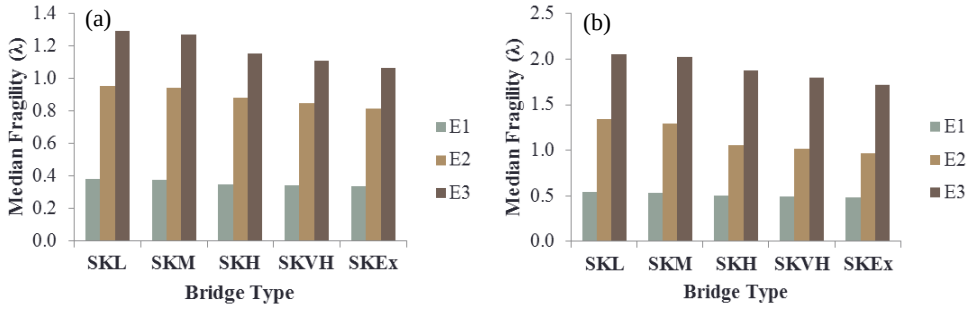

Figure 7.20: Comparison of the median system fragilities of skewed bridges based on various design eras: (a) BBST-2; (b) BBST-3

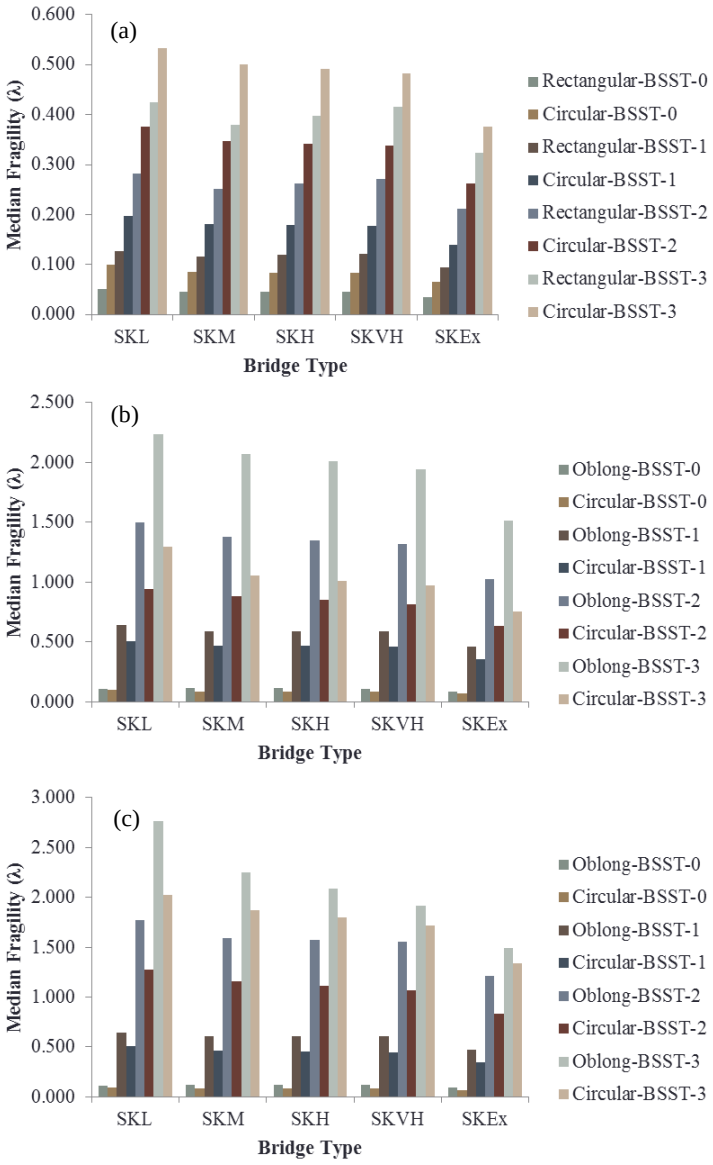

Figure 7.21: Comparison of the median system fragilities of skewed bridges based on various column cross-section shapes: (a) pre-1970 design era; (b) 1970-1990 design era; (c) post-1990 design era

The fragility parameters for the class of highly skewed bridges with various configurations are presented in Table 7.15, and the values are compared in Figure 7.22 and Figure 7.23. The results (Figure 7.22) affirm that skewed bridges with seat abutments are more vulnerable than skewed bridges with rigid diaphragm abutments, particularly at higher damage levels. It is noted from Figure 7.23 that bridges with multiple columns per

bent are more vulnerable than those with single columns. Although the difference between the median fragilities is negligible at the slight damage state, the median changes considerably at higher damage levels such as BSST-3.

Table 7.15: Fragility parameters for the skewed bridge types (specifications: multi-span continuous concrete box-girder bridges with circular column cross-sections and various abutment types and number of columns per bent)

Bridge type*	BSST-0		BSST-1		BSST-2		BSST-3	
	λ	ζ	λ	ζ	λ	ζ	λ	ζ
SC-Rg-E2	0.154	0.555	0.622	0.531	1.487	0.642	2.014	0.639
SC-St-E2	0.085	0.551	0.465	0.541	0.850	0.603	1.012	0.609
TC-Rg-E2	0.100	0.468	0.411	0.436	1.057	0.531	1.430	0.531
TC-St-E2	0.089	0.464	0.414	0.460	0.757	0.539	1.013	0.538
MC-Rg-E2	0.095	0.568	0.377	0.521	0.801	0.725	1.080	0.729
MC-St-E2	0.061	0.609	0.325	0.596	0.596	0.913	0.831	0.951
SC-Rg-E3	0.153	0.546	0.629	0.530	2.030	0.646	3.051	0.634
SC-St-E3	0.081	0.549	0.455	0.543	1.110	0.598	1.797	0.600
TC-Rg-E3	0.099	0.464	0.413	0.435	1.420	0.530	2.160	0.547
TC-St-E3	0.090	0.482	0.416	0.454	0.971	0.521	1.450	0.526
MC-Rg-E3	0.095	0.570	0.381	0.527	1.073	0.731	1.616	0.728
MC-St-E3	0.062	0.590	0.326	0.585	0.807	0.874	1.272	0.902

* refer to Appendix I, Table I.1 for the nomenclature

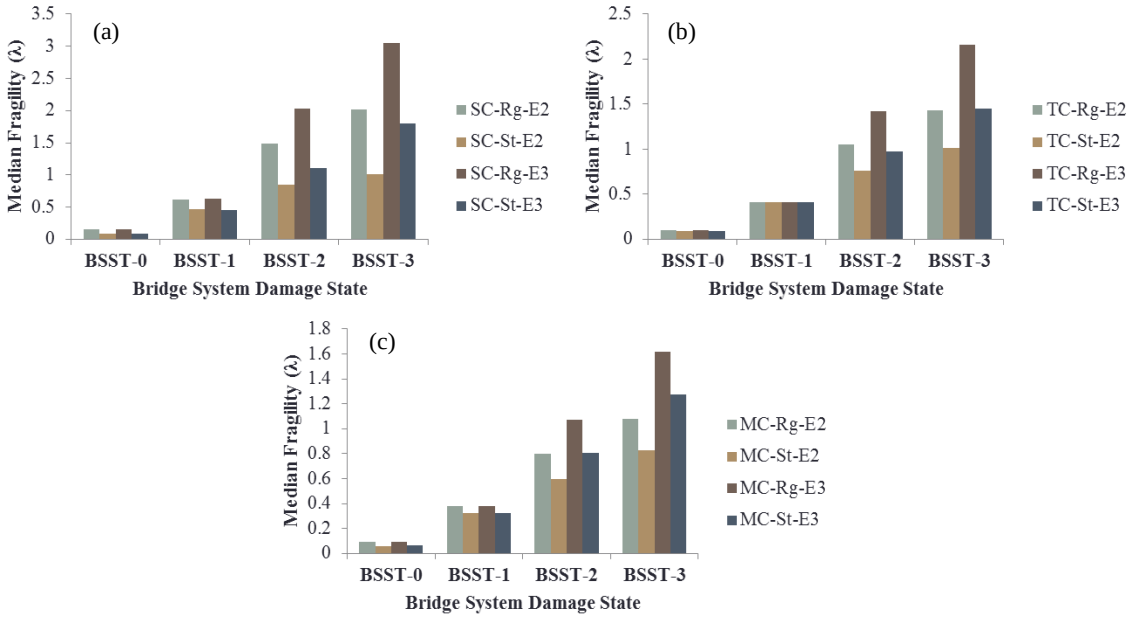

Figure 7.22: Comparison of the median system fragilities of skewed bridges based on various abutment types: (a) single column per bent; (b) two columns per bent; (c) three columns per bent

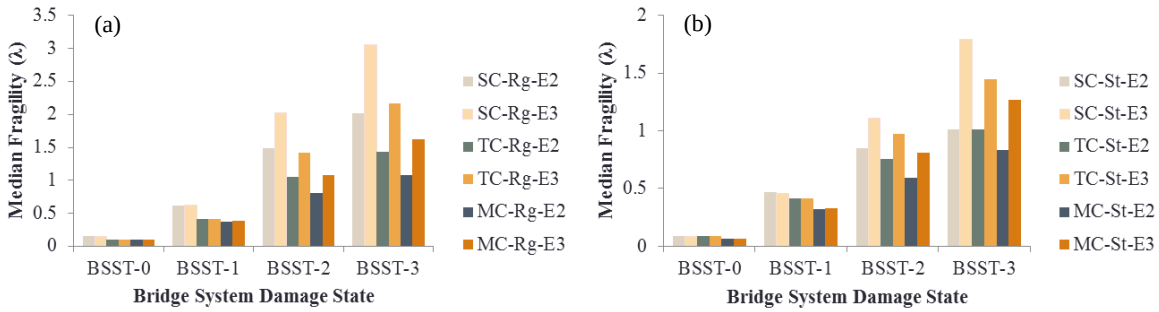

Figure 7.23: Comparison of the median system fragilities of skewed bridges based on different number of columns per bent: (a) rigid diaphragm abutment; (b) seat type abutment

In order to illustrate the impact of skew angle on the generated fragility curves, Figure 7.24 demonstrates a sample of the fragility curves constructed for the four levels of damage (slight, moderate, extensive, and complete). The results indicate that the fragility curve does not significantly shift at lower skew angles (i.e., SKL). As the skew angle increases, the changes in fragility curves lead to higher vulnerability. At BSST-0 and BSST-1, the fragility curves of SKM are very close to those of SKH and SKVH, while at BSST-2 and BSST-3, as the skew angle increases, the curve shifts with a constant rate. At all damage states, extremely skewed bridges appear to be more vulnerable than other skewed classes, particularly when compared to the slightly skewed class.

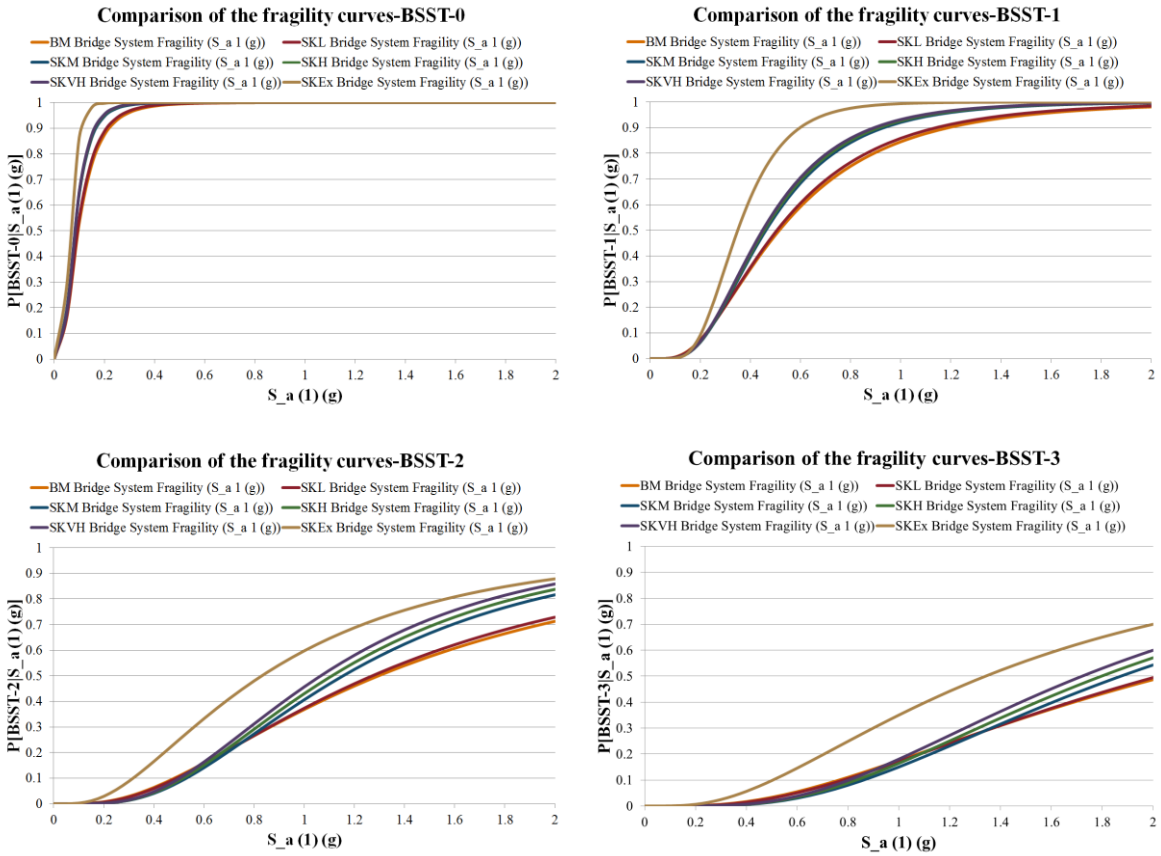

Figure 7.24: Comparison of the system fragility curves for the class of skewed bridges (specifications: SC-St-E3 and circular column cross-sections)

7.2.4 Comparison with HAZUS

One well-known seismic assessment tools is Hazard US Multi-Hazard (HAZUS-MH), which uses fragility analysis to assess the seismic performance of structures (HAZUS, 2003). However, HAZUS has some limitations for geometric irregularities that require some improvements. HAZUS proposed fragility curves for 28 primary bridge types and defined modification factors to be applied to the median fragilities to reflect the impact of specific bridge features listed as skew angle, number of spans, span width, and span length. These bridge specifications are assigned to three factors called K_{skew}, K_{shape}, and K_{3D} and are multiplied by the median fragilities of the primary bridges. The new

median fragility values, along with a constant dispersion of 0.6, are used to form the fragility curves in HAZUS. This section is devoted to the comparison of the generated fragilities for skewed bridges with those obtained from HAZUS-MH. The HAZUS modification factor for skewed bridges is calculated as

$$K_{skew} = \sqrt{\sin(90 - \alpha)} \tag{3}$$

$\alpha = 15^{\circ} \rightarrow K_{skew} = 0.983$
$\alpha = 30^{\circ} \rightarrow K_{skew} = 0.930$
$\alpha = 45^{\circ} \rightarrow K_{skew} = 0.841$
$\alpha = 60^{\circ} \rightarrow K_{skew} = 0.707$
$\alpha = 77^{\circ} \rightarrow K_{skew} = 0.474$

Figure 7.25 presents a comparison of the modification factors calculated from Equation 3 and those computed in the present study. The calculated adjustment factors for bridges with low skew angles (SKL) agree with the values proposed by HAZUS-M. However, the factors differ for bridges with higher skew angles. In particular, the HAZUS-MH suggests lower modification factors for bridges in the SKVH and SKEx category, which lead to overestimating the probability of damage. Although HAZUS provides conservative estimates of the median fragilities for two classes of skewed bridges, the general trend of the adjustment factors for various damage levels agree fairly well with those proposed by HAZUS-MH, as seen in Figure 7.25. However, the fragilities of irregular bridges are underestimated by HAZUS-MH, as shown in Figure 7.26.

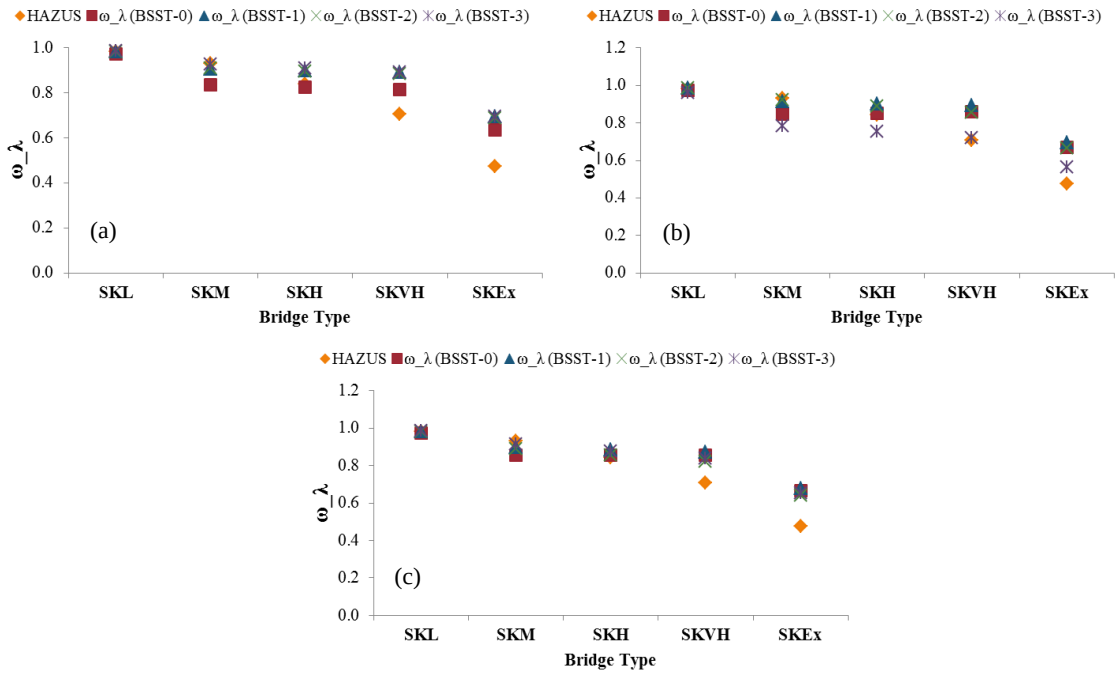

Figure 7.25: Comparison of the developed adjustment factors with the HAZUS proposed modification factors: (a) pre-1970 design era; (b) 1970-1990 design era; (c) post-1990 design era

The discrepancies between the adjustment factors and the median fragilities derived in the current study and those suggested by HAZUS occur for several reasons, including variation in the structural modeling strategy and assessment algorithm. The other major differences involve the treatment of uncertainty, definition of bridge design eras, and selection of capacity models. Overall, the current study improves the HAZUS fragility estimation of bridges in several key aspects:

- The current study utilized the most up-to-date modeling techniques to conduct three-dimensional nonlinear time history analyses on irregular bridges. However, HAZUS used simplified two-dimensional structural analyses.
- This study considers the material uncertainty along with the uncertainties associated with the geometric attributes and ground motions pertinent to concrete box-girder bridges. These uncertainties were identified according to a

plan review of thousands of existing bridges in California and in communication with bridge design engineers and experts. However, the HAZUS fragilities were derived based on limited consideration of uncertainty, including the material properties such as concrete strength and the reinforcement ratios, which can significantly affect the ductility of bridge columns and hence the final vulnerability results.

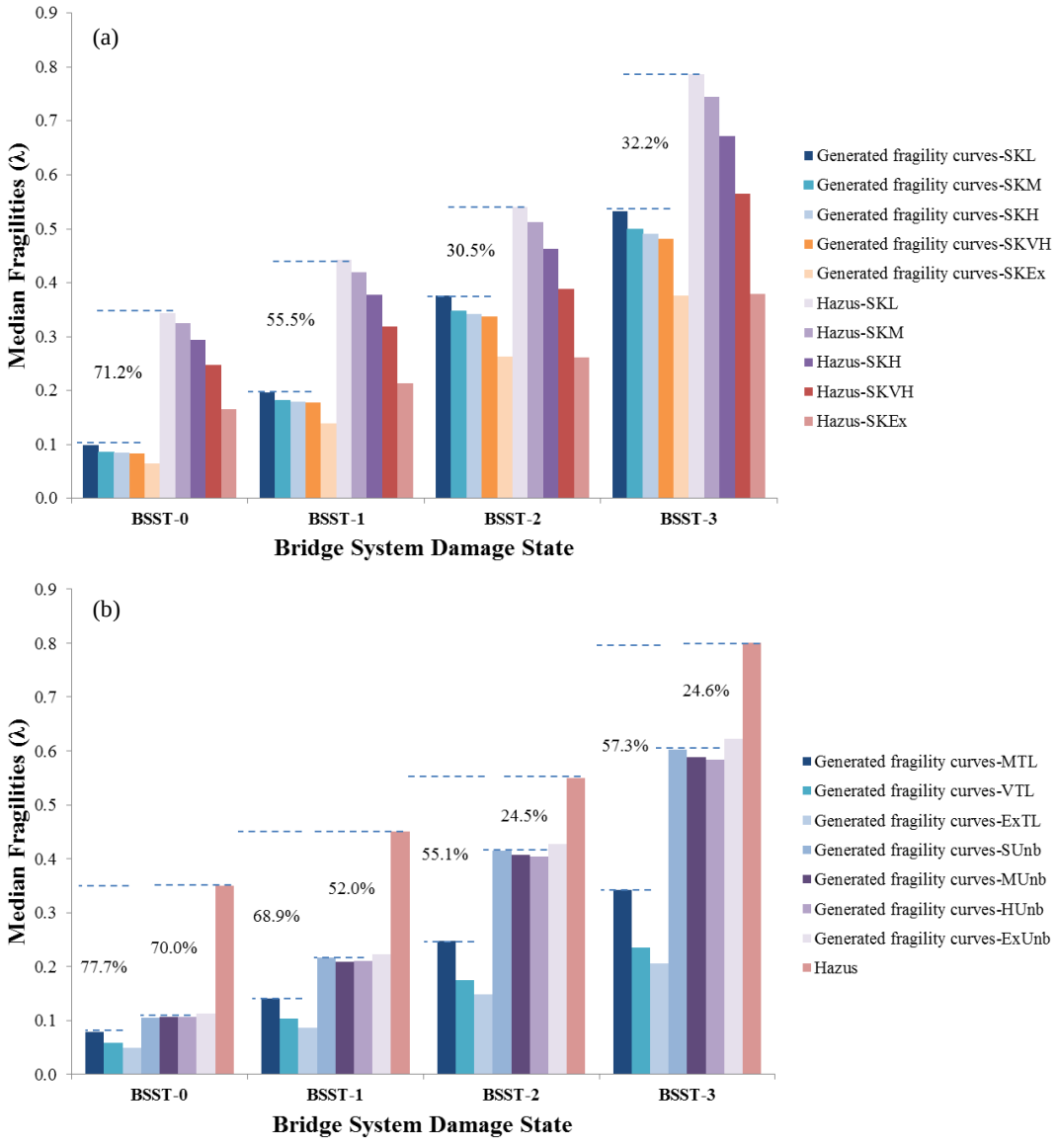

Figure 7.26: Comparison of the calculated and HAZUS median fragilities for (a) skewed bridges and (b) tall and unbalanced bridges

- Although there is a lack of information about the capacity models used to develop HAZUS fragility values (except that a qualitative description of visible damage is described in the report), the current work provides a database to approximate capacity models summarizing the experimental investigations combined with the expert opinions. The capacity models used in this study are the first iteration of exploring a comprehensive database for the capacity models. The collaboration between Georgia Tech's research team and Caltrans is ongoing, and will continue to offer refinements for the limit states in future research phases.
- The current study provides adjustment factors for major geometric irregularities: skew angle, tall column bents, and unbalanced stiffness frames. Among these factors, HAZUS suggested a single modification factor for skew angle and did not provide recommendations for the other geometric attributes (e.g., column height).
- Although it is apparent from the fragility analysis of this study that system fragility is dominated by column fragility, other components such as abutment type and deck also contribute to bridge vulnerability and therefore they are included in the development of bridge system fragility curves. In this regard, HAZUS only relied on the vulnerability of bridge columns to develop the system fragility curves, which underestimates the bridge system fragility.
- The current study provides individual adjustment factors for each of the four damage levels. However, HAZUS-MH proposed a single factor for all damage states.

7.3 Closure

In order to assess the influence of geometric irregularities on the bridge vulnerability, this chapter provided a general description of the fragility analysis framework that has been used in this study to generate fragility curves of selected bridges with irregularities. The fragilities of irregular bridges were compared to those of regular bridges, and appropriate adjustment factors were derived for estimating the fragility of bridges with geometric irregularities. The proposed adjustment factors mainly contribute to the development of reliable fragility curves that are applicable to the class of irregular bridges. Among the three evaluated irregularities, tall column heights showed the highest influence on the fragilities of concrete box-bridge bridges. The skew angle was the second most-influential parameter. The computed adjustment factors were compared with HAZUS-MH modification factors. Overall, the comparison between the established adjustment factors in this study and the HAZUS modification factors demonstrated that the application of the HAZUS factors for bridges with very high and/or extreme skew angles results in a higher level of vulnerability than the proposed factors in this study, while both factors for the lower levels of irregularity (i.e., SKL, SLM, and SKH) are almost similar.

CHAPTER 8

CONCLUSIONS AND FUTURE RESEARCH

This work assessed the impacts of selected geometric irregularities on the vulnerability analyses of concrete box-girder bridges. This Chapter summarizes the notable findings from this work and highlights key contributions as well as the potential future research outlines.

8.1 Summary and Conclusions

The development of analytical fragility curves is advantageous for the risk assessment of bridges with complex configurations and geometries for which the computation of the probability of damage requires challenging programing and extensive simulations. Moreover, the curves provide valuable insight for decision makers who must choose suitable rehabilitation plans.

Prior to the evaluation of bridges in this study, suitable numerical approaches for creating finite element models of regular and irregular bridges were discovered; in order to account for the uncertainty in bridge modeling parameters, appropriate distributions of parameters were obtained based on the review of thousands of bridge plans provided by the California Department of Transportation (Caltrans). The implemented strategies to develop three-dimensional finite element OpenSees models of the bridge components along with their corresponding accounted uncertainties were presented in Chapter 3.

Clearly, it was not feasible to perform seismic analysis on all the possible permutations of bridge configurations. Consequently, a suitable set of bridges was selected for consideration in the present research study, based on statistical distributions

and sensitivity analysis. The identified bridges, provided in Chapter 4, correspond to the most common bridge configurations and were used for the vulnerability assessment in this study.

In order to improve our understanding of the seismic performance of irregular bridges, this study examined the influential parameters of irregular bridges by performing sensitivity analyses of skewed, tall, and unbalanced bridges in Chapter 5. The recently developed statistical techniques were implemented in this study to identify the most- and the least-influential parameters affecting the irregular bridge responses. Although the relative significance of various predictors varied over different bridge responses and irregularity ranges, there existed many common influential parameters, including ground motion intensity, longitudinal reinforcement ratio, column diameter, the number of columns per bent, column height, span length, and concrete compressive strength. It is essential that the identified influential parameters be included in the seismic demand modeling of irregular bridges. To accomplish this, bridge databases must be enhanced to reflect realistic information for the influential parameters. Where the information is not accessible, suitable uncertainty in the assignment of these parameters needs to be considered.

A major task of the current study was to propose an efficient approach for developing probabilistic seismic demand models. In order to accomplish this task, a mathematical optimization methodology was developed in Chapter 6. In order to estimate the confidence intervals, the model was formulated in a Bayesian framework.

Seeking an understanding of the impact of irregularities on the seismic vulnerability of bridges, the component and system fragility curves of regular and

irregular bridges were compared in this study. In Chapter 7, the applied fragility analysis framework was described. Initially, NLTHA was performed on the selected bridge models to obtain the seismic demands for the desired components of a bridge. Next, appropriate adjustment factors were developed for each level of irregularity at various damage states. Among the three evaluated irregularities, tall column heights showed the highest influence on the fragilities of concrete box-bridge bridges. Skew angle was the second most-influential parameter. Eventually, the proposed adjustment factors were compared to those proposed by HAZUS, which is the existing seismic assessment tool for earthquake risk assessment.

In addition to the primary objective of this research, which was the development of modification factors for probabilistic seismic demand models and the fragility curves, the seismic performances of various bridge components were thoroughly investigated for each type of irregularity. The results from this study illustrate the necessity to capture the influences of irregularities on the seismic performance of bridges and also indicate the importance of considering irregularities on the prediction of bridge vulnerability.

8.2 Research Impact

The key impact of this study is its contribution to broaden the insight regarding the impact of geometric irregularities on the seismic response and vulnerability of bridges. The outcomes of this research study help bridge engineers to better understand the performance of irregular bridges under seismic loads. Design engineers, as well, may find this research beneficial to gain insights as to how to modify the particular design procedures. In the aspect of retrofitting bridges, the findings of this study can provide valuable information regarding the bridge components with higher damage potentials for

the class of bridges with the studied irregularities. A number of important contributions are highlighted in the following:

- Development of three-dimensional nonlinear finite element models of single-frame concrete box-girder bridges with geometric irregularities: skew angles, tall columns, and unbalanced stiffness frame. The modeling characteristics, including geometric and material uncertainties, are derived based on the plan review of existing bridges in California.
- Classification of box-girder bridges with various configurations (e.g., number of spans, abutment type, and interior support type) to reduce computational costs for developing the seismic demands.
- Determination of key modeling parameters that affect the development of probabilistic seismic demands of each irregular bridge family.
- Development of modified probabilistic seismic demand models, that is beneficial since the numerical analyses are computationally burdensome. The modified approaches improve the estimation of irregular bridge responses by considering the effects of irregularity parameter.
- Development of the adjustment factors for each individual irregularity range and various levels of damage. In addition to clarifying the impacts of irregularities on the bridge vulnerability, the proposed factors facilitate estimating seismic fragility curves of irregular bridges when only the fragility parameters of the base models are accessible. In general, fragility curves help decision makers prioritize and optimize retrofit cost and strategies.

8.3 Recommendations for Future Research

The presented study can be extended through several research schemes, including the following areas:

- Performing multi-hazard assessment of the addressed bridge families.
- Studying the seismic performance of box-girder bridges with other types of irregularities, such as horizontal and vertical curvature of the bridge superstructure.
- Extending the vulnerability study to other bridge types, including I-girder, T-girder, and slab bridges.
- Investigating the effects of soil liquefaction on the seismic response and fragility of irregular bridges.
- Evaluating the effectiveness of existing retrofit strategies and recommending improved retrofit techniques pertinent to the irregular bridges.
- Improving capacity models for bridge components, particularly the bridge column and the abutment, based on the existing experimental or empirical damage observations.
- Analyzing the effects of irregularities on the seismic performance of bridges with multiple frames.

APPENDIX A

Column Cross-Sections

Table A. 1: Idealization of existing cross-sections of bridge columns

Column cross-sections	Assigned to (Idealized as)	Column cross-sections	Assigned to (Idealized as)
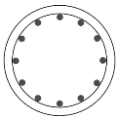	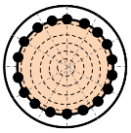	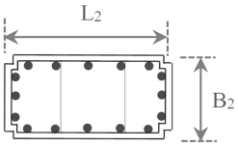	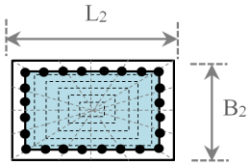
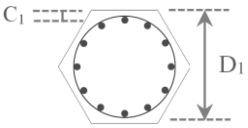	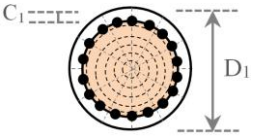	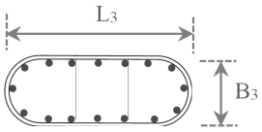	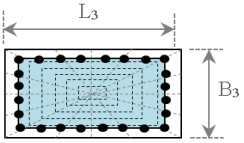
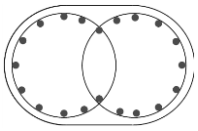	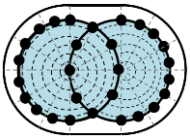	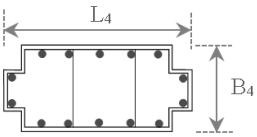	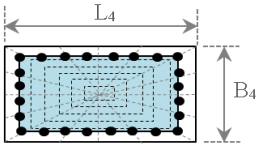
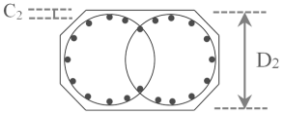	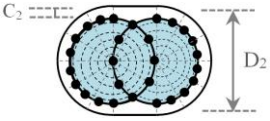	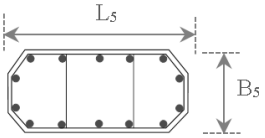	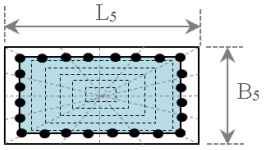
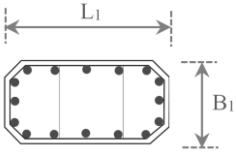	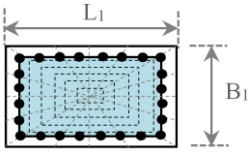		

Performance of Various Cross-Sections

Table A. 2: Mean and standard deviation of system fragility curves

Case	Type	Damage State							
		Slight		Moderate		Extensive		Collapse	
		Median (λ)	Dispersion (ξ)	Median (λ)	Dispersion (ξ)	Median (λ)	Dispersion (ξ)	Median (λ)	Dispersion (ξ)
DBSC	CP	0.120	0.89	0.205	0.96	0.324	1.08	1.040	1.11
DBSC	RP	0.146	1.03	0.251	1.09	0.394	1.20	1.253	1.22
DBSC	OP	0.172	0.98	0.399	1.02	0.642	1.15	2.090	1.23
DBSC	Fl	0.110	0.91	0.177	0.96	0.282	1.09	0.932	1.14
SBSC	CP	0.084	0.58	0.153	0.66	0.217	0.81	0.545	0.83
SBSC	RP	0.072	0.60	0.107	0.68	0.153	0.83	0.409	0.86
SBSC	OP	0.107	0.60	0.261	0.65	0.404	0.85	1.043	0.88
SBSC	Fl	0.084	0.59	0.142	0.67	0.204	0.82	0.533	0.85
DBMC	CP	0.122	0.73	0.178	0.77	0.249	0.86	0.566	0.89
DBMC	RP	0.152	0.74	0.243	0.84	0.342	0.94	0.832	0.96
DBMC	OP	0.164	0.69	0.322	0.76	0.458	0.87	1.114	0.90
DBMC	Fl	0.120	0.73	0.165	0.77	0.231	0.86	0.528	0.88
SBMC	CP	0.074	0.51	0.135	0.57	0.183	0.68	0.390	0.70
SBMC	RP	0.064	0.59	0.102	0.65	0.138	0.76	0.309	0.77
SBMC	OP	0.085	0.56	0.211	0.60	0.302	0.76	0.672	0.78
SBMC	Fl	0.069	0.55	0.115	0.60	0.154	0.70	0.326	0.72
DASC	CP	0.126	0.82	0.225	0.88	0.345	1.01	1.029	1.03
DASC	RP	0.148	0.98	0.271	1.06	0.426	1.18	1.362	1.21
DASC	OP	0.169	0.94	0.411	0.97	0.667	1.11	2.131	1.19
DASC	Fl	0.117	0.87	0.191	0.91	0.295	1.03	0.897	1.06
SASC	CP	0.085	0.56	0.162	0.63	0.233	0.80	0.597	0.82
SASC	RP	0.073	0.56	0.117	0.66	0.164	0.80	0.445	0.85
SASC	OP	0.101	0.58	0.264	0.62	0.414	0.82	1.057	0.84
SASC	Fl	0.084	0.56	0.146	0.64	0.208	0.80	0.534	0.83
DAMC	CP	0.118	0.83	0.195	0.86	0.269	0.93	0.593	0.95
DAMC	RP	0.154	0.71	0.267	0.80	0.374	0.91	0.885	0.93
DAMC	OP	0.161	0.69	0.347	0.75	0.499	0.88	1.211	0.89
DAMC	Fl	0.116	0.83	0.175	0.86	0.240	0.93	0.533	0.95
SAMC	CP	0.068	0.52	0.137	0.58	0.188	0.69	0.406	0.71
SAMC	RP	0.061	0.78	0.110	0.81	0.154	0.93	0.325	0.94
SAMC	OP	0.083	0.50	0.220	0.56	0.324	0.73	0.711	0.75
SAMC	Fl	0.067	0.53	0.124	0.59	0.169	0.68	0.355	0.69

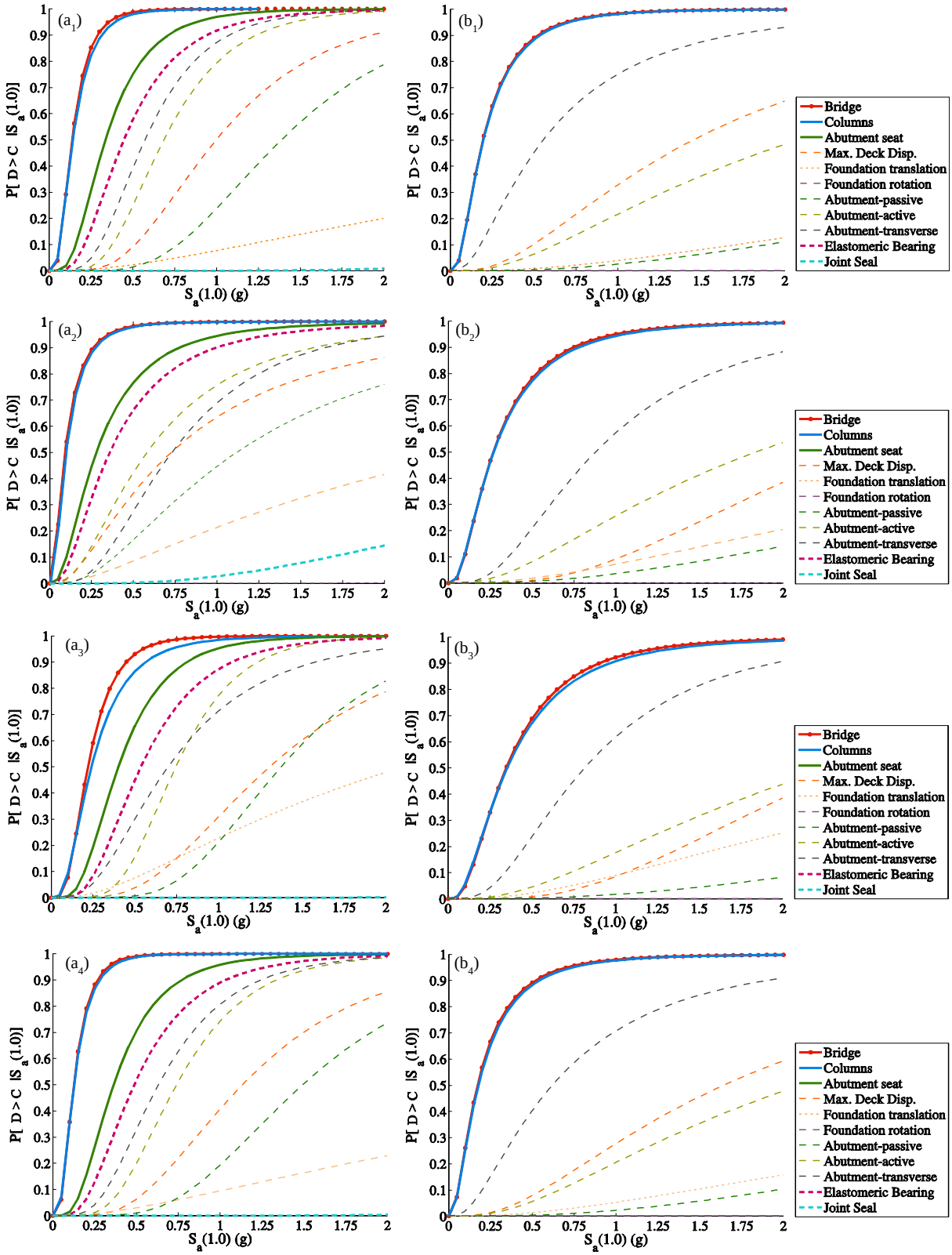

Figure A. 1: Fragility curves at moderate damage state for the bridge system and components for bridges designed after 1970 with multi-columns per bent and (a) seat, (b) integral type abutment

Failure Modes

Generally, analytical modeling of the columns, as the most susceptible component of a bridge under earthquake excitation, is challenging. Capturing and considering the column failure modes according to each design era is an essential part of the numerical modeling. In this study, some strategies, validated by the experimental results, were developed to consider various failure modes of a column. Considered types of a bridge column failure and numerical approaches to capture these failures are explained here.

Flexural failure is the typical type of column failure of bridges designed, in the period of 1971-1990 and post-1990. Respective numerical model of the column to capture flexural failure was validated with the experimental studies conducted by (Lehman, et al., 2004). Figure A.1 shows the validations for Specimens No. 415 and No. 815 of (Lehman, et al., 2004). The comparison shows that the numerical model captures the force-deformation relations.

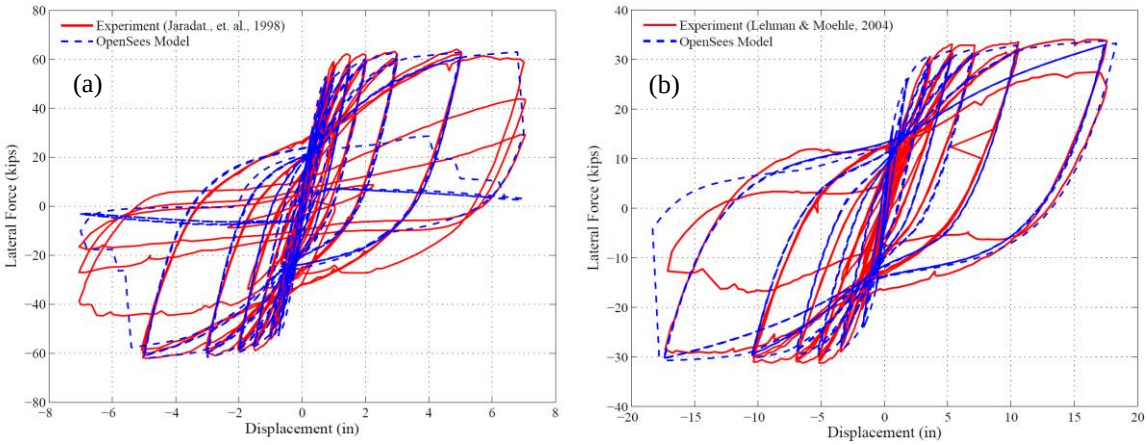

Figure A. 2: Comparison of experimental and numerical results; a) Specimen No. 415, b) Specimen No. 815

In addition to flexural failure, shear failure mode is common in bridges designed before 1971 (i.e., prior to developing the seismic design code). Numerical modeling to capture shear failure is challenging. For the purpose of this study, the column shear capacity of bridges, constructed in pre-1971, was evaluated. Initially, the pushover analysis was carried out on

bridge columns with properties associated with the old era bridges. Afterward, the shear demand was compared with the shear capacity estimated using (Caltrans, 2013) and San Diego shear model (Priestley, et al., 1994). Three possible scenarios are illustrated in Figure A.2. A similar evaluation was performed on various bridge columns, and the distribution of the three mentioned possible cases are shown in Figure A.3. The column shear failure is more critical if happen in the transverse direction. As noted in Figure A.3, the majority of failures are flexural. In this study, the shear force of bridge columns for each dynamic analysis will be recorded in the NLTHA, and will be used later in the production analysis to compare with capacity limits and capture the shear failure.

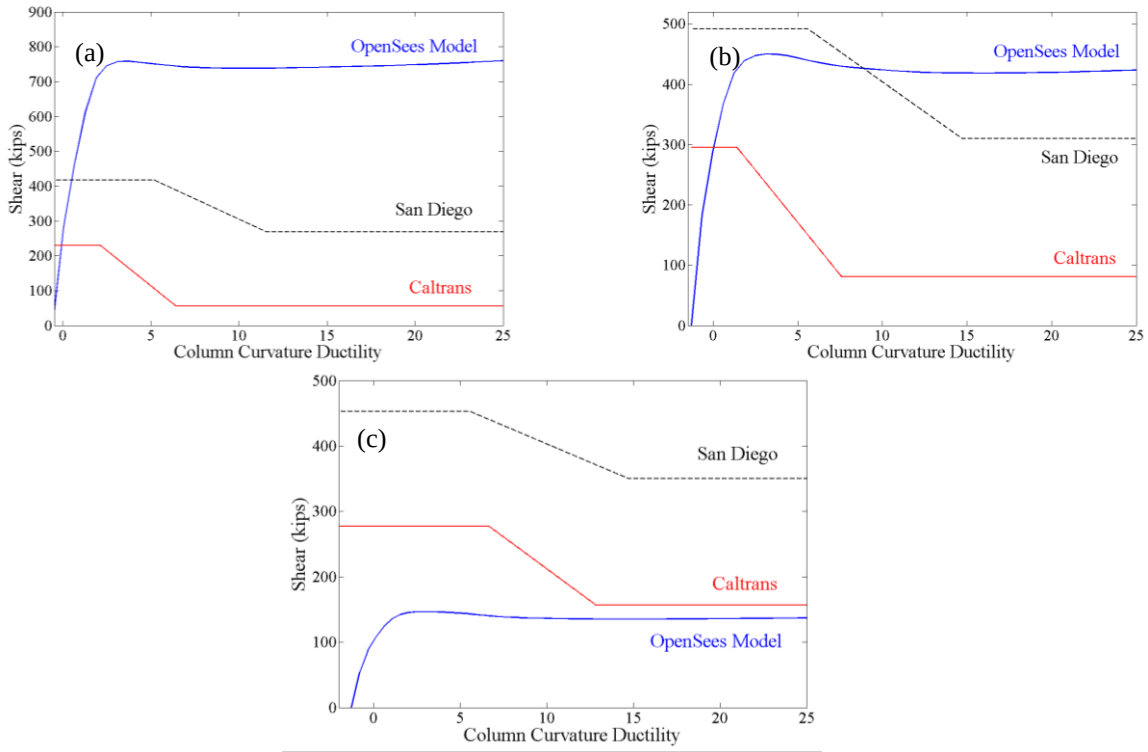

Figure A. 3: Shear capacity evaluation of bridge columns; a) shear failure happens before the flexural yielding of the column (i.e., brittle mode of failure), b) flexural failure, c) shear mode of failure after flexural yielding

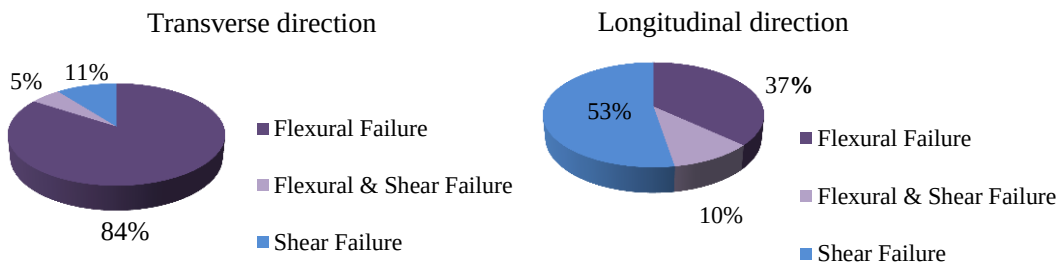

Figure A. 4: Statistical distribution of possible scenarios

APPENDIX B

A brief summary of changes in modeling bridges with tall bents and unbalanced frames was presented in Chapter 3. In this Appendix, supplementary plots are provided.

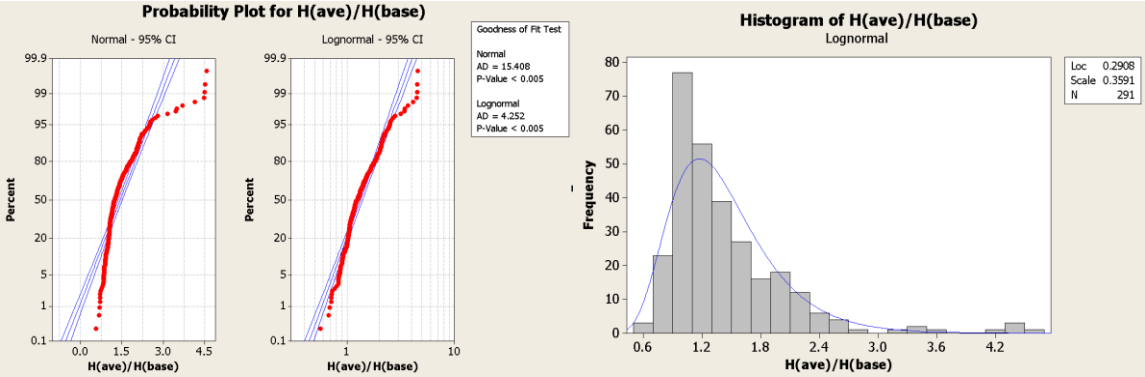

Figure B. 1: Considering all average bridge-height ratios (for pre-1971 bridges)

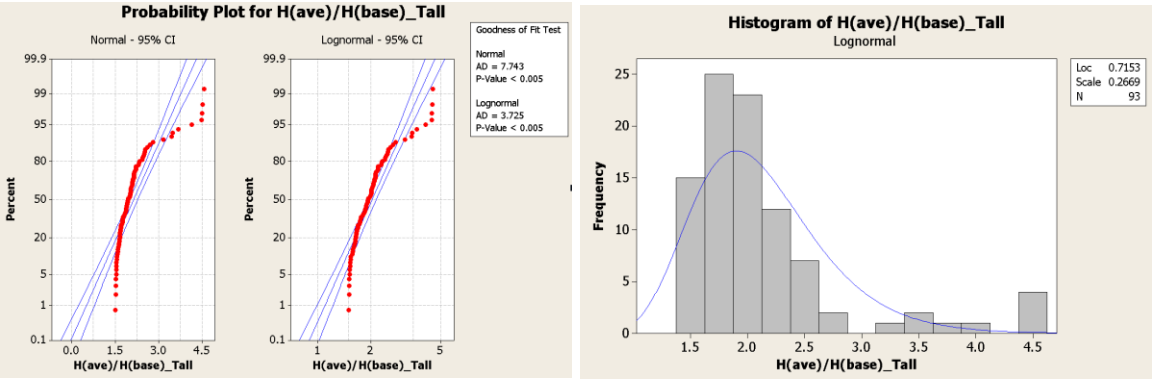

Figure B. 2: Considering average bridge-height ratios > 1.5 (for pre-1971 bridges)

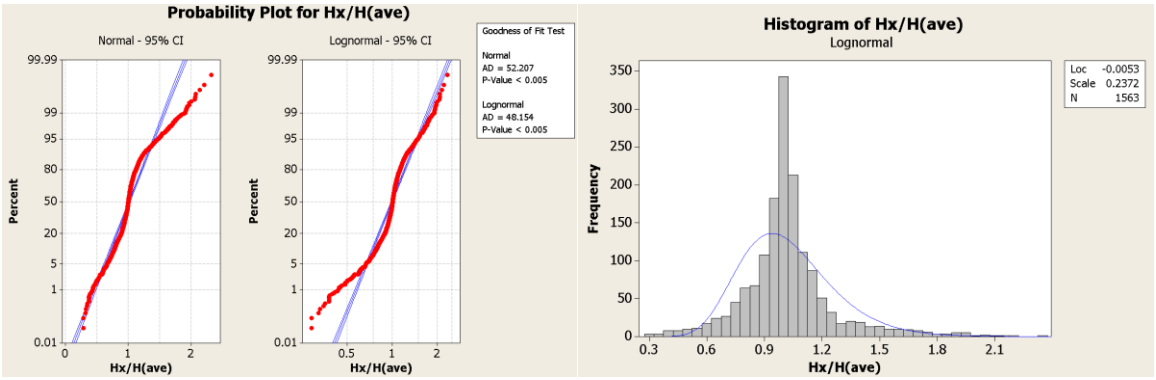

Figure B. 3: Intra-bridge bent-height ratios (for pre-1971 bridges)

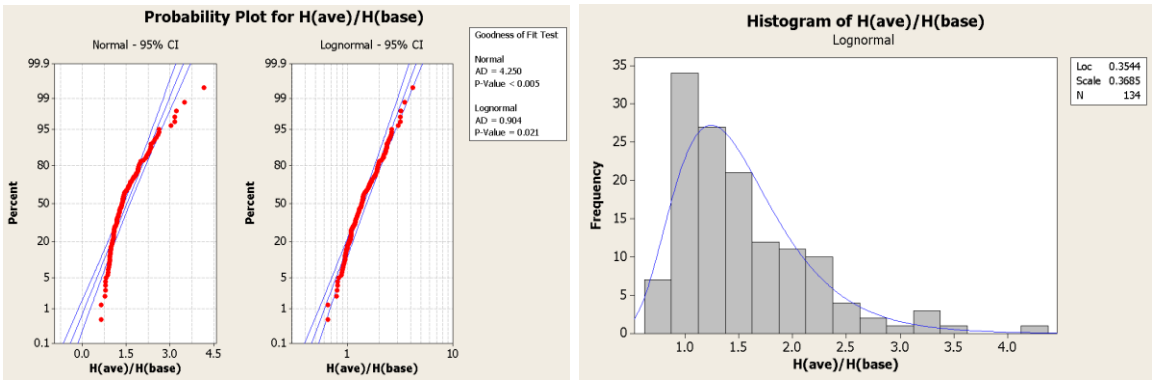

Figure B. 4: Considering all average bridge-height ratios (for 1971-1990 bridges)

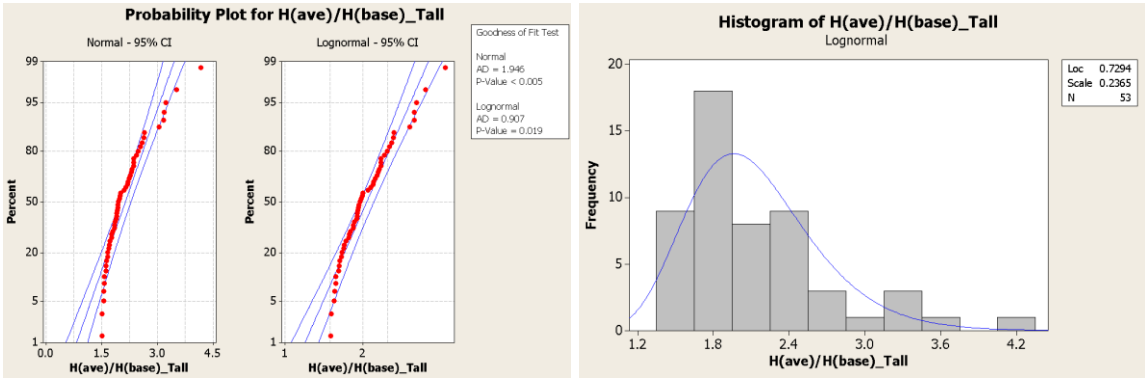

Figure B. 5: Considering average bridge-height ratios > 1.5 (for 1971-1990 bridges)

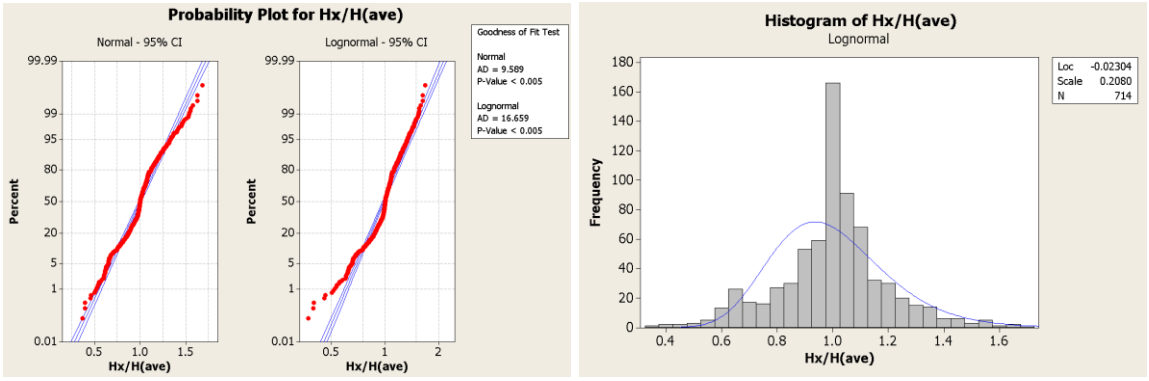

Figure B. 6: Intra-bridge bent-height ratios (for 1971-1990 bridges)

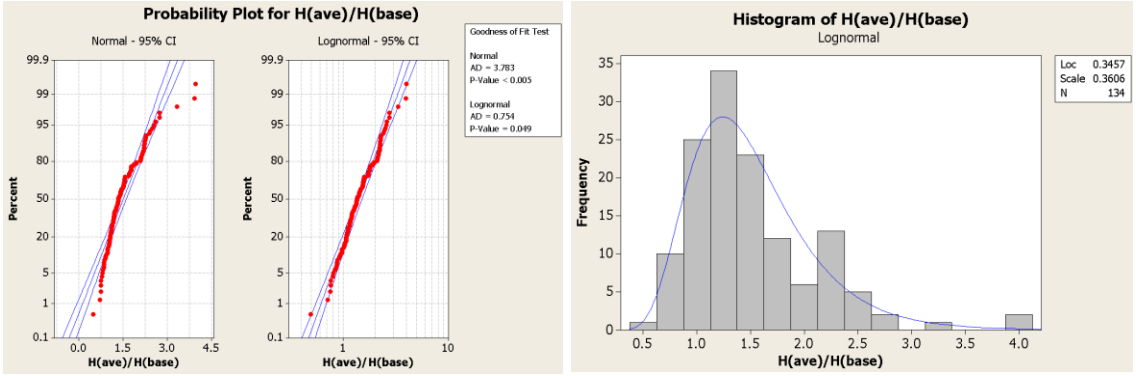

Figure B. 7: Considering all average bridge-height ratios (for post-1990 bridges)

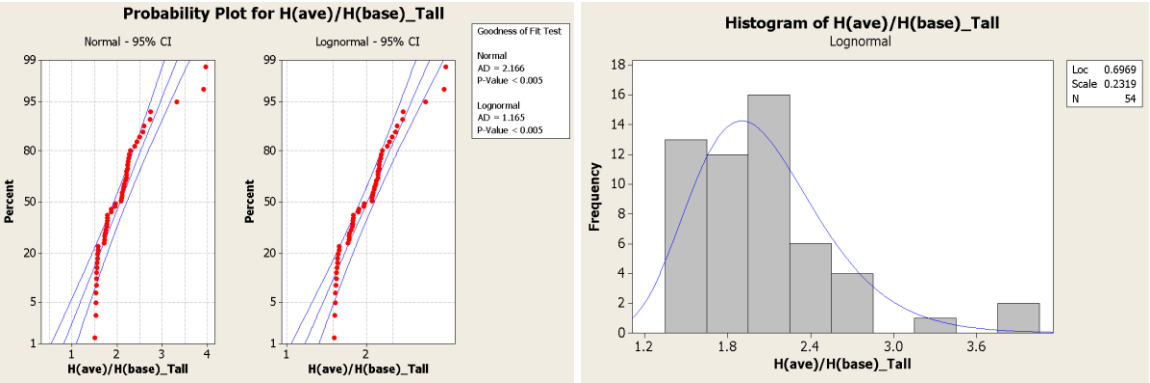

Figure B. 8: Considering average bridge-height ratios > 1.5 (for post-1990 bridges)

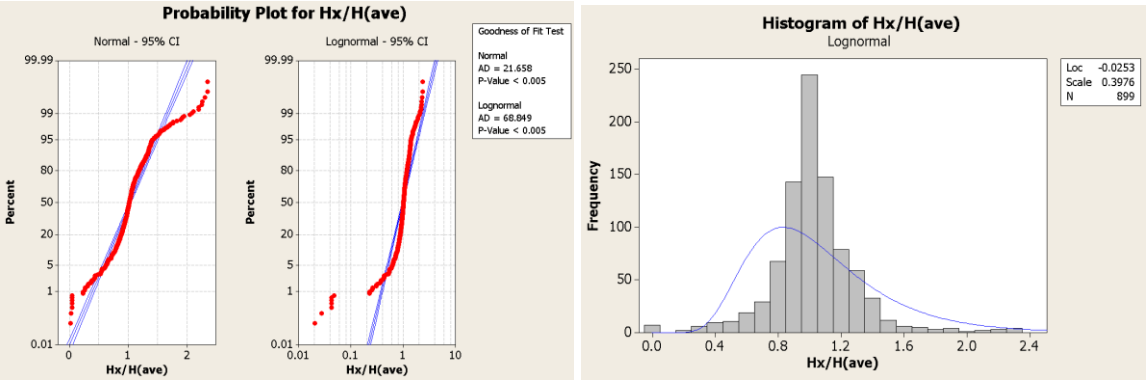

Figure B. 9: Intra-bridge bent-height ratios (for post-1990 bridges)

APPENDIX C

The sensitivity analysis results for the chosen dynamic responses and the individual range of irregularities are detailed in this section.

Table C. 1: Identified influential parameters for moderately tall and very tall bridges

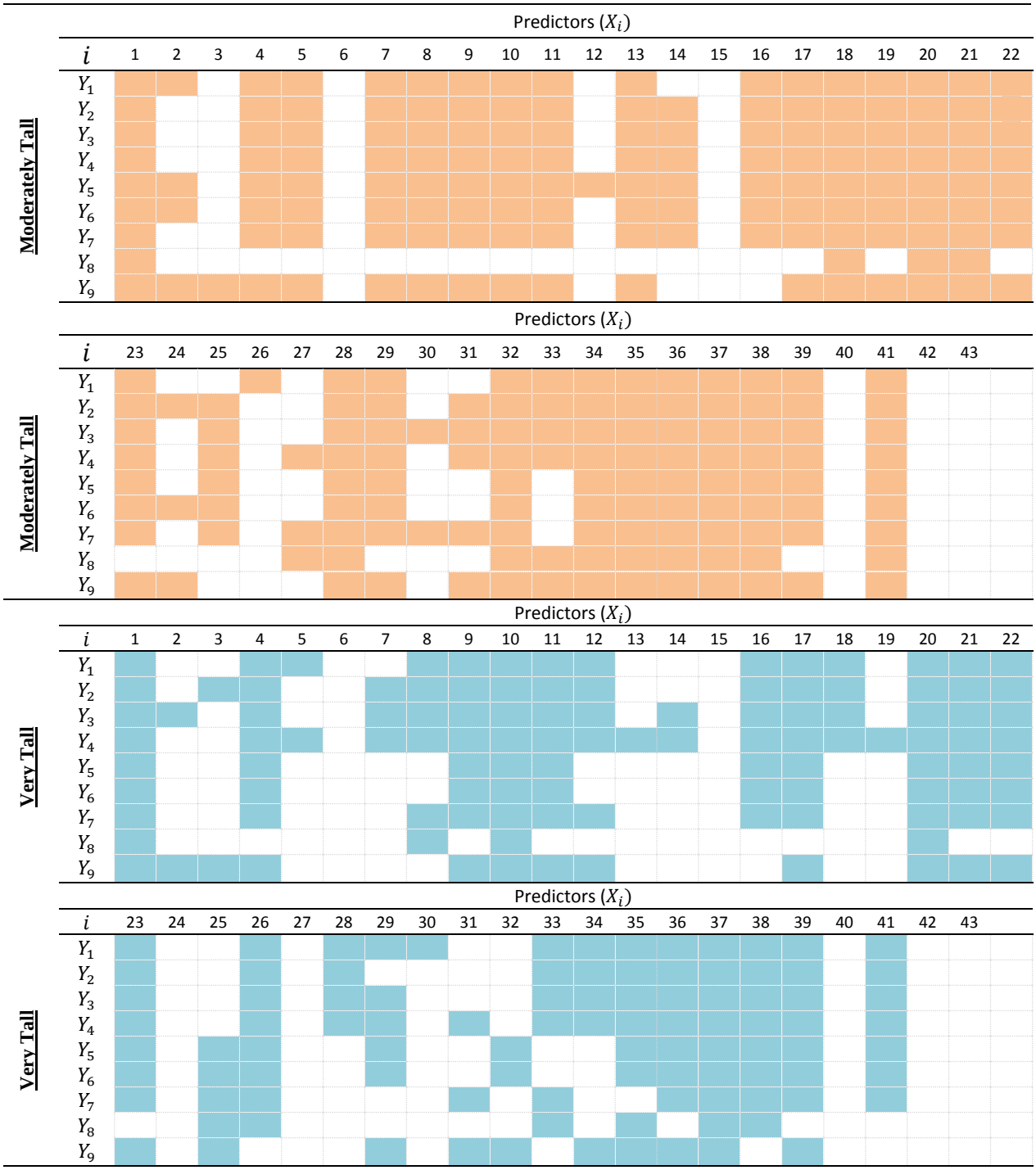

Table C. 2: Identified influential parameters for extremely tall and slightly unbalanced bridges

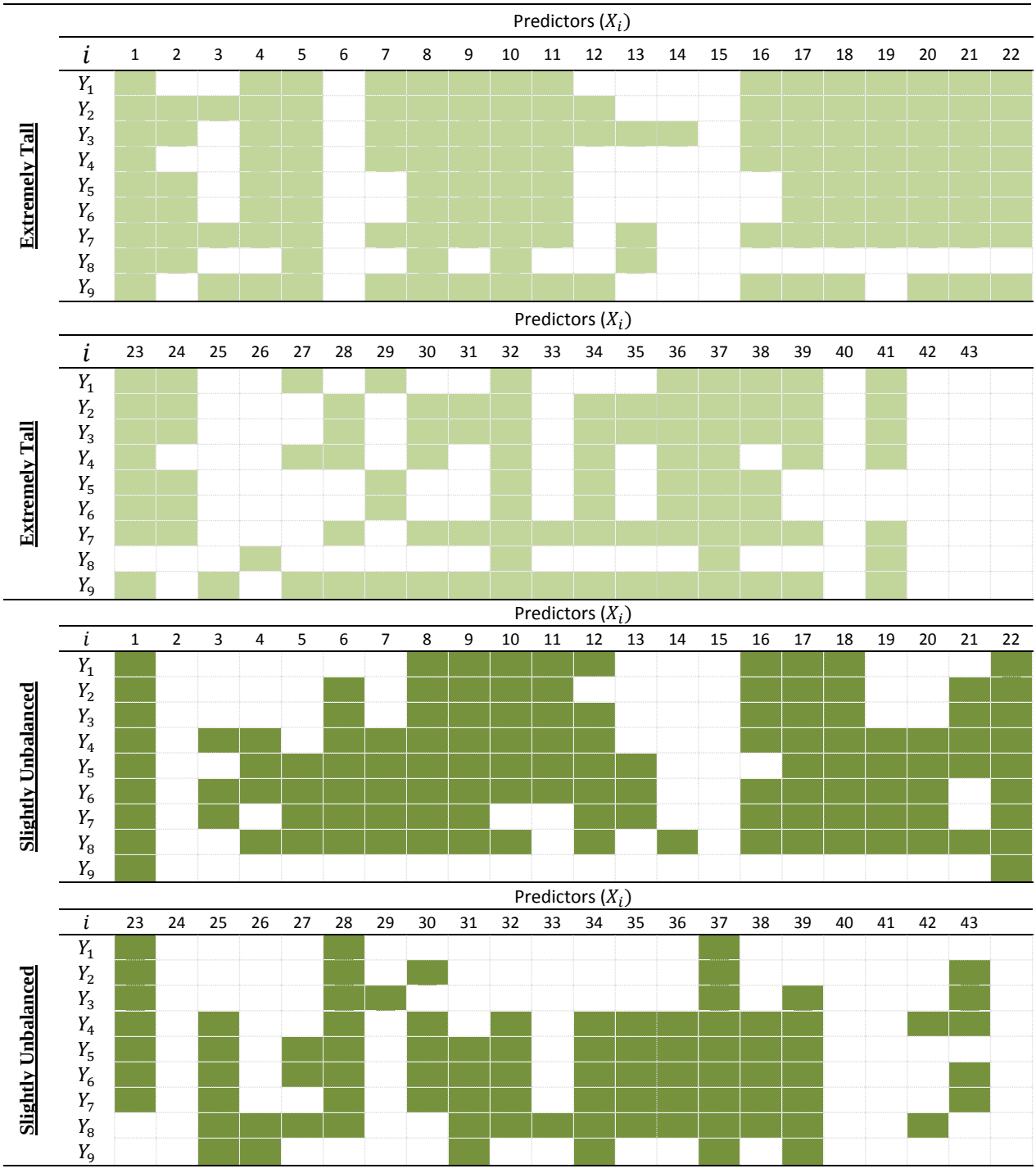

Table C. 3: Identified influential parameters for moderately unbalanced and highly unbalanced bridges

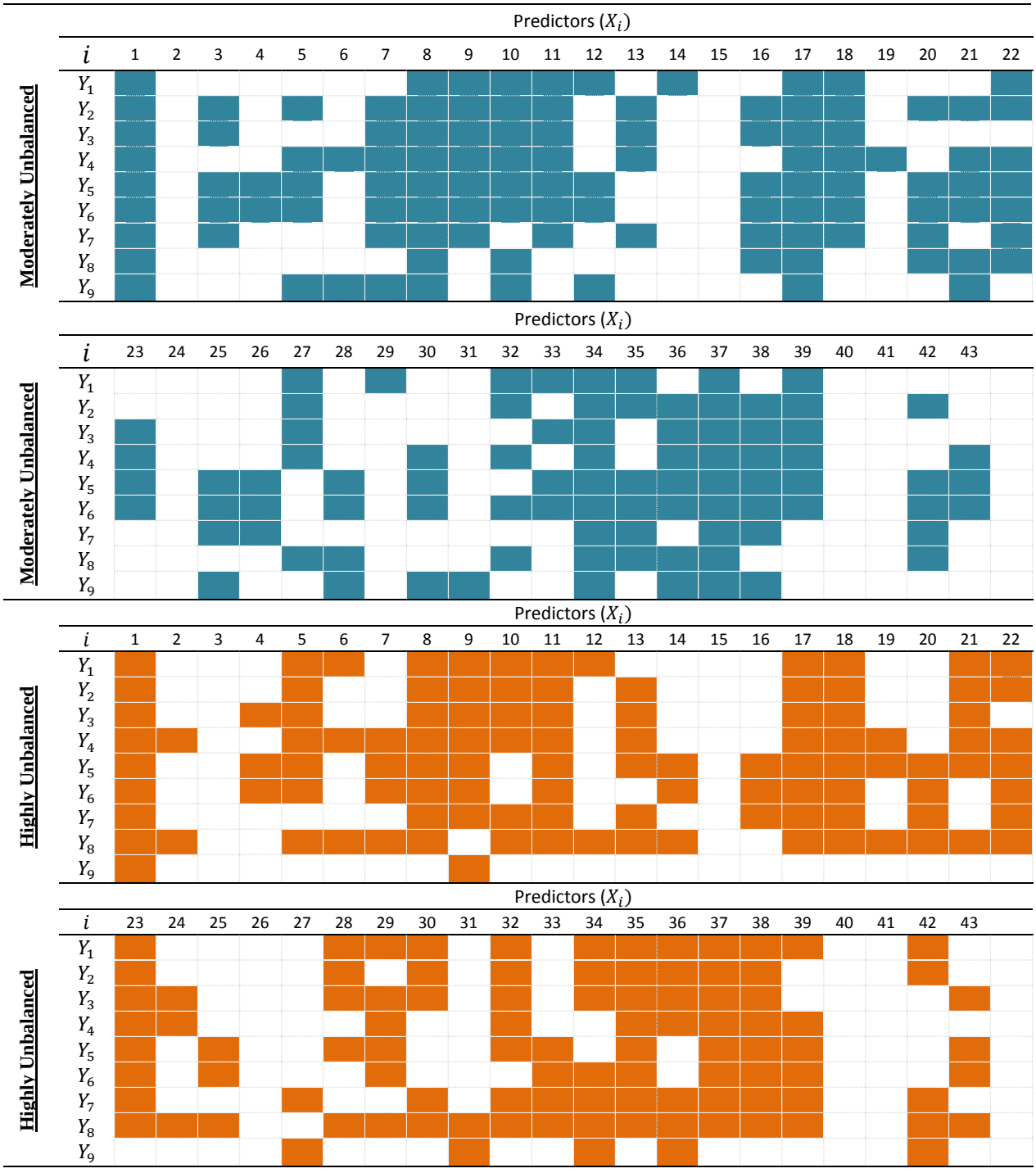

Table C. 4: Identified influential parameters for extremely unbalanced and bridges with low skew angles

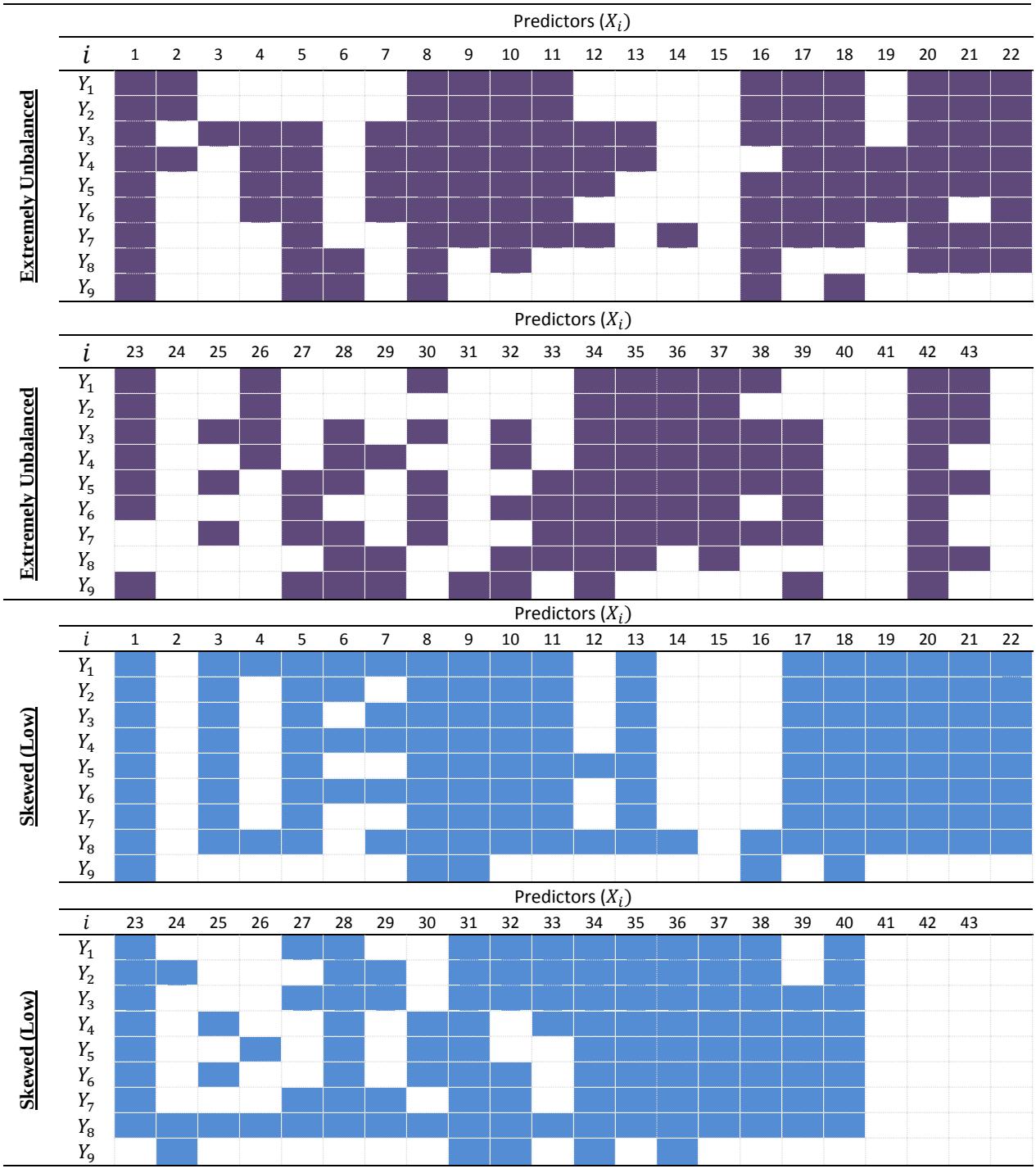

Table C. 5: Identified influential parameters for bridges with medium and high skew angles

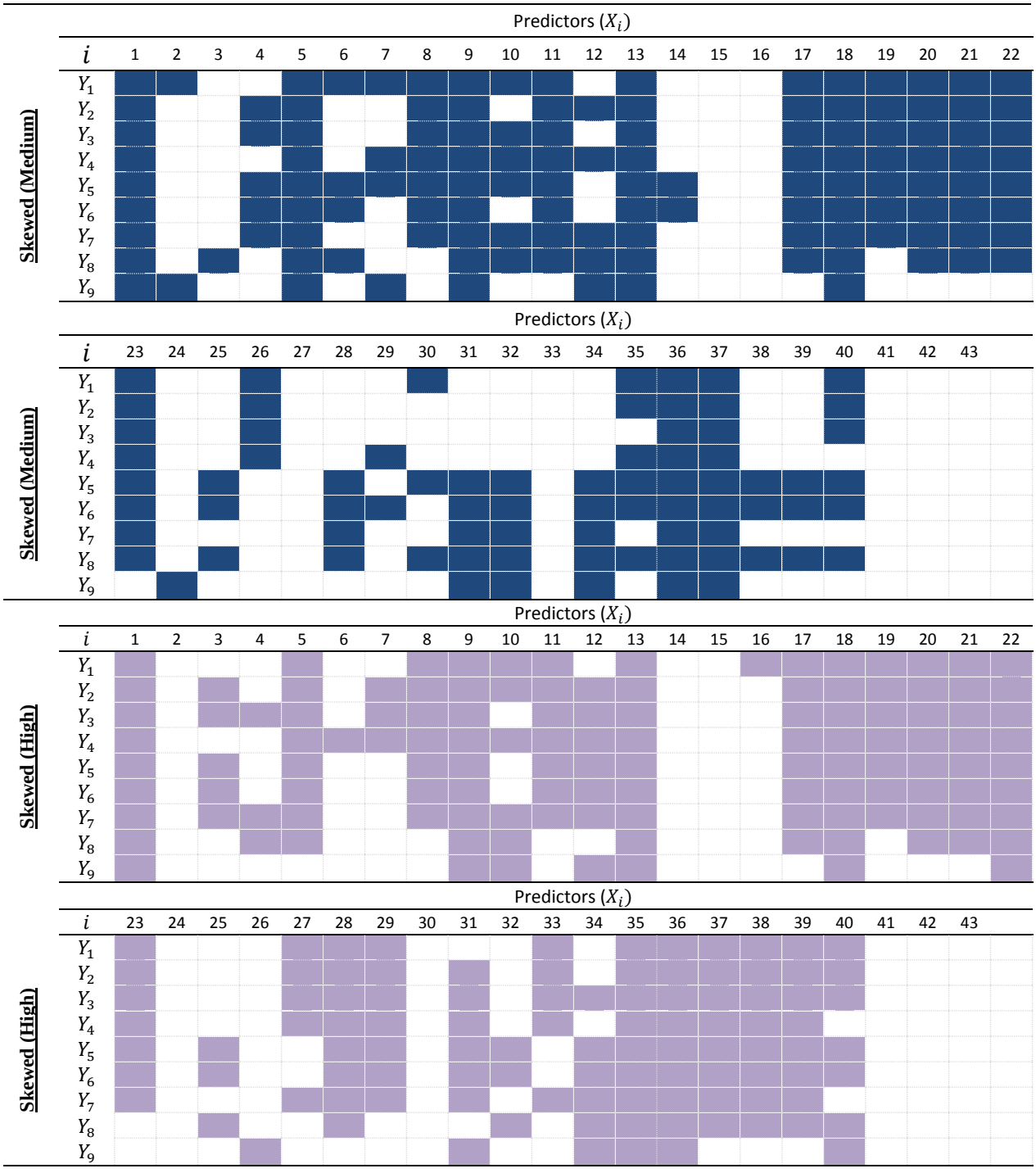

Table C. 6: Identified influential parameters for bridges with very high and extreme skew angles

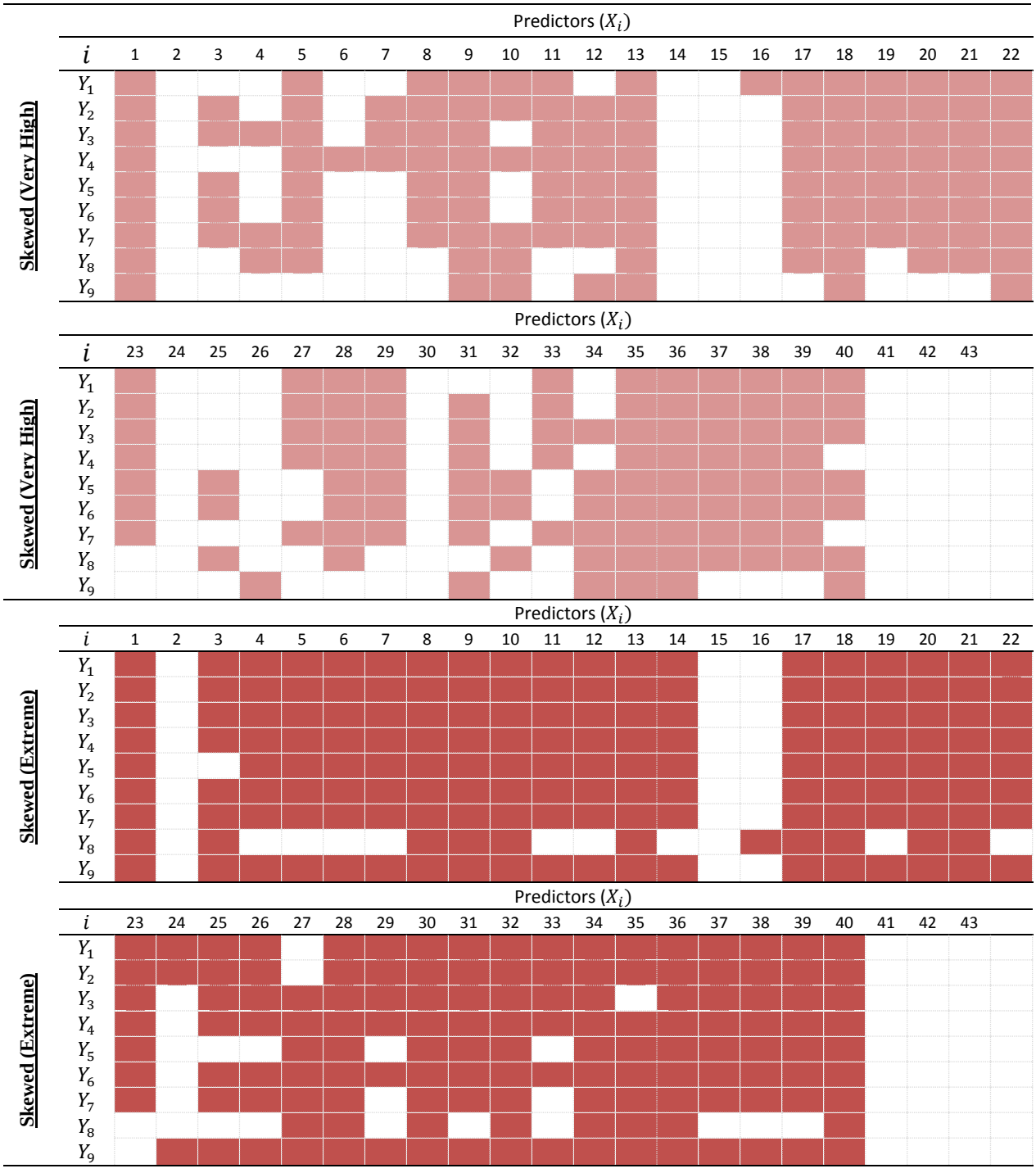

APPENDIX D

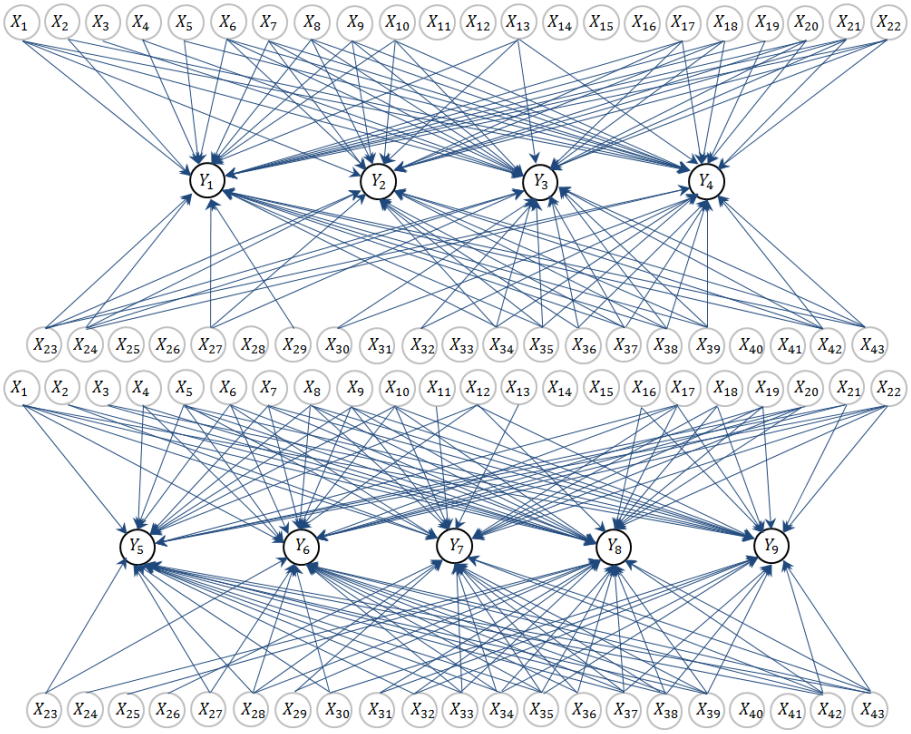

Figure D.1: System network diagram for the class of unbalanced bridges

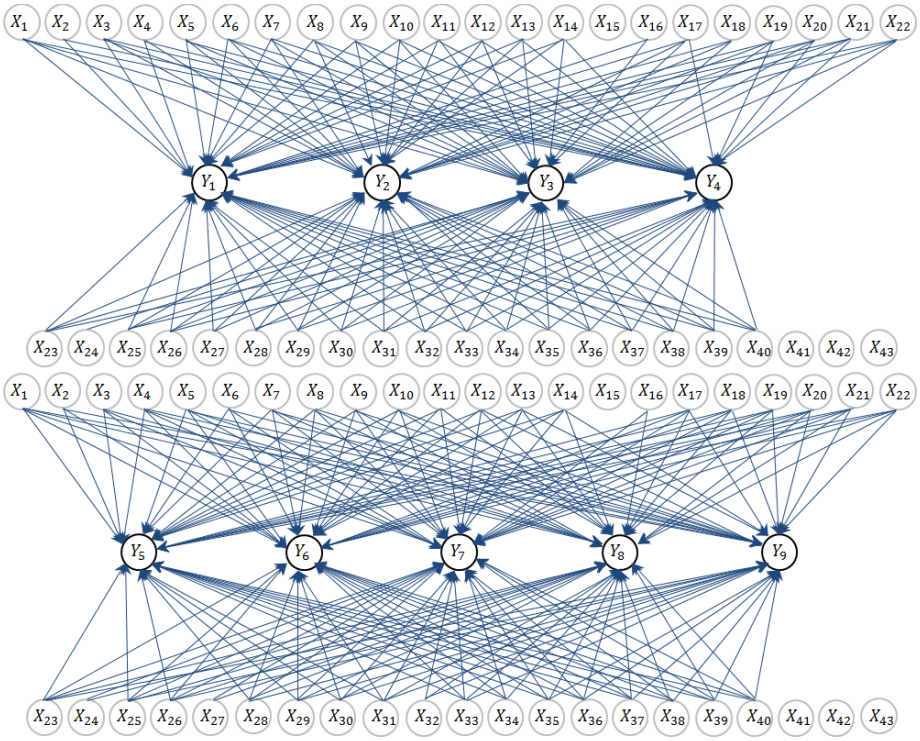

Figure D.2: System network diagram for the class of skewed bridges

APPENDIX E

An example of the statistical response surface model is presented of the column's response for the tall bridge class as

$$\ln\left(\hat{Y}_{1_{tall}}\right) = \beta_0 + \beta_1 \ln(X_1) + \sum_{j=2}^{8} \beta_j X_j + \sum_{j=9}^{43} \beta_j \ln(X_j)\,, \qquad (E.1)$$

where the coefficients are listed in Table E. 1. In Equation E.1, $\boldsymbol{\beta}_j$ and $\boldsymbol{X}_j$ $(j = 2, \ldots, 8)$ are shown as vectors since they include dummy variables for each categorical variable.

Table E. 1: Values for the coefficients in equation *E.1*

Coefficients	Values	Coefficients	Values	Coefficients	Values	Coefficients	Values
Intercept (β_0)	11.673	$\beta_{7_{nine-cells}}$	-0.199	β_{18}	-1.270	β_{33}	-0.619
β_1	1.133	$\beta_{7_{eleven-cells}}$	-0.278	β_{19}	-0.279	β_{35}	-0.020
$\beta_{2_{seat}}$	1.988	$\beta_{8_{trans}}$	0.142	β_{20}	0.167	β_{36}	-0.505
$\beta_{4_{two-col}}$	-0.942	β_9	2.185	β_{21}	-5.288	β_{37}	2.205
$\beta_{4_{three-col}}$	4.638	β_{10}	-2.012	β_{22}	0.058	β_{38}	0.162
$\beta_{4_{four-col}}$	3.518	β_{11}	-0.073	β_{23}	0.223	β_{39}	-0.275
$\beta_{4_{five-col}}$	2.81	β_{13}	8.382	β_{26}	-0.021	β_{41}	-1.421
$\beta_{5_{sand}}$	0.078	β_{16}	0.419	β_{28}	-0.607		
$\beta_{7_{seven-cells}}$	-1.582	β_{17}	-4.425	β_{29}	-1.116		

APPENDIX F

Table F. 1: List of ground motions assembled by Caltrans for application to this project

No.	PEER Record Sequence Number*	Scale Factor	SA-1 (g)	Vs30 (m/sec)	Tp-Pulse Period (sec)	Arias Intensity (m/sec)	Earthquake Name	Year	Station Name	Magnitude	Mechanism	Rjb (km)	Rrup (km)
1	825	2.294	1.388	567.78	-	6	"Cape Mendocino"	1992	"Cape Mendocino"	7.01	Reverse	0	6.96
2	983	1.930	1.925	525.79	3.535	6.5	"Northridge-01"	1994	"Jensen Filter Plant Generator Building"	6.69	Reverse	0	5.43
3	1063	1.857	2.716	282.25	1.246	7.5	"Northridge-01"	1994	"Rinaldi Receiving Sta"	6.69	Reverse	0	6.5
4	1119	2.267	1.863	312.00	1.806	3.9	"Kobe Japan"	1995	"Takarazuka"	6.9	strike slip	0	0.27
5	1120	1.617	2.088	256.00	1.554	8.7	"Kobe Japan"	1995	"Takatori"	6.9	strike slip	1.46	1.47
6	1492	2.216	2.274	579.10	11.956	2.9	"Chi-Chi Taiwan"	1999	"TCU052"	7.62	Reverse Oblique	0	0.66
7	1503	1.896	2.224	305.85	5.74	7.7	"Chi-Chi Taiwan"	1999	"TCU065"	7.62	Reverse Oblique	0.57	0.57
8	1605	2.362	1.510	281.86	-	2.9	"Duzce Turkey"	1999	"Duzce"	7.14	strike slip	0	6.58
9	3968	1.843	2.584	310.21	-	11.8	"Tottori Japan"	2000	"TTRH02"	6.61	strike slip	0.83	0.97
10	4040	2.283	1.739	487.40	2.023	8	"Bam Iran"	2003	"Bam"	6.6	strike slip	0.05	1.7
11	4219	2.246	1.723	480.40	-	8.8	"Niigata Japan"	2004	"NIGH01"	6.63	Reverse	0.49	9.46
12	4856	2.166	1.797	294.38	-	3.9	"Chuetsu-oki Japan"	2007	"Kashiwazaki City Center"	6.8	Reverse	0	11.09
13	4894	1.361	2.151	329.00	-	16.5	"Chuetsu-oki Japan"	2007	"Kashiwazaki NPP Unit 1: ground surface"	6.8	Reverse	0	10.97
14	5657	1.848	1.400	506.44	-	26.1	"Iwate Japan"	2008	"IWTH25"	6.9	Reverse	0	4.8
15	5992	2.499	1.515	196.25	-	5.5	"El Mayor-Cucapah Mexico"	2010	"El Centro Array #11"	7.2	strike slip	15.36	16.21
16	6906	1.785	1.815	344.02	6.23	4.7	"Darfield New Zealand"	2010	"GDLC"	7	strike slip	1.22	1.22
17	126	2.106	1.332	259.59	-	5.7	"Gazli USSR"	1976	"Karakyr"	6.8	Reverse	3.92	5.46
18	180	2.245	1.326	205.63	4.13	1.7	"Imperial Valley-06"	1979	"El Centro Array #5"	6.53	strike slip	1.76	3.95
19	181	2.370	1.152	203.22	3.773	1.8	"Imperial Valley-06"	1979	"El Centro Array #6"	6.53	strike slip	0	1.35
20	723	2.224	1.596	348.69	2.394	3.7	"Superstition Hills-02"	1987	"Parachute Test Site"	6.54	strike slip	0.95	0.95
21	821	2.420	1.874	352.05	-	1.8	"Erzican Turkey"	1992	"Erzincan"	6.69	strike slip	0	4.38
22	828	2.357	1.931	422.17	2.996	3.8	"Cape Mendocino"	1992	"Petrolia"	7.01	Reverse	0	8.18
23	1084	1.621	2.236	251.24	2.982	6	"Northridge-01"	1994	"Sylmar - Converter Sta"	6.69	Reverse	0	5.35
24	1086	1.754	1.143	440.54	2.436	5	"Northridge-01"	1994	"Sylmar - Olive View Med FF"	6.69	Reverse	1.74	5.3
25	1244	2.346	1.733	258.89	5.341	3	"Chi-Chi Taiwan"	1999	"CHY101"	7.62	Reverse Oblique	9.94	9.94

Table F. 1 (Continued): List of ground motions assembled by Caltrans for application to this project

No.	PEER Record Sequence Number*	Scale Factor	SA-1 (g)	Vs30 (m/sec)	Tp-Pulse Period (sec)	Arias Intensity (m/sec)	Earthquake Name	Year	Station Name	Magnitude	Mechanism	Rjb (km)	Rrup (km)
26	1549	2.417	1.372	511.18	-	9.3	"Chi-Chi Taiwan"	1999	"TCU129"	7.62	Reverse Oblique	1.83	1.83
27	1602	2.234	2.157	293.57	0.882	3.7	"Duzce Turkey"	1999	"Bolu"	7.14	strike slip	12.02	12.04
28	4876	2.114	1.975	655.45	-	8.6	"Chuetsu-oki Japan"	2007	"Kashiwazaki Nishiyamacho Ikeura"	6.8	Reverse	0	12.63
29	5264	1.774	1.663	198.26	-	5	"Chuetsu-oki Japan"	2007	"NIG018"	6.8	Reverse	0	10.78
30	5658	2.366	1.060	371.06	-	14.1	"Iwate Japan"	2008	"IWTH26"	6.9	Reverse	5.97	6.02
31	5818	2.354	1.238	512.26	-	7.3	"Iwate Japan"	2008	"Kurihara City"	6.9	Reverse	12.83	12.85
32	6911	2.041	1.424	326.01	9.919	3.2	"Darfield New Zealand"	2010	"HORC"	7	strike slip	7.29	7.29
33	160	2.272	1.006	223.03	-	6.1	"Imperial Valley-06"	1979	"Bonds Corner"	6.53	strike slip	0.44	2.66
34	182	2.270	1.534	210.51	4.375	1.7	"Imperial Valley-06"	1979	"El Centro Array #7"	6.53	strike slip	0.56	0.56
35	779	1.578	1.188	594.83	-	7.9	"Loma Prieta"	1989	"LGPC"	6.93	Reverse Oblique	0	3.88
36	982	1.744	2.475	373.07	3.157	5.3	"Northridge-01"	1994	"Jensen Filter Plant Administrative Building"	6.69	Reverse	0	5.43
37	1044	1.706	1.710	269.14	1.372	5.7	"Northridge-01"	1994	"Newhall - Fire Sta"	6.69	Reverse	3.16	5.92
38	1106	1.693	2.343	312.00	1.092	8.4	"Kobe Japan"	1995	"KJMA"	6.9	strike slip	0.94	0.96
39	1505	1.508	1.061	487.34	12.285	3.3	"Chi-Chi Taiwan"	1999	"TCU068"	7.62	Reverse Oblique	0	0.32
40	1507	2.046	1.432	624.85	-	9.5	"Chi-Chi Taiwan"	1999	"TCU071"	7.62	Reverse Oblique	0	5.8
41	2114	2.397	1.791	329.40	3.157	1.9	"Denali Alaska"	2002	"TAPS Pump Station #10"	7.9	strike slip	0.18	2.74
42	4874	2.425	1.279	561.59	-	5.3	"Chuetsu-oki Japan"	2007	"Oguni Nagaoka"	6.8	Reverse	10.31	20
43	4895	1.326	1.506	265.50	-	13.3	"Chuetsu-oki Japan"	2007	"Kashiwazaki NPP Unit 5: ground surface"	6.8	Reverse	0	10.97
44	5663	2.382	0.961	479.37	-	9.4	"Iwate Japan"	2008	"MYG004"	6.9	Reverse	20.17	20.18
45	5664	2.379	1.068	361.24	-	4.2	"Iwate Japan"	2008	"MYG005"	6.9	Reverse	10.71	13.47
46	5827	2.351	1.377	242.05	-	6.1	"El Mayor-Cucapah Mexico"	2010	"MICHOACAN DE OCAMPO"	7.2	strike slip	13.21	15.91
47	6927	2.264	1.278	263.20	7.371	2.7	"Darfield New Zealand"	2010	"LINC"	7	strike slip	5.07	7.11
48	8161	2.490	1.668	196.88	8.722	3.2	"El Mayor-Cucapah Mexico"	2010	"El Centro Array #12"	7.2	strike slip	9.98	11.26
49	179	2.128	1.140	208.91	4.788	1.4	"Imperial Valley-06"	1979	"El Centro Array #4"	6.53	strike slip	4.9	7.05
50	183	2.237	0.776	206.08	-	1.6	"Imperial Valley-06"	1979	"El Centro Array #8"	6.53	strike slip	3.86	3.86
51	753	2.466	1.245	462.24	-	3.2	"Loma Prieta"	1989	"Corralitos"	6.93	Reverse Oblique	0.16	3.85
52	1004	1.660	1.415	380.06	0.931	7	"Northridge-01"	1994	"LA - Sepulveda VA Hospital"	6.69	Reverse	0	8.44

Table F. 1 (Continued): List of ground motions assembled by Caltrans for application to this project

No.	PEER Record Sequence Number*	Scale Factor	SA-1 (g)	Vs30 (m/sec)	Tp-Pulse Period (sec)	Arias Intensity (m/sec)	Earthquake Name	Year	Station Name	Magnitude	Mechanism	Rjb (km)	Rrup (km)
53	1013	2.326	1.457	628.99	1.617	1.8	"Northridge-01"	1994	"LA Dam"	6.69	Reverse	0	5.92
54	1114	2.310	2.152	198.00	2.828	1.8	"Kobe Japan"	1995	"Port Island (0 m)"	6.9	strike slip	3.31	3.31
55	1176	2.333	0.896	297.00	4.949	1.3	"Kocaeli Turkey"	1999	"Yarimca"	7.51	strike slip	1.38	4.83
56	1197	1.488	1.515	542.61	-	5.9	"Chi-Chi Taiwan"	1999	"CHY028"	7.62	Reverse Oblique	3.12	3.12
57	1509	1.851	2.106	549.43	-	6.4	"Chi-Chi Taiwan"	1999	"TCU074"	7.62	Reverse Oblique	0	13.46
58	3748	2.477	1.631	387.95	-	1.7	"Cape Mendocino"	1992	"Ferndale Fire Station"	7.01	Reverse	16.64	19.32
59	4886	2.220	1.190	338.32	-	4.9	"Chuetsu-oki Japan"	2007	"Tamati Yone Izumozaki"	6.8	Reverse	0	11.48
60	4894	0.968	1.531	329.00	-	16.5	"Chuetsu-oki Japan"	2007	"Kashiwazaki NPP Unit 1: ground surface"	6.8	Reverse	0	10.97
61	5656	2.340	0.781	486.41	-	3.5	"Iwate Japan"	2008	"IWTH24"	6.9	Reverse	3.1	5.18
62	5825	2.336	0.914	242.05	-	3.3	"El Mayor-Cucapah Mexico"	2010	"CERRO PRIETO GEOTHERMAL"	7.2	strike slip	8.88	10.92
63	5837	2.268	1.223	229.25	-	3.7	"El Mayor-Cucapah Mexico"	2010	"El Centro - Imperial & Ross"	7.2	strike slip	19.39	20.08
64	6962	2.229	0.853	295.74	7.14	1.6	"Darfield New Zealand"	2010	"ROLC"	7	strike slip	0	1.54
65	174	2.448	0.583	196.25	-	2	"Imperial Valley-06"	1979	"El Centro Array #11"	6.53	strike slip	12.56	12.56
66	184	1.852	0.791	202.26	6.265	2.1	"Imperial Valley-06"	1979	"El Centro Differential Array"	6.53	strike slip	5.09	5.09
67	741	2.299	1.228	476.54	-	5.4	"Loma Prieta"	1989	"BRAN"	6.93	Reverse Oblique	3.85	10.72
68	803	2.273	1.371	347.90	5.649	1.3	"Loma Prieta"	1989	"Saratoga - W Valley Coll."	6.93	Reverse Oblique	8.48	9.31
69	1054	2.116	2.475	325.67	1.232	3.1	"Northridge-01"	1994	"Pardee - SCE"	6.69	Reverse	5.54	7.46
70	1080	2.316	1.655	557.42	-	4.1	"Northridge-01"	1994	"Simi Valley - Katherine Rd"	6.69	Reverse	0	13.42
71	1111	2.313	0.661	609.00	-	3.4	"Kobe Japan"	1995	"Nishi-Akashi"	6.9	strike slip	7.08	7.08
72	1120	1.015	1.311	256.00	1.554	8.7	"Kobe Japan"	1995	"Takatori"	6.9	strike slip	1.46	1.47
73	1158	2.006	0.982	281.86	-	1.3	"Kocaeli Turkey"	1999	"Duzce"	7.51	strike slip	13.6	15.37
74	1231	1.114	2.336	496.21	-	9.3	"Chi-Chi Taiwan"	1999	"CHY080"	7.62	Reverse Oblique	0.11	2.69
75	1517	1.058	1.989	665.20	-	20.3	"Chi-Chi Taiwan"	1999	"TCU084"	7.62	Reverse Oblique	0	11.48
76	3746	2.232	0.969	459.04	1.967	1.6	"Cape Mendocino"	1992	"Centerville Beach Naval Fac"	7.01	Reverse	16.44	18.31
77	4228	2.418	0.963	375.00	1.799	2.2	"Niigata Japan"	2004	"NIGH11"	6.63	Reverse	6.27	8.93
78	4895	1.032	1.050	265.50	-	13.3	"Chuetsu-oki Japan"	2007	"Kashiwazaki NPP Unit 5: ground surface"	6.8	Reverse	0	10.97
79	5985	2.185	1.218	202.26	-	4.3	"El Mayor-Cucapah Mexico"	2010	"El Centro Differential Array"	7.2	strike slip	22.83	23.42

Table F. 1 (Continued): List of ground motions assembled by Caltrans for application to this project

No.	PEER Record Sequence Number*	Scale Factor	SA-1 (g)	Vs30 (m/sec)	Tp-Pulse Period (sec)	Arias Intensity (m/sec)	Earthquake Name	Year	Station Name	Magnitude	Mechanism	Rjb (km)	Rrup (km)
80	6906	1.121	1.140	344.02	6.23	4.7	"Darfield New Zealand"	2010	"GDLC"	7	strike slip	1.22	1.22
81	721	2.266	0.661	192.05	-	1.1	"Superstition Hills-02"	1987	"El Centro Imp. Co. Cent"	6.54	strike slip	18.2	18.2
82	767	2.111	0.668	349.85	2.639	2.1	"Loma Prieta"	1989	"Gilroy Array #3"	6.93	Reverse Oblique	12.23	12.82
83	779	1.085	0.816	594.83	-	7.9	"Loma Prieta"	1989	"LGPC"	6.93	Reverse Oblique	0	3.88
84	983	1.069	1.067	525.79	3.535	6.5	"Northridge-01"	1994	"Jensen Filter Plant Generator Building"	6.69	Reverse	0	5.43
85	1084	1.014	1.399	251.24	2.982	6	"Northridge-01"	1994	"Sylmar - Converter Sta"	6.69	Reverse	0	5.35
86	1101	1.865	1.579	256.00	-	2	"Kobe Japan"	1995	"Amagasaki"	6.9	strike slip	11.34	11.34
87	1106	1.164	1.610	312.00	1.092	8.4	"Kobe Japan"	1995	"KJMA"	6.9	strike slip	0.94	0.96
88	1505	1.036	0.729	487.34	12.285	3.3	"Chi-Chi Taiwan"	1999	"TCU068"	7.62	Reverse Oblique	0	0.32
89	1510	1.986	0.693	573.02	4.998	3	"Chi-Chi Taiwan"	1999	"TCU075"	7.62	Reverse Oblique	0.89	0.89
90	3968	1.021	1.432	310.21	-	11.8	"Tottori Japan"	2000	"TTRH02"	6.61	strike slip	0.83	0.97
91	4031	2.282	0.760	410.66	-	1.9	"San Simeon CA"	2003	"Templeton - 1-story Hospital"	6.52	Reverse	5.07	6.22
92	4451	1.968	1.713	462.23	1.442	3	"Montenegro Yugoslavia"	1979	"Bar-Skupstina Opstine"	7.1	Reverse	0	6.98
93	5264	1.110	1.041	198.26	-	5	"Chuetsu-oki Japan"	2007	"NIG018"	6.8	Reverse	0	10.78
94	5657	1.024	0.775	506.44	-	26.1	"Iwate Japan"	2008	"IWTH25"	6.9	Reverse	0	4.8
95	5991	1.763	1.007	202.85	-	3.6	"El Mayor-Cucapah Mexico"	2010	"El Centro Array #10"	7.2	strike slip	19.36	20.05
96	6893	2.142	0.857	344.02	-	2.8	"Darfield New Zealand"	2010	"DFHS"	7	strike slip	11.86	11.86
97	776	1.766	1.259	282.14	-	2.2	"Loma Prieta"	1989	"Hollister - South & Pine"	6.93	Reverse Oblique	27.67	27.93
98	825	1.122	0.679	567.78	-	6	"Cape Mendocino"	1992	"Cape Mendocino"	7.01	Reverse	0	6.96
99	1063	0.908	1.328	282.25	1.246	7.5	"Northridge-01"	1994	"Rinaldi Receiving Sta"	6.69	Reverse	0	6.5
100	1086	0.968	1.121	440.54	2.436	5	"Northridge-01"	1994	"Sylmar - Olive View Med FF"	6.69	Reverse	1.74	5.3
101	1119	1.108	0.911	312.00	1.806	3.9	"Kobe Japan"	1995	"Takarazuka"	6.9	strike slip	0	0.27
102	1197	1.022	1.041	542.61	-	5.9	"Chi-Chi Taiwan"	1999	"CHY028"	7.62	Reverse Oblique	3.12	3.12
103	1503	0.927	1.087	305.85	5.74	7.7	"Chi-Chi Taiwan"	1999	"TCU065"	7.62	Reverse Oblique	0.57	0.57
104	1605	1.155	0.738	281.86	-	2.9	"Duzce Turkey"	1999	"Duzce"	7.14	strike slip	0	6.58
105	3749	2.058	0.679	355.18	-	1.3	"Cape Mendocino"	1992	"Fortuna Fire Station"	7.01	Reverse	16.54	20.41
106	4219	1.098	0.843	480.40	-	8.8	"Niigata Japan"	2004	"NIGH01"	6.63	Reverse	0.49	9.46
107	4863	1.995	1.349	514.30	-	2.2	"Chuetsu-oki Japan"	2007	"Nagaoka"	6.8	Reverse	3.97	16.27

Table F. 1 (Continued): List of ground motions assembled by Caltrans for application to this project

No.	PEER Record Sequence Number*	Scale Factor	SA-1 (g)	Vs30 (m/sec)	Tp-Pulse Period (sec)	Arias Intensity (m/sec)	Earthquake Name	Year	Station Name	Magnitude	Mechanism	Rjb (km)	Rrup (km)
108	4875	1.077	0.886	282.57	-	6.4	"Chuetsu-oki Japan"	2007	"Kariwa"	6.8	Reverse	0	12
109	5780	1.912	0.810	345.55	-	1.8	"Iwate Japan"	2008	"Iwadeyama"	6.9	Reverse	20.77	20.78
110	5975	1.867	0.599	231.23	-	2.4	"El Mayor-Cucapah Mexico"	2010	"Calexico Fire Station"	7.2	strike slip	19.12	20.46
111	6911	1.127	0.786	326.01	9.919	3.2	"Darfield New Zealand"	2010	"HORC"	7	strike slip	7.29	7.29
112	6953	2.158	0.639	206.00	-	1.3	"Darfield New Zealand"	2010	"Pages Road Pumping Station"	7	strike slip	24.55	24.55
113	126	1.026	0.649	259.59	-	5.7	"Gazli USSR"	1976	"Karakyr"	6.8	Reverse	3.92	5.46
114	180	1.094	0.646	205.63	4.13	1.7	"Imperial Valley-06"	1979	"El Centro Array #5"	6.53	strike slip	1.76	3.95
115	723	1.083	0.778	348.69	2.394	3.7	"Superstition Hills-02"	1987	"Parachute Test Site"	6.54	strike slip	0.95	0.95
116	900	2.183	0.918	353.63	7.504	0.9	"Landers"	1992	"Yermo Fire Station"	7.28	strike slip	23.62	23.62
117	982	0.933	1.324	373.07	3.157	5.3	"Northridge-01"	1994	"Jensen Filter Plant Administrative Building"	6.69	Reverse	0	5.43
118	1044	0.913	0.915	269.14	1.372	5.7	"Northridge-01"	1994	"Newhall - Fire Sta"	6.69	Reverse	3.16	5.92
119	1492	0.956	0.981	579.10	11.956	2.9	"Chi-Chi Taiwan"	1999	"TCU052"	7.62	Reverse Oblique	0	0.66
120	1513	1.391	0.879	363.99	-	7.7	"Chi-Chi Taiwan"	1999	"TCU079"	7.62	Reverse Oblique	0	10.97
121	1602	1.089	1.051	293.57	0.882	3.7	"Duzce Turkey"	1999	"Bolu"	7.14	strike slip	12.02	12.04
122	3750	2.080	0.509	515.65	-	0.9	"Cape Mendocino"	1992	"Loleta Fire Station"	7.01	Reverse	23.46	25.91
123	4040	0.985	0.750	487.40	2.023	8	"Bam Iran"	2003	"Bam"	6.6	strike slip	0.05	1.7
124	4458	1.949	1.061	318.74	1.974	1.8	"Montenegro Yugoslavia"	1979	"Ulcinj - Hotel Olimpic"	7.1	Reverse	3.97	5.76
125	4856	0.934	0.775	294.38	-	3.9	"Chuetsu-oki Japan"	2007	"Kashiwazaki City Center"	6.8	Reverse	0	11.09
126	4876	1.030	0.962	655.45	-	8.6	"Chuetsu-oki Japan"	2007	"Kashiwazaki Nishiyamacho Ikeura"	6.8	Reverse	0	12.63
127	5658	1.153	0.516	371.06	-	14.1	"Iwate Japan"	2008	"IWTH26"	6.9	Reverse	5.97	6.02
128	5992	1.078	0.654	196.25	-	5.5	"El Mayor-Cucapah Mexico"	2010	"El Centro Array #11"	7.2	strike slip	15.36	16.21
129	160	1.109	0.491	223.03	-	6.1	"Imperial Valley-06"	1979	"Bonds Corner"	6.53	strike slip	0.44	2.66
130	181	1.053	0.512	203.22	3.773	1.8	"Imperial Valley-06"	1979	"El Centro Array #6"	6.53	strike slip	0	1.35
131	821	1.075	0.833	352.05	-	1.8	"Erzican Turkey"	1992	"Erzincan"	6.69	strike slip	0	4.38
132	828	1.047	0.858	422.17	2.996	3.8	"Cape Mendocino"	1992	"Petrolia"	7.01	Reverse	0	8.18
133	953	1.176	1.155	355.81	-	4.5	"Northridge-01"	1994	"Beverly Hills - 14145 Mulhol"	6.69	Reverse	9.44	17.15
134	1004	0.918	0.783	380.06	0.931	7	"Northridge-01"	1994	"LA - Sepulveda VA Hospital"	6.69	Reverse	0	8.44
135	1244	1.042	0.770	258.89	5.341	3	"Chi-Chi Taiwan"	1999	"CHY101"	7.62	Reverse Oblique	9.94	9.94

Table F. 1 (Continued): List of ground motions assembled by Caltrans for application to this project

No.	PEER Record Sequence Number*	Scale Factor	SA-1 (g)	Vs30 (m/sec)	Tp-Pulse Period (sec)	Arias Intensity (m/sec)	Earthquake Name	Year	Station Name	Magnitude	Mechanism	Rjb (km)	Rrup (km)
136	1507	0.999	0.699	624.85	-	9.5	"Chi-Chi Taiwan"	1999	"TCU071"	7.62	Reverse Oblique	0	5.8
137	2114	1.170	0.874	329.40	3.157	1.9	"Denali Alaska"	2002	"TAPS Pump Station #10"	7.9	strike slip	0.18	2.74
138	4874	1.183	0.624	561.59	-	5.3	"Chuetsu-oki Japan"	2007	"Oguni Nagaoka"	6.8	Reverse	10.31	20
139	4896	0.930	0.912	201.00	-	5.1	"Chuetsu-oki Japan"	2007	"Kashiwazaki NPP Service Hall Array 2.4 m depth"	6.8	Reverse	0	10.97
140	5664	1.161	0.521	361.24	-	4.2	"Iwate Japan"	2008	"MYG005"	6.9	Reverse	10.71	13.47
141	5818	1.046	0.550	512.26	-	7.3	"Iwate Japan"	2008	"Kurihara City"	6.9	Reverse	12.83	12.85
142	5827	1.147	0.672	242.05	-	6.1	"El Mayor-Cucapah Mexico"	2010	"MICHOACAN DE OCAMPO"	7.2	strike slip	13.21	15.91
143	6927	1.105	0.624	263.20	7.371	2.7	"Darfield New Zealand"	2010	"LINC"	7	strike slip	5.07	7.11
144	8161	1.215	0.814	196.88	8.722	3.2	"El Mayor-Cucapah Mexico"	2010	"El Centro Array #12"	7.2	strike slip	9.98	11.26
145	182	0.977	0.660	210.51	4.375	1.7	"Imperial Valley-06"	1979	"El Centro Array #7"	6.53	strike slip	0.56	0.56
146	184	1.024	0.437	202.26	6.265	2.1	"Imperial Valley-06"	1979	"El Centro Differential Array"	6.53	strike slip	5.09	5.09
147	753	1.203	0.607	462.24	-	3.2	"Loma Prieta"	1989	"Corralitos"	6.93	Reverse Oblique	0.16	3.85
148	1013	1.134	0.711	628.99	1.617	1.8	"Northridge-01"	1994	"LA Dam"	6.69	Reverse	0	5.92
149	1054	1.170	1.368	325.67	1.232	3.1	"Northridge-01"	1994	"Pardee - SCE"	6.69	Reverse	5.54	7.46
150	1114	1.126	1.050	198.00	2.828	1.8	"Kobe Japan"	1995	"Port Island (0 m)"	6.9	strike slip	3.31	3.31
151	1176	1.138	0.437	297.00	4.949	1.3	"Kocaeli Turkey"	1999	"Yarimca"	7.51	strike slip	1.38	4.83
152	1509	0.903	1.027	549.43	-	6.4	"Chi-Chi Taiwan"	1999	"TCU074"	7.62	Reverse Oblique	0	13.46
153	1549	0.947	0.537	511.18	-	9.3	"Chi-Chi Taiwan"	1999	"TCU129"	7.62	Reverse Oblique	1.83	1.83
154	3748	1.208	0.796	387.95	-	1.7	"Cape Mendocino"	1992	"Ferndale Fire Station"	7.01	Reverse	16.64	19.32
155	4451	1.233	1.073	462.23	1.442	3	"Montenegro Yugoslavia"	1979	"Bar-Skupstina Opstine"	7.1	Reverse	0	6.98
156	4886	1.083	0.581	338.32	-	4.9	"Chuetsu-oki Japan"	2007	"Tamati Yone Izumozaki"	6.8	Reverse	0	11.48
157	5656	1.141	0.381	486.41	-	3.5	"Iwate Japan"	2008	"IWTH24"	6.9	Reverse	3.1	5.18
158	5663	1.025	0.413	479.37	-	9.4	"Iwate Japan"	2008	"MYG004"	6.9	Reverse	20.17	20.18
159	5991	1.104	0.630	202.85	-	3.6	"El Mayor-Cucapah Mexico"	2010	"El Centro Array #10"	7.2	strike slip	19.36	20.05
160	6962	1.087	0.416	295.74	7.14	1.6	"Darfield New Zealand"	2010	"ROLC"	7	strike slip	0	1.54
161	179	0.859	0.460	208.91	4.788	1.4	"Imperial Valley-06"	1979	"El Centro Array #4"	6.53	strike slip	4.9	7.05
162	183	0.904	0.313	206.08	-	1.6	"Imperial Valley-06"	1979	"El Centro Array #8"	6.53	strike slip	3.86	3.86

Table F. 1 (Continued): List of ground motions assembled by Caltrans for application to this project

No.	PEER Record Sequence Number*	Scale Factor	SA-1 (g)	Vs30 (m/sec)	Tp-Pulse Period (sec)	Arias Intensity (m/sec)	Earthquake Name	Year	Station Name	Magnitude	Mechanism	Rjb (km)	Rrup (km)
163	767	1.095	0.346	349.85	2.639	2.1	"Loma Prieta"	1989	"Gilroy Array #3"	6.93	Reverse Oblique	12.23	12.82
164	776	1.038	0.740	282.14	-	2.2	"Loma Prieta"	1989	"Hollister - South & Pine"	6.93	Reverse Oblique	27.67	27.93
165	1080	1.060	0.757	557.42	-	4.1	"Northridge-01"	1994	"Simi Valley - Katherine Rd"	6.69	Reverse	0	13.42
166	1101	0.967	0.819	256.00	-	2	"Kobe Japan"	1995	"Amagasaki"	6.9	strike slip	11.34	11.34
167	1111	1.059	0.303	609.00	-	3.4	"Kobe Japan"	1995	"Nishi-Akashi"	6.9	strike slip	7.08	7.08
168	1158	0.918	0.449	281.86	-	1.3	"Kocaeli Turkey"	1999	"Duzce"	7.51	strike slip	13.6	15.37
169	1510	1.030	0.359	573.02	4.998	3	"Chi-Chi Taiwan"	1999	"TCU075"	7.62	Reverse Oblique	0.89	0.89
170	1513	0.927	0.585	363.99	-	7.7	"Chi-Chi Taiwan"	1999	"TCU079"	7.62	Reverse Oblique	0	10.97
171	3746	1.021	0.443	459.04	1.967	1.6	"Cape Mendocino"	1992	"Centerville Beach Naval Fac"	7.01	Reverse	16.44	18.31
172	4228	1.107	0.441	375.00	1.799	2.2	"Niigata Japan"	2004	"NIGH11"	6.63	Reverse	6.27	8.93
173	4863	1.173	0.793	514.30	-	2.2	"Chuetsu-oki Japan"	2007	"Nagaoka"	6.8	Reverse	3.97	16.27
174	5825	0.943	0.369	242.05	-	3.3	"El Mayor-Cucapah Mexico"	2010	"CERRO PRIETO GEOTHERMAL"	7.2	strike slip	8.88	10.92
175	5837	0.916	0.494	229.25	-	3.7	"El Mayor-Cucapah Mexico"	2010	"El Centro - Imperial & Ross"	7.2	strike slip	19.39	20.08
176	6893	1.111	0.445	344.02	-	2.8	"Darfield New Zealand"	2010	"DFHS"	7	strike slip	11.86	11.86
177	174	0.910	0.217	196.25	-	2	"Imperial Valley-06"	1979	"El Centro Array #11"	6.53	strike slip	12.56	12.56
178	721	0.954	0.278	192.05	-	1.1	"Superstition Hills-02"	1987	"El Centro Imp. Co. Cent"	6.54	strike slip	18.2	18.2
179	741	0.855	0.456	476.54	-	5.4	"Loma Prieta"	1989	"BRAN"	6.93	Reverse Oblique	3.85	10.72
180	803	0.845	0.510	347.90	5.649	1.3	"Loma Prieta"	1989	"Saratoga - W Valley Coll."	6.93	Reverse Oblique	8.48	9.31
181	1052	0.970	0.501	508.08	0.728	1.8	"Northridge-01"	1994	"Pacoima Kagel Canyon"	6.69	Reverse	5.26	7.26
182	1551	1.040	0.449	652.85	-	1.7	"Chi-Chi Taiwan"	1999	"TCU138"	7.62	Reverse Oblique	9.78	9.78
183	3744	1.064	0.398	566.42	5.362	0.6	"Cape Mendocino"	1992	"Bunker Hill FAA"	7.01	Reverse	8.49	12.24
184	3749	0.982	0.324	355.18	-	1.3	"Cape Mendocino"	1992	"Fortuna Fire Station"	7.01	Reverse	16.54	20.41
185	4031	0.961	0.320	410.66	-	1.9	"San Simeon CA"	2003	"Templeton - 1-story Hospital"	6.52	Reverse	5.07	6.22
186	4207	0.977	0.328	274.17	-	3.4	"Niigata Japan"	2004	"NIG017"	6.63	Reverse	4.22	12.81
187	4218	0.955	0.324	430.71	-	5.2	"Niigata Japan"	2004	"NIG028"	6.63	Reverse	0.46	9.79
188	4458	1.054	0.574	318.74	1.974	1.8	"Montenegro Yugoslavia"	1979	"Ulcinj - Hotel Olimpic"	7.1	Reverse	3.97	5.76
189	5780	0.913	0.387	345.55	-	1.8	"Iwate Japan"	2008	"Iwadeyama"	6.9	Reverse	20.77	20.78

Table F. 1 (Continued): List of ground motions assembled by Caltrans for application to this project

No.	PEER Record Sequence Number*	Scale Factor	SA-1 (g)	Vs30 (m/sec)	Tp-Pulse Period (sec)	Arias Intensity (m/sec)	Earthquake Name	Year	Station Name	Magnitude	Mechanism	Rjb (km)	Rrup (km)
190	5975	0.891	0.286	231.23	-	2.4	"El Mayor-Cucapah Mexico"	2010	"Calexico Fire Station"	7.2	strike slip	19.12	20.46
191	5985	0.812	0.453	202.26	-	4.3	"El Mayor-Cucapah Mexico"	2010	"El Centro Differential Array"	7.2	strike slip	22.83	23.42
192	6953	1.030	0.305	206.00	-	1.3	"Darfield New Zealand"	2010	"Pages Road Pumping Station"	7	strike slip	24.55	24.55
193	20	1.100	0.345	219.31	-	0.5	"Northern Calif-03"	1954	"Ferndale City Hall"	6.5	strike slip	26.72	27.02
194	161	1.010	0.263	208.71	4.396	0.4	"Imperial Valley-06"	1979	"Brawley Airport"	6.53	strike slip	8.54	10.42
195	587	0.995	0.207	551.30	-	0.7	"New Zealand-02"	1987	"Matahina Dam"	6.6	Normal	16.09	16.09
196	764	1.059	0.393	308.55	1.638	0.7	"Loma Prieta"	1989	"Gilroy - Historic Bldg."	6.93	Reverse Oblique	10.27	10.97
197	900	0.875	0.368	353.63	7.504	0.9	"Landers"	1992	"Yermo Fire Station"	7.28	strike slip	23.62	23.62
198	952	0.882	0.261	545.66	-	3	"Northridge-01"	1994	"Beverly Hills - 12520 Mulhol"	6.69	Reverse	12.39	18.36
199	1006	1.091	0.253	398.42	-	1.6	"Northridge-01"	1994	"LA - UCLA Grounds"	6.69	Reverse	13.8	22.49
200	1107	0.975	0.325	312.00	-	1.7	"Kobe Japan"	1995	"Kakogawa"	6.9	strike slip	22.5	22.5
201	1116	1.020	0.265	256.00	-	0.8	"Kobe Japan"	1995	"Shin-Osaka"	6.9	strike slip	19.14	19.15
202	3750	0.834	0.204	515.65	-	0.9	"Cape Mendocino"	1992	"Loleta Fire Station"	7.01	Reverse	23.46	25.91
203	4456	0.925	0.419	543.26	-	4.6	"Montenegro Yugoslavia"	1979	"Petrovac - Hotel Olivia"	7.1	Reverse	0	8.01
204	4849	0.958	0.363	342.74	-	0.8	"Chuetsu-oki Japan"	2007	"Kubikiku Hyakken Joetsu City"	6.8	Reverse	20.71	22.18
205	4879	1.095	0.574	265.82	-	0.7	"Chuetsu-oki Japan"	2007	"Yan Sakuramachi City watershed"	6.8	Reverse	12.98	18.97
206	5774	0.939	0.190	276.30	-	1	"Iwate Japan"	2008	"Nakashinden Town"	6.9	Reverse	29.37	29.38
207	6886	1.003	0.159	280.26	-	0.9	"Darfield New Zealand"	2010	"Canterbury Aero Club"	7	strike slip	14.48	14.48
208	8166	1.009	0.193	425.00	-	-	"Duzce Turkey"	1999	"IRIGM 498"	7.14	strike slip	3.58	3.58
209	68	0.924	0.164	316.46	-	0.7	"San Fernando"	1971	"LA - Hollywood Stor FF"	6.61	Reverse	22.77	22.77
210	162	0.921	0.147	231.23	-	0.9	"Imperial Valley-06"	1979	"Calexico Fire Station"	6.53	strike slip	10.45	10.45
211	285	0.989	0.272	649.67	1.71332	0.4	"Irpinia Italy-01"	1980	"Bagnoli Irpinio"	6.9	Normal	8.14	8.18
212	730	1.073	0.317	343.53	-	0.3	"Spitak Armenia"	1988	"Gukasian"	6.77	Reverse Oblique	23.99	23.99
213	737	0.947	0.157	239.69	-	0.5	"Loma Prieta"	1989	"Agnews State Hospital"	6.93	Reverse Oblique	24.27	24.57
214	739	0.905	0.163	488.77	-	0.8	"Loma Prieta"	1989	"Anderson Dam (Downstream)"	6.93	Reverse Oblique	19.9	20.26
215	881	0.942	0.203	396.41	-	1.2	"Landers"	1992	"Morongo Valley Fire Station"	7.28	strike slip	17.36	17.36
216	998	1.004	0.178	315.06	-	1.4	"Northridge-01"	1994	"LA - N Westmoreland"	6.69	Reverse	23.4	26.73
217	1115	1.023	0.178	256.00	-	0.6	"Kobe Japan"	1995	"Sakai"	6.9	strike slip	28.08	28.08

Table F. 1 (Continued): List of ground motions assembled by Caltrans for application to this project

No.	PEER Record Sequence Number*	Scale Factor	SA-1 (g)	Vs30 (m/sec)	Tp-Pulse Period (sec)	Arias Intensity (m/sec)	Earthquake Name	Year	Station Name	Magnitude	Mechanism	Rjb (km)	Rrup (km)
218	1121	0.905	0.369	256.00	-	1.1	"Kobe Japan"	1995	"Yae"	6.9	strike slip	27.77	27.77
219	1486	1.099	0.183	465.55	8.043	0.4	"Chi-Chi Taiwan"	1999	"TCU046"	7.62	Reverse Oblique	16.74	16.74
220	1628	0.966	0.269	306.37	-	0.9	"St Elias Alaska"	1979	"Icy Bay"	7.54	Reverse	26.46	26.46
221	4212	1.096	0.133	193.20	-	0.8	"Niigata Japan"	2004	"NIG022"	6.63	Reverse	17.57	18.03
222	4842	0.959	0.165	655.45	-	1.4	"Chuetsu-oki Japan"	2007	"Joetsu Uragawaraku Kamabucchi"	6.8	Reverse	18.6	22.74
223	4859	0.953	0.366	274.23	-	0.8	"Chuetsu-oki Japan"	2007	"Mitsuke Kazuiti Arita Town"	6.8	Reverse	11.35	20.33
224	6928	0.983	0.171	649.67	10.633	0.7	"Darfield New Zealand"	2010	"LPCC"	7	strike slip	25.21	25.67
225	175	0.909	0.160	196.88	-	0.4	"Imperial Valley-06"	1979	"El Centro Array #12"	6.53	strike slip	17.94	17.94
226	724	1.056	0.159	316.64	-	0.6	"Superstition Hills-02"	1987	"Plaster City"	6.54	strike slip	22.25	22.25
227	827	0.949	0.173	457.06	-	0.3	"Cape Mendocino"	1992	"Fortuna - Fortuna Blvd"	7.01	Reverse	15.97	19.95
228	990	0.981	0.152	365.22	-	1.1	"Northridge-01"	1994	"LA - City Terrace"	6.69	Reverse	35.03	36.62
229	1001	0.976	0.191	285.28	-	0.7	"Northridge-01"	1994	"LA - S Grand Ave"	6.69	Reverse	29.52	33.99
230	1166	0.943	0.207	476.62	-	0.4	"Kocaeli Turkey"	1999	"Iznik"	7.51	strike slip	30.73	30.73
231	1234	0.920	0.214	665.20	-	1	"Chi-Chi Taiwan"	1999	"CHY086"	7.62	Reverse Oblique	27.57	28.42
232	1636	1.082	0.126	302.64	-	0.4	"Manjil Iran"	1990	"Qazvin"	7.37	strike slip	49.97	49.97
233	1794	0.917	0.275	379.32	-	0.6	"Hector Mine"	1999	"Joshua Tree"	7.13	strike slip	31.06	31.06
234	3758	1.010	0.205	333.89	-	0.5	"Landers"	1992	"Thousand Palms Post Office"	7.28	strike slip	36.93	36.93
235	3908	1.074	0.135	293.37	-	0.8	"Tottori Japan"	2000	"OKY005"	6.61	strike slip	28.81	28.82
236	4208	0.905	0.136	198.26	-	0.8	"Niigata Japan"	2004	"NIG018"	6.63	Reverse	21.55	25.84
237	4872	1.042	0.266	640.14	-	0.3	"Chuetsu-oki Japan"	2007	"Sawa Mizuguti Tokamachi"	6.8	Reverse	21.17	27.3
238	5799	1.036	0.083	552.38	-	0.4	"Iwate Japan"	2008	"Misato Akita City - Tsuchizaki"	6.9	Reverse	39.86	41.72
239	5972	0.910	0.112	208.71	-	0.8	"El Mayor-Cucapah Mexico"	2010	"Brawley Airport"	7.2	strike slip	41.15	41.48
240	6965	0.947	0.118	263.20	-	0.7	"Darfield New Zealand"	2010	"SBRC"	7	strike slip	21.31	24.34
241	70	1.118	0.365	425.34	-	0.3	"San Fernando"	1971	"Lake Hughes #1"	6.61	Reverse	22.23	27.4
242	78	1.043	0.141	452.86	-	0.3	"San Fernando"	1971	"Palmdale Fire Station"	6.61	Reverse	24.16	28.99
243	172	1.036	0.085	237.33	-	0.3	"Imperial Valley-06"	1979	"El Centro Array #1"	6.53	strike slip	19.76	21.68
244	288	1.004	0.102	561.04	-	0.5	"Irpinia Italy-01"	1980	"Brienza"	6.9	Normal	22.54	22.56
245	726	1.081	0.194	191.14	-	0.4	"Superstition Hills-02"	1987	"Salton Sea Wildlife Refuge"	6.54	strike slip	25.88	25.88

Table F. 1 (Continued): List of ground motions assembled by Caltrans for application to this project

No.	PEER Record Sequence Number*	Scale Factor	SA-1 (g)	Vs30 (m/sec)	Tp-Pulse Period (sec)	Arias Intensity (m/sec)	Earthquake Name	Year	Station Name	Magnitude	Mechanism	Rjb (km)	Rrup (km)
246	748	0.989	0.139	627.59	-	0.2	"Loma Prieta"	1989	"Belmont - Envirotech"	6.93	Reverse Oblique	43.94	44.11
247	800	1.000	0.101	279.56	-	0.2	"Loma Prieta"	1989	"Salinas - John & Work"	6.93	Reverse Oblique	28.66	32.78
248	880	1.009	0.092	355.42	-	0.4	"Landers"	1992	"Mission Creek Fault"	7.28	strike slip	26.96	26.96
249	968	0.968	0.146	271.90	-	0.6	"Northridge-01"	1994	"Downey - Co Maint Bldg"	6.69	Reverse	43.2	46.74
250	984	1.054	0.138	301.00	-	0.4	"Northridge-01"	1994	"LA - 116th St School"	6.69	Reverse	36.39	41.17
251	1162	1.056	0.141	347.62	-	0.3	"Kocaeli Turkey"	1999	"Goynuk"	7.51	strike slip	31.74	31.74
252	1289	1.073	0.260	484.97	-	0.3	"Chi-Chi Taiwan"	1999	"HWA041"	7.62	Reverse Oblique	43.37	47.76
253	3937	1.094	0.113	182.30	-	0.2	"Tottori Japan"	2000	"SMN005"	6.61	strike slip	45.73	45.73
254	3994	1.046	0.101	365.15	-	0.2	"San Simeon CA"	2003	"San Luis Obispo - Lopez Lake Grounds"	6.52	Reverse	48.07	48.11
255	4844	0.934	0.181	640.14	-	0.3	"Chuetsu-oki Japan"	2007	"Tokamachi Matsunoyama"	6.8	Reverse	23.01	28.75
256	5471	1.084	0.089	158.16	-	0.3	"Iwate Japan"	2008	"AKT016"	6.9	Reverse	46.77	48.36
257	9	1.169	0.062	213.44	-	0.1	"Borrego"	1942	"El Centro Array #9"	6.5	strike slip	56.88	56.88
258	65	1.201	0.075	308.35	-	0.1	"San Fernando"	1971	"Gormon - Oso Pump Plant"	6.61	Reverse	43.95	46.78
259	122	0.814	0.106	249.28	-	0.1	"Friuli Italy-01"	1976	"Codroipo"	6.5	Reverse	33.32	33.4
260	191	0.877	0.058	242.05	-	0.3	"Imperial Valley-06"	1979	"Victoria"	6.53	strike slip	31.92	31.92
261	745	0.905	0.051	422.79	-	0.2	"Loma Prieta"	1989	"Bear Valley #14 Upper Butts Rn"	6.93	Reverse Oblique	71.28	71.39
262	860	1.155	0.107	328.09	-	0.3	"Landers"	1992	"Hemet Fire Station"	7.28	strike slip	68.66	68.66
263	966	0.996	0.078	324.79	-	0.1	"Northridge-01"	1994	"Covina - W Badillo"	6.69	Reverse	53.21	53.45
264	1154	0.998	0.121	612.78	-	0.1	"Kocaeli Turkey"	1999	"Bursa Sivil"	7.51	strike slip	65.53	65.53
265	1626	1.070	0.051	649.67	-	0.2	"Sitka Alaska"	1972	"Sitka Observatory"	7.68	strike slip	34.61	34.61
266	1782	1.033	0.083	436.14	-	0.1	"Hector Mine"	1999	"Forest Falls Post Office"	7.13	strike slip	74.92	74.92
267	2111	0.882	0.092	341.56	-	0.1	"Denali Alaska"	2002	"R109 (temp)"	7.9	strike slip	42.99	43
268	3915	1.228	0.076	296.96	-	0.1	"Tottori Japan"	2000	"OKY012"	6.61	strike slip	66.24	66.25
269	4054	0.828	0.045	574.88	-	0.2	"Bam Iran"	2003	"Mohammad Abad-e-Madkoon"	6.6	strike slip	46.2	46.22
270	4222	1.046	0.043	244.84	-	0.2	"Niigata Japan"	2004	"NIGH05"	6.63	Reverse	70.59	71.52
271	5258	1.003	0.069	229.95	-	0.3	"Chuetsu-oki Japan"	2007	"NIG012"	6.8	Reverse	65.54	67.77
272	6933	1.085	0.053	342.70	-	0.1	"Darfield New Zealand"	2010	"MAYC"	7	strike slip	33.54	35.23
273	7	1.180	0.039	219.31	-	0	"Northwest Calif-02"	1941	"Ferndale City Hall"	6.6	strike slip	91.15	91.22

Table F. 1 (Continued): List of ground motions assembled by Caltrans for application to this project

No.	PEER Record Sequence Number*	Scale Factor	SA-1 (g)	Vs30 (m/sec)	Tp-Pulse Period (sec)	Arias Intensity (m/sec)	Earthquake Name	Year	Station Name	Magnitude	Mechanism	Rjb (km)	Rrup (km)
274	51	1.017	0.047	280.56	-	0	"San Fernando"	1971	"2516 Via Tejon PV"	6.61	Reverse	55.2	55.2
275	56	0.901	0.027	235.00	-	0.1	"San Fernando"	1971	"Carbon Canyon Dam"	6.61	Reverse	61.79	61.79
276	188	0.955	0.044	316.64	-	0.1	"Imperial Valley-06"	1979	"Plaster City"	6.53	strike slip	30.33	30.33
277	294	0.868	0.053	496.46	-	0	"Irpinia Italy-01"	1980	"Tricarico"	6.9	Normal	51.74	53.16
278	897	1.042	0.028	635.01	-	0.1	"Landers"	1992	"Twentynine Palms"	7.28	strike slip	41.43	41.43
279	975	0.912	0.094	362.31	-	0.1	"Northridge-01"	1994	"Glendora - N Oakbank"	6.69	Reverse	53.71	53.94
280	1061	1.138	0.067	580.03	-	0.1	"Northridge-01"	1994	"Rancho Palos Verdes - Hawth"	6.69	Reverse	48.02	52.18
281	1109	0.909	0.035	609.00	-	0.1	"Kobe Japan"	1995	"MZH"	6.9	strike slip	69.04	70.26
282	1627	1.067	0.032	432.58	-	0.1	"Caldiran Turkey"	1976	"Maku"	7.21	strike slip	50.78	50.82
283	3583	1.225	0.066	309.41	-	0	"Taiwan SMART1(25)"	1983	"SMART1 I08"	6.5	Reverse	95.5	95.98
284	3946	0.986	0.048	271.29	-	0.1	"Tottori Japan"	2000	"SMN018"	6.61	strike slip	85.31	85.31
285	4997	0.999	0.088	305.54	-	0.1	"Chuetsu-oki Japan"	2007	"FKS028"	6.8	Reverse	52.63	55.38
286	5648	1.124	0.038	534.71	-	0.1	"Iwate Japan"	2008	"IWTH16"	6.9	Reverse	48.43	49.97
287	5768	0.987	0.027	291.48	-	0.1	"Iwate Japan"	2008	"YMTH09"	6.9	Reverse	47.01	48.59
288	5864	1.014	0.075	384.66	-	0	"El Mayor-Cucapah Mexico"	2010	"Frink"	7.2	strike slip	81.63	81.8
289	287	0.861	0.039	356.39	-	0	"Irpinia Italy-01"	1980	"Bovino"	6.9	Normal	44.62	46.25
290	432	1.006	0.048	267.67	-	0	"Taiwan SMART1(25)"	1983	"SMART1 O01"	6.5	Reverse	97.16	97.63
291	436	1.011	0.018	279.97	-	0	"Borah Peak ID-01"	1983	"CPP-601"	6.88	Normal	82.6	82.6
292	747	0.808	0.029	509.87	-	0	"Loma Prieta"	1989	"Bear Valley #7 Pinnacles"	6.93	Reverse Oblique	68.22	69.38
293	1037	0.955	0.030	422.73	-	0	"Northridge-01"	1994	"Mojave - Oak Creek Canyon"	6.69	Reverse	75.64	75.8
294	1097	0.978	0.030	506.00	-	0	"Northridge-01"	1994	"Wrightwood - Nielson Ranch"	6.69	Reverse	81.54	81.69
295	1620	1.121	0.022	411.91	-	0	"Duzce Turkey"	1999	"Sakarya"	7.14	strike slip	45.16	45.16
296	1767	0.970	0.023	667.42	-	0	"Hector Mine"	1999	"Banning - Twin Pines Road"	7.13	strike slip	83.43	83.43
297	3594	1.038	0.062	300.22	-	0	"Taiwan SMART1(25)"	1983	"SMART1 M11"	6.5	Reverse	96.52	97
298	3882	1.223	0.018	571.63	-	0	"Tottori Japan"	2000	"HRS016"	6.61	strike slip	82.42	82.42
299	3981	0.861	0.049	333.61	-	0	"San Simeon CA"	2003	"Coalinga - Fire Station 39"	6.52	Reverse	69.51	70.23
300	3987	0.866	0.031	280.64	-	0	"San Simeon CA"	2003	"Greenfield - Police Station"	6.52	Reverse	69.08	69.8
301	4198	0.981	0.025	220.65	-	0	"Niigata Japan"	2004	"NIG008"	6.63	Reverse	83.83	84.28

Table F. 1 (Continued): List of ground motions assembled by Caltrans for application to this project

No.	PEER Record Sequence Number*	Scale Factor	SA-1 (g)	Vs30 (m/sec)	Tp-Pulse Period (sec)	Arias Intensity (m/sec)	Earthquake Name	Year	Station Name	Magnitude	Mechanism	Rjb (km)	Rrup (km)
302	5254	0.964	0.024	220.65	-	0	"Chuetsu-oki Japan"	2007	"NIG008"	6.8	Reverse	81.51	83.31
303	5467	0.977	0.020	449.45	-	0.1	"Iwate Japan"	2008	"AKT012"	6.9	Reverse	57.37	58.67
304	8163	1.018	0.025	483.02	-	0	"El Mayor-Cucapah Mexico"	2010	"SANTA ISABEL VIEJO"	7.2	strike slip	55.19	57.49
305	58	0.875	0.019	477.22	-	0	"San Fernando"	1971	"Cedar Springs Pumphouse"	6.61	Reverse	92.25	92.59
306	92	0.808	0.014	347.67	-	0	"San Fernando"	1971	"Wheeler Ridge - Ground"	6.61	Reverse	68.38	70.23
307	427	1.028	0.022	671.52	-	0	"Taiwan SMART1(25)"	1983	"SMART1 E02"	6.5	Reverse	91.54	92.04
308	440	0.907	0.011	324.20	-	0	"Borah Peak ID-01"	1983	"TRA-642 ETR Reactor Bldg(Bsmt)"	6.88	Normal	79.59	79.59
309	441	1.074	0.015	324.20	-	0	"Borah Peak ID-01"	1983	"TRA-670 ATR Reactor Bldg(Bsmt)"	6.88	Normal	80	80
310	2093	1.078	0.020	382.50	-	0	"Nenana Mountain Alaska"	2002	"TAPS Pump Station #09"	6.7	strike slip	104.73	104.73
311	3899	1.003	0.012	617.44	-	0	"Tottori Japan"	2000	"HYGH02"	6.61	strike slip	88.75	88.75
312	3945	0.860	0.018	262.19	-	0	"Tottori Japan"	2000	"SMN017"	6.61	strike slip	77.85	77.85
313	5003	0.801	0.013	245.88	-	0	"Chuetsu-oki Japan"	2007	"FKSH04"	6.8	Reverse	93.48	95.05
314	5064	1.032	0.027	342.36	-	0	"Chuetsu-oki Japan"	2007	"GNM005"	6.8	Reverse	86.23	87.94
315	5461	0.886	0.019	279.36	-	0	"Iwate Japan"	2008	"AKT006"	6.9	Reverse	112.78	113.45
316	5490	1.136	0.013	232.58	-	0.1	"Iwate Japan"	2008	"AKTH14"	6.9	Reverse	95.32	96.11
317	5839	1.009	0.016	388.01	-	0	"El Mayor-Cucapah Mexico"	2010	"El Cajon - Marshall"	7.2	strike slip	115	115
318	5970	0.820	0.010	619.00	-	0	"El Mayor-Cucapah Mexico"	2010	"Borrego Springs"	7.2	strike slip	91.9	91.9
319	6515	0.952	0.020	279.58	-	0	"Niigata Japan"	2004	"FKS016"	6.63	Reverse	111.33	111.4
320	6783	1.012	0.018	265.60	-	0	"Niigata Japan"	2004	"TCG008"	6.63	Reverse	109.14	109.21

APPENDIX G

- **Conventioanl PSDMs:**

The conventional PSDM refers to the simplest form $S_d = a.IM^b$. In the plots, y and x refer to the seismic demand and ground motion intensity measure in the logarithmic space.

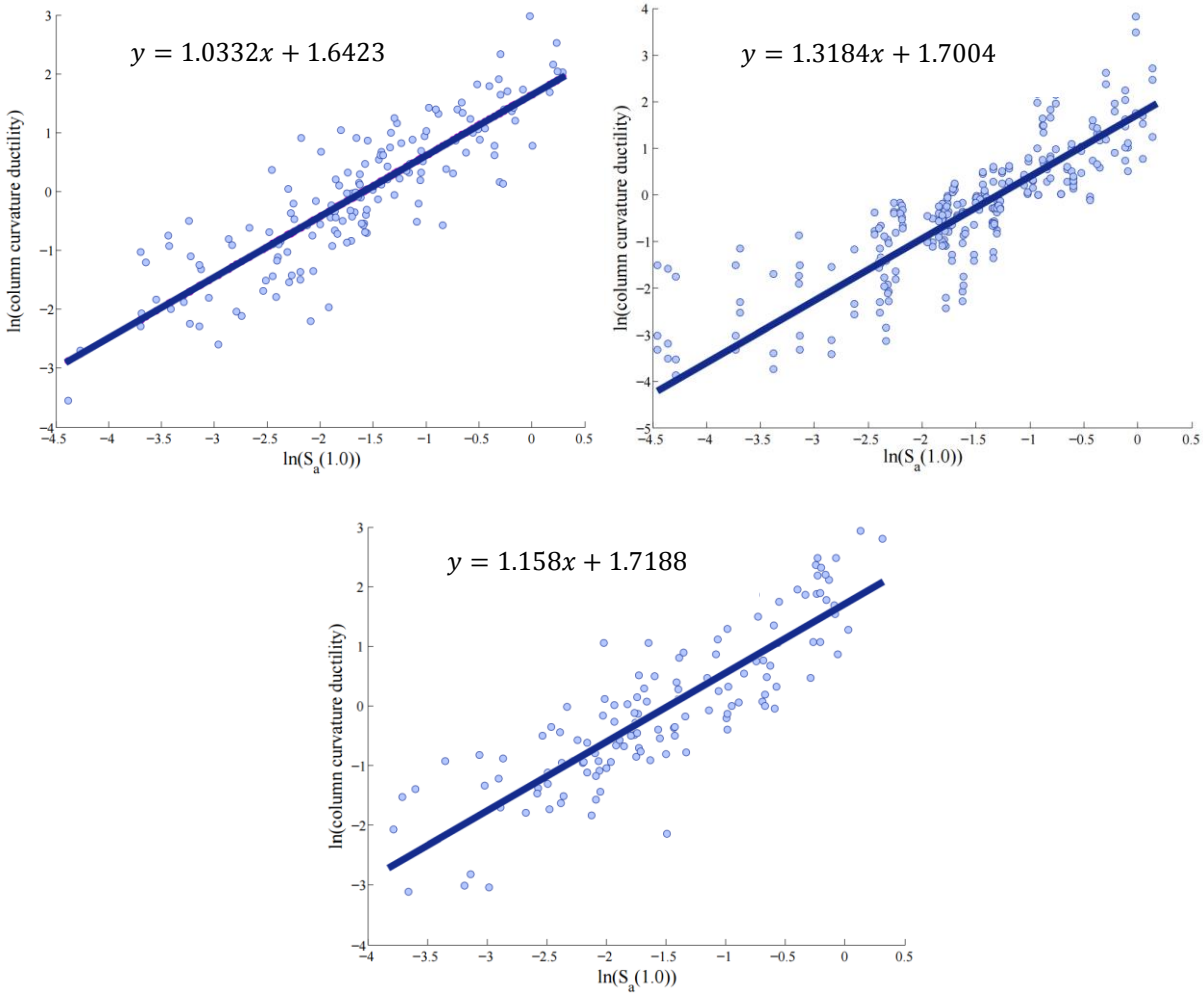

Figure G. 1: The conventional probabilistic seismic demand models generated for (a) skewed, (b) tall, and (c) unbalanced bridges

- **Modified PSDMs Using Optimization Approach:**

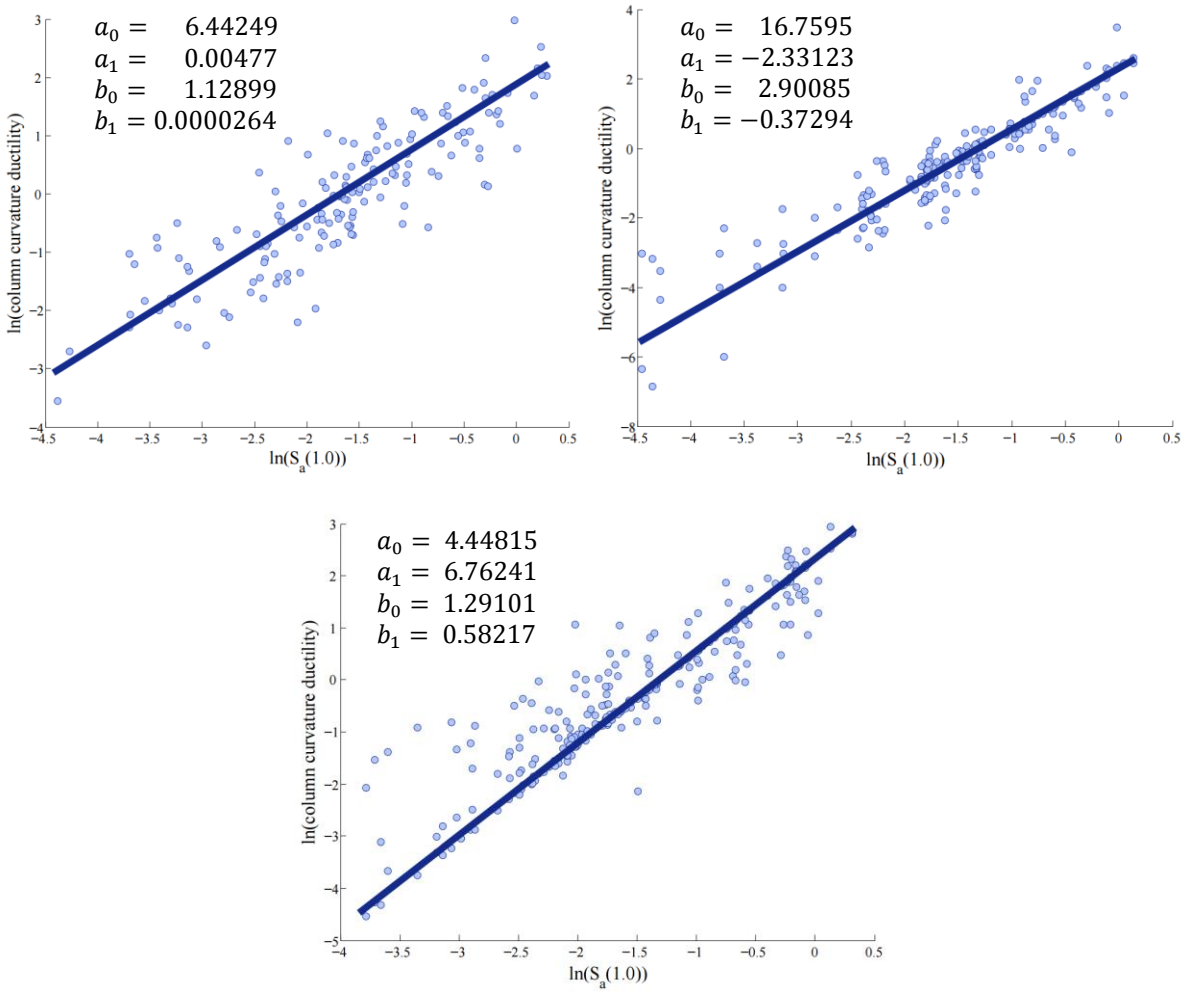

Figure G. 2: The conventional probabilistic seismic demand models generated for (a) skewed, (b) tall, and (c) unbalanced bridges

- **Modified PSDMs Using Bayesian Appraoch:**

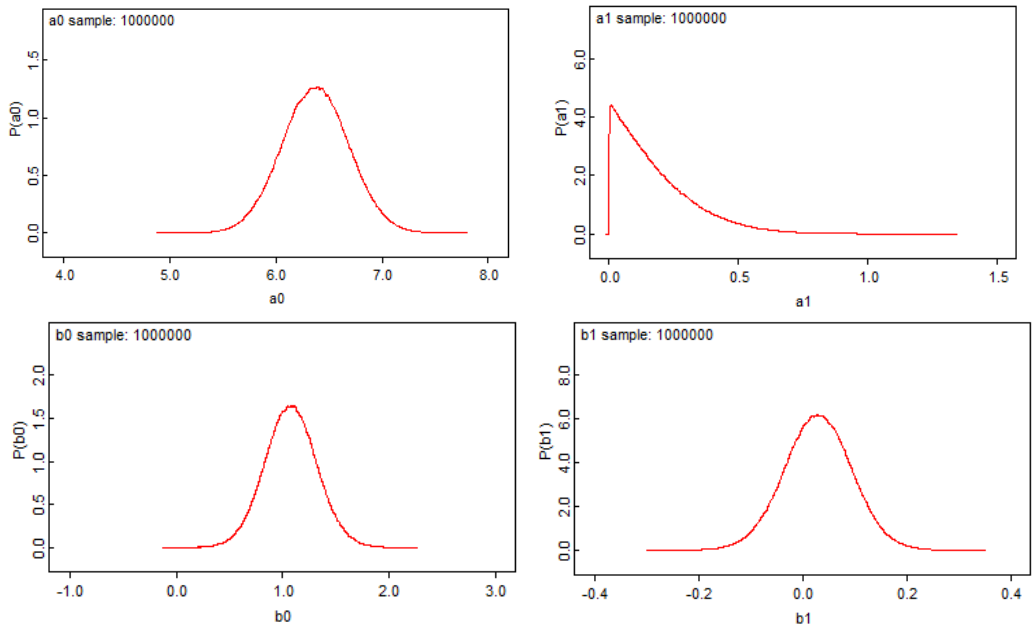

Figure G. 3: The estimated posterior distributions for the coefficients of PSDM for skewed bridges (produced by WinBUGs)

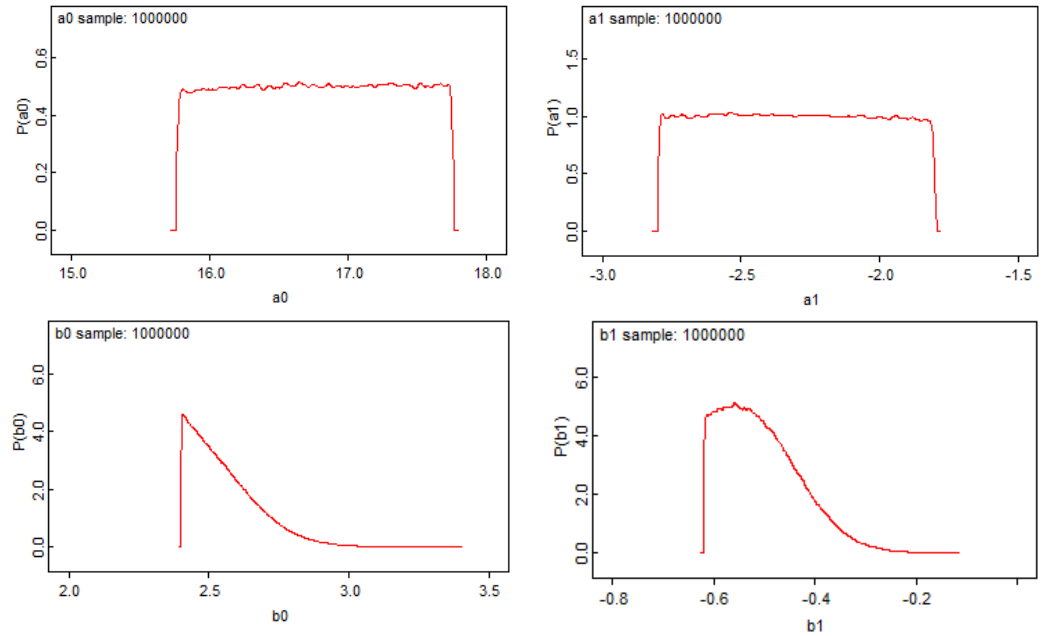

Figure G. 4: The estimated posterior distributions for the coefficients of PSDM for tall bridges (produced by WinBUGs)

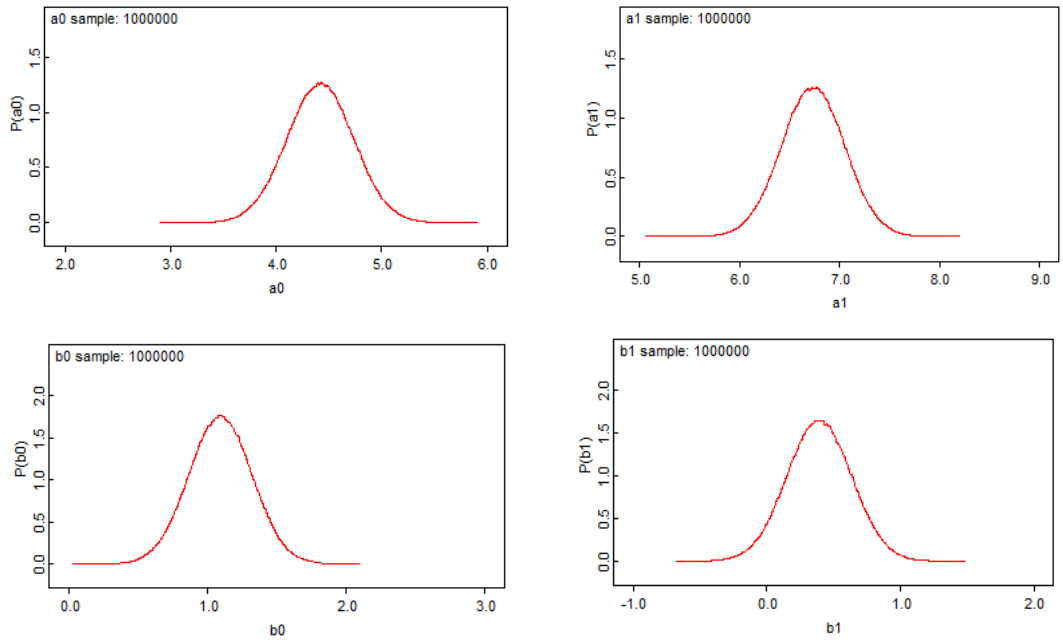

Figure G. 5: The estimated posterior distributions for the coefficients of PSDM for unbalanced bridges (produced by WinBUGs)

Table G. 1: The statistical inference of the posterior distributions for the column curvature ductility of skewed bridge

Parameter	Mean	median	Std	MC_error	val2.5pc	val5.0pc	val95.0pc	val97.5pc
a_0	6.373	6.373	0.3155	0.001311	5.756	5.854	6.893	6.992
a_1	0.1769	0.1378	0.1503	6.60E-04	0.005476	0.01122	0.4757	0.5568
b_0	1.079	1.078	0.2451	9.90E-04	0.6006	0.6786	1.485	1.567
b_1	0.02959	0.0297	0.06541	2.60E-04	-0.09981	-0.07817	0.1363	0.1576

Table G. 2: The statistical inference of the posterior distributions for the column curvature ductility of tall bridge

Parameter	Mean	median	Std	MC_error	val2.5pc	val5.0pc	val95.0pc	val97.5pc
a_0	16.77	16.77	0.5757	0.002482	15.81	15.86	17.66	17.71
a_1	-2.303	-2.304	0.2876	0.001271	-2.775	-2.75	-1.852	-1.826
b_0	2.556	2.528	0.1247	6.03E-04	2.405	2.411	2.796	2.86
b_1	-0.5059	-0.5175	0.07817	3.64E-04	-0.6145	-0.6092	-0.3618	-0.3287

Table G. 3: The statistical inference of the posterior distributions for the column curvature ductility of unbalanced bridge

Parameter	Mean	median	Std	MC_error	val2.5pc	val5.0pc	val95.0pc	val97.5pc
a_0	4.418	4.419	0.3173	0.001124	3.795	3.896	4.94	5.041
a_1	6.735	6.735	0.3168	0.001116	6.115	6.213	7.257	7.356
b_0	1.092	1.091	0.2279	8.35E-04	0.6452	0.7171	1.465	1.537
b_1	0.3933	0.3928	0.2422	8.81E-04	-0.08091	-0.00373	0.7923	0.8684

- **Multivariate PSDMs:**

$$\ln(\varphi c) = \beta_0 + \beta_1 \ln(X_1) + \sum_{j=2}^{8} \beta_j X_j + \sum_{j=9}^{43} \beta_j \ln(X_j) \qquad (G.1)$$

Table G. 4: Values for the coefficients in equation *G.1* for tall bridge

Coefficients	Values	Coefficients	Values	Coefficients	Values	Coefficients	Values
Intercept (β_0)	-33.9	β_9	1.970	β_{21}	-6.227	β_{37}	2.276
β_1	1.118	β_{10}	-2.107	β_{22}	0.111	β_{38}	0.144
$\beta_{2_{rigid}}$	1.910	β_{11}	6.009	β_{23}	0.235	β_{39}	-0.281
$\beta_{4_{single-col}}$	0.463	β_{13}	2.157	β_{26}	0.160	β_{41}	-1.368
$\beta_{5_{clay}}$	0.057	β_{16}	0.560	β_{28}	-0.793		
$\beta_{5_{sand}}$	0.115	β_{17}	4.057	β_{29}	-1.029		
$\beta_{7_{three-cells}}$	-0.754	β_{18}	-1.237	β_{33}	-0.567		
$\beta_{8_{long}}$	0.102	β_{19}	0.098	β_{35}	0.032		
$\beta_{8_{trans}}$	0.203	β_{20}	0.089	β_{36}	-0.183		

Table G. 5: Values for the coefficients in equation *G.1* for unbalanced bridge

Coefficients	Values	Coefficients	Values	Coefficients	Values	Coefficients	Values
Intercept (β_0)	-0.530	$\beta_{8_{trans}}$	0.233	β_{22}	0.047	β_{39}	0.066
β_1	1.248	β_9	0.862	β_{23}	0.025	β_{42}	0.478
$\beta_{4_{single-col}}$	-0.056	β_{10}	0.027	β_{24}	0.083	β_{43}	0.594
$\beta_{5_{clay}}$	-0.011	β_{13}	2.616	β_{27}	0.010		
$\beta_{5_{sand}}$	-0.022	β_{17}	-0.107	β_{29}	-0.536		
$\beta_{6_{RC}}$	0.047	β_{18}	-0.978	β_{34}	0.041		
$\beta_{6_{PC}}$	0.094	β_{19}	-0.053	β_{35}	0.011		
$\beta_{7_{three-cells}}$	0.060	β_{20}	-0.051	β_{37}	0.929		
$\beta_{8_{long}}$	0.116	β_{21}	-0.401	β_{38}	0.078		

Table G. 6: Values for the coefficients in equation *G.1* for skewed bridge

Coefficients	Values	Coefficients	Values	Coefficients	Values	Coefficients	Values
Intercept (β_0)	104.826	$\beta_{8_{long}}$	-0.001	β_{19}	-0.013	β_{32}	0.019
β_1	0.012	$\beta_{8_{trans}}$	-0.002	β_{20}	0.001	β_{33}	-0.007
$\beta_{2_{rigid}}$	-11.054	β_9	-1.002	β_{21}	0.026	β_{34}	-0.001
$\beta_{3_{1970-1990}}$	0.510	β_{10}	-0.004	β_{23}	0.001	β_{36}	-0.008
$\beta_{3_{post-1990}}$	0.764	β_{11}	0.026	β_{25}	-0.006	β_{37}	0.022
$\beta_{4_{single-col}}$	-0.002	β_{12}	-0.058	β_{26}	2.877	β_{38}	0.001
$\beta_{5_{clay}}$	-0.001	β_{13}	0.190	β_{27}	2.890	β_{39}	-0.001
$\beta_{5_{sand}}$	-0.002	β_{14}	-3.446	β_{28}	-0.015	β_{40}	0.069
$\beta_{6_{RC}}$	13.388	β_{16}	0.250	β_{29}	-0.018		
$\beta_{6_{RC}}$	-13.388	β_{17}	-0.011	β_{30}	0.019		
$\beta_{7_{three-cells}}$	-0.003	β_{18}	-0.013	β_{31}	0.008		

APPENDIX H

Bridge columns have different design features based on their design and construction era, which can be classified into three main periods: Pre-1970, 1970-1990, and Post-1990. These eras are defined based on the evolution of the seismic design codes after the 1971 San Fernando and 1989 Loma Prieta Earthquakes. The distinction between the attributes of the bridge columns designed in different eras is summarized in Table H. 1, and more details are provided by Ramanathan (2012). This section explains the literature review of previous experiments on the bridge columns for every individual design era. The geometric features of the specimens and the corresponding values for the column capacity limit states are provided in Table H. 2, Table H. 3, and Table H. 4 for each level of damage.

Table H. 1: Comparison of the design details of the bridge columns according to various design eras

Bridge design era	Lateral seismic force	Column shear reinforcement	Additional features	Force-displacement backbone curve (schematic)
Pre-1970	6% of structural dead weight	#4 @ 12 inches irrespective of column size	• Lap-splice of longitudinal bars near footing. • Inadequate development length of the longitudinal bars into the footing without any standard hook. • Absence of the ductility concept (failure modes are brittle, shear, or lap-splice). • Rapid degradation of the column strength once yield moment is attained. • No 90 degree hooks when column bars are embedded into footing. • Short splice length of longitudinal bars.	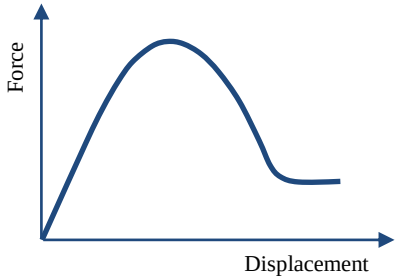
1970-1990	2- 2.5 times higher than the corresponding values for Pre-1970; Based on ATC-6 guidelines	Spacing: 3-6 inches; However, confinement in the plastic hinge region is absent in most cases.	• No bar lap-splice at the location of maximum moment. • Increase in the negative moment reinforcement in footing and pile caps without any shear reinforcement. • Absence of the joint reinforcement between either the column and the bent cap or the column and the footing. • Column shear in the plastic hinge region. • Shear failure was seen in columns with flares due to the poor flare details.	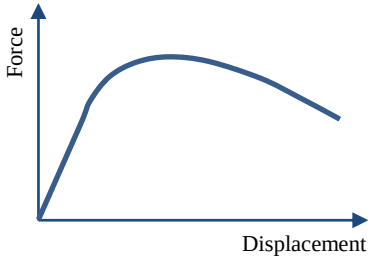
Post-1990	Based on ATC-32; Capacity-based design to ensure the ductile mode of failure	Spacing: <6 times the longitudinal bar diameter; Confinement exists in the plastic hinge region.	• Minimal usage of column flares. • Tight confinement reinforcement in the column plastic hinge zones. • Improvised flare details by isolating the flare from the superstructure (i.e., a gap of 2–4 in). • No lap splices in the plastic hinge zones. • Shear reinforcement in the footing and pile caps. • Joint reinforcement between both the column and the bent cap, and the column and the footing.	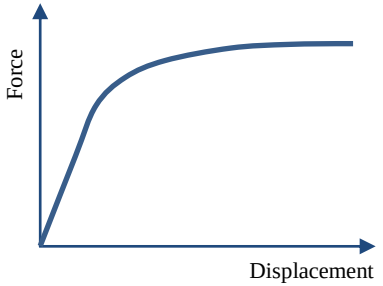

Table H. 2: Review of selected experiments to develop the capacity models for the bridge columns designed in the Pre-1970 era

Specimen properties						Displacement ductility				Curvature ductility				
	Cross-section													
Specimen	Shape	Size (in.)	Height (ft.)	Design code	Long. Steel ratio (%)	CCLS-0	CCLS--1	CCLS--2	CCLS--3	CCLS-0	CCLS--1	CCLS--2	CCLS--3	Reference
R-I	Rectangular	28.75 ×19.25	12	Caltrans	2.55	0.8	1	2	3	0.8	2	6	10	Sun et al. (1993)
R-5	Rectangular	28.75 × 19.25	12	Caltrans	5	0.8	2	3	4	0.8	2.5	3.5	6	
SRPH-6	Circular	24	7	Caltrans	5.4	0.8	1	1.5	2	0.8	1	1.54	2.56	Hose et al. (1997)
col #2	Circular	24	6	ACI	1.06	0.8	1.5	2	4	0.8	2.26	3.52	8.56	Priestley and Benzoni (1996)
col-1	Circular	24	12	Caltrans	2.53	0.8	1	1.5	4	0.8	1	2.31	8.87	Chai et al. (1991)
col-3	Circular	24	12	Caltrans	2.53	1	1.5	3	5	1	2.31	6.25	11.49	
T1	Circular	10	3.33	Caltrans	2	0.8	2	3	5	0.8	2.93	4.85	8.71	Jaradat et al. (1998)
T2	Circular	10	3.33	Caltrans	1.1	0.8	2	4	5	0.8	2.93	6.78	8.71	
T3	Circular	10	3.33	Caltrans	2	0.8	2	3	4	0.8	2.93	4.85	6.78	
S1	Circular	10	5.83	Caltrans	2	0.8	1	1.5	2	0.8	1	2.33	3.65	
S2	Circular	10	5.83	Caltrans	1.1	0.8	2	3	5	0.8	3.65	6.31	11.62	
S3	Circular	10	5.83	Caltrans	1.1	1	2	3	4	1	3.65	6.31	8.96	
S1	Circular	20	5	Washington	0.99	0.8	1.82	5.04	8.27	0.8	2.48	8.28	14.1	Ranf et al. (2006)
S3	Circular	20	5	Washington	0.99	0.8	1.34	2.45	3.56	0.8	1.61	3.61	5.61	
S15	Circular	20	5	Washington	0.99	0.8	2.05	4.03	6	0.8	2.89	6.46	10.01	
C2	Circular	20	5	Washington	0.99	0.8	1.47	2.65	3.83	0.8	1.85	3.97	6.1	
C4	Circular	20	5	Washington	0.99	0.8	1.52	4.6	7.68	0.8	1.94	7.49	13.04	
C3R	Circular	20	5	Washington	0.99	0.8	1.32	3.51	5.7	0.8	1.58	5.52	9.47	

Table H. 3: Review of selected experiments to develop the capacity models for the bridge columns designed in the 1970-1990

Specimen properties						Displacement ductility				Curvature ductility				
	Cross-section													
Specimen	Shape	Size (in.)	Height (ft.)	Design code	Long. Steel ratio (%)	CCLS-0	CCLS--1	CCLS--2	CCLS--3	CCLS-0	CCLS--1	CCLS--2	CCLS--3	Reference
SRPH-1	Circular	24	-	Caltrans	2.7	0.77	1	6	8	0.77	2.77	7	9.26	Hose et al. (1997)
SRPH-2	Circular	24	-	Caltrans	5.4	0.72	1.5	3	4.5	0.72	1.6	4.15	7.8	
SRPH-3	Circular	24	-	Caltrans	5.4	0.69	2.5	5	7.3	0.69	3.1	5.8	9.23	
SRPH-7	Circular	24	-	Caltrans	5.4	0.75	2	4	6	0.75	1.6	4.56	7.32	
MG-2	Circular	28.8	8.8	Caltrans	2	0.86	2.3	2.88	3.45	0.86	4.48	6.04	7.57	Sanchez et al. (1997)
RDS-2	Oblong	24 ×36	13	Caltrans	2	2	6	8	10	3.75	14.77	20.28	25.79	
PEER-COL-1	Circular	16	6	Caltrans	1.17	1.3	5.08	4.16	5.55	1.75	11.27	8.95	12.46	Esmaeily and Xiao (2005)
PEER-COL-3	Circular	16	6	Caltrans	1.17	1.11	2.8	4.17	5.55	1.277	5.534	8.984	12.46	
Flexure	Circular	60	30	Caltrans	2	1	3	5	6.6	3.87	6.74	12.49	17.08	Stone and Cheok (1989)
Shear	Circular	60	15	Caltrans	2	1	4	6	10	3.09	7.26	11.44	19.79	

Table H. 4: Review of selected experiments to develop the capacity models for the bridge columns designed in the Post-1990 era

Specimen properties						Displacement ductility				Curvature ductility				
	Cross-section													
Specimen	Shape	Size (in.)	Height (ft.)	Design code	Long. Steel ratio (%)	CCLS-0	CCLS--1	CCLS--2	CCLS--3	CCLS-0	CCLS--1	CCLS--2	CCLS--3	Reference
328	Circular	24	6	Caltrans	2.72	1.4	3.51	4.91	9.12	2.07	7.64	11.36	22.51	Calderone et al. (2001)
328T	Circular	24	6	Caltrans	2.72	1.57	4.71	7.84	10.2	2.51	10.81	19.12	25.35	
828	Circular	24	16	Caltrans	2.72	1.26	4.41	4.41	7.77	1.91	12.9	12.9	24.63	
1028	Circular	24	20	Caltrans	2.72	1.81	5.81	6.46	9.04	3.94	18.47	20.82	30.19	
ISL 1.0	Oblong	12×17.5	4.83	Caltrans	2	0.8	1.5	5.6	9.6	0.5	2.24	12.4	22.31	Correal. et al. (2007)
ISL 1.5	Oblong	12×20.25	6	Caltrans	2	1.5	2.4	7.5	10.4	2.35	4.78	18.53	26.35	
ISH 1.0	Oblong	10× 14.5	7.62	Caltrans	2.9	0.9	1.4	3.6	4.7	1	2.19	8.72	11.99	
ISH 1.25	Oblong	10×16.75	8.15	Caltrans	2.8	0.7	1.4	3.7	4.7	1	2.22	9.22	12.26	
ISH 1.5	Oblong	10×15.62	8.79	Caltrans	2.9	1	1.6	2.2	4.7	1	2.86	4.72	12.46	
ISH1.5T	Oblong	10×16.75	8.79	Caltrans	2.9	1	1.7	2.8	3.8	1	3.18	6.6	9.71	
415	Circular	24	8	Caltrans	1.5	1	2.7	5	8	1	5.04	10.59	17.78	Lehman and Moehle (2000)
407	Circular	24	8	Caltrans	0.75	1	2.5	3	6	1	4.6	5.8	12.99	
430	Circular	24	8	Caltrans	1.5	1	3	5	7	1	5.88	10.59	15.41	
815	Circular	24	8	Caltrans	1.5	1	2	3	5	1	3.47	5.94	10.89	
1015	Circular	24	8	Caltrans	1.5	1	2	3	5	1	3.47	5.94	10.89	
SRPH-4	Circular	24	7	Caltrans	5.4	1	2.5	8	-	1	2	14.6	-	Hose et al. (1997)
VP-2	Circular	16	6	Caltrans	1.17	1	3.4	7	8.3	1	5.1	10.8	13.85	Orozco (2001)
RDS-1	Oblong	24×36	13	Caltrans	1.64	2	4	8	12	2.3	4.5	10.9	17.3	Sanchez et al. (1997)
RDS-6	Oblong	24×36	13	Caltrans	2	2	6	8	12	1.5	5.3	11.4	17.4	
H/D (6)	Circular	24	12	Caltrans	2.1	0.75	4.5	6	18	0.75	8.71	12.01	38.43	Shanmugam (2009)
H/D (3)	Circular	24	6	Caltrans	2.1	0.75	4.33	13.75	17	0.75	5.03	16.42	20.36	

APPENDIX I

Table I. 1: The assigned nomenclature for bridges with various configurations

Bridge design era	No. of columns per bent	Abutment type	Nomenclature
Pre-1970	Single column	Rigid	SC-Rg-E1
	Single column	Seat	SC-St-E1
	Two columns	Rigid	TC-Rg-E1
	Two columns	Seat	TC-St-E1
	Multiple columns	Rigid	MC-Rg-E1
	Multiple columns	Seat	MC-St-E1
1970-1990	Single column	Rigid	SC-Rg-E2
	Single column	Seat	SC-St-E2
	Two columns	Rigid	TC-Rg-E2
	Two columns	Seat	TC-St-E2
	Multiple columns	Rigid	MC-Rg-E2
	Multiple columns	Seat	MC-St-E2
Post-1990	Single column	Rigid	SC-Rg-E3
	Single column	Seat	SC-St-E3
	Two columns	Rigid	TC-Rg-E3
	Two columns	Seat	TC-St-E3
	Multiple columns	Rigid	MC-Rg-E3
	Multiple columns	Seat	MC-St-E3

The fragility values provided in Chapter 7 correspond to the bridges with circular column cross-sections. The following tables provide fragility values and adjustment factors for the irregular bridges with rectangular and oblong column cross-sections. According to the review of bridge plans, the rectangular column sections are only common in bridges designed before 1970, and the oblong columns are more common in the other two design eras. Therefore, in the following tables, the values provided for the Pre-1970 design era correspond to the bridges with rectangular cross-sections, and the values given for the other two eras relate to the bridges with oblong columns.

Table I. 2: Fragility parameters for the tall bridge types (specifications: multi-span continuous concrete box-girder bridges with seat abutments, single column per bent, and rectangular and oblong column cross-sections)

Bridge design era	Bridge type	BSST-0		BSST-1		BSST-2		BSST-3	
		λ	ζ	λ	ζ	λ	ζ	λ	ζ
Pre-1970	BM	0.053	0.641	0.130	0.612	0.288	0.580	0.435	0.559
	MTL	0.046	0.554	0.095	0.561	0.182	0.549	0.266	0.550
	VTL	0.040	0.578	0.077	0.595	0.143	0.588	0.205	0.602
	ExTL	0.038	0.572	0.073	0.600	0.131	0.604	0.183	0.600
1970-1990	BM	0.111	0.619	0.652	0.662	1.524	0.849	2.272	0.901
	MTL	0.082	0.482	0.409	0.461	0.965	0.563	1.426	0.571
	VTL	0.060	0.556	0.296	0.539	0.718	0.643	1.049	0.632
	ExTL	0.037	0.686	0.207	0.673	0.580	0.824	0.870	0.882
Post-1990	BM	0.111	0.634	0.653	0.662	1.815	0.764	2.872	0.788
	MTL	0.082	0.483	0.410	0.461	1.055	0.507	1.576	0.513
	VTL	0.060	0.541	0.293	0.536	0.752	0.610	1.097	0.573
	ExTL	0.037	0.682	0.206	0.672	0.602	0.784	0.925	0.809

Table I. 3: Fragility adjustment factors for the tall bridge types (specifications: multi-span continuous concrete box-girder bridges with seat abutments, single column per bent, and rectangular and oblong column cross-sections)

Bridge design era	Bridge type	BSST-0		BSST-1		BSST-2		BSST-3	
		ω_λ	ω_ζ	ω_λ	ω_ζ	ω_λ	ω_ζ	ω_λ	ω_ζ
Pre-1970	BM	1.000	1.000	1.000	1.000	1.000	1.000	1.000	1.000
	MTL	0.868	0.864	0.731	0.917	0.632	0.947	0.611	0.984
	VTL	0.755	0.902	0.592	0.972	0.497	1.014	0.471	1.077
	ExTL	0.717	0.892	0.562	0.980	0.455	1.041	0.421	1.073
1970-1990	BM	1.000	1.000	1.000	1.000	1.000	1.000	1.000	1.000
	MTL	0.739	0.779	0.627	0.696	0.633	0.663	0.628	0.634
	VTL	0.541	0.898	0.454	0.814	0.471	0.757	0.462	0.701
	ExTL	0.333	1.108	0.317	1.017	0.381	0.971	0.383	0.979
Post-1990	BM	1.000	1.000	1.000	1.000	1.000	1.000	1.000	1.000
	MTL	0.739	0.762	0.628	0.696	0.581	0.664	0.549	0.651
	VTL	0.541	0.853	0.449	0.810	0.414	0.798	0.382	0.727
	ExTL	0.333	1.076	0.315	1.015	0.332	1.026	0.322	1.027

Table I. 4: Fragility parameters for the tall bridge types (specifications: multi-span continuous concrete box-girder bridges with rectangular and oblong column cross-sections and various abutment types and number of columns per bent)

Bridge type*	BSST-0		BSST-1		BSST-2		BSST-3	
	λ	ζ	λ	ζ	λ	ζ	λ	ζ
SC-Rg-E2	0.110	0.472	0.392	0.471	1.766	0.799	2.405	0.787
SC-St-E2	0.060	0.556	0.296	0.539	0.718	0.643	1.049	0.632
TC-Rg-E2	0.094	0.510	0.328	0.503	1.544	0.721	2.016	0.725
TC-St-E2	0.039	0.478	0.216	0.469	0.557	0.527	0.837	0.549
MC-Rg-E2	0.014	0.740	0.232	0.645	1.252	2.499	2.529	2.531
MC-St-E2	0.051	0.592	0.265	0.563	0.657	0.662	0.969	0.699
SC-Rg-E3	0.110	0.482	0.401	0.473	2.388	0.772	3.652	0.786
SC-St-E3	0.060	0.541	0.293	0.536	0.752	0.610	1.097	0.573
TC-Rg-E3	0.094	0.514	0.326	0.502	2.025	0.724	2.904	0.708
TC-St-E3	0.039	0.483	0.216	0.486	0.575	0.504	0.866	0.497
MC-Rg-E3	0.013	0.747	0.230	0.638	2.423	2.380	6.196	2.394
MC-St-E3	0.051	0.594	0.267	0.556	0.690	0.628	1.023	0.593

* refer to Appendix I, Table I.1 for the nomenclature

Table I. 5: Fragility parameters for the unbalanced bridge types (specifications: multi-span continuous concrete box-girder bridges with seat abutments, single column per bent, and rectangular and oblong column cross-sections)

Bridge design era	Bridge type	BSST-0		BSST-1		BSST-2		BSST-3	
		λ	ζ	λ	ζ	λ	ζ	λ	ζ
Pre-1970	BM	0.089	0.477	0.173	0.469	0.329	0.480	0.470	0.468
	SUnb	0.087	0.480	0.171	0.475	0.328	0.481	0.472	0.478
	MUnb	0.084	0.482	0.169	0.500	0.329	0.505	0.479	0.504
	HUnb	0.084	0.501	0.168	0.505	0.322	0.502	0.469	0.500
	ExUnb	0.089	0.649	0.177	0.640	0.356	0.627	0.527	0.631
1970-1990	BM	0.138	0.503	0.716	0.488	1.598	0.513	2.252	0.516
	SUnb	0.137	0.513	0.710	0.497	1.555	0.519	2.190	0.528
	MUnb	0.133	0.513	0.690	0.494	1.464	0.525	2.022	0.543
	HUnb	0.127	0.516	0.649	0.489	1.334	0.523	1.822	0.535
	ExUnb	0.119	0.554	0.577	0.533	1.096	0.602	1.431	0.612
Post-1990	BM	0.138	0.502	0.725	0.496	1.859	0.513	2.862	0.532
	SUnb	0.136	0.510	0.707	0.490	1.828	0.514	2.864	0.565
	MUnb	0.130	0.503	0.682	0.491	1.745	0.515	2.647	0.520
	HUnb	0.128	0.513	0.650	0.485	1.633	0.513	2.439	0.520
	ExUnb	0.120	0.563	0.573	0.527	1.403	0.596	2.031	0.591

Table I. 6: Fragility adjustment factors for the unbalanced bridge types (specifications: multi-span continuous concrete box-girder bridges with seat abutments, single column per bent, and rectangular and oblong column cross-sections)

Bridge design era	Bridge type	BSST-0		BSST-1		BSST-2		BSST-3	
		λ	ζ	λ	ζ	λ	ζ	λ	ζ
Pre-1970	BM	1.000	1.000	1.000	1.000	1.000	1.000	1.000	1.000
	SUnb	0.978	1.006	0.988	1.013	0.997	1.002	1.004	1.021
	MUnb	0.944	1.010	0.977	1.066	1.000	1.052	1.019	1.077
	HUnb	0.944	1.050	0.971	1.077	0.979	1.046	0.998	1.068
	ExUnb	1.000	1.361	1.023	1.365	1.082	1.306	1.121	1.348
1970-1990	BM	1.000	1.000	1.000	1.000	1.000	1.000	1.000	1.000
	SUnb	0.993	1.020	0.992	1.018	0.973	1.012	0.972	1.023
	MUnb	0.964	1.020	0.964	1.012	0.916	1.023	0.898	1.052
	HUnb	0.920	1.026	0.906	1.002	0.835	1.019	0.809	1.037
	ExUnb	0.862	1.101	0.806	1.092	0.686	1.173	0.635	1.186
Post-1990	BM	1.000	1.000	1.000	1.000	1.000	1.000	1.000	1.000
	SUnb	0.986	1.016	0.975	0.988	0.983	1.002	1.001	1.062
	MUnb	0.942	1.002	0.941	0.990	0.939	1.004	0.925	0.977
	HUnb	0.928	1.022	0.897	0.978	0.878	1.000	0.852	0.977
	ExUnb	0.870	1.122	0.790	1.063	0.755	1.162	0.710	1.111

Table I. 7: Fragility parameters for the unbalanced bridge types (specifications: multi-span continuous concrete box-girder bridges with rectangular and oblong column cross-sections and various abutment types and number of columns per bent)

Bridge type*	BSST-0		BSST-1		BSST-2		BSST-3	
	λ	ζ	λ	ζ	λ	ζ	λ	ζ
SC-Rg-E2	0.202	0.589	0.903	0.587	2.733	0.686	3.875	0.712
SC-St-E2	0.127	0.516	0.649	0.489	1.334	0.523	1.822	0.535
TC-Rg-E2	0.120	0.674	0.546	0.645	1.763	0.885	2.456	0.893
TC-St-E2	0.089	0.463	0.436	0.436	0.867	0.464	1.188	0.467
MC-Rg-E2	0.137	0.551	0.610	0.534	1.634	0.710	2.333	0.713
MC-St-E2	0.103	0.456	0.463	0.443	0.883	0.488	1.195	0.494
SC-Rg-E3	0.205	0.597	0.904	0.586	3.784	0.676	5.946	0.698
SC-St-E3	0.128	0.513	0.650	0.485	1.633	0.513	2.439	0.520
TC-Rg-E3	0.119	0.661	0.550	0.649	2.458	0.885	3.926	0.905
TC-St-E3	0.089	0.457	0.435	0.432	1.045	0.452	1.560	0.457
MC-Rg-E3	0.138	0.549	0.607	0.535	2.337	0.708	3.914	0.743
MC-St-E3	0.104	0.456	0.462	0.445	1.053	0.474	1.547	0.477

* refer to Appendix I, Table I.1 for the nomenclature

Table I. 8: Fragility parameters for the skewed bridge types (specifications: multi-span continuous concrete box-girder bridges with seat abutments, single column per bent, and rectangular and oblong column cross-sections)

Bridge design era	Bridge type	BSST-0		BSST-1		BSST-2		BSST-3	
		λ	ζ	λ	ζ	λ	ζ	λ	ζ
Pre-1970	BM	0.053	0.641	0.130	0.612	0.288	0.580	0.435	0.559
	SKL	0.052	0.612	0.128	0.590	0.282	0.564	0.425	0.547
	SKM	0.045	0.474	0.117	0.489	0.252	0.490	0.380	0.492
	SKH	0.045	0.491	0.119	0.509	0.261	0.510	0.398	0.516
	SKVH	0.045	0.508	0.122	0.528	0.271	0.530	0.416	0.539
	SKEx	0.035	0.396	0.095	0.411	0.211	0.413	0.324	0.420
1970-1990	BM	0.111	0.619	0.652	0.662	1.524	0.849	2.272	0.901
	SKL	0.111	0.600	0.641	0.633	1.499	0.794	2.237	0.838
	SKM	0.114	0.508	0.590	0.498	1.379	0.532	2.074	0.542
	SKH	0.113	0.503	0.588	0.494	1.348	0.526	2.009	0.530
	SKVH	0.111	0.498	0.587	0.490	1.317	0.519	1.945	0.517
	SKEx	0.087	0.388	0.458	0.382	1.027	0.404	1.515	0.403
Post-1990	BM	0.111	0.634	0.653	0.662	1.815	0.764	2.872	0.788
	SKL	0.112	0.612	0.645	0.635	1.776	0.723	2.764	0.759
	SKM	0.118	0.509	0.608	0.505	1.594	0.529	2.254	0.621
	SKH	0.119	0.507	0.608	0.499	1.573	0.524	2.085	0.536
	SKVH	0.121	0.504	0.608	0.492	1.553	0.518	1.916	0.450
	SKEx	0.094	0.393	0.474	0.383	1.210	0.404	1.493	0.351

Table I. 9: Fragility adjustment factors for the skewed bridge types (specifications: multi-span continuous concrete box-girder bridges with seat abutments, single column per bent, and rectangular and oblong column cross-sections)

Bridge design era	Bridge type	BSST-0		BSST-1		BSST-2		BSST-3	
		λ	ζ	λ	ζ	λ	ζ	λ	ζ
Pre-1970	BM	1.000	1.000	1.000	1.000	1.000	1.000	1.000	1.000
	SKL	0.973	0.954	0.982	0.965	0.978	0.973	0.978	0.979
	SKM	0.848	0.739	0.897	0.799	0.875	0.845	0.872	0.880
	SKH	0.848	0.766	0.918	0.831	0.908	0.879	0.915	0.922
	SKVH	0.848	0.793	0.938	0.863	0.941	0.914	0.957	0.964
	SKEx	0.660	0.618	0.731	0.672	0.733	0.712	0.746	0.751
1970-1990	BM	1.000	1.000	1.000	1.000	1.000	1.000	1.000	1.000
	SKL	1.004	0.969	0.983	0.957	0.983	0.935	0.985	0.930
	SKM	1.025	0.821	0.904	0.752	0.905	0.627	0.913	0.602
	SKH	1.015	0.813	0.903	0.746	0.885	0.619	0.884	0.588
	SKVH	1.004	0.805	0.901	0.740	0.864	0.611	0.856	0.574
	SKEx	0.782	0.627	0.702	0.577	0.674	0.476	0.667	0.447
Post-1990	BM	1.000	1.000	1.000	1.000	1.000	1.000	1.000	1.000
	SKL	1.010	0.965	0.988	0.958	0.979	0.946	0.962	0.963
	SKM	1.059	0.803	0.931	0.763	0.878	0.692	0.785	0.788
	SKH	1.074	0.799	0.931	0.753	0.867	0.685	0.726	0.680
	SKVH	1.089	0.795	0.931	0.743	0.855	0.678	0.667	0.571
	SKEx	0.849	0.619	0.726	0.579	0.667	0.528	0.520	0.445

Table I. 10: Fragility parameters for the skewed bridge types (specifications: multi-span continuous concrete box-girder bridges with rectangular and oblong column cross-sections and various abutment types and number of columns per bent)

Bridge type*	BSST-0		BSST-1		BSST-2		BSST-3	
	λ	ζ	λ	ζ	λ	ζ	λ	ζ
SC-Rg-E2	0.185	0.544	0.792	0.551	2.264	0.541	3.102	0.578
SC-St-E2	0.113	0.503	0.588	0.494	1.348	0.526	2.009	0.530
TC-Rg-E2	0.123	0.624	0.574	0.586	1.973	0.852	2.787	0.857
TC-St-E2	0.096	0.471	0.504	0.459	1.093	0.530	1.558	0.548
MC-Rg-E2	0.120	0.570	0.587	0.541	1.853	0.802	2.796	0.845
MC-St-E2	0.106	0.470	0.506	0.442	1.040	0.510	1.465	0.519
SC-Rg-E3	0.187	0.537	0.796	0.552	3.180	0.612	5.941	0.755
SC-St-E3	0.119	0.507	0.608	0.499	1.573	0.524	2.085	0.536
TC-Rg-E3	0.124	0.618	0.577	0.582	2.731	0.801	4.744	0.911
TC-St-E3	0.095	0.479	0.515	0.468	1.345	0.499	2.081	0.511
MC-Rg-E3	0.121	0.569	0.581	0.530	2.764	0.802	5.580	0.951
MC-St-E3	0.105	0.463	0.500	0.442	1.268	0.498	1.918	0.508

* refer to Appendix I, Table I.1 for the nomenclature

REFERENCES

Abbasi, M., Zakeri, B. & Amiri, G. G., 2015. Probabilistic Seismic Assessment of Multiframe Concrete Box-Girder Bridges with Unequal-Height Piers. *Journal of Performance of Constructed Facilities,* p. 04015016.

Abdel-Mohti, A. & Peckan, G., 2008. Seismic response of skewed RC box-girder bridges. Volume 7, pp. 415-426.

Ayyub, B. M. & Lai, K. L., 1989. Structural reliability assessment using latin hypercube sampling. *Structural Safety and Reliability*, pp. 1177-1184.

Baker, J. W., Lin, T., Shahi, S. K. & Jayaram, N., 2011. New ground motion selection procedures and selected motions for the PEER transportation research program. *Pacific Earthquake Engineering Research Center.*

Buckle, I. G., 1994. The Northridge, California earthquake of January 17, 1994: performance of highway bridges. *NCEER-94-0008.*

Calderone, A., Lehman, D. E. & Moehle, J. P., 2001. Behavior of reinforced concrete bridge columns having varying aspect ratios and varying lengths of confinement. *Pacific Earthquake Engineering Research Center.*

Caltrans, 2006. Seismic Design Criteria, Version 1.4.. *California Department of Transportation.*

Caltrans, 2013-2016. Georgia Tech team communication with the Caltrans engineers involved in P266, Task 1780 Fragility project.

Caltrans, 2013. Caltrans Seismic Design Criteria version 1.7. *California Department of Transportation.*

Caltrans, S., 2010. *Caltrans Seismic Design Criteria version 1.6,* Sacramento, CA: California Department of Transportation.

Catacoli, S. S. M., 2014. Displacement demands for performance based design of skewed bridges with seat type abutments.

Chai, Y. H., Priestley, M. N. & Seible, F., 1991. Seismic retrofit of circular bridge columns for enhanced flexural performance. *ACI Structural Journal,* 88(5).

Choi, E., DesRoches, R. & Nielson, B., 2004. Seismic fragility of typical bridges in moderate seismic zones. *Engineering Structures,* 26(2), pp. 187-199.

Cornell, C., Jalayer, F., Hamburger, R. & Foutch, D., 2002. Probabilistic Basis for 2000 SAC Federal Emergency Management Agency Steel Moment Frame Guidelines. *Journal of Structural Engineering,* 128(4), pp. 526-533.

Correal, J. F., Saiidi, M. S., Sanders, D. & El-Azazy, S., 2007. Shake table studies of bridge columns with double interlocking spirals. *ACI structural journal*, 104(4), p. 393.

Derksen, S. & Keselman, H. J., 1992. Backward, forward and stepwise automated subset selection algorithms: Frequency of obtaining authentic and noise variables. *British Journal of Mathematical and Statistical Psychology*, 45(2), pp. 265-282.

DesRoches, R., Padgett, J., Ramanathan, K. & Dukes, J., 2012. Feasibility Studies for Improving Caltrans Bridge Fragility Relationships. *No. CA12-1775*.

Dukes, J., DesRoches, R. & Padgett, J. E., 2012. Sensitivity Study of Design Parameters Used to Develop Bridge Specific Fragility Curves. *In Proc. 15 th World Conf. Earthquake Eng.*.

Esmaeily, A. & Xiao, Y., 2005. Behavior of reinforced concrete columns under variable axial loads: analysis. *ACI Structural Journal*, 102(5), p. 736.

Filippou, F. C., Popov, E. P. & Bertero, V. V., 1983. *Effects of bond deterioration on hysteretic behavior of reinforced concrete joints*, Washington DC: SAC Joint Venture: s.n.

Flores, L. M., 2004. *PEFORMANCE OF EXISTING REINFORCED CONCRETE COLUMNS UNDER BIDIRECTIONAL SHEAR AND AXIAL LOADING*, s.l.: s.n.

Gardoni, P., Mosalam, K. M. & der Kiureghian, A., 2003. Probabilistic seismic demand models and fragility estimates for RC bridges. *Journal of Earthquake Engineering*, Volume 7, pp. 79-106.

Ghobarah, A. A. & Tso, W. K., 1973. Seismic analysis of skewed highway bridges with intermediate supports. *Earthquake Engineering & Structural Dynamics*, 2(3), pp. 235-248.

Golub, G. H. & Van Loan, C. F., 1996. Matrix Computations, third edition. *The Johns Hopkins University Press*, pp. 52-53.

Hastie, T., Taylor, J., Tibshirani, R. & Walther, G., 2007. Forward stagewise regression and the monotone lasso. *Electronic Journal of Statistics*, Volume 1, pp. 1-29.

HAZUS, M., 2003. MR4 Technical Manual. *Multihazard Loss Estimation Methodology*.

Hocking, R. R. & Leslie, R. N., 1967. Selection of the best subset in regression analysis. *Technometrics*, 9(4), pp. 531-540.

Hose, Y. D., Priestley, M. & Seible, F., 1997. Strategic relocation of plastic hinges in bridge columns. *Structural Systems Research Project, 97/05, University of California, San Diego.*

Hwang, H., Jernigan, J. B. & Lin, Y. W., 2000. Evaluation of seismic damage to Memphis bridges and highway systems. *Journal of Bridge Engineering*, Volume 5, pp. 322-330.

James, G., Witten, D., Hastie, T. & Tibshirani, R., 2013. *An introduction to statistical learning*. New York: springer.

Jaradat, O. A., McLean, D. I. & Marsh, M. L., 1998. Performance of Existing Bridge Columns under Cyclic Loading Part 1: Experimental Results and Observed Behavior. *ACI Structural Journal*, 95(6).

Jara, J. M., Reynoso, J. R., Olmos, B. A. & Jara, M., 2015. Expected seismic performance of irregular medium-span simply supported bridges on soft and hard soils. *Engineering Structures*, Volume 98, pp. 174-185.

Jeong, S. & Elnashai, A., 2007. Probabilistic Fragility Analysis Parameterized by Fundamental Response Quantities. *Engineering Structures*, Volume 29, pp. 1238-1251.

John, G. H., Kohavi, R. & Pfleger, K., 1994. Irrelevant features and the subset selection problem. *Machine learning: proceedings of the eleventh international conference,* pp. 121-129.

Kaviani, P., Zareian, F. & Taciroglu, E., 2012. Seismic behavior of reinforced concrete bridges with skew-angled seat-type abutments. *Engineering Structures,* Volume 45, pp. 137-150.

Kawashima, K., Unjoh, S., Hoshikuma, J. & Josa, K., 2010. Damage of transportation facility due to 2010 Chile earthquake. *Bridge Team Dispatched by Japan Society of Civil Engineers.*

Lehman, D. E. & Moehle, J. P., 2000. Seismic performance of well-confined concrete bridge columns. *Pacific Earthquake Engineering Research Center.*

Lehman, D. J., Mahin, S., Calderone, A. & Henry, L., 2004. Experimental evaluation of the seismic performance of reinforced concrete bridge columns. *Journal of Structural Engineering,* Volume 130, pp. 869-879.

Li, R., Ning, X. J., Ye, L. Y. & Li, X. I., 2001. Earthquake Response Analysis of Girder Bridge With High Pier. *Journal of Kunming University of Science and Technology,* Volume 5.

LPILE v6.0, n.d. *A program for the Analysis and Design of Piles and Drilled Shafts under Lateral Loads,* Austin, TX: ENsoft, Inc. Engineering Software.

Mackie, K. R. & Stojadinovic, B., 2005. Fragility basis for California highway overpass bridge seismic decision making. *Pacific Earthquake Engineering Research Center.*

Madsen, K., Bruun, H. & Tingleff, O., 1999. *Methods for non-linear least squares problems.* s.l.:s.n.

Madsen, k., Nielsen, H. & Tingleff, O., 2004. Methods for non-linear least squares problems. *Technical University of Denmark.*

Maleki, S., 2005. Seismic modeling of skewed bridges with elastomeric bearings and side retainers. *Journal of Bridge Engineering,* 10(4), pp. 442-449.

Mander, J. B., Kim, D., Chen, S. & Premus, G., 1996. Response of steel bridge bearings to reversed cyclic loading ,Technical Report NCEER-96-0014. *NCEER.*

Mander, J. B., Priestley, M. J. N. & Park, R., 1988. Theoretical Stress-Strain Model for Confined Concrete. *Journal of Structural Engineering ASCE,* pp. 1804-1825.

Mangalathu, S., 2017. PERFORMANCE BASED GROUPING AND FRAGILITY ANALYSIS OF BOX-GIRDER BRIDGES IN CALIFORNIA.

Maragakis, E. A. & Jennings, P. C., 1987. Analytical models for the rigid body motions of skew bridges. *Earthquake Engineering & structural Dynamics,* 45(8), pp. 923-944.

Mazzoni, S., McKenna, F., Scott, M. H. & Fenves, G. L., 2006. *OpenSees command language manual,* s.l.: Pacific Earthquake Engineering Research (PEER) Center.

Megally, S. H., Silva, F. P. & Seible, F., 2002. Seismic Response of Sacrificial Shear Keys in Bridge Abutments.

Menegotto, M. & Pinto, P. E., 1973. *Method of Analysis for Cyclically Loaded RC Frames Including Changes in Geometry and Non-elastic Behaviour of Elements Under Combined Normal Force and Bending.* s.l., In LABSE Congress Reports of the Working Commision.

Meng, J. Y., Ghasemi, H. & Lui, E. M., 2004. Analytical and experimental study of a skew bridge model. *Engineering Structures,* Volume 26, pp. 1127-1142.

Meng, J. Y. & Lui, E. M., 2000. Seismic analysis and assessment of a skew highway bridge. *Engineering Structures,* Volume 22, pp. 1433-1452.

Miller, A., 2002. *Subset selection in regression.* s.l.:CRC Press.

Muthukumar, S. & DesRoches, R., 2006. A Hertz contact model with non-linear damping for pounding simulation. *Earthquake Engineering & Structural Dynamics,* 35(7), pp. 811-828.

Nada, H., Sanders, D. & Saiidi, M. S., 2003. Seismic performance of RC bridge frames with architectural-flared columns (No. CCEER 03-03). *Center for Earthquake Engineering Research, University of Nevada.*

Nielson, B. G., 2005. *Analytical fragility curves for highway bridges in moderate seismic zones.* Atlanta: School of Civil and Environmental Engineering, Georgia Institute of Technology.

Nielson, B. G. & DesRoches, R., 2006. Influence of modeling assumptions on the seismic response of multi-span simply supported steel girder bridges in moderate seismic zones. *Engineering Structures,* 28(8), pp. 1083-1092.

Orozco, G. L., 2001. The effects of a large velocity pulse on reinforced concrete bridge columns. *Dept. of Structural Engineering, University of California, San Diego.*

Ou, Y. C. et al., 2014. Shear behavior of oblong bridge columns with innovative seven-spiral transverse reinforcement. *ACI Structural Journal,* 111(6), p. 1339.

Padgett, J. E. & DesRoches, R., 2007. Sensitivity of seismic response and fragility to parameter uncertainty. *Journal of Structural Engineering.*

Padgett, J. E. & DesRoches, R., 2008. Methodology for the development of analytical fragility curves for retrofitted bridges. *Earthquake Engineering and Structural Dynamics,* 37(8), pp. 1157-1174.

Priestley, M. N. & Benzoni, G., 1996. Seismic performance of circular columns with low longitudinal reinforcement ratios. *ACI Structural Journal,* 93(4).

Priestley, M. N., Seible, F. & Calvi, G., 1996. Seismic design and retrofit of bridges.

Priestley, M. N., Verma, R. & Xiao, Y., 1994. Seismic shear strength of reinforced concrete columns. *Journal of Structural Engineering,* Volume 120, pp. 2310-2329.

Qian, L., Kehai, W. & Han, W., 2006. Seismic response analysis for girder bridges with tall piers. *Earthquake Engineering and Engineering Vibration-Chineese Edition,* 26(3), p. 74.

Ramanathan, K. N., 2012. *Next generation seismic fragility curves for California bridges incorporating the evolution in seismic design philosophy,* s.l.: s.n.

Ranf, R. T. et al., 2006. Damage accumulation in lightly confined reinforced concrete bridge columns. *Pacific Earthquake Engineering Research Center.*

Sahs, S., Veletzos, M., Panagiutou, M. & Restrepo, J., 2008. Visual Inspection & Capacity Assessment of Earthquake Damaged Reinforced Concrete Bridge Element: Integrated Research & Deployment Final Report. *Report No CA08-0284 and SSRP-06,* Volume 19.

Sanchez, A. V., Priestley, M. & Seible, F., 1997. Seismic performance of flared bridge columns. *UC San Diago, Division of Structural Engineering.*

Scharge, L., 1981. Anchoring of bearings by friction, joint sealing and bearing systems for concrete structures. *World Congress on Joints and Bearings,* Volume 1.

Schoettler, M. J. et al., 2012. A full-scale, single-column bridge bent tested by shake-table excitation. *Center for Civil Engineering Earthquake Research , Department of Civil Engineering, University of Nevada.*

Shamsabadi, A. & Rollins, K. M., 2014. Three-dimensional nonlinear continuum seismic soil-structure interaction analysis of skewed bridge abutments. *NUMGE, 8th European Conference on Numerical Methods in Geotechnical Engineering,* Volume 1.

Shamsabadi, A. & Yan, L., 2008. Closed-form force-displacement backbone curves for bridge abutment-backfill systems. *Proceedings of the Geotechnical Earthquake Engineering and Soil Dynamics IV Congress.*

Shanmugam, S. P., 2009. Seismic behavior of circular reinforced concrete bridge columns under combined loading including torsion. *Missouri University of Science and Technology.*

Shinozuka, M., Feng, M. Q., Lee, J. & Naganuma, T., 2000. Statistical analysis of fragility curves. *Journal of Engineering Mechanics-ASCE,* Volume 126, pp. 1224-1231.

Soleimani, F. et al., 2016. Cyclic Testing and Assessment of Columns Containing Recycled Concrete Debris. *ACI Structural Journal,* 113(5).

Soleimani, F., Vidakovic, B., DesRoches, R. & Padgett, J., 2017. Identification of the Significant Parameters in the Seismic Response of Irreular Bridges. *Engineering Structures. In Press.*

Song, J. & Ellingwood, B. R., 1999. Seismic reliability of special moment steel frames with welded connections: II. *Journal of Structural Engineering,* 125(4), pp. 372-384.

Spiegelhalter, D., Thomas, A., Best, N. & Lunn, D., 2003. WinBUGS user manual.

Stone, W. C. & Cheok, G. S., 1989. Inelastic behavior of full-scale bridge columns subjected to cyclic loading. *Gaithersburg, MD, National Institute of Science and Technology.*

Sullivan, I., 2010. Analytical seismic fragility curves for skewed multi-span steel girder bridges.

Sun, Z., Priestley, M. & Seible, F., 1993. Diagnostics and retrofit of rectangular bridge columns for seismic loads. *Department of Applied Mechanics & Engineering Sciences, University of California, San Diego.*

Tanaka, H. & Park, R., 1993. Seismic design and behavior of reinforced concrete columns with interlocking spirals. *Structural Journal,* 90(2), pp. 192-203.

Tibshirani, R., 1996. Regression shrinkage and selection via the lasso. *Journal of the Royal Statistical Society. Series B (Methodological),* pp. 267-288.

Tirasit, P. & Kawashima, K., 2005. Seismic torsion response of skewed bridge piers. *Journal of Earthquake Engineering,* Volume 28, p. Paper No. 116.

Vidakovic, B., 2011. *Statistics for bioengineering sciences: with MATLAB and WinBUGS Support.* s.l.:Springer Science and Business Media.

Wehbe, N. I., Saiidi, M. S. & Sanders, D. H., 1997. *Effects of confinement and flares on the seismic performance of reinforced concrete bridge columns,* s.l.: (No. RDT-01-004, CCEER-97-2).

Wu, T. L. et al., 2013. Behavior of oblong and rectangular bridge columns with conventional tie and multi-spiral transverse reinforcement under combined axial and flexural loads. *Journal of the Chinese Institute of Engineers,* 36(8), pp. 980-993.

Yang, C. S. W., Werner, S. D. & DesRoches, R., 2015. Seismic fragility analysis of skewed bridges in the central southeastern United States. *Engineering Structures,* Volume 83, pp. 116-128.

Yashinsky, M. et al., 2010. Performance of highway and railway structures during the February 27, 2010 Maule Chile earthquake. *EERI/PEER/FEMA bridge team report.*

Yu, O., Allen, D. L. & Drenvich, V. P., 1991. Seismic vulnerability assessment of bridges on earthquake priority routes in Western Kentucky. *Lifeline Earthquake Engineering,* pp. 817-826.

Zakeri, B., Padgett, J. E. & Amiri, G. G., 2013. Fragility analysis of skewed single-frame concrete box-girder bridges. *Journal of Performance of Constructed Facilities,* 28(3), pp. 571-582.

Zhang, J. & Huo, Y. L., 2009. Evaluating effectiveness and optimum design of isolation devices for highway bridges using the fragility function method. *Engineering Structures,* Volume 31, pp. 1648-1660.

Zheng, Q. & Wenhua, L., 2006. Seismic design of high piers for mountain bridges.

Zhong, J., Gardoni, P., Rosowky, D. & Haukaas, T., 2008. Probabilistic seismic demand models and fragility estimates for reinforced concrete bridges with two-column bents. *Journal of Engineering Mechanics,* Volume 134, pp. 495-504.

VITA

Farahnaz Soleimani

Farahnaz was born in 1986 in Tehran, Iran. She received her Bachelor of Science in Civil Engineering in 2009 from Sharif University of Technology (SUT) in Tehran, Iran. She then entered Tufts University in Boston, US, in the Spring of 2010 to pursue her Master of Engineering in Civil Engineering with an emphasis in Sturtcural Engineering. Upon completion of her Master's degree in Fall 2011, she joined the Georgia Institue of Technology where she obtained her Master of Science and Ph.D. degrees in Civil Engineering with a focus on Structural Engineering in Fall 2015 and Spring 2017, respectively. Her minor field during her Ph.D. was Statistics and Mathematics.